

A New Analytical Design Method of Ultra-low-noise Voltage Controlled VHF Crystal Oscillators and it's Validation

von der Fakultät 1 - MINT - Mathematik, Informatik, Physik, Elektro- und
Informationstechnik der
Brandenburgischen Technischen Universität Cottbus–Senftenberg
genehmigte Dissertation zur Erlangung
des akademischen Grades eines “Dr.-Ing.”

vorgelegt von

Anisha M. Apte (Mungi)

Geboren am 13. Januar 1972 in Pune, Indien

Vorsitzender: Prof. Dr.-Ing. Alexander Kolpin

Gutachter: Prof. Dr.-Ing habil Ulrich L. Rohde
Prof. Dr.-Ing. Matthias Rudolph
Prof. Klaus Buchenrieder, PhD, (Universität der Bundeswehr München)
Prof. Dr.-Ing. Ignaz Eisele, (EMFT-Fraunhofer München)

Tag der mündlichen Prüfung: 11 Februar 2020

Preface, Appreciation, and Acknowledgement

Modern synthesizers and related products require very stable and low phase noise crystal oscillators. The lack of comprehensive know-how in the literature on how to design high performance voltage controlled VHF (very high frequency) VCXO (voltage controlled crystal oscillator) in the 100MHz-200 MHz frequency ranges seems to be one of the greatest difficulties.

These VHF crystal oscillators exhibit extremely low phase noise and are locked against low-aging standards like 10MHz crystal oscillators. As the aging and drifting is compensated by locking the VHF oscillators against the 10MHz standards, the crystal itself can be used at a much higher dissipation, resulting in a better phase noise.

This research work started in 2012, took unusually long time as the available test equipment limited the accuracy of the measurements. It was observed many times, the DUT (Device under test) exhibited superior phase noise performance as compared to the phase noise measurement of the test equipments, and these findings invited lot of technical discussions at IEEE sponsored Frequency Control Symposium and International Microwave Symposium. Suitable phase noise measurement test equipment from Rohde & Schwarz, Keysight, Holzworth, and Noise XT became available after 2016.

This dissertation is based on my research work in the area of microwave oscillators at Synergy Microwave Corporation, Paterson, NJ and looks at all the variables to design a stable, high performance VCXO. By participating at several student design contests I was able to show my research work with positive outcomes and was recipient of student awards in 2014 (First place), (IMS 2014, Tampa, Florida) and 2016 (IMS, San Francisco) for this work. Some of this work was published in IEEE Microwave Magazine Sept/Oct 2013; June 2017, as a winning entry of the Student Design Contests at IMS, "Low Phase-Noise 100MHz Crystal Oscillator, Optimizing phase-noise performance", and another in The Microwave Journal April 2013, "Phase Noise Measurements and System Comparisons". For verification of the design methodology, I have worked on high frequency metamaterial inspired 10 GHz planar/printed resonator oscillator, that won a student paper award at IEEE BenMAS, Philadelphia Sept 2014. What was found was that the noise cancellation techniques incorporated in VCXO design can be applied to high frequency printed resonator oscillator for the applications in current and later generation radio communication systems.

I am very thankful to the IEEE for providing such opportunities for the benefit of the students that helps them grow in their career.

I am extremely grateful for the support of Synergy Microwave Corporation, New Jersey, USA, for sponsoring this work and its Engineering Design team for helping with the board layouts and prototype building and facilitating some overnight or time consuming measurements.

I am indebted to Prof. Dr.-Ing.-habil. Dr. h. c. mult. Ulrich L. Rohde for imparting his guidance, support and encouragement, every step of the way.

I am truly thankful to Prof. Dr.-Ing Matthias Rudolph for his support and providing thorough and effective insights during the course of this work.

I must thank Dr. Afshin Daryoush (Drexel University, PA, USA), Prof. Ignaz Eisele (EMFT, Fraunhofer) and Dr. Klaus Buchenrieder (Bundeswehr University Munich) for their valuable suggestions and timely feedback.

My discussions with Dr.-Ing.-habil Ajay K. Poddar have been of a great impact not just for the helpful suggestions and comments but for relentlessly pushing my limits to get me through this exciting though tiring and challenging endeavor.

This whole effort would not have been possible without Croven Crystals from Canada and Axtal and Morion Inc. for supplying high performance and also purposely some noisy crystals.

Interesting enough the manufactures could not clearly identify what went wrong in the manufacturing of the noisy crystals that were identified by a selection process with a test oscillator.

My acknowledgements would not be complete without expressing gratitude to those who have deeply influenced my life in one way or another. My father, Prof. Arun Mungi (Dept. of Instrumentation and Control, Govt. College of Engineering Pune, India, who I wish was alive and well today) was the reason I became interested in Engineering at a very young age. My mother Dr. Manjusha Mungi (Retired Vice-Principal of Jnana Prabodhini Prashala, (a school for the Gifted), Pune, India) is a role model and a source of inspiration from my childhood.

“Thank you” is not enough to acknowledge the unconditional support and patience of my husband Mahesh Apte and our wonderful daughters Aaroahi Apte and Ananya Apte with whom I have missed many special occasions and events including birthdays and anniversaries during this time, and also my in-laws who have graciously extended their support in every way they could.

I cannot forget to thank Dr. C.P. Gadgil, (Retired Head of the Dept. of Instrumentation and Control, Govt. College of Engineering Pune, India) for his guidance and faith in my abilities in continuing higher studies after leaving my native land.

A special thank you goes to my well-wisher friend, Unmesh Narkar (Innovative Analyticals, Pune, India), where I began my career in Engineering, for the highly motivational conversations and for genuinely believing in me and my capabilities.

Last but not the least, my gratitude to my spiritual Guru Dr. Ashok Marathe (Retired Prof. at the Deccan College, Pune, India) who is an ongoing guiding light, helping me to stay focused and strive to enhance ourselves in every dimension of life.

Warum diese Dissertation?

Die Entwicklung von Oszillatoren mit Resonatoren hoher Güte unter Verwendung von Schwingquarzen für niedrigeren Frequenzen (ebenso wie von dielektrischen Resonatoren bei viel höheren Frequenzen) wurde lange Zeit als schwarze Kunst angesehen. Dies kann daran liegen, dass ein systematischer Ansatz mit optimierter Entwurfsrichtlinien für ersten Quarz-Oszillators trotz umfangreicher Literaturrecherche nicht gefunden werden konnte.

In dieser Dissertation werden nach der Analyse des ersten bekannten Quarz-Oszillators von W. G. Cady (1921) andere Hochleistung Quarz-Oszillators diskutiert, analysiert und berechnet.

Der HP10811A ist ein Einzeltransistor-Quarz-Oszillator, wie von HP (Hewlett Packard) in einem ihrer Designs verwendet. In dieser Arbeit wird die die Schaltung mathematisch und mithilfe von Computer Aided Design Simulation (CAD) analysiert. Die Schaltung wurde auch mit einem Signalquellenanalysator nach dem neuesten Stand der Technik gemessen. Nach der Bestätigung der Daten wird dieses Design auf 100 MHz skaliert, die Frequenz, die für diese Dissertation von Interesse ist.

Obwohl die meisten Entwickler eine Oszillatorschaltung auf Einzeltransistorbasis verwenden, handelt es sich nicht um ein optimiertes Design, da die Kontrolle über wichtige Designparameter wie Schleifenverstärkung, Gleichstrom usw. begrenzt ist.

Diese Dissertation präsentiert einen Ansatz, die Einschränkung aufgrund der Einzeltransistorschaltung zu überwinden und zeigt eine schrittweise Vorgehensweise, in der die Bedeutung eines Zwei-Transistor-Entwurfs mit gründlichen Analyse- und Entwurfssimulationsergebnissen erläutert wird. Diese zweistufige Transistorschaltung ist jedoch noch nicht die optimale Lösung hinsichtlich des Phasenrauschens und der Ausgangsleistung, und für eine optimierte Leistung wird eine zusätzliche Schaltungen benötigt.

Ein wichtiger Beitrag dieser Arbeit ist es zu zeigen, dass das Oszillator-Design durch eine Schaltungstopologie optimiert werden kann, bei der die Schleifen-Spannungsverstärkung durch das Verhältnis des Kollektorwiderstands zum Emitterwiderstand festgelegt ist. Dadurch werden die die Schaltung bestimmenden Parameter praktisch unabhängig vom VHF-Transistor, was eine bessere Kontrolle der Parameter des Oszillators ermöglicht.

In der mathematischen Analyse des Oszillator werden auch die Empfindlichkeit der Abstimm-diode und der Beitrag des Flicker-Rauschens berücksichtigt und die Genauigkeit der Schaltungsberechnung verifiziert.

Quarz-Resonatoren mit AT Schnitt und stressskompensierte (SC) Schnitte werden als die beste Lösung angesehen. Der Oszillator vom Colpitts-Typ mit einem "Tor" wird zuerst betrachtet und der Transistor mit zwei "Toren" später. Beide benötigen eine Nachverstärker- bzw. Pufferstufe.

Anschließend wird ein vollständiges schrittweises Entwurfsverfahren für einen optimierten 100-MHz-Quarzoszillator vorgestellt.

Der Vollständigkeit halber werden CAD-Simulations- und Versuchsergebnisse für 10-MHz-, 128-MHz- und 155-MHz-VCO-Schaltungen bereitgestellt.

Abschließend wird ein Nachverstärker in Basisschaltung eingeführt, um die Isolation und die Ausgangsleistung zu verbessern. Im Gegensatz zu den meisten Oszillatoren, die den Ausgang vom Kollektor beziehen, wird hier ein innovatives Konzept von Rohde [14] benutzt, bei dem der Quarzresonator als Filter und Resonator verwendet wird, bevor es durch den Nachverstärker angekoppelt wird. Diese Technik wurde inzwischen von vielen Herstellern übernommen. Diese Dissertation zeigt, dass diese Schaltungstechnik die Ausgangsleistung erhöht, ohne das Phasenrauschen wesentlich zu beeinflussen. Dieser Nachweis ist zum besseren Verständnis erforderlich und wurde meines Wissens bisher noch nicht erbracht.

Why this dissertation?

The design of high Q oscillators, using Crystals at lower frequencies, (and dielectric resonators at much higher frequencies), has long been considered a black art. This may be due to the fact that a systematic approach with optimized design guideline for crystal oscillators could not be found after extensive literature search.

In this dissertation, after analyzing the first crystal oscillator by W.G. Cady (1921), other high performance crystal oscillators will be discussed, analyzed and calculated.

A single transistor crystal oscillator design as used by HP (Hewlett Packard) in one of their designs, the HP10811A is considered in this thesis for mathematical analysis and CAD (Computer aided Design) simulation. This was also measured on state-of-the-art signal source analyzer. After validation, this design is scaled to 100MHz, the frequency of interest for this dissertation.

Though most designers use a single transistor based oscillator circuit, it is not an optimized design because of limited control over key design parameters such as loop gain, dc current etc.

This dissertation is an attempt to overcome the limitation due to the single transistor circuit and to give a step by step procedure, explaining the significance of a two transistor design with thorough analysis and design simulation results. This two stage transistor circuit is also not yet a best solution in terms of phase noise performance and output power, and some add-on circuitry will be needed for an optimized performance.

An important contribution of this work is to show that since the voltage gain is the ratio of the collector resistor and the emitter resistor, the performance is practically independent of the VHF transistor and gives better control over various parameters of the oscillator, in order to optimize the design.

A grounded-base amplifier is then introduced and added for improving the isolation and the output power. Unlike most oscillators, that take the output from the collector, a novel concept introduced by Rohde [14], is incorporated here, where the crystal is used as a filter that is then connected to the grounded base amplifier, a technique which many companies have been using. This dissertation will show that this technique increases the output power without significantly affecting the phase noise. Such a validation is needed for better understanding and as per my knowledge, has not been done so far.

For the oscillator, the tuning diode sensitivity and flicker noise contribution are also taken into consideration, by calibrating the mathematics and its validation is shown.

Crystal resonators of the type AT and stress-compensated (SC) cut devices will be considered as they give the best performance. The one port Colpitts type oscillator is considered first and the two port two transistor design later. Both will need a post amplifier/buffer stage.

A complete step by step design procedure for an optimized 100MHz crystal oscillator is then presented.

For completeness, CAD Simulation and Experimental results are provided for 10 MHz, 128 MHz and 155 MHz VCO circuits.

Outcome of the Research Work

Awards and Recognition:

Recipient of Student Design Contest Award at IEEE sponsored conferences

- **IMS 2016 - [Low Phase Noise 100 MHz Crystal Oscillator](#)** - To Design, construct, measure and demonstrate a 100MHz Crystal Oscillator using Crystal resonator supplied by organizer

Advisor: Prof. Dr.-Ing. Matthias Rudolph, Brandenburg University of Technology Cottbus
Cottbus 03046, Germany

First Place Award (\$2000 cash, Certificate and an invitation to publish in the IEEE Microwave Magazine, an article based on the winning entry)

- **IMS 2014 – Low Phase Noise X-Band Oscillator** - To Design, construct, measure and demonstrate a 10GHz Oscillator using printed transmission line (microstrip/stripline) resonator

Advisor: Prof. Dr.-Ing. Matthias Rudolph, Brandenburg University of Technology Cottbus
Cottbus 03046, Germany

First Place Award (\$2000 cash, Certificate and an invitation to publish in the IEEE Microwave Magazine, an article based on the winning entry)

- **Recipient Best student paper award**

- **2014** - Anisha Apte, Vivek Madhavan, Ajay Poddar, Ulrich Rohde, and Matthias Rudolph, “**A Novel Low Phase Noise X-band Oscillator**”, IEEE Benjamin Franklin Symposium on Microwave and Antenna Sub-systems for RADAR, Telecommunications, and Biomedical Applications (BenMAS)

Cash \$500, Plaque and Certificate

- ***Productionization of Signal sources based on the research work carried out as a part of Dr. Ing. Thesis***
- 100 MHz Crystal oscillator for reference signal source applications in Synthesizers
- 125 MHz Crystal oscillator for reference signal source applications in Synthesizers
- 128 MHz Crystal oscillator for reference signal source applications in Synthesizers
- 10 GHz Microwave reference signal source applications in RADAR and Test & measurement Equipments applications
- ***Publications***

Total 10 papers published in the international conference, magazine and journals

List of Published papers:

1. Anisha Apte, Ulrich Rohde, Ajay Poddar, and Matthias Rudolph, “Optimizing phase noise performance: Theory and Design Techniques for a Crystal Oscillator”, IEEE Microwave Magazine, vol. 18, Issue 4, pp. 108-123, 2017
2. Ulrich Rohde, Anisha Apte, “Everything you always wanted to know about Colpitts oscillators”, IEEE Microwave Magazine, vol. 17, Issue 8, pp. 59-76, 2016

3. Anisha Apte, Ajay Poddar, Ulrich Rohde, Enrico Rubiola, "Colpitts Oscillator: A new Criterion of Energy Saving for high performance signal sources", IEEE International Frequency Control Symposium (IFCS), pp. 1-7, 2016
4. Ajay Poddar, Ulrich Rohde, Vivek Madhavan, Anisha Apte, Shibam Koul. "Ka-Band Metamaterial Möbius Oscillator (MMO) Circuit", IEEE International Microwave Symposium, MTT-S Digest, pp. 1-4, 2016
5. Anisha Apte, Ajay Poddar, Matthias Rudolph, and Ulrich Rohde, " A Novel Low Phase Noise X-Band Oscillator", IEEE Microwave Magazine, Vol. 16, Issue 1, pp. 127-135, 2015.
6. Anisha Apte, Vivek Madhavan, Ajay Poddar, Ulrich Rohde, and Matthias Rudolph, "A Novel Low Phase Noise X-band Oscillator", 2014 IEEE Benjamin Franklin Symposium on Microwave and Antenna Sub-systems for RADAR, Telecommunications, and Biomedical Applications (BenMAS), pp. 1-3, 2014
7. Ajay Poddar, Ulrich Rohde, Anisha Apte, Vivek Madhavan, Tatsuo Itoh, "Phase Noise Measurement: Uncertainty & Limitations", 2014 IEEE Benjamin Franklin Symposium on Microwave and Antenna Sub-systems for RADAR, Telecommunications, and Biomedical Applications (BenMAS), pp. 1-3, 2014
8. Ulrich Rohde, Ajay Poddar, Anisha Apte, "Getting Its Measure: Oscillator phase noise measurement techniques and limitations", IEEE Microwave Magazine, Vol. 14, No. 6, pp. 73-86, 2013
9. Ajay Poddar, Ulrich Rohde, Anisha Apte, " How Low Can They Go ?: Oscillator Phase noise model, Theoretical, Experimental Validation, and Phase Noise Measurements", IEEE Microwave Magazine , Vol. 14, Issue 6, pp. 50-72, 2013.
10. Ulrich Rohde, Ajay Poddar, Anisha Apte, "Phase noise measurements and System Comparisons", Microwave journal, pp. 22-46, April 2013.

Table of Contents

Cover Page

Preface Acknowledgement

Summary

Table of Contents

Chapter 1: Introduction

- 1.1 Dynamics of Time and Timing Devices
- 1.2 Quartz Crystal Oscillators
- 1.3 Overview of Thesis
- 1.4 Prediction of Phase Noise
- 1.5 Sanity check - (establishing a base line)
- 1.6 Highlights of this dissertation
- 1.7 Conclusion

Chapter 2: Definition of the parameters typically used in Crystal Oscillators

- 2.1 A short description of the most relevant parameters for crystal oscillators
- 2.2 Noise in Semiconductors and Circuits
- 2.3 Conclusion

Chapter 3: Quartz Crystal Resonators

- 3.1 Timing Devices
- 3.2 Resonators and Resonator types
- 3.3 Quartz Crystal Resonators
- 3.4 Fundamental Physics of Crystal Theory
- 3.5 Equivalent Circuit of Crystal and Resonance
- 3.6 Selection of Desired Resonant Modes and Mode Jumping
- 3.7 Behavior of Crystal over Temperature and Aging Factor
- 3.8 Environmental Effects (Excluding static temperature effects)
- 3.9 Thermal Transients
- 3.10 Thermal-Frequency Hysteresis
- 3.11 Acceleration Effects
- 3.12 The Polarization Effect
- 3.13 Crystal Cuts
- 3.14 B-mode trapping
- 3.15 What is Q and Why is it Important?
- 3.16 Drive level Effects
 - 3.16.1 Second Level of Drive
- 3.17 Amplitude Frequency Effect
- 3.18 Conclusion

Chapter 4: Semiconductor Components

- 4.1 Diodes
- 4.2 AM-to-PM Conversion from tuning diodes operated in reverse bias
- 4.3 Diode Noise Model in forward bias
- 4.4 Notes on the Diode Noise Model
- 4.5 Transistors
- 4.6 BJT Noise Model
- 4.7 Notes on the BJT Noise Model
- 4.8 Conclusion

Chapter 5: Crystal Oscillators

- 5.1 Introduction
- 5.2 Cady's Crystal Oscillators
- 5.3 Circuit Analysis using Colpitts Topology
 - 5.3.1 Important consideration for selection of the transistor found during the course of this work
- 5.4 Derivation of the Bessel functions
- 5.5 A Simulation exercise using the available HP10811A/B circuit – a 10 MHz crystal oscillator
- 5.6 Mode-Suppression circuit
- 5.7 A Discussion on some of the findings in this work - considering the 100 MHz case
- 5.8 The Meissner circuit approach
- 5.9 Two Transistor Design
 - 5.9.1 Transistor Selection Criteria
- 5.10 What's new?
- 5.11 Limiting action
- 5.12 Conclusion

Chapter 6: Phase Noise Measurements

- 6.1 Primary phase noise measurement techniques
 - 6.1.1 Direct Spectrum Technique
 - 6.1.2 Frequency Discriminator Method
 - 6.1.3 Phase Detector Technique
 - 6.1.4 Residual method
 - 6.1.5 Two-Channel Cross-Correlation Technique
- 6.2 Conventional Phase Noise Measurement System (Hewlett-Packard)
- 6.3 General Discussion on Phase Noise
- 6.4 Prediction and Validation of Oscillator Phase Noise Measured on Different Equipments
- 6.5 Verification of 100 MHz Crystal Oscillator using CAD simulation Tool (Ansoft Designer from Ansys)
- 6.6 Verification of 100 MHz Crystal Oscillator (LNXO 100) using Analytical Model
- 6.7 Verification of 100 MHz Crystal Oscillator using Phase Noise Measurement Equipments

- 6.7.1 Experimental Verification of 100 MHz Crystal Oscillator using Agilent E5052B
- 6.7.2 Experimental Verification of 100 MHz Crystal Oscillator using R&S (FSUP 26)
- 6.7.3 Experimental Verification of 100 MHz Crystal Oscillator using Anapico (APPH6000-IS)
- 6.7.4 Experimental Verification of 100 MHz Crystal Oscillator using Holzworth (HA7402A)
- 6.7.5 Experimental Verification of 100 MHz Crystal Oscillator using Noise XT (DCNTS)
- 6.8 Phase Noise Measurement Evaluation and Uncertainties
- 6.9 Phase Noise Measurement Issues
- 6.10 Applying the Cross-Correlation
- 6.11 Uncertainties in Phase Noise Measurement
- 6.12 Measurement: This work is to perform analysis of harmonics, phase, and delay and load variations during ultra-low phase noise measurement
- 6.13 Some inferences, findings and suggestions
- 6.14 Factors Influence Phase Noise Measurement
- 6.15 Conclusion

Chapter 7: Experimental Validations-Design Methodology of High Performance Crystal Oscillators

- 7.1 Design Specification based on IMS 2016 SDC (Student Design Contest)
- 7.2 Example: 100MHz crystal oscillator
- 7.3 Example 125 MHz Crystal Oscillator
- 7.4 Example: 155.6 MHz Crystal Oscillator
- 7.5 Conclusion
- 7.6 Acknowledgement

Chapter 8: Future Work, Market trends and Conclusions

- 8.1 Summary
- 8.2 Vibration and Shock Sensitivity
- 8.3 Current and Next Generation Crystal Oscillators
- 8.4 Conclusions

Appendix: Typical questions in the context of this dissertation

Chapter 9: Symbols and Abbreviations

List of Figures and Tables

List of Figures:

Figure 1-1: Cady's first quartz oscillator application [15]

Figure 1-2: Relative phase noise versus the ratio of loaded and unloaded Q of the resonator for noise factor F_1 and F_2 , ($F_1 > F_2$) [9]

Figure 1-3: Calculated phase noise for a 100MHz crystal oscillator

Figure 1-4: Shows the US Patent - Low Noise VHF Crystal Harmonic Oscillator [2]

Figure 1-5: Driscoll crystal oscillator (1974) US Patent 3,836,873 [2] vs. this work

Figure 1-6: HP 10811A/B Crystal Oscillator [17]

Figure 2-1 typical characterization of the noise sideband in the time and frequency domain and its contributions: (a) time domain and (b) frequency domain. Note that two different effects are considered, such as aging in (a) and phase noise in (b) [19].

Figure 3-1: Typical datasheet of a 100MHz Quartz Crystal [Courtesy CROVEN][31]

Figure 3-2: Typical crystal resonator: (a) Quartz resonator, (b) AT Cut crystal thickness at different overtones, (c) Equivalent circuit and (d) Impedance characteristics (fundamental & overtones) [29][31]

Fig 3-3 Impedance characteristics of electro-mechanical crystal resonator [30]

Figure 3-4: Maximum crystal series resistance R , as a function of frequency [7]

Figure 3-5: Maximum crystal power dissipation as a function of frequency [7]

Figure 3-6: Maximum crystal-drive voltage at series resonance as a function of frequency [7]

Figure 3-7: Crystal resonances with and without the effects of load capacitance, C_L [10]

Figure 3-8: Frequency changes in precision quartz crystal units due to interruptions in oscillation and oven control. A: solder bonding and glass encapsulation. B: thermos-compression bonding and high-temperature processing [35]

Fig 3-9 FT for AT cut resonators [19]

Fig 3-10 FT for SC cut resonators [19]

Fig 3-11 FT for AT cut, SC cut, IT cut resonators showing UTP, LTP and inflection angle [10]

Fig 3-12 Typical warm-up for AT and SC cut oven oscillators [19]

Figure 3-13: Idealized frequency-time behavior of a quartz oscillator [35]

Figure 3-14: Thermal hysteresis in quartz resonators. Cycling over wide temperature extremes produces hysteretic behavior that approaches a semi-reproducible loop after a number of repetitions; changing the temperature excursions modifies the loop [35]

Figure 3-15: Crystal resonance spectrum showing vibration-induced sideband at modulation frequency f_m . Sideband level, referred to the crystal resonance, is a measure of the crystal's acceleration sensitivity [35]

Figure 3-16a: The b-mode trap schematic in a Colpitts oscillator [10]

Figure 3-16b: The net impedance for the b-mode trap implementation [10]

Figure 3-17: Diagram showing how crystal plane is rotated about the X axis to obtain the AT cut [35]

Figure 3-18: Shows the measured phase noise of SC-cut and BT-cut 100 MHz crystal oscillator

Figure 3-19: Shows the schematic representation of the variation of resonator motional resistance with crystal current. At very low values anomalously high resistances are sometimes encountered; at high drive levels nonlinear effects increase the resistance [35]

Figure 3-20: (a) Anomalous starting resistance occurring as abrupt transitions leading to a hysteresis loop (b) Nonlinear starting resistance occurring as a single-valued function of crystal voltage V_x (c) Normal linear resistance extending down to very low values of V_x [35]

Figure 3-21 (a): Amplitude-frequency effect. As drive level is increased the crystal resonance curve becomes a multiple-valued function of frequency. Curve heights have been scaled to the same value. (b) Amplitude-frequency curves superimposed, showing the locus of maxima. The resonator is an AT-cut at 1 MHz [35]

Figure 3-22: Activity dips in the frequency-temperature plots of an AT-cut when operated without and with load capacitors [35]

Figure 3-23: Phase noise simulation showing the effect of feedback vs. drive level adjusted by selecting C1 and C2 values

Figure 3-24: Two different crystal resonators – in same oscillator circuit give different performance

Figure 4-1: Part of the datasheet of Infineon diode BB555 [123]

Figure 4-2: Parallel tuned circuit with tuning diodes [20]

Figure 4-3: Part of the datasheet of AXTAL AXIOM75ULN-21– Section for Frequency adjustment range [124]

Figure 4-4: Showing influence of different tuning diodes [Courtesy AXTAL, www.axtal.com]

Figure 4-5: Typical Phase Noise for 10MHz Crystal oscillator [20]

Figure 4-6: Equivalent noise circuit for a diode chip [41]

Figure 4-7(a): Part of Infineon BFP196W NPN Silicon RF transistor datasheet showing Electrical Characteristics [126]

Figure 4-7(b): Part of Infineon BFP196W NPN Silicon RF transistor datasheet showing Transistor chip data Spice parameters [127]

Figure 4-7(c): Part of Infineon BFP196W NPN Silicon RF transistor datasheet showing package equivalent circuit [127]

Figure 4-8: BJT noise model (not showing extrinsic parasitics). Current sources with n are noise sources [41]

Figure 4-9: Phase noise plots showing influence of different transistor types [courtesy AXTAL, www.axtal.com]

Figure 5-1: Schematic of common types of tube oscillator circuits [1]

Figure 5-2: Typical measured phase noise of a free-running tube oscillator at about 100MHz (18.27 dBm output power, operating DC bias 250 volts) [121][Courtesy Synergy Microwave]

Figure 5-3: Simulated Phase Noise of a typical free-running 100 MHz FET based oscillator with a 2N4416 Siliconix transistor, 13.56 dBm output power, operating DC bias 12 volts [43]

Figure 5-4- Simulation schematic of the Cady circuit

Figure 5-5: Output power spectrum of Cady's simulated circuit of Figure 5-4

Figure 5-6: Voltage waveform of the Cady's simulated circuit

Figure 5-7: Simulated single sideband phase noise of this Cady based crystal oscillator

Figure 5-8: General topology of the Colpitts oscillator [9]

Figure 5-9: Colpitts oscillator circuit [9]

Figure 5-10: Colpitts Oscillator schematic

Figure 5-11: Imaginary part of the impedance - Im (Z_{in})

Figure 5-12: Real part of the impedance Re (Z_{in})

Figure 5-13: Simulated phase noise plot showing the effect of the value of $C_2=150\text{pF}$ and $C_2=270\text{pF}$

Figure 5-14: Simulated Phase noise plot with and without the effect of flicker

Figure 5-15: Output power for the Colpitts Circuit in Figure 5-11

Figure 5-16: Base current of the Transistor of the 10MHz Colpitts Crystal Oscillator Circuit in Figure 5-11

Figure 5-17: Collector current of the transistor for the 10MHz Colpitts Crystal Oscillator Circuit in Figure 5-11

Figure 5-18: Collector-Emitter voltage of the transistor of the 10MHz Colpitts Crystal Oscillator Circuit in Figure 5-11

Figure 5-19: Base-Emitter voltage of the transistor of the 10MHz Colpitts Crystal Oscillator Circuit in Figure 5-11

Figure 5-20: A closer look at the base-emitter voltage – RF swing over the DC bias ($0.77\text{V}\approx 100\text{mV}$)

Figure 5-21: 10MHz Crystal datasheet (Courtesy: AXTAL)

Figure 5-22a: Part of the actual circuit schematic of the HP10811A [53]

Figure 5-22b: Modified Part of the actual circuit schematic of the HP10811A [53]

Figure 5-23: Base-Emitter voltage of the transistor in circuit of figure 5-22b

Figure 5-24: Collector current of the transistor in circuit of Figure 5-22b

Figure 5-25: Example of the transient simulation of a high-Q crystal oscillator showing the DC-offset [9].

Figure 5-26: Simulated base current of the first transistor in figure 5-22

Figure 5-27: Simulated Collector-Emitter voltage (V_{ce}) of the first transistor in figure 5-22

Figure 5-28: Simulated Output power of the circuit in figure 5-22

Figure 5-29: Simulated phase noise of the circuit in figure 5-22

Figure 5-30: Sub-harmonics suppression circuit

Figure 5-31: Linear analysis (of the circuit in figure 5-22) showing the Real part of the negative impedance

Figure 5-32: A simple Block Diagram showing the configuration to implement aging of the 100MHz and get phase noise of the 10MHz [19]

Figure 5-33a: Scaled to 100MHz based on the 10MHz HP10811A circuit [17]

Figure 5-33b: Simulated imaginary part of the negative impedance $\text{Im}(Z_{11})$ of the circuit in fig 5-33a

Figure 5-33c: Simulated real part of the negative impedance $\text{Re}(Z_{11})$ of the circuit in fig 5-33a

Figure 5-33d: Simulated phase noise of the circuit in fig 5-33a

Figure 5-34: Effect of different drive levels on phase noise

Figure 5-35: Schematic of the modified circuit based on figure 5-33a for better phase noise performance

Figure 5-36: Simulated phase noise of the circuit in fig 5-35

Figure 5-37: Meissner oscillator [9]

Figure 5-38: A typical representation of 2- transistor design topology for high performance crystal oscillator circuit [7]

Figure 5-39: Portions of the datasheet of the transistor BFG540 [www.nxp.com]

Figure 5-40: Portions of the datasheet of the transistor BFG540 showing typical values of associated available gain and noise figure as a function of collector current [www.nxp.com]

Figure 5-41: Schematic for simulation of the modified 100MHz XO [7, Fig 5.23]

Figure 5-42: Shows the base-emitter junction of the first transistor limits the RF voltage

Figure 5-43: Collector voltage clipping

Figure 5-44: Collector current of the second transistor indicates the voltage limiting/clipping

Figure 5-45: Simulated Output power

Figure 5-46: Simulated phase noise of the crystal oscillator of figure 5-41

Figure 5-47: Two transistor design with grounded base amplifier

Figure 5-48a: Simulated phase noise performance of the circuit of Figure 5-47

Figure 5-48b: Simulated output power of the circuit of Figure 5-47

Figure 5-49: Measured phase noise of the 100MHz crystal oscillator

Figure 6-1: Direct Spectrum Measurement Technique [24]

Figure 6-2: Shows the basic block diagram of frequency discriminator method (Courtesy: Agilent Company) [21]

Figure 6-3: The ideal phase detector sensitivity in terms of RF power (assuming LO power is great than RF) and phase detector constant $K\phi$. The noise floor sensitivity is 1:1 to mixer power input [90]

Figure 6-4: Basic block diagram of heterodyne (digital) discriminator method (Courtesy: Agilent) [91]

Figure 6-5: Basic concept of Phase detector techniques [21]

Figure 6-6: Shows the basic block diagram Phase Detector Method using reference source/PLL techniques). Small fluctuations from nominal voltages are equivalent to phase variations. The phase lock loop keeps two signals in quadrature, which cancels carriers and converts phase noise to fluctuating DC voltage (Courtesy of Agilent Technologies) [21][24]

Figure 6-7: Shows the response of DBM as a phase detector varies as $\cos(\Delta\phi + \pi)$, (VIF) is reasonably linear in the region $(\Delta\phi = \frac{\pi}{2} + \delta\phi)$ [90]

Figure 6-8: Residual method set-up (Simplified single channel residual phase noise measurement system) [24]

Figure 6-9: Automatic system to measure residual phase noise of two 8662A synthesizers (Courtesy of Hewlett-Packard Company) [21]

Figure 6-10: Shows the basic block diagram of 2-channel cross-correlation technique (Courtesy: Agilent) [21][24]

Figure 6-11: Phase Noise system with two sources maintaining phase quadrature [21][24]

Figure 6-12: Shows phase noise plots and noise floor for 3-techniques (PLL, Delay line, and cross-correlation) [REF?? Not found in 90]

Figure 6-13: 100 MHz Colpitts Crystal Oscillator with the Grounded-Base low noise Amplifier [24]

Figure 6-14: Simulated plot showing NF of 100 MHz Oscillator shown in Fig 6-13

Figure 6-15: CAD simulated Polar Plot of Noise of the Oscillator Circuit shown in Figure 6-13

Figure 6-16: CAD simulated Phase Noise Plot of 100MHz Crystal Oscillator with Buffer Stage

Figure 6-17: Simulated Power Output Plot of 100MHz Crystal Oscillator with Buffer Stage

Figure 6-18 shows the theoretical phase noise model expressed in (6-29) [3]

Figure 6-19: Theoretically calculated Phase Noise Plot for 100MHz Crystal Oscillator (LNXO 100) [3]

Figure 6-20 shows the picture of E5052B (Courtesy: Agilent) with the phase noise plot of 100 MHz crystal oscillator circuit for the purpose of the verification of measurement uncertainty (IMS show 2012, Montreal, Canada) [3]

Figure 6-21: 100MHz Crystal Oscillator Measured on Agilent E5052B (Corr_4000) (measurement performed in IMS show 2012, Montreal, Canada) [3]

Figure 6-22 shows the picture of R&S FSUP 26 (Courtesy: R&S) while taking measurement [3]

Figure 6-23: 100MHz Crystal Oscillator Measured on R&S FSUP [3]

Figure 6-24: shows the picture of phase noise plots and equipment setting (Courtesy: Anapico APPH6000-IS) 100MHz Crystal Oscillator Measured on Anapico phase noise engine [3]

Figure 6-25: shows the picture of phase noise plots and equipment setting (Courtesy: Holzworth) 100MHz Crystal Oscillator Measured on Holzworth Phase Noise Engine (measurement performed in IMS show 2012, Montreal, Canada) [3]

Figure 6-26: Phase noise measurement using cross-correlation techniques using Noise XT DCNTS Engine [3]

Figure 6-27: Undetected Discrete Spurious Signal [52]

Figure 6-28: Correct and Erroneous Display of Phase Noise Data [3][112]

Figure 6-29 – Picture shows Low Phase Noise Measurement Setup in Faraday Cage [24]

Figure 6-30: Display of a typical phase noise measurement using the delay line principle. This method is applicable only where $x \propto \sin(x)$. The measured values above the solid line violate this relationship and therefore are not valid [9]

Figure 6-31: Dynamic range as a function of cable delay. A delay line of 1ms is ideal for microwave frequencies [9]

Figure 6-32: A typical Signal source analyzer [[63], ch4]

Figure 6-33: Phase noise measurement of 1GHz SAW Oscillator (SSA#1: -151.9dBc/Hz @ 10 kHz for 1GHz carrier frequency, SSA#2: -142.3dBc/Hz @ 10 kHz) HFSO 100 [63, ch4]

Figure 7-1: A typical 100MHz conventional crystal oscillator (tuning diodes are not included for simplification) [31]

Figure 7-2: 100 MHz 5th overtone crystal oscillator circuit (DC Bias: 5V, 42mA), heater circuit is not included, typical power consumption in steady-state with heater is typically 660mW, startup power consumption with heater 1120 mW) [31]

Figure 7-3: Prototype board of the 100MHz Crystal Oscillator (Top and Bottom sides) [13]

Figure 7-4: Shows the measurement setup with 100 MHz 5th overtone OCXO, the measured Phase Noise is -141dBc/Hz @ 100Hz offset with -193 dBm/ Hz noise floor [31]

Figure 7-5: CAD simulated PN plots for 100 MHz 5th overtone OCXO (ovenized crystal oscillator): trace T1 and T2 show the conventional 100 MHz OCXO, PI+MC+NF (phase-injection, mode-coupled, and noise filtering), noise floor of trace T2 is -190 dBm/Hz@ 1MHz offset [31]

Figure 7-6: Calculated Phase Noise from the different noise sources [9]

Figure 7-7a: Measured PN plots for 100 MHz 5th overtone OCXO: trace T1, T2, and T3 show the conventional 100 MHz OCXO, MC+NF (mode-coupled and noise filtering), and PI+MC+NF (phase-injection, mode-coupled, noise filtering), noise floor of trace T3 is -189.85dBc/Hz@ 1MHz offset (with heater) [31]

Figure 7-7b: Measured PN plots for 100 MHz 5th overtone OCXO: optimized using PI+MC+NF (phase-injection, mode-coupled, noise filtering) [31]

Figure 7-8: Improvement in close-in noise is seen after using some low tolerance metal film resistors (this needs to be optimized in future work)

Figure 7-8b: Part of datasheet of a typical crystal oscillator with its phase noise table [Courtesy Wenzel, www.wenzel.com]

Figure 7-9: shows the prototype 5th overtone 125 MHz crystal (crstal resonator unloaded $Q=90,000$) [13]

Figure 7-10: Measured Phase Noise of the 125MHz Crystal Oscillator [13]

Figure 7-11: 155.6 MHz Mode-Feedback 5th overtone crystal oscillator; resonator $Q=100k$ [122]

Figure 7-12: Measured phase noise plots for 155.6 MHz 5th overtone crystal oscillator [122]

Figure 7-13: Pictures taken at IEEE conferences

Figure 8.1: shows the phase noise plots of reference and 100 MHz crystal oscillator as DUT (Device under test), yellow plot depicts reference phase noise plot in z-direction and DUT-phase noise plot along x, y, and z-axis directions under vibration

Figure 8.2: shows the phase noise plots of reference and 100 MHz crystal oscillator as DUT (Device under test), yellow plot depicts reference phase noise plot in XY-direction and DUT-phase noise plot along x, y, and z-axis directions under vibration

List of Tables:

Table 1.1: Phase Noise – Calculation based on Leeson’s (Rohde Modified) equation with values as per actual crystal

Table 4-1: Diode Noise Model Keywords

Table 4-2: BJT Noise Model Keywords [41]

Table 5-1 For $T=300$ K, data are generated at a different drive-level

Table 5-2: The measured crystal parameters of HP 10811A

Table 5-3: Measured and simulated data of modern day and older crystal oscillators

Table 5-4: This work so far as compared with a typical crystal oscillator on the market

Table 6-1: Correction factor if the phase noise of the reference oscillator is near the phase noise of DUT

Table 6-2: Calculated Noise Figure and Phase Noise for 100MHz Crystal Oscillator

Table 6-3: Theoretical and measured phase noise on different test equipments available in market [3][36]

Table 6-4: Phase noise measurement related problems and possible remedy [63][77]

Table 7-1: Comparison of Simulated and Measured results after optimization [31]

Table 7-2: Recent published Crystal oscillator performance and this work [31]

Table 7-3: Specification of the 125 MHz Crystal Oscillator circuit [Courtesy: Synergy Microwave Corp.]

Chapter 1: Introduction

1.1 Dynamics of Time and Timing Devices

The very concept of “time” is very abstract and that makes it challenging to define “time” in an absolute sense, as it has no beginning and no end and thus is “Timeless”! But, we as humans have come to relate time with events or happenings and thus give meaning to this abstract idea. With the evolution of technology, we as engineers have made significant progress in developing devices to measure and control timing and frequency (inverse of time) even though the definition of “time” itself is so mysterious. Time has become a critical aspect of many concepts that are defined based on timing or frequency measured as (1/time such as 1milisecond translates to 1 kHz). Researchers have dedicated enormous efforts in making devices with increasing accuracy (short-term (milliseconds to picoseconds and long-term accuracy; aging and drift) and reliability. With more and more challenges facing today’s technology, devices with smaller size and lower power consumption have become the need of the hour [1]-[4][8]-[15].

1.2 Quartz Crystal Oscillators

Many scientists were fascinated by pyro-or piezo-electricity. Piezoelectricity was discovered by Jacques and Pierre Curie in 1880. The German (Prof.) Voigt became famous in 1910, for his monumental work, “ALehrbuch der Kristallphysik”. According to Cady, Voigt (in his book) proved the differential equations for the elastic vibrations of the piezo-electric-vibrators [16].

Resonators are considered as energy storing elements in oscillator circuits. Many scientists were searching for a technique to explore the elastic vibrations in quartz crystals, though none of them had so far designed a working circuit.

During World War I, Paul Langevin first investigated quartz resonators for use in sonar. The first crystal-controlled oscillator was built in 1917, using a crystal of Rochelle salt, and patented in 1918 by Alexander M. Nicholson at Bell Telephone Laboratories, although his priority was disputed by Walter Guyton Cady. Some early innovators in quartz crystal oscillators also include G. W. Pierce and Louis Essen [4]-[7].

Cady built the first quartz crystal oscillator in 1921 and proved that the piezo-electric phenomenon could really control frequency stability [6][16]. Cady applied for an American Patent on 28 January 1920 which was granted on 3 April 1923 under number 1,450,246. He claimed a *Piezo electric resonator*; his second patent 1,472,583 claimed a *method of maintaining electric currents of constant frequency*, which was granted on 30 October 1923. Probably due to legal obstructions these patents were (had to be) reissued (registered) in 1929. On 1 October 1925 Cady filed another patent; in this was claimed: *method of mounting piezo electric resonators for the excitation of various overtones*; which was classified on 18 November 1930 under the patent number 1,782,117 [7].

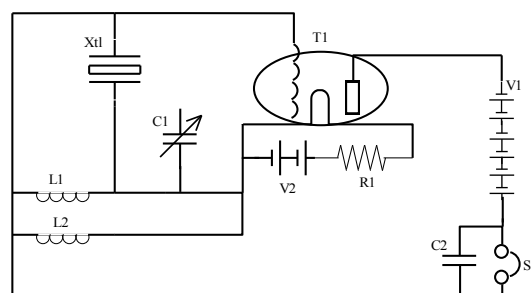


Figure 1-1: Cady’s first quartz oscillator application [15]

The circuit in Figure 1-1 shows quartz-clocks designed by the German Bureau of Standards and the revolutionary quartz-clock invented by Rohde and Leonardt, of the Rohde and Schwarz Company, in 1937 [15]. To validate the circuit in Figure 1-1, a CAD simulation was carried out (Ch. 6, Figure 6-4), which works very well with the modern crystals and transistors!

Today, quartz crystal resonator based oscillators, have established their position as very stable, low noise, high Q, reference frequency signal sources that typically work best in the range of a few kHz up to a few hundred MHz. In this dissertation the frequency range of 100 MHz-128 MHz is being considered.

1.3 Overview of Thesis

The purpose of this work is to give, for the first time, a complete and efficient way to “synthesize” the circuit design of high performance, low noise crystal oscillators. Various circuit configurations and the design criteria along with the challenges for designing crystal oscillators are studied in an effort to present an optimum design in terms of FOM (Figure of Merit) [10][11], which characterizes the phase noise, size, and power consumption, DC-to-RF conversion efficiency, cost and reliability with the objective to meet the real world requirements for efficient and cost-effective quartz crystal resonator based signal source solutions.

This modern concept is used in an extremely low aging and low drifting oscillator, specialty of a crystal manufacturer, Morion Inc. The “noise reference” of the system is a 100, 120, 125 or 128 MHz oscillator, locked against the 10 MHz standard of lesser drift and aging. Other needed auxiliary frequencies are then derived from this VHF crystal oscillator. In a frequency synthesizer system, stabilized against the VHF reference, the oscillator within the loop bandwidth is cleaned up, is no longer free-running and its noise outside the loop depends on the resonator Q and post amplifier performance (AM/PM conversion and noise floor).

The general solution is discussed and derived from the popular Colpitts/Clapp circuit (where the inductor is replaced by a quartz crystal), which is then a valid approach for crystal oscillators up to the third, fifth and seventh overtones.

1.4 Prediction of Phase Noise

The definition of phase noise was first given by E. J. Baghdady, R. N. Lincoln and B. D. Nelin, “*Short-Term Frequency Stability: Characterization Theory, and Measurement*,” in *Short-Term Frequency Stability*, NASA SP-80, 1965, pp. 65-87.

To gain better understanding of the design criteria in the perspective of noise, the prevalent oscillator noise models are studied starting with the popular Leeson’s Noise model and their advantages and drawbacks are discussed.

The first phase noise plot was suggested by Leeson in 1966 [113]. The key quality factor considered here is the phase noise. Leeson developed an approximation equation in which Dieter Scherer added the flicker component (f_c/f_m). Jeremy Everard showed the best ratio between the unloaded and loaded Q (see definition of m in (1.1)) and Rohde added the VCO noise term, the last term in the equation (1.1) which uses the voltage gain of the oscillator for noise modulation.

In designing an oscillator it is important to have a concept of how to do this and hopefully validate the same.

The basic equation (Rohde’s Modified Leeson’s Equation) needed to calculate the phase noise is found in *The Design of Modern Microwave Oscillators for Wireless Applications: Theory and Optimization* [9].

$$E(f_m) = 10 \log \left\{ \left[1 + \frac{f_0^2}{[2f_m Q_0 m(1-m)]^2} \right] \left(1 + \frac{f_c}{f_m} \right) \frac{FkT}{2P_0} + \frac{2kTRK_0^2}{f_m^2} \right\} \quad (1.1)$$

where $\mathcal{E}(f_m)$, f_m , f_0 , f_c , Q_L , Q_0 , F , k , T , P_o , R , K_0 and m are the ratio of the sideband power in a 1 Hz bandwidth at f_m to total power in dB, offset frequency, flicker corner frequency, loaded Q, unloaded Q, noise factor, Boltzmann's constant, temperature in degree Kelvin, average output power, equivalent noise resistance of tuning diode, voltage gain and ratio of the loaded and unloaded Q, respectively.

From (1.1), the minimum phase noise can be found by differentiating Equation (1.1b) and equating to zero as $\frac{\partial}{\partial m} [\mathcal{E}(f_m)]_{m=m_{opt}} = 0$

$$\mathcal{E}(f_m) = \frac{d}{dm} \left\{ 10 \log \left\{ \left[1 + \frac{f_0^2}{[2f_m Q_0 m(1-m)]^2} \right] \left(1 + \frac{f_c}{f_m} \frac{FkT}{2P_0} + \frac{2kTRK_0^2}{f_m^2} \right) \right\} \right\}_{m \neq 1} = 0$$

$$\rightarrow m_{opt} \cong 0.5 \quad (1.2)$$

Figure 1-2 shows the relative phase noise of the typical oscillator [9, pp.333] versus the ratio of loaded and unloaded Q of the resonator for noise factor F_1 and F_2 , ($F_1 > F_2$).

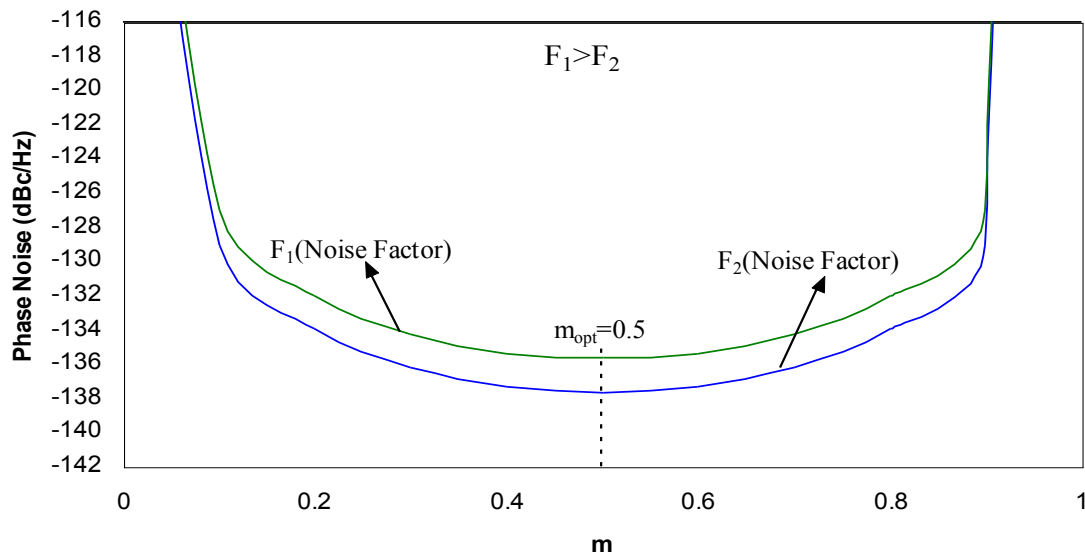


Figure 1-2: Relative phase noise versus the ratio of loaded and unloaded Q of the resonator for noise factor F_1 and F_2 , ($F_1 > F_2$) [9]

This implies that for low noise wideband application, the value of m should be dynamically controlled over the tuning range and it should lie in the vicinity of $m_{opt} \cong 0.5$ for low phase noise performance over the frequency band.

Based on research, modern SC-crystals have a Figure of Merit of $12.5E12$. This means for a 5 MHz crystal, the unloaded Q will be $12.5E12/5E6=2.5E6$ (2.5million); or at a 100 MHz Q will be $12.5E12/100E6 = 125000$. The datasheets typically specify a 'Q' of 130000 for 100 MHz crystals.

The definition and importance of 'Q' is discussed in Chapter 3.

1.5 Sanity check - (establishing a base line):

Published data which are much better in this case, may be misleading if the same parameters are used.

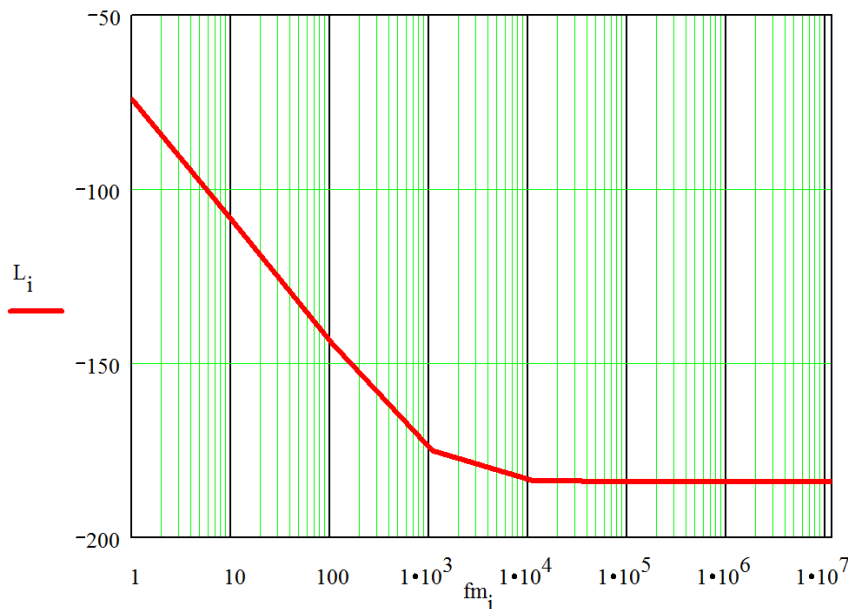
The two key variables are more output power (higher drive level of the crystal) which typically results in worse phase noise close-in and better phase noise far out, or crystals which have a much higher Q_0 than 130000. CAD Simulation shows that an increase of 10% of the Q results in about 1dB better phase noise throughout. A higher output level of 19dBm instead of 14 dBm will result in only better phase noise far out as the close-in phase noise is determined by the oscillator stage/s and the final output stage/s which contributes little if anything to the phase noise below 1 MHz.

A typical 100 MHz crystal oscillator (this frequency is relevant to this dissertation) will have a 14dBm output power =25mW. For ideal phase noise performance, we assume the VCO term has negligible or zero noise contribution at $m \approx 0.5$ (Eq. 1.1). Typically, noise factor is more than 5 for oscillator circuit, for this thesis, noise factor = 5 selected for comparative analysis. The phase noise for this 100 MHz crystal oscillator calculated as per Equation 1-2 is shown in Table 1.1 and is also plotted using MathCad as is shown in Figure 1-3.

Table 1.1: Phase Noise - Calculation based on Leeson's (Rohde Modified) equation with values as per actual crystal

f_0 is the center frequency (Hz)	$f_0=100 \times 10^6$	$\omega_0 = 2\pi f_0$	
f_m is the offset frequency (Hz)	$f_{mi} = 10^i$	$i = 0 \text{ to } 7$	$\omega_{mi} = 2\pi f_{mi}$
f_c is the flicker frequency (Hz)	$f_c=10 \times 10^3$		
Q_L is the loaded Q of the tuned circuit	$Q_L=65000$	$Q_0=130000$	
kT where k =Boltzmann Constant and $T=300K$	$kT=4.1 \times 10^{-21}$		
F is the Noise factor	$F = 5$		
P_{sav} is the average power at oscillator output in W	$P_{sav}=25 \times 10^{-3}$		
K_0 is the oscillator voltage gain in MHz/V	$K_0=5$		
R is the equivalent noise resistor of the tuning diode, typically 5 Ω to 10k Ω	$R = 1 \Omega$		

Phase noise plot based on Leeson's (Rohde Modified) Equation



$\mathcal{E}(f_m)$ is the ratio of the sideband power in 1 Hz bandwidth at f_m to total power in dB

f_{mi}	$\mathcal{E}(f_m)=L_i$
1	-74.11
10	-109.106
100	-143.984
1.10^3	-175.049
1.10^4	-183.6
1.10^5	-183.866
1.10^6	-183.872
1.10^7	-183.872

Figure 1-3: Calculated phase noise for a 100 MHz crystal oscillator

Why is this equation in the introduction? The example considered above shows the best possible physics-based result and is actually quite close to the measured values.

The Leeson equation is quite useful after the design. In the beginning the loaded Q, the output power, the flicker corner frequency and the noise factor are not known. It can be shown that the tuning diode is coupled so loosely that the VCO term can be neglected.

The Leeson equation does not really look at the contribution of the transistor used. Therefore in [9, pg185] a phase noise equation based on the feedback model is discussed using a Colpitts oscillator for microwave application. The equation has to be reconfigured to fit the crystal oscillator case. This is done by the transformation from the Colpitts to the Clapp oscillator. The Clapp oscillator circuit substitutes the inductor with a LC-series circuit which represents the equivalent circuit of the crystal with no contribution from the holder.

The drawback of the Colpitts oscillator is that it is difficult to obtain the best feedback circuit and at the same time limit the crystal drive level and power dissipation. Crystal drive level is the amount of power dissipated in a crystal, typically quantified in microwatts or milliwatts. It can be estimated by computing the excitation current flowing through the crystal. The maximum drive level is the most power the crystal can dissipate, still maintaining operation with necessary electrical parameters guaranteed. For a stable design, drive level must be sustained at the minimum levels essential to initiate proper start-up and guarantee steady-state oscillation. To safeguard from early aging or damage to the crystal, drive level is a key parameter to be considered.

By rotating the Colpitts circuit and using the feedback between the base and collector and using the emitter via the quartz crystal as power source there is more control over the feedback. If a second transistor is used to generate the required 180 degree phase shift between emitter and collector, an additional order of freedom is accomplished, to adjust feedback and phase. This is the key circuit for this dissertation.

A brief look in the past:

In this dissertation, references are made to the probably first crystal oscillator by Cady, and using a harmonic balance simulator, its behavior is predicted [16].

While there are some interesting design rules in the literature, mostly a compromise, not always successful, the analysis of noise in crystal oscillators was only recently possible. Reliable phase noise measurements, of a good rubidium standard, from 1 Hz to 1 MHz offset, has become possible only in the last 5 years, with Wenzel, USA, (5 to 100 MHz) and Morion, USSR, (5 to 100 MHz) being the leading crystal oscillator suppliers.

As far as the phase noise is concerned one of the first complete design rules for crystal oscillators was published by Driscoll, commonly referred to as the "Driscoll Oscillator".

United States Patent [19]		[11] Patent Number: 4,797,639
Driscoll		[45] Date of Patent: Jan. 10, 1989
[54] LOW NOISE CRYSTAL CONTROLLED OSCILLATOR	[56] References Cited	
[75] Inventor: Michael M. Driscoll, Baltimore, Md.	U.S. PATENT DOCUMENTS	
[73] Assignee: The United States of America as represented by the Secretary of the Air Force, Washington, D.C.	4,160,183 7/1979 Kusters et al. 310/315	
[21] Appl. No.: 57,461	4,520,326 5/1985 Clemens 331/116 R	
[22] Filed: May 22, 1987	4,536,721 8/1985 Charbonnier 331/116 R	
[51] Int. Cl.⁴ H03B 5/32	4,577,165 3/1986 Uehara et al. 331/109	
[52] U.S. Cl. 331/158; 331/77	4,580,109 4/1986 Lockwood 331/117 FE	
[58] Field of Search 331/158, 159, 116 R, 331/116 FE, 77	4,600,900 7/1986 Renouit et al. 331/116 R	
	<i>Primary Examiner</i> —Siegfried H. Grimm	
	<i>Attorney, Agent, or Firm</i> —Donald J. Singer; Jacob N. Erlich; Richard J. Donahue	
	[57] ABSTRACT	
	A low noise crystal controlled oscillator utilizes a single low impedance modular amplifier in conjunction with matching low impedance fixed element subcircuits to achieve predictable and repeatable frequency stability. A low component count enhances circuit reliability.	
	6 Claims, 1 Drawing Sheet	

Figure 1-4: Shows the US Patent - Low Noise Crystal Controlled Oscillator [2]

Some of the important contributions by Driscoll dealt with vibration sensitivity and its effect in deteriorating phase noise and phase noise performance itself. In 1974, Driscoll introduced a highly optimized crystal oscillator, which for its time was the best design. It is described in his patent (Figure 1-4) [2]. He selected the crystal as a resonant device from the emitter to ground and collected the output from the collector of the cascode. Therefore, while obtaining a good close-in phase noise, the far-out noise was about -175dBc below the carrier level. The phase noise of this Driscoll oscillator is shown in Figure 1-5. The phase noise results obtained for the optimized Driscoll oscillator circuit scaled and CAD simulated for a 100MHz crystal oscillator is shown superimposed using a red trace in the Figure 1-5, to show past and present day oscillators at a glance.

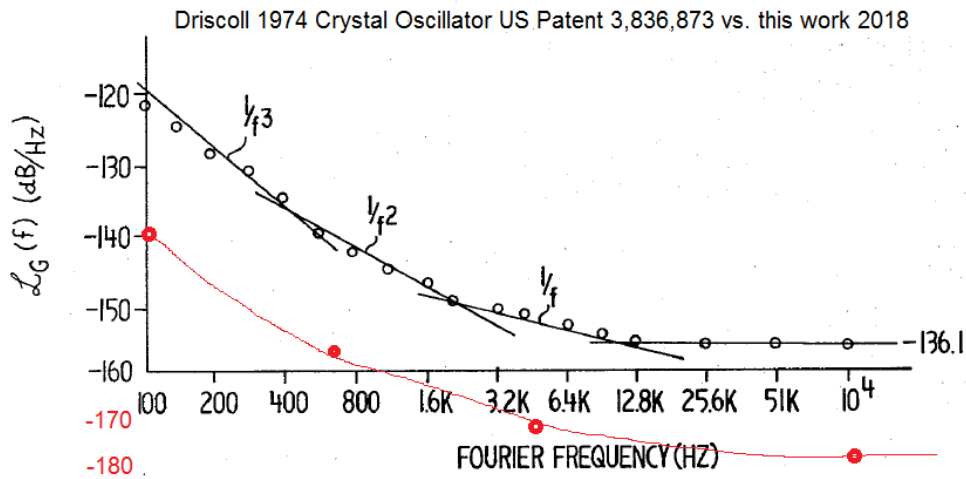


Figure 1-5: Driscoll crystal oscillator (1974) US Patent 3,836,873 [2] vs. this work (marked in red)

A key contribution to low phase noise oscillators was made by Rohde [14]. This circuit did not optimize the oscillator, but using the crystal as a filter device, connecting to the output amplifier stage, greatly improved its far-out noise. A far-out phase noise of -180dBc/Hz became possible.

This principle was first picked up by Hewlett Packard in their popular HP10811A/B crystal oscillator, shown in Figure 1-6.



Figure 1-6: HP 10811A/B Crystal Oscillator [17]

In order to demonstrate the systematic approach, a simplified circuit of this 10 MHz crystal oscillator will be described and analyzed as a part of this dissertation. The circuit diagram shows the actual use of the crystal as a filter and its result. This 10 MHz crystal is a 3rd overtone crystal and the sub-harmonic suppression of the feedback circuit will be explained. This suppression circuit has become the state-of-the-art.

1.6 Highlights of this dissertation:

This dissertation will mainly address the design of very low noise crystal oscillators with emphasis on low noise, short term and long term stability. After providing a brief history of crystal oscillators, its most relevant literature, when phase noise became an issue, the first pioneer on this topic and today's evolution along with the definitions of stability (short term and long term, drift), the definition of phase noise are considered and takes a look at today's phase noise systems along with its mathematical and physics based limitations. An intensive literature search has been done to mention the most relevant publications on crystal oscillators. A few good books on this topic are [35] [46] [105] and [118].

Since the often quoted Driscoll oscillator has some similarity, a published 100 MHz design has been analyzed and the results are shown. The Driscoll oscillator while an intelligent design had the drawback that the grounded base circuit of the cascode oscillator in the feedback circuit frequently became unstable and was uncontrollably oscillating at microwave frequencies. The patent [2] quite old now, claims stability where fairly low frequency transistors were used which are no longer available.

The circuit used in this dissertation also has a grounded base output stage which is not part of the loop and therefore acts as an isolation stage. By putting a small resistor in the RF part, from base to ground, reduces its cut-off frequency and makes it unconditionally stable.

The contribution of this dissertation is the use of a two-transistor feedback circuit with additional level of freedom for adjusting phase and gain and by applying strong feedback at the second transistor the circuit is fairly immune to tolerances due to external environment, thereby the noise performance only depends upon the quartz crystal and its tolerances or its internal environment. The actual circuit was built with the heater circuit stabilizing the crystal temperature at 85°C.

An interesting test was to obtain on purpose some noisy crystals from Croven Crystals, to show its influence.

The actual and final circuit will be determined by first calculating the DC parameters for an acceptable operating point, then calculating the open loop gain, necessary for good steady-state oscillations and then validation with a microwave harmonic-balance CAD simulation for stability

analysis and the measured results are presented, photographs of the hardware are shown and the scope for further development is discussed.

State-of-the art Phase Noise measurement systems and the various techniques for accurate noise measurements are considered as a part of this research study and was also published in [3][24][71].

1.7 Conclusion

This dissertation comes just in time as the modern test equipment for phase noise have become sensitive and accurate enough to really observe and measure very small differences in noise levels.

The purpose of this dissertation is to:

1) Look back in time from Cady's [15] invention until the 1980's where crystal oscillators have been primarily used as secondary frequency sources. (Hydrogen Masers and Cesium standards are called Primary standards), and look at the circuitry used now with semiconductors (Bipolar transistors) and note the stability achieved with crystal oscillators.

2) Introduce the concept and details of low phase noise oscillators, starting with Driscoll's important discussions on Phase Noise of crystal oscillators [2], followed by the trendsetter, the HP 10811A, 10 MHz Crystal Oscillator [17].

3) As the major noise contributors in an oscillator are the transistor and the lossy resonator, their noise contribution needs to be analyzed.

4) For many years, reference oscillators were built at 5 MHz, later 10 MHz but they were optimized for long term frequency stability, not short term stability.

There are actually two classes of oscillators –

i) With extremely low aging and drift (hydrogen masers, Cesium standards, Rubidium standards and finally crystal oscillators)

ii) Extremely good short term stability, phase noise, rather than good aging.

This is achieved by driving the crystal (crystal oscillator at 100 MHz to 128 MHz) with upto 10mW crystal dissipation (poor aging) but locking this against an ultra-stable 10 MHz reference of a loop bandwidth of less than 10 Hz. This provides the best of both worlds.

5) Therefore we take a look at the design rules of a 10 MHz low aging crystal oscillator and then transforming this into a 128 MHz design. Many modern synthesizers require an auxiliary frequency of 640 MHz which is derived from a 128 MHz oscillator, (since $640 \text{ MHz}/5=128 \text{ MHz}$). The crystal resonator at 128 MHz is mechanically very thin and fragile and the quality factor Q deteriorates rapidly beyond 128 MHz.

This dissertation provides a thorough understanding of the complexity of designing and building low phase noise crystal oscillators and the specific things needed to do to make them better.

It will also become apparent that low phase noise and low aging (long term stability) do not come hand in hand. The oscillator for low aging will not have the same low phase noise as the one that is optimized for low phase noise. Some of these things are applicable for other high Q resonators also but the main focus is on crystal oscillators.

One final comment as test equipments requires both high long term stability (aging) and low phase noise at 10 Hz from the carrier and further out, the oscillator design will be different, specifically the power dissipation in the crystal resonator.

This thesis is also partly based on the work that has been published as student - paper, poster, design competitions and reviewed articles in various reputed journals, conferences and magazines many of which have been co-authored [3][4][24][31][71].

A list of the various outcomes during the course of this work is also given in Section 1.8.

The organization of this dissertation is as outlined below:

Chapter 1: Introduction – a brief outline of the topic including overview of the work.

Chapter 2: Definitions of the most relevant parameters of crystal oscillators

Chapter 3: Quartz Crystal Resonator

The theory and physics of the quartz crystal are studied, and also the various modes and mode jumping phenomena are discussed. Resonator Q-factor is also considered and its effects on the performance of the oscillator are discussed.

Chapter 4: Semiconductor Components (used in crystal oscillators are discussed)

Chapter 5: Crystal Oscillators – Some prevalent configurations are discussed and also the typical configurations used for crystal oscillators and step by step design methods are presented.

Chapter 6: Phase Noise

Chapter 7: Optimized Design of a low phase noise crystal oscillator

Chapter 8: Future Work

Chapter 2: Definition of the parameters typically used in Crystal Oscillators

In this chapter, brief definitions of some of the parameters that are typically used in the design, manufacture and measurement of crystal oscillators are considered.

2.1 A short description of the most relevant parameters for crystal oscillators:

a) Output Power

The output power is measured at the designated output port of the oscillator circuit. Practical designs require one or more isolation stages between the oscillator and the output. The VCO output power can vary as much as ± 2 dB over the tuning range. A typical output level ranges from 0 to +10 dBm [9].

b) Frequency Range and Tuning Characteristics

The output frequency of Voltage Controlled Oscillators (VCOs) can vary over a wide range. The frequency range is determined by the architecture of the oscillator. A standard tunable oscillator has a frequency range typically less than 2:1. This specification shows the relationship, depicted as a graph, between the VCO operating frequency and the tuning voltage applied. Ideally, the correspondence between operating frequency and tuning voltage is linear [9].

c) Tuning Linearity

For stable oscillators, a linear deviation of frequency versus tuning voltage is desirable. It is also important to make sure that there are no breaks in tuning range, for example, that the oscillator does not stop operating with a tuning voltage of 0V [9].

d) Tuning Sensitivity, Tuning Performance

This datum, typically expressed in megahertz per volt (MHz/V), characterizes how much the frequency of a VCO changes per unit of tuning voltage change [9].

e) Tuning Speed

This characteristic is defined as the time necessary for the VCO to reach 90% of its final frequency upon the application of a tuning voltage step. Tuning speed depends on the internal components between the input pin and the tuning diode, including, among other things, the capacitance present at the input port. The input port's parasitic elements, as well as the tuning diode, determine the VCOs maximum possible modulation bandwidth [9].

f) Post-tuning Drift

After a voltage step is applied to the tuning diode input, the oscillator frequency may continue to change until it settles to a final value. The post-tuning drift is one of the parameters that limit the bandwidth of the VCO input and the tuning speed [9].

g) Harmonic Suppression

The oscillator/VCO has a typical harmonic suppression of better than 15 dB. For high performance applications, a low pass filter at the output will reduce the harmonic contents to a desired level.

h) Output Power as a Function of Temperature

All active circuits vary in performance as a function of temperature. This variation in output power with temperature should be less than a specified value, such as 1dB [9].

i) Spurious Response

Spurious outputs are signals found around the carrier of an oscillator, which are not harmonically related. A good, clean oscillator needs to have a spurious-free range of 90 dB, but these

requirements make it expensive. Oscillators typically have no spurious frequencies besides possibly 60 Hz and 120 Hz pick-up. The digital electronics in a synthesizer generates many signals, and when modulated on the VCO, are responsible for these unwanted output products [9].

j) Frequency Pushing

Frequency pushing characterizes the degree to which an oscillator's frequency is affected by its supply voltage. For example, a sudden current surge caused by activating a transceiver's RF power amplifier may produce a spike on the VCOs DC power supply and a consequent frequency jump. Frequency pushing is specified in frequency/voltage form and is tested by varying the VCOs DC supply voltage (typically $\pm 1V$) with its tuning voltage held constant. Frequency pushing must be minimized, especially in cases where power stages are close to the VCO unit and short pulses may affect the output frequency. Poor isolation can make phase locking impossible [9].

k) Sensitivity to Load Changes (Pulling factor)

To keep manufacturing costs down, many wireless applications use a VCO alone, without the buffering action of a high reverse-isolation amplifier stage. In such applications, frequency pulling, the change of frequency resulting from partially reactive loads is an important oscillator characteristic. Pulling is commonly specified in terms of the frequency shift that occurs when the oscillator is connected to a load that exhibits a non-unity VSWR (such as 1.75, usually referenced to 50W), compared to the frequency that results with unity-VSWR load (usually 50W) [9].

l) Power Consumption

This characteristic conveys the DC power, usually specified in milliwatts and sometimes qualified by operating voltage, required by the oscillator to function properly. [9][22]

m) Phase Noise

An important feature is the stability of the oscillator (low phase noise) and its freedom from spurious signals and noise. While the oscillator is almost always used as a voltage-controlled oscillator (VCO) in a frequency synthesizer system, its free-running noise performance outside the loop is still extremely important and solely determined by the oscillator.

Unfortunately, oscillators do not generate perfect signals. The various noise sources in and outside of the active device (transistor) modulate the VCO, resulting in energy or spectral distribution on both sides of the carrier due to modulation and frequency conversion. AM and FM noise is expressed as the ratio of noise power in a 1 Hz bandwidth divided by the output power. It is measured at frequency offset of the carrier. The x-axis is the frequency offset from the carrier on a logarithmic scale. The y-axis is the phase noise in dBc/Hz. – Add relevant plots.

The stability or phase noise of an oscillator can be determined in the time or frequency domain. Phase noise is a short-term phenomenon and has various components. Figure 2-1 (a) shows the typical illustration of the stability and phase noise in the time and frequency domain. The major noise contributors are thermal noise, Schottky noise and the flicker noise from the active device. Flicker noise depends on the transistor type and its biasing. The noise contribution from the resonator is mainly thermal noise. The minimum phase noise is at far offsets from the carrier, the best number being $[-P_{out} \text{ (dBm)} + kT \text{ (-174dBm)} + NF \text{ (large-signal noise figure of the amplifier transistor of the oscillator in dB)}]$ [19].

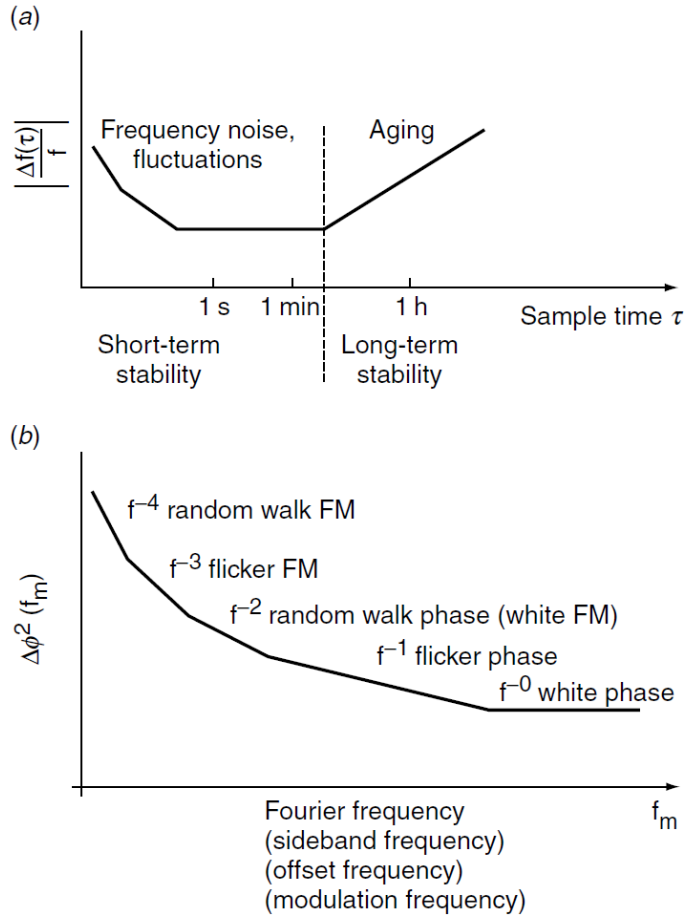


Figure 2-1: Typical characterization of the noise sideband in the time and frequency domain and its contributions: (a) time domain and (b) frequency domain [19]

Note that two different effects are considered, such as aging in Figure 2-1(a) and phase noise in Figure 2-1(b).

2.2 Noise in Semiconductors and Circuits [21]-[24]

Microwave applications generally use bipolar transistors and following are their noise contributions [3][6][12]-[14].

Johnson noise [21]-[24]

- The Johnson noise (thermal noise) is due to the movement of molecules in solid state devices called “Brown’s molecular movements”
- It is expressed as $v_n^2 = 4kT_0RB$ (emf) (volt²/Hz)
- The power of thermal noise can thus be written as

$$\text{Noise Power} = \frac{v_n^2}{4R} = kT_0B \text{ (W/Hz)}$$

It is most common to do noise evaluations using a noise power density, in Watts per Hz. By setting B=1 Hz we get:

For $B = 1\text{Hz}$, $\text{Noise Power} = kT_0$

$T = 290\text{K}$ and k – Boltzmann’s constant = $1.38 \times 10^{-23} \text{ J/K}$

by Thevinin, $\text{Noise Power} = 1.38 \times 10^{-23} \times 290 = 4 \times 10^{-23} \text{ W}$

- Noise floor below the carrier for zero dBm output is given by:

$$L(\omega) = 10 \log \left(\frac{v_n^2/R}{1mW} \right) = -173.97dBm \text{ or about } -174dBm$$

- In order to reduce this noise, the only option is to lower the temperature, since noise power is directly proportional to temperature.
- The Johnson noise sets the theoretical noise floor.
- The available noise power does not depend on the value of resistor but it is a function of temperature T. The noise temperature can thus be used as a quantity to describe the noise behavior of a general lossy one-port network.
- For high frequencies and/or low temperature a quantum mechanical correction factor has to be incorporated for the validation of equation. This correction term results from Planck's radiation law, which applies to blackbody radiation.

$$P_{av} = kT \cdot B \cdot p(f, T), \text{ with } p(f, T) = \left[\frac{hf}{kT} / \left(e^{\left(\frac{hf}{kT} \right)} - 1 \right) \right]$$

- where $h = 6.626 \cdot 10^{-34} \text{ J} \cdot \text{s}$, Planck's Constant (**Planck's Radiation Noise**)

Schottky/Shot noise [21]-[24]

- The Schottky noise occurs in conducting PN junctions (semiconductor devices) where electrons are freely moving. The root mean square (RMS) noise current in 1 Hz bandwidth given by

$$\overline{i_n^2} = 2 \times q \times I_{dc} \quad P = i_n^2 \times R_L$$

Where, q is the charge of the electron, P is the noise power, and I_{dc} is the dc bias current, R_L is the termination load (can be complex).

- Since the origin of this noise generated is totally different, they are independent of each other.

Flicker noise [21]-[24]

- The electrical properties of surfaces or boundary layers are influenced energetically by states, which are subject to statistical fluctuations and therefore, lead to the flicker noise or $1/f$ noise for the current flow.
- $1/f$ noise is observable at low frequencies and generally decreases with increasing frequency f according to the $1/f$ -law until it will be covered by frequency independent mechanism, like thermal noise or shot noise.

Example: The noise for a conducting diode is bias dependent and is expressed in terms of Af and Kf .

$$\langle i_{Dn}^2 \rangle_{AC} = 2qI_{dc}B + Kf \frac{I_{DC}^{Af}}{f} B$$

- The Af is generally in range of 1 to 3 (dimensionless quantity) and is a bias dependent curve fitting term, typically 2.
- The Kf value is ranging from $1E^{-12}$ to $1E^{-6}$, and defines the flicker corner frequency.

Transit time and Recombination Noise [21]-[24]

- When the transit time of the carriers crossing the potential barrier is comparable to the periodic signal, some carriers diffuse back and this causes noise. This is really seen in the collector area of NPN transistor.

- The electron and hole movements are responsible for this noise. The physics for this noise has not been fully established.

Avalanche Noise [21]-[24]

- When a reverse bias is applied to semiconductor junction, the normally small depletion region expands rapidly.
- The free holes and electrons then collide with the atoms in depletion region, thus ionizing them and produce spiked current called the avalanche current.
- The spectral density of avalanche noise is mostly flat. At higher frequencies the junction capacitor with lead inductance acts as a low-pass filter.
- Zener diodes are used as voltage reference sources and the avalanche noise needs to be reduced by big bypass capacitors.

2.3 Conclusion

The definitions of the various relevant parameters in Crystal oscillators and its measurements have been considered in this chapter. The different types of noise are also defined and explained briefly.

Chapter 3: Quartz Crystal Resonators

3.1 Timing Devices

Today's research in the field of electronic timing and frequency generation devices is intended towards the development of making such devices with increasing accuracy, lower power consumption, reduced size and cost; the solutions of which depends upon the various design criteria and measurable parameters such as phase noise, thermal drift, harmonics, tuning sensitivity, stability, aging, and so on. The foremost types of clock sources used with a microcontroller have been the crystal oscillators, SAW (Surface Acoustic Wave), CRO (Ceramic Resonator Oscillator), RC oscillators and silicon resonator oscillators. Even though many characteristics define the performance, phase noise is usually the most important parameter defining the performance of today's frequency generating signal sources [1]–[25].

3.2 Resonators and Resonator types

The key component in crystal oscillator circuit design is a resonator, an energy storing element that is capable of storing both frequency-dependent electric and magnetic energy, as shown in Fig. 1.1 and 1.2 and plotted in Fig 1.3.

Their broad classification is based upon their principle of operation.

A simple example is a series or parallel combination of an inductor (L) and a capacitor (C), where the magnetic energy is stored in the inductance L and the electric energy is stored in the capacitance C. The resonant frequency of a resonator is the frequency at which the energy stored in electric field equals the energy stored in the magnetic field. As components, resonator components allow a selective transmission or blocking of signals and serve as 1-port or 2-port frequency-determining elements for oscillator applications [10][11][19][25][29]-[32].

3.3 Quartz Crystal Resonators

Quartz is a crystalline mineral made of silicon dioxide (SiO_2) that forms hexagonal (six sided) crystals or masses of crystals. The curie brothers, Jacques and Pierre, discovered an electrical effect in quartz in 1880 and called this phenomenon piezoelectricity, derived from the Greek word Piezein, meaning to press.

Reference frequency sources require high Q (quality factor) energy storage element such as crystal resonators for stable low phase noise operation. Quartz crystal resonator based oscillators, have established their position as very stable, low noise, reference frequency signal sources and typically work best in the range of a few kHz up to a few hundred MHz. [10][11]

Before delving deeper in the theory of Quartz crystals, Figure 3-1a shows a typical datasheet of a 100 MHz quartz crystal for an oven controlled crystal oscillator (OCXO) and Figure 3-1b shows a typical datasheet of a 10 MHz oven controlled crystal oscillator (OCXO). It is important that before designing a crystal oscillator, one must know the various specifications of the crystal, their definitions and the impact that these parameters have on the performance of the oscillator. This chapter gives an overview of the important crystal parameters that are useful while designing an oscillator with optimum performance. Sometimes manufacturers can provide preselected crystals to the user sorted out for certain specifications such as phase noise, aging or temperature stability. Nevertheless, this chapter discusses the most relevant aspects of a quartz crystal that the designer should know while selecting or buying such crystals.



CROVEN CRYSTALS has provided high quality and reliability products to the frequency control industry for more than fifty years and is a world leader in the development and manufacture of the highest precision quartz resonators for demanding applications.

The HC-35 series of crystal resonators provides a broad range of frequencies and designs in a rugged, high reliability enclosure.

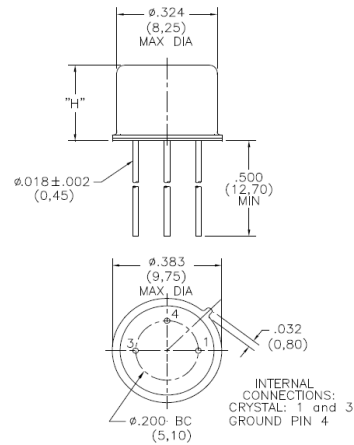
Features:

- cold weld sealed for **low aging** and **low phase noise** applications
- available in AT, SC and IT-cut designs
- low g-sensitivity design options available
- RoHS compatible (if required)

Applications:

- precision OCXO, VCXO and TCXO oscillators
- data telemetry
- instrumentation
- military and high reliability (multiple CR references)

HC-35 (TO-5)



Quartz Crystal Specification

Frequency	100.000000 MHz
Cut	SC-cut
Vibration Mode	5 th overtone
Holder	HC-35, 0.220" (5.58 mm) maximum height
Calibration Tolerance	± 5 ppm at +85 °C
Load Capacitance	Series
Frequency-Temperature Stability	Lower TOP 75 to 90 °C or Slope < +20 ppb/°C @ +85 °C
Motional Resistance Rs	100 ohms maximum (<i>typically 70 ohms</i>)
Motional Capacitance C1	0.15 fF typical
Shunt Capacitance C0	2.7 pF typical
Quality Factor Q	> 110,000 (<i>typically 130,000</i>)
Phase Noise	< -130 dB/Hz @ 100 Hz
Drive Level	100 µW; (<i>4mW when locked in a PLL system</i>)
G-sensitivity	< ± 0.5 ppb/g per axis
Aging	< ± 0.1 ppm/year after 30 days of operation
Marking	1. Bar code label with Serial Number - data to be provided
Environmental	Shock: MIL-STD-202G, M213 Condition C - 100 g, 6 msec, ½ sine Vibration: MIL-STD-202G, M204 Condition C, 10 g peak, 55 to 2000 Hz 1 sweep per axis Solderability, Seal and Workmanship per MIL-PRF-3098
RoHS	Parts are RoHS compliant

Figure 3-1a: Typical datasheet of a 100 MHz Quartz Crystal [Courtesy CROVEN][31]



Specification	AXX43-54	Rev.: 1	Date: 2014-02-18
---------------	----------	---------	------------------

Type: Precision Quartz Crystal Unit for OCXO

Parameter	min.	typ.	max.	Unit	Condition
Nominal frequency f_0	10.000			MHz	
Crystal cut	SC				
Overtone	3				
Load capacitance C_L	20			pF	
Adjustment tolerance			±2.0	ppm	@ L.T.P.
Frequency stability					
Lower turn-over temperature (L.T.P.)	+82	+85	+88	°C	Option A
	+88	+91	+94	°C	Option B
Long term (aging) per year @ 25°C			±100	ppb	after 30 days operation
Retrace after 24 hours			±10	ppb	2 hours off and 1 hour on
Resonance resistance R_r			100	Ω	
Motional capacitance C_1	0.16	0.19	0.22	fF	
Shunt capacitance C_0			3.8	pF	
Quality factor Q		1200		k	
Drive level		100		μW	
Drive level dependence (DLD) $\gamma=R_{rmax}/R_{rmin}$			1.1		0.3 μW ~ 200 μW
Unwanted responses R_{spur}/R_1	2				Except B-Mode
Insulation resistance	500			MΩ	100 V DC
Operable temperature range	-45		+100	°C	
Storage temperature range	-55		+105	°C	
Enclosure (see drawing)	HC-43/U				IEC 60122-3
Can height H	13.5 max.			mm	
SMD configuration	N.A.				
Marking	IQD-FOQ Marking AXX43-54A or B 10.000 MHz wwAXFyy				Side 1 Side 2
Packing	Tape & Reel				

Notes:

1. Terminology and test conditions are according to IEC standard IEC60122-1, unless otherwise stated
2. Measurement technique according to IEC 60444-5 or equivalent

Ordering Code:

Mode [Specification]	L.T.P. Option	Frequency [MHz]	Equivalent to
AXX43-54	A	10.000	IQXC-119
AXX43-54	B	10.000	IQXC-118

Figure 3-1b: Typical datasheet of a 10 MHz Quartz Crystal (Courtesy: AXTAL)

3.4 Fundamental Physics of Crystal Theory

The resonant frequency (also described as “nominal frequency” on the datasheet) of the crystal resonator is determined by the effective thickness of the quartz wafer, which is controlled by mechanical sawing and lapping of the quartz wafer to the desired thickness ($frequency \propto 1/thickness$). For achieving higher oscillation frequency, reducing wafer thickness beyond certain limit makes the crystal fragile and as it gets thinner, processing the component becomes more

difficult, thus posing a physical limit to the manufacturing process under the constraints of cost and reliability.

The piezoelectric effect that Quartz exhibits is that, when a dc voltage is applied to the opposing surfaces of a piece of properly oriented quartz it will change its shape mechanically (and vice versa). This is the reason why crystals are primarily used to form a resonator or the frequency selective element in oscillator circuits. The physical dimensions of this small thin piece of quartz, with two opposite surfaces metallized to make electrical connections, are tightly controlled as they control the frequency of oscillation. Figure 3-2(a) shows the typical structure of quartz crystal. An oscillator circuit with a crystal resonator permits vibrations at the resonant frequency thus performing like a very high-Q tuned network. The lowest fundamental frequency available in a quartz crystal is about 1 kHz. The highest fundamental frequency is about 20-25 MHz, above which the crystal becomes too thin and delicate to be handled. Oscillations can be continued to about 200 MHz by operating the crystal on its third, fifth, seventh, or ninth overtones; (mentioned on the datasheet). Proportional dimensions of the different overtones are shown in Figure 3-2(b) [29]-[31].

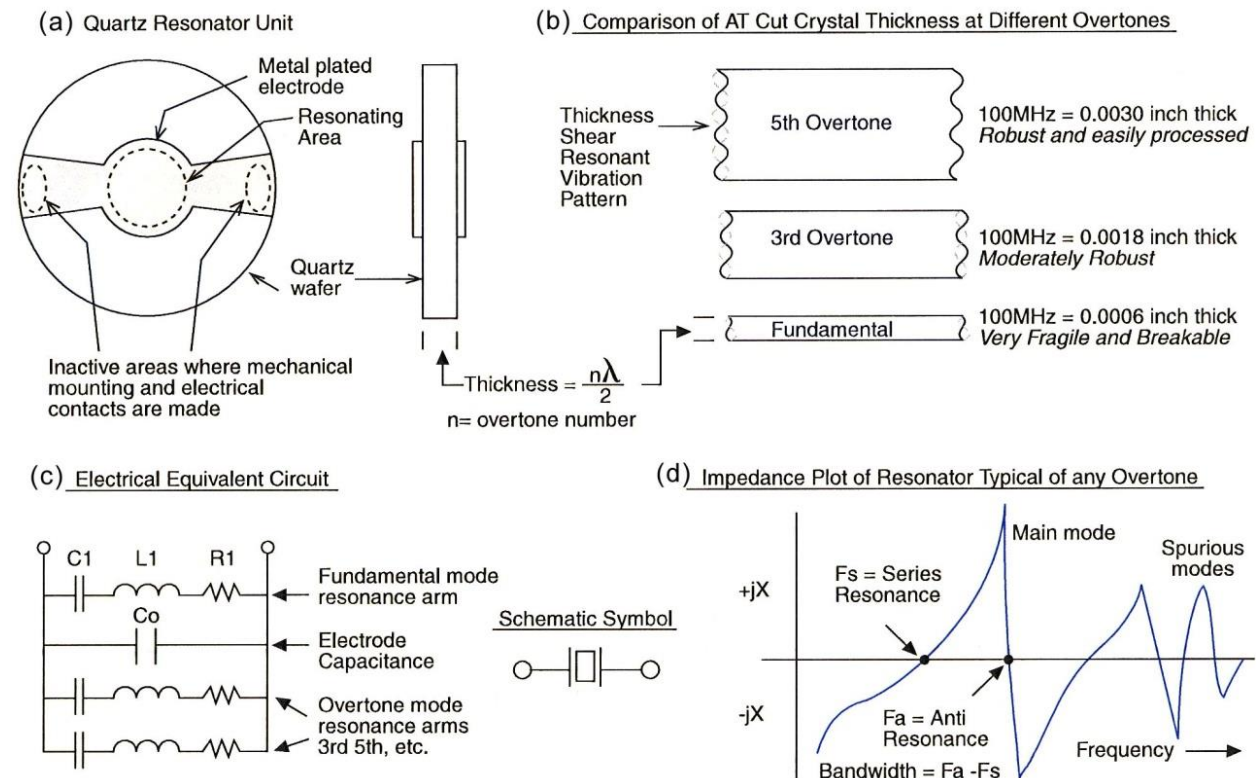


Figure 3-2: Typical crystal resonator: (a) Quartz resonator, (b) AT Cut crystal thickness at different overtones, (c) Equivalent circuit and (d) Impedance characteristics (fundamental & overtones) [29]-[31]

More details about crystal cuts are considered in section 3.13 Crystal Cuts.

3.5 Equivalent Circuit of Crystal and Resonance

Figure 3-2(c) shows the most basic equivalent circuit of a crystal using lumped constant elements known as the *Van dyke model*, where the crystal is shown as a series combination of RLC in parallel with a holding capacitor. Inductance L_1 and the series capacitance C_1 , represent the crystal's frequency-sensitive elements. Capacitance C_0 , specified as "*shunt capacitance*" on the datasheet, is the capacitance between the two metallized surfaces used as electrode contacts on the crystal and

runs about 3-15 pF for most crystals. The series resistance R_1 , (also represented by R_s or “*resonance resistance*” on the datasheets) of a typical crystal of any cut, increases with the harmonic, and varies from about 10Ω , at 20 MHz, to a few hundred ohms at 1 MHz, up to a few thousand ohms at 100 kHz, and up to $200,000\Omega$ at 1 kHz and the process of frequency multiplication increases the power in the sidebands by the square of the multiplication factors ($P_m=P_0/m^2$) [10][29].

Figure 3-2d shows the typical impedance characteristics of such an electromechanical crystal resonator, which vibrates due to piezoelectric effect and exhibits multimode resonances. [31]

Figure 3-3 explains the reactance characteristics of electro-mechanical crystal resonator [30].

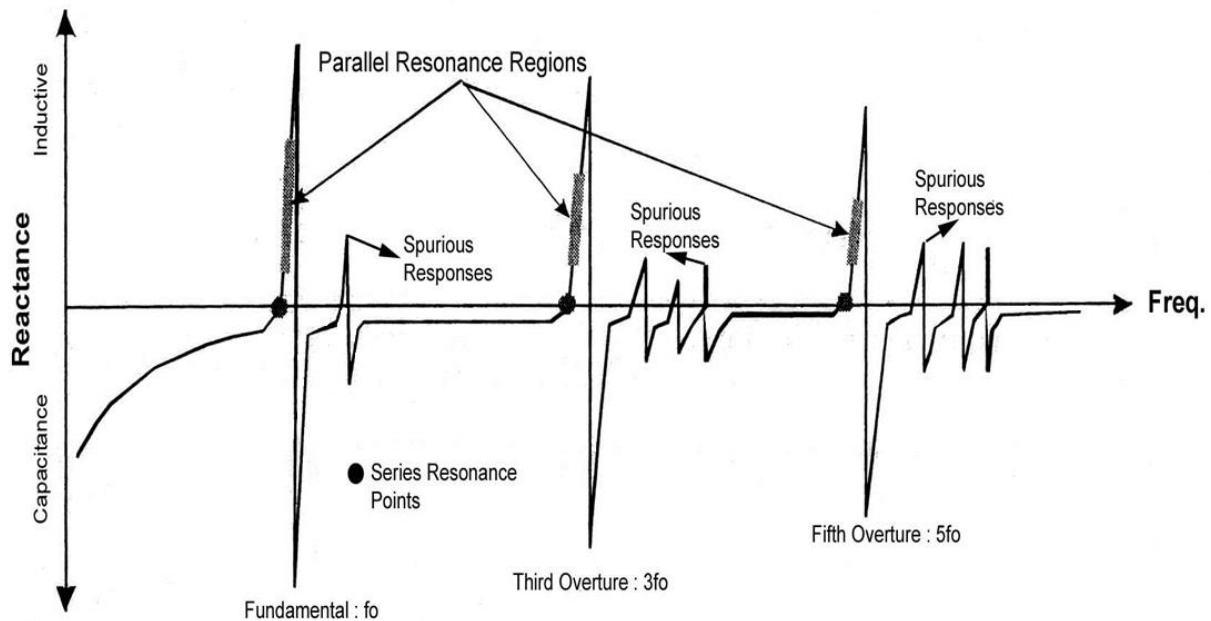


Figure 3-3: Reactance characteristics of electro-mechanical crystal resonator [30]

Figure 3-4 shows the maximum series resistance of quartz crystals over a frequency range of 1 kHz-200 MHz. These data are taken from several specifications, so more than one limit is shown at some frequencies. A typical crystal will have about two-thirds the maximum resistance specified in Fig. 3-4. This wide variation in series resistance from 10Ω to $200,000\Omega$, R is the largest single factor in oscillator design and dominates the design of every oscillator circuit [7].

Figure 3-5 shows the maximum drive power that can be put into a crystal without excessive heating and frequency shift in the crystal. Figure 3-6 shows the maximum permissible drive voltage across the crystal *at exact series resonance*. Figure 3-6 is derived from the series resistance and maximum power data given in Fig. 3-4 and Fig. 3-5. Figures 3-4-to-3-6 apply to crystals of all common types of cuts mounted in a gas-filled container. Note that in Fig. 3-6 the maximum crystal voltage falls off rapidly above 1 MHz. This maximum voltage curve is a useful design tool [7][10][11][19].

Since crystals frequently operate slightly off resonance, measuring the voltage across the crystal is meaningless as a measure of current through the crystal. The practical solution is to measure the current through the crystal by means of the voltage drop across a series element and calculate the crystal's power dissipation by I^2R , where 'I' is the current through the crystal and R is the crystal's internal series resistance; ($1/2(I^2)R = \text{RMS power}$). At frequencies above about 2 MHz, the AC voltage swing from an oscillator circuit operating from a 5 V power supply can be higher than what should be put across the crystal at series resonance. An amplitude-limiting scheme is frequently needed to take care of this problem [7][10][19][31].

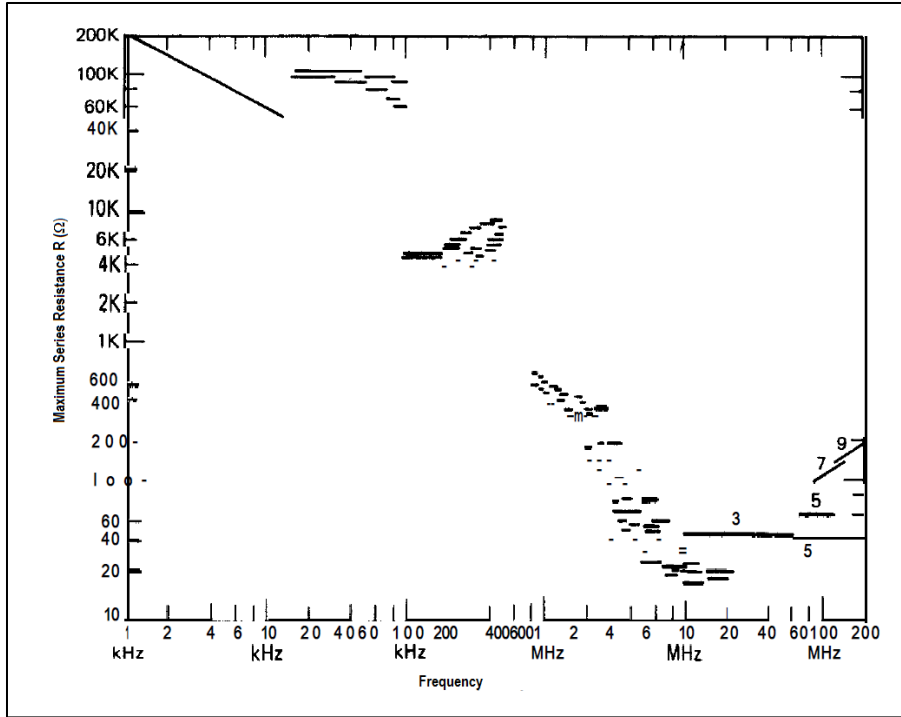


Figure 3-4: Maximum crystal series resistance R , as a function of frequency [7]

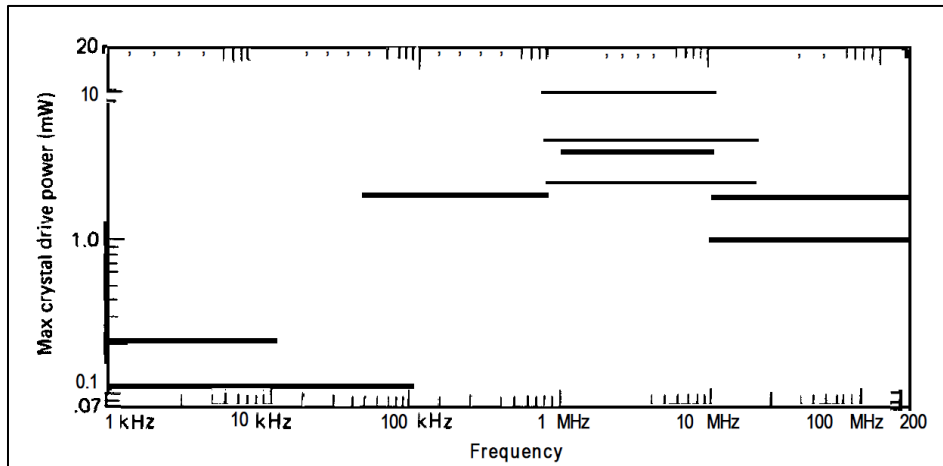


Figure 3-5: Maximum crystal power dissipation as a function of frequency [7]

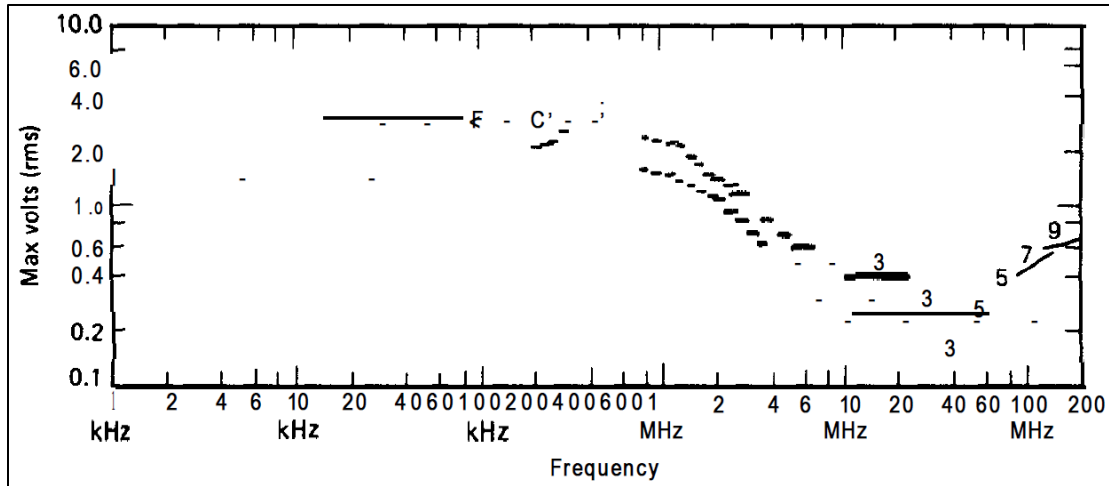


Figure 3-6: Maximum crystal-drive voltage at series resonance as a function of frequency [7]

The package capacitances and lead inductance are generally ignored till the VHF frequencies. The equivalent circuit for crystal shows two resonances, one due to the series branch alone and the other with the inductor L in combination with the effective capacitance of C_0 and $C_1 \dots C_n$. These resonances termed as the series resonant frequency and the anti-resonant frequency of the crystal and are computed as

$$f_s = \frac{1}{2\pi\sqrt{L_1 C_1}}$$

$$f_p = \frac{1}{2\pi\sqrt{L_1 \left(\frac{C_1 C_0}{C_1 + C_0} \right)}}$$
(3-1)

where f_s is series resonant frequency and f_p is the anti-resonant frequency [10].

When an oscillator presents some amount of load capacitance to a crystal, the crystal is said to be parallel resonant, and a value of load capacitance, C_L , must be specified. If the circuit does not exhibit capacitive loading, the crystal is said to be series-resonant, and no value of load capacitance is specified. It is important to note that when a capacitor is placed in series with a crystal, the new series frequency is displaced slightly to a higher frequency than the original series resonance. Conversely, when the capacitor is placed in parallel with the resonator, the new parallel resonant frequency is displaced slightly to a lower frequency. This phenomenon has caused a great deal of perplexity between the terms series and parallel resonance. Figure 3-7 shows the crystal resonances with and without the effects of load capacitance, C_L [10].

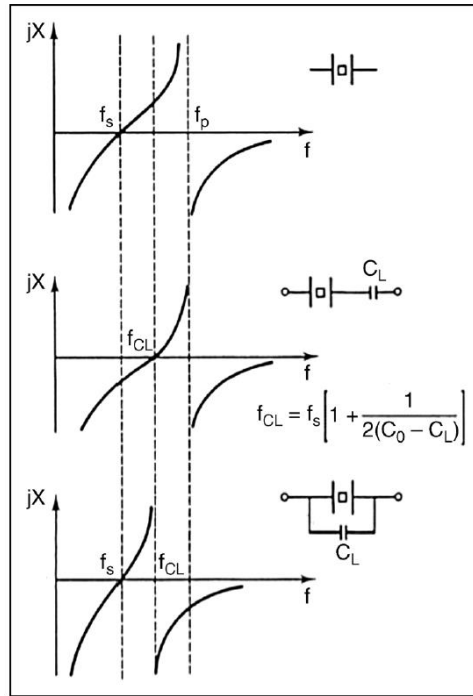


Figure 3-7: Crystal resonances with and without the effects of load capacitance, CL [10]

Series mode resonance of the crystal is represented by a small resistance in series with a resonant reactance, whereas, in parallel mode by a large resistor in parallel to a resonant susceptance. The series (f_s) and parallel resonance (f_p) are described by the impedance function [10][31],

$$Z(s) = \frac{1}{sC_0 + \frac{1}{1/sC_i + sL_i + R_i}} = \frac{s^2 + sR_i/L_i + 1/L_iC_i}{sC_0[s^2 + sR_i/L_i + (C_0 + C_i)/L_iC_0C_i]} \tag{3-2}$$

The further evaluation from the imaginary part of the zeroes

$$s_{z1,2} = -\frac{\omega_0}{2Q} \pm j\omega_0 \sqrt{1 - \frac{1}{4Q^2}} \approx -\frac{\omega_0}{2Q} \pm j\omega_0, \quad \text{for } Q \gg 1 \tag{3-3a}$$

and poles as below,

$$s_{p1,2} = -\frac{\omega_0}{2Q} \pm j\omega_0 \sqrt{1 + \frac{C_i}{C_0} - \frac{1}{4Q^2}} \approx -\frac{\omega_0}{2Q} \pm j\omega_0 \left(1 + \frac{C_i}{2C_0}\right) \tag{3.3b}$$

$$\omega_i = \frac{1}{\sqrt{L_iC_i}} \Rightarrow f_s(\text{series}) = \frac{1}{2\pi\sqrt{L_iC_i}} \quad (i = 1,3,5 \dots) \tag{3.3c}$$

$$\omega_p \approx \omega_0 \left(1 + \frac{C_i}{2C_0}\right) \Big|_{C_0 \gg C_i} \Rightarrow f_p(\text{parallel}) \approx \frac{1}{2\pi\sqrt{L_iC_i}} \left(1 + \frac{C_i}{2C_0}\right) \Big|_{C_0 \gg C_i} \tag{3.3d}$$

$$M = \frac{2Q(\omega_p - \omega_0)}{\omega_0} = \frac{2Q(f_p - f_0)}{f_0} \tag{3-4}$$

Where Q=quality factor, f_0 =resonant frequency

gives us M, which is the mode separation ($f_p - f_0$) equation. The degree to which an oscillator generates a constant frequency f_i throughout a specified period of time is defined as the frequency stability of the signal source. Some problems faced during the days of tube technology are now

easier to handle with the advent of transistor technology. The lower power supply voltage used in transistor circuits has reduced the crystal overdrive problem to more manageable proportions. And to get better frequency stability, oscillator circuits are now routinely designed with low power output, since it costs so little to add an amplifier stage [10][31].

3.6 Selection of Desired Resonant Modes and Mode Jumping

Crystal does not produce harmonics and the overtone response of crystal is not harmonics of fundamental. For designing the high performance crystal oscillator, the oscillator circuit topology determines the crystal configuration, like use of fundamental, overtone, parallel and the series configuration. In other words, the oscillator circuit topology forces the crystal resonator into either the fundamental (lowest major resonant response), overtone (major responses other than fundamental), parallel (one of the inductive regions of the crystal's reactance curve) or series mode (one of the resistive points on the crystal's reactance curve) of operation.

For overtones the equivalent circuit of crystal gets an additional branch in parallel with a combination of RLC. The values of R, L and C in the overtone branch can be computed by scaling the values of R, L and C in the fundamental resonant branch. If 'f₁' is the fundamental frequency then the nth overtone frequency should be computed as [10],

$$f_n = n * f_1 = \frac{1}{2\pi\sqrt{L_n C_n}} = \frac{n}{2\pi\sqrt{L_1 C_1}} = \frac{1}{2\pi\sqrt{L_1 \frac{C_1}{n^2}}}$$

$$\Rightarrow L_n = L_i$$

$$\Rightarrow C_n = \frac{C_1}{n^2}, \text{ where } n \text{ is } 3, 5, 7 \text{ etc. ... overtone number} \quad (3-5)$$

Wide pull Voltage controlled crystal oscillator (VCXO) typically utilizes fundamental crystals with large motional capacitance C₁. Overtone operation is precluded if wide tuning range is desired. Also the resistor for the overtone branch gets scaled as, R_n = R₁ × n² which implies that the negative resistance required to get oscillations on overtone is much larger than the value for fundamental mode. The fundamental frequency (lowest-mode) response is the most active due to lowest value of R_n. If a large negative resistance is provided for the fundamental resonance, it could result in exciting an overtone mode also. When crystal oscillators are designed for higher frequency, excitation is on its higher modes and care should be taken to suppress the unwanted fundamental resonance in such cases.

3.7 Behavior of Crystal over Temperature and Aging Factor

Another property of a crystal is aging and can be described as slow changes in the oscillation frequency with time. The various reasons for aging, particularly in quartz crystals are stresses in the mounting and electrodes that are relieved with time, excessive crystal drive power, out-gassing of materials in crystal support structure and electrodes, cleanliness of the resonator and slow leaks in the enclosure and oilcanning, where the enclosure is stressed by changes in atmospheric pressure outside the envelope. Negative aging is usually caused by enclosure leakage.

A typical aging curve is given in Fig 3-8 [35]. The curve marked 'A' also known as positive aging, ages upward in frequency in approximately logarithmic fashion and is more common. This may occur from the response to turn-off and subsequent restart. The cleaner crystal of curve B has a much reduced aging.

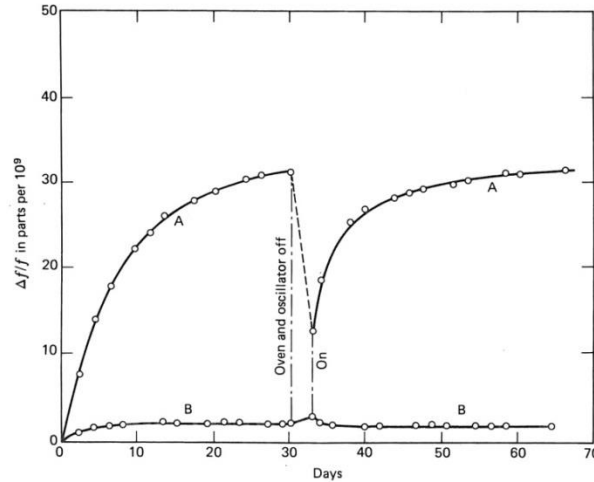


Figure 3-8: Frequency changes in precision quartz crystal units due to interruptions in oscillation and oven control. A: solder bonding and glass encapsulation. B: thermos-compression bonding and high-temperature processing [35]

Aging is also a function of drive level of the crystal unless contamination and stresses have been minimized by use of high-temperature high-vacuum bakeout and sealing and use of SC-cuts.

In high-volume production aging rates of less than 1 part in 10⁸ per day can be achieved; for high precision units the figure can be improved to 5 parts in 10¹¹ per day on a low-yield selective basis.

Apart from the spurious resonances, the cut of the quartz resonator changes the angle of the crystalline orientation that leads to change in crystals behavior over the temperature. The temperature behavior is modeled by a third order polynomial of the form

$$\frac{\Delta f}{f} = a(t - T_0) + b(t - T_0)^2 + c(t - T_0)^3 \tag{3-6}$$

where T₀ is the inflection temperature at which the change in frequency is minimum [19][35].

General examples of frequency changes over temperature are referred to as F-T behavior observed in the range of -50°C to +125°C.

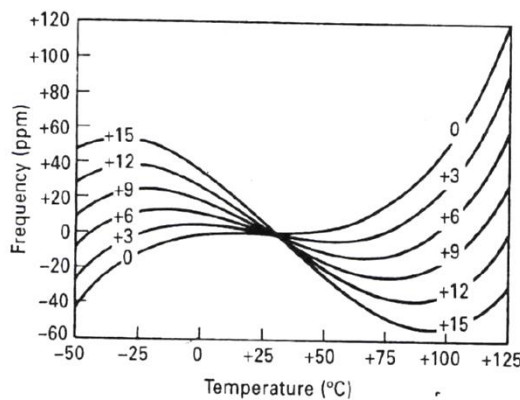


Figure 3-9: F-T curve for AT cut resonators [19]

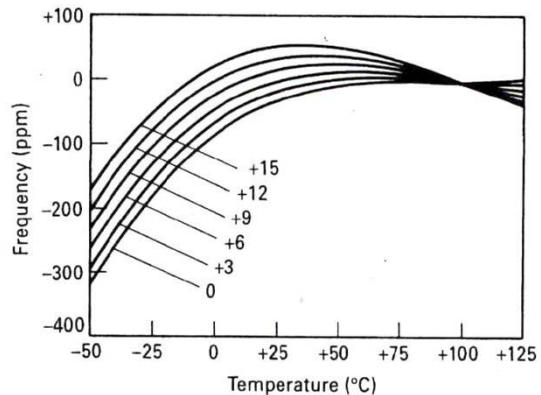


Figure 3-10: F-T curve for SC cut resonators [19]

Figure 3-9 and Figure 3-10 show the frequency response of AT and SC cuts to a thermal transient due to oven warmup. Thermal gradients in AT produce a dramatic overshoot and a long approach

to steady state; the thermally compensated SC approaches final frequency in a time, dictated solely by the oven parameters. Changes in the quartz are usually negligible for most applications [35].

The frequency variations in AT cut resonator are dependent on temperature as well as the thermal gradient of temperature across the crystals surface, whereas the SC cut is immune to the thermal gradients.

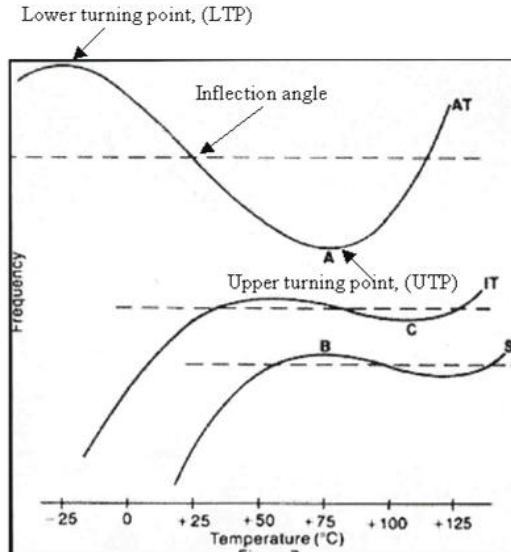


Figure 3-11: F-T curves for AT cut, SC cut, IT cut resonators showing UTP, LTP and inflection angle [10]

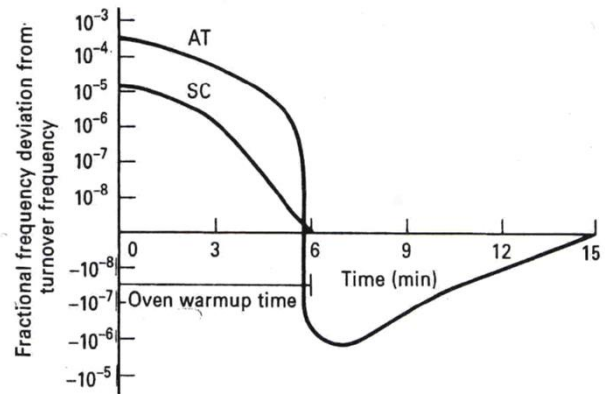


Figure 3-12: Typical warm-up for AT and SC cut oven oscillators [19]

Figure 3-11 shows the difference of the temperature characteristics for different crystal oscillators and the classification of crystal oscillators based on the compensation techniques. Figure 3-11 also shows the FT behavior where the crystals upper and lower turning points along with the inflection angle are seen. To minimize the frequency changes resulting from temperature the oven of the OCXO is adjusted to the turning point of the crystal.

In an SC cut and IT cut resonators the change in frequency is more towards the cold end but tend to flatten out as the temperature approaches the inflection angle as shown in Figure 3-12. This makes them very suitable for Oven controlled oscillators where the temperature of the oven is set to the turn temperature. The AT cut on other hand has inflection angle around 270c, and that makes it suitable for TCXO application. Note: an AT cut crystal of 9 minutes, shows frequency change of about ± 30 ppm and inflection angle at 27°c while an SC cut crystal of 9 minutes, shows the inflection angle around +1000c with the changes in frequency from -225ppm to +50ppm.

The typical warm-up time for AT and SC cut oven oscillators is shown in Figure 3-12. Since SC cut is nearly insensitive to the thermal gradients that invariably occur during oven warm-up, it is expected that SC cut resonators will give much faster warm-up in ovenized oscillators. The packaging and the control circuitry play a critical role in warm-up time of ovenized crystal oscillator [10][11][19][35].

3.8 Environmental Effects (Excluding static temperature effects)

Figure 3-13 shows an idealized curve of frequency versus time for a crystal resonator subjected to a variety of environmental disturbances. A thermal transient occurs at t_1 : mechanical accelerations in the forms of vibration, shock, and tuning the crystal over in a gravitational field (tip-over) occur between t_2 and t_1 . At t_5 the oscillator is turned off, causing another thermal transient, and at t_6 it is

turned back on again. Superimposed on these disturbances is the long term aging slope. If the curve is sufficiently magnified, it will be found to contain noisy fluctuations about the mean frequency.

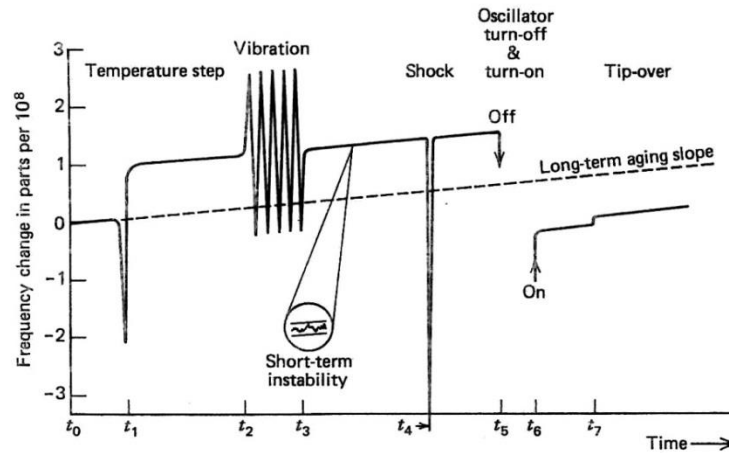


Figure 3-13: Idealized frequency-time behavior of a quartz oscillator [35]

The greatest contributors to frequency change are thermal transients, accelerations, cessation and reestablishment of vibration, and long-term aging [35].

3.9 Thermal Transients:

The f - T curves in Section 3.7 assumed slow temperature variations. If $dT/dt=T$ is sufficiently large to produce thermal gradients across the resonator, then it is found that the f - T curve must be modified to read

$$\frac{\Delta f}{f} = a_0 \Delta T + a_1 \Delta T^2 + c_0 \Delta T^3 + (\bar{a} \Delta T + \dot{a}) \dot{T} \quad (3-7)$$

Where $\Delta T = \Delta T(t) = T(t) - T_0$

In the above equation, \bar{a} and \dot{a} depend upon material constants of quartz as well as the resonator design. For tests involving a ramp function of temperature, the \bar{a} coefficient has the effect of changing the apparent angle of orientation of the resonators: that is, it rotates the S-shaped cubic curve. The \bar{a} coefficient translates the cubic curve up or down in frequency. If and when an abrupt temperature change is encountered, as with oven turn-on, AT-cuts will behave as seen in Fig 3-12, producing an overshoot and slow approach to equilibrium. SC cuts on the other hand experience no such transients and simply follow the static f - T curve irrespective of \dot{T} .

The consequences of this difference in behavior are striking when one has to adjust the oven of a high precision unit to the turnover (zero-slope) point of the f - T curve. Even minute changes in temperature will send the AT-cut oscillator's frequency far from where the static curve would predict, and many oven time constants have to be waited for the frequency to settle finally at the static point. Creeping up on the turn-over temperature in this manner is exceedingly time-consuming and costly.

Moreover, when the oven has been set at its reference point it can only maintain the temperature within a finite range. If this range is used then the $\Delta f/f$ so predicted will be found to be many times smaller than that observed. The \bar{a} and \dot{a} terms can cause substantial frequency departures in high-precision AT oscillators.

In SC-cut resonators the effect is nearly absent, and the "setting the oven temperature to the turn-over point" is a simple rapid procedure. [35]

3.10 Thermal-Frequency Hysteresis

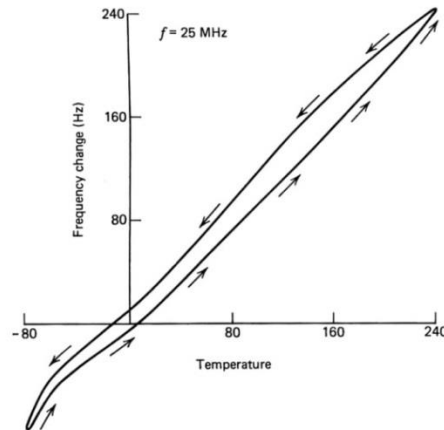


Figure 3-14: Thermal hysteresis in quartz resonators. Cycling over wide temperature extremes produces hysteretic behavior that approaches a semi-reproducible loop after a number of repetitions; changing the temperature excursions modifies the loop [35]

Figure 3-14 gives an example of thermal hysteresis when cycling a quartz resonator over an extended temperature range. The effect is a function of the temperature range; its causes are poorly understood. It should be bore in mind that the effect varies from unit to unit and is very difficult to model for the purpose of compensation by microprocessor programming. [35]

3.11 Acceleration Effects

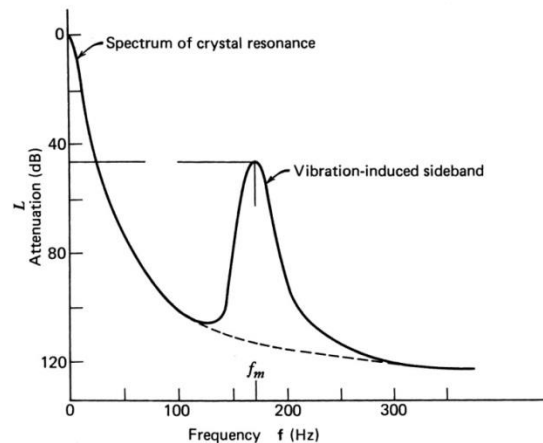


Figure 3-15: Crystal resonance spectrum showing vibration-induced sideband at modulation frequency f_m . Sideband level, refereed to the crystal resonance, is a measure of the crystal's acceleration sensitivity [35]

Shock, vibration, and change in attitude (tip-over) are acceleration effects. For a given design and direction of applied acceleration, the frequency shift is proportional to the acceleration \bar{a} :

$$\frac{\Delta f}{f} = \bar{a}\gamma \quad (3-8)$$

\bar{a} is expressed in g units and γ is the acceleration sensitivity coefficient. Values for γ normally run, "a few parts in 10^9 per...", for the AT-cut. Recent work has led to units with γ values in the 10^{-10} range, but with relatively labor-intense methods. Figure 3-15 shows a typical crystal resonance spectrum showing vibration-induced sideband at modulation frequency f_m .

If a resonator operating at its resonance frequency is subjected to a sinusoidal vibration at frequency f_m , where $f_m \ll f_R$, then sidebands will be produced at the carrier frequency $\pm f_m$. A measurement of the sideband level L in dB normalized to the carrier level, determines γ from

$$\gamma = \left(\frac{2f_m}{af} \right) \times 10^{L/20} \quad (3-9)$$

3.12 The Polarization Effect

A dc voltage impressed on the electrodes of an AT-cut will produce a very small frequency shift; for an SC-cut the effect is considerably larger and may be utilized for compensation purposes. Expressed in terms of a constant \bar{e} , we obtain

$$\frac{\Delta f}{f} = \bar{e}E \quad (3-10)$$

E is the vacuum electric field strength. For AT-cuts, $\bar{e} = 0.04$ and for SC-cuts $\bar{e} = 2.3$; the units of e are 10^{-9} mm/V, and of E are V/mm. If 10 V dc is applied to a typical 5 MHz fundamental SC-cut, the normalized frequency shift is approximately 6×10^{-8} . In some circuits static electricity can accumulate across the crystal terminals, leading to a frequency shift caused by the polarization effect. If this charge fluctuates with time, an added contribution to noise will then be present. By shunting the crystal by a high resistance, this influence can be overcome [35].

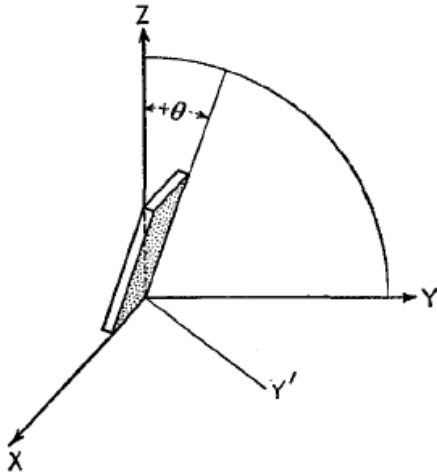


Figure 3-16: Diagram showing how crystal plane is rotated about the X axis to obtain the AT cut [35]

3.13 Crystal Cuts

The crystal resonator is obtained from the abundant natural resource of quartz. The quartz stone gets cut into thin slices called “blank”, which are coated with metallic films that form the leads for exciting the crystal. The quartz is cut in various ways either in single rotation or double rotation, which results in significant change in the operating parameters mainly the operational frequency stability. The commonly used blanks are formed from AT cut and SC cut quartz.

The cut of the quartz also results in additional resonances, specifically in SC and IT cut crystals. These additional resonances termed as b-mode are located at

approximately 10% higher in frequency from the desired c-mode. Apart from b-mode we also get the a-mode resonance at 188/100 times the c-mode [35].

Although there are many crystal cuts, the AT-cut crystal is extensively used at high frequencies (1 MHz and above)

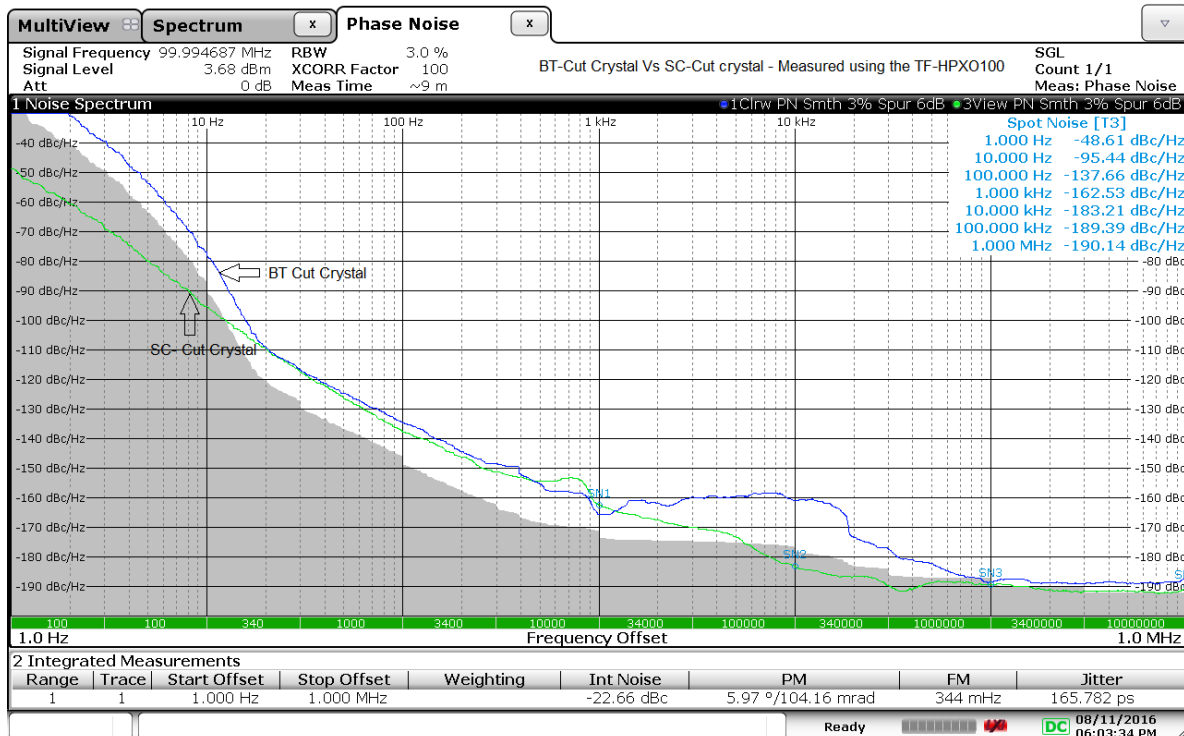
ranging from about 500 kHz upward to about 10 MHz. The AT-cut crystal is a thin piece of quartz with two parallel or slightly convex surfaces, usually about the size of a nickel or less. This type of plate is cut from a plane that is rotated about an X axis so that the angle θ made with the Z axis, as indicated in Fig. 3-16, is approximately 35.5° . When voltage is applied across the flat sides of such a plate, the AT crystal moves sideways internally in a thickness shear vibrations, causing displacements [29]. Electrical connections are made to the crystal by metallizing the two parallel faces on opposite sides of the crystal. The crystal’s resonant frequency is inversely proportional to the crystal’s thickness between these two metallized surfaces.

$$\text{Frequency (kHz) for AT cut} = \frac{1,675}{\text{thickness, mm}} \quad (3-11)$$

Today most of the high-precision crystals use the Stress Compensated (SC) cut [35].

- **Advantages of the SC-cut [34]**
 - Thermal transient compensated (allows faster warmup OCXO)
 - Static and dynamic f vs. T allow higher stability OCXO and MCXO
 - Better f vs. T repeatability allows higher stability OCXO and MCXO
 - Far fewer activity dips
 - Lower drive level sensitivity
 - Planar stress compensated; lower Δf due to edge forces and bending
 - Lower sensitivity to radiation
 - Higher capacitance ratio (less Δf for oscillator reactance changes)
 - Higher Q for fundamental mode resonators of similar geometry
 - Less sensitive to plate geometry - can use wide range of contours
- **Disadvantage of the SC-cut :** More difficult to manufacture for OCXO (but is easier to manufacture for MCXO than is an AT-cut for precision TCXO)
- **Other Significant Differences**
 - B-mode is excited in the SC-cut, although not necessarily in LFR's
 - The SC-cut is sensitive to electric fields (which can be used for compensation)

Figure 3-17 shows two 100 MHz crystals with different cuts, the BT and the SC that was measured on R&S FSWP as a part of this research study. The grey area shows the possible measurement limit of the equipment during the measurement of the BT-cut crystal. The plot of the SC-cut measurement was then overlaid for comparison of the two measurements, and can be a little misleading as it does not show the grey portion for the measurement of the SC-cut crystal.



Date: 11.AUG.2016 18:03:34

Figure 3-17: Shows the measured phase noise of SC-cut and BT-cut 100 MHz crystal oscillator

The measurement shows that the SC-cut has a better phase noise performance especially at close-in offset frequencies, relative to the BT-cut crystal. The spot noise table shown on the top right corner in the figure is for the SC-cut measurement.

3.14 B-mode trapping:

The b-mode has a linear temperature characteristic and can be used as a sensitive thermometer of the resonator temperature. This effect has been used to design extremely stable microcomputer-compensated oscillators, where the frequency of b-mode is used to compensate the fundamental mode and oscillations are present on both modes at all times. However more typically it's required the crystal is operated only on a single mode. A resonant circuit must then be employed to trap out the b-mode and force the oscillations to occur on the desired mode at all times. This is b-mode trapping. Depending upon the circuit configuration, several different methods can be employed. This can be accomplished in Colpitts and Pierce oscillator by forcing one of the capacitive elements to be inductive at the frequency of unwanted mode.

As shown below in the schematic of Figure 3-18a, the inductors L2 and capacitor C2 are series resonant at frequency just below the b-mode. This means that they appear inductive at the b-mode frequency, thus they serve as b-mode trap.

The net impedance of this circuit is shown in Figure 3-18b.

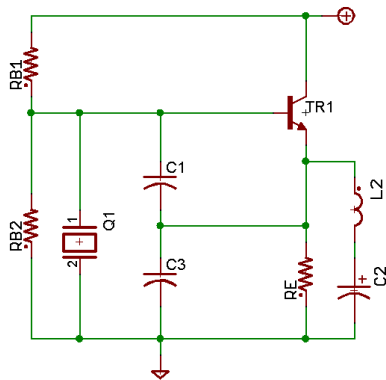


Figure 3-18a: The b-mode trap schematic in a Colpitts oscillator [10]

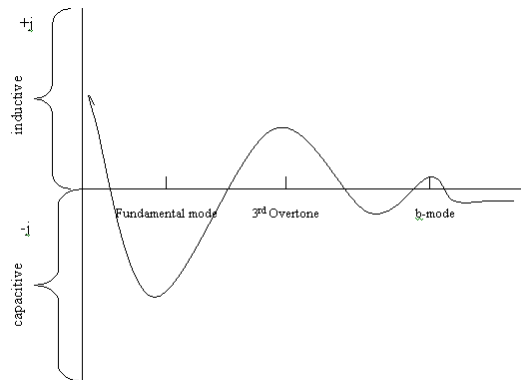


Figure 3-18b: The net impedance for the b-mode trap implementation [10]

It can be very convenient to measure thermal performance of an oven using the b-mode. By returning the resonant circuit to force oscillations to occur on the b-mode, the linear frequency verses temperature characteristics can provide a means to precisely measure the performance of the thermal enclosure.

To accomplish this, the frequency variations caused by temperature changes of the b-mode are first measured with the oven off. This step provides a means of characterizing the frequency-temperature characteristics of the b-mode. Next, the frequency changes caused by external temperature variations are computed from this. Of course, the trap can then be re-tuned to set the oscillation back to the desired mode [10][11].

3.15 What is Q and Why is it Important?

The Figure of Merit, Q, can be defined in different ways for a crystal oscillator.

Energy storage definition:

$$Q \equiv 2\pi \frac{\text{Energy stored during a cycle}}{\text{Energy dissipated during a cycle}} \quad (3-12)$$

Q factor is 2π times the ratio of the stored energy to the energy dissipated per oscillation cycle, or equivalently the ratio of the stored energy to the energy dissipated per radian of the oscillation. For a microwave or optical resonator, one oscillation cycle is understood as corresponding to the field oscillation period, not the round-trip period [34].

A major reason for the wide use of crystal oscillators is their high Q factor. A typical Q value for a quartz oscillator ranges from $10E4$ to $10E6$, compared to perhaps $10E2$ for an LC oscillator, 500 for a helix resonator. The maximum Q for a high stability quartz oscillator can be estimated as $Q = 1.3 \times 10E7/f$, where f is the resonance frequency in megahertz. As an example, a 5 MHz 3rd overtone crystal has a Q of $2.6E6$, the product of both is $5E6 \times 2.6E6 = 1.3 \times 10E7$ MHz. So at 100 MHz, the Q is 130,000. This is consistent with the published literature.

Factors that Determine Resonator Q

The maximum Q at “normal” temperatures can be expressed as: $Q_{max} = \frac{1}{2\pi f \tau}$

where f is the frequency in Hz, and τ is an empirically determined “motional time constant” in seconds, which varies with the angles of cut and the mode of vibration. For example, $\tau = 1 \times 10^{-14}$ s for the AT-cut's c-mode ($Q_{max} = 3.2$ million at 5 MHz), $\tau = 9.9 \times 10^{-15}$ s for the SC-cut's c-mode, and $\tau = 4.9 \times 10^{-15}$ s for the BT-cut's b-mode. ($Q > 10^9$ can be achieved at cryogenic temperatures.)

Other factors which affect the Q of a resonator include:

- Overtone
- Blank geometry (contour, dimensional ratios)
- Surface finish
- Material impurities and defects
- Drive level
- Mounting stresses
- Gases inside the enclosure (pressure, type of gas)
- Bonding stresses
- Interfering modes
- Temperature
- Ionizing radiation
- Electrode geometry and type

The motional time constant $\tau = R_1 C_1$ ($= 10^{-14}$ s for an AT-cut) is related to the internal friction, i.e., to the attenuation of an acoustic wave as the wave travels in a resonator. It is independent of frequency [34].

3.16 Drive level Effects:

The apparent resistance of a resonator is often found to be a function of the crystal current I_x . The effect is sketched in Figure 3-19. The motional capacitance C_1 may also vary with drive, but its variation is much less than that of R_1 [35].

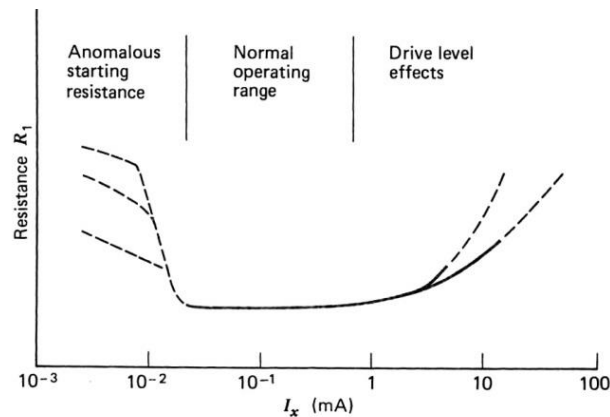


Figure 3-19: Shows the schematic representation of the variation of resonator motional resistance with crystal current. At very low values anomalously high resistances are sometimes encountered; at high drive levels nonlinear effects increase the resistance [35]

3.16.1 Second Level of Drive [35]:

At low drive levels, the resistance R_1 of many crystals increases appreciably, and very often abruptly. Examples are given in Figs. 3-20a and 3.20b. In Fig. 3-20a as the voltage across the crystal is increased from 0 to B, the current remains zero. It rises abruptly to point C, where its value is consistent with the rated R_1 . Further increases in V_x produce no change in R_1 , nor do decreases until point E is reached when I_x again falls to zero. The hysteresis-like effect is called second level of drive [35]. In some resonator units the behavior shown in Fig. 3-20b is encountered where the curve shows a continuous increase in R_1 with decrease in V_x from point D to point A, and no crystal activity for V_x values below this.

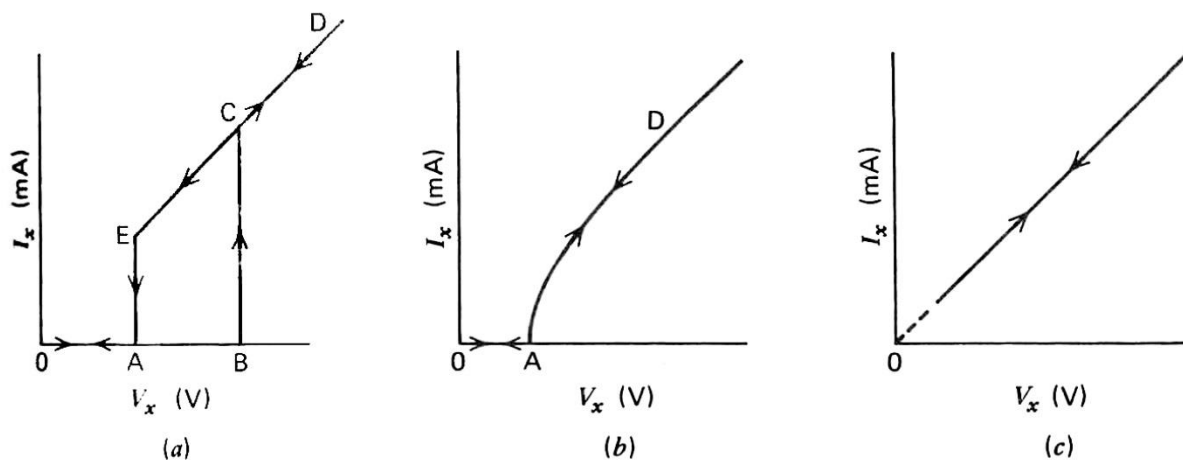


Figure 3-20: (a) Anomalous starting resistance occurring as abrupt transitions leading to a hysteresis loop (b) Nonlinear starting resistance occurring as a single-valued function of crystal voltage V_x (c) Normal linear resistance extending down to very low values of V_x [35]

This effect is almost exclusively due to the surface preparation of the resonator. It becomes apparent at current densities below about $10\mu\text{A}/\text{mm}^2$, which for units in HC-6 and HC-18 enclosures, and for frequencies in the 1-30 MHz range, works out to mA currents and μW power levels.

It is obvious that the presence of this effect can produce serious starting and operating effects in the oscillator. Furthermore the effect can be insidious and not show up in tests on a newly made resonator, only to appear after a period of storage.

Production of units without this defect requires attention to surface cleanliness. Maintaining the resonator surface free from contaminating particles of lapping and polishing compound and use of chemical etching to remove microcracks effectively removes the phenomenon and results in units with the characteristics shown in Fig. 3-20c. The effect is thought to be much less severe with SC-cuts than that with AT. It may be dealt with in the specification of the unit [35].

3.17 Amplitude Frequency Effect [35]

As drive level is increased the crystal resonance curve becomes a multiple-valued function of frequency. Figure 3-21 (a) shows the amplitude-frequency effect. At higher levels of drive, the resonance curve ceases to be symmetric and bends to one side as shown in Fig 3-21(b).

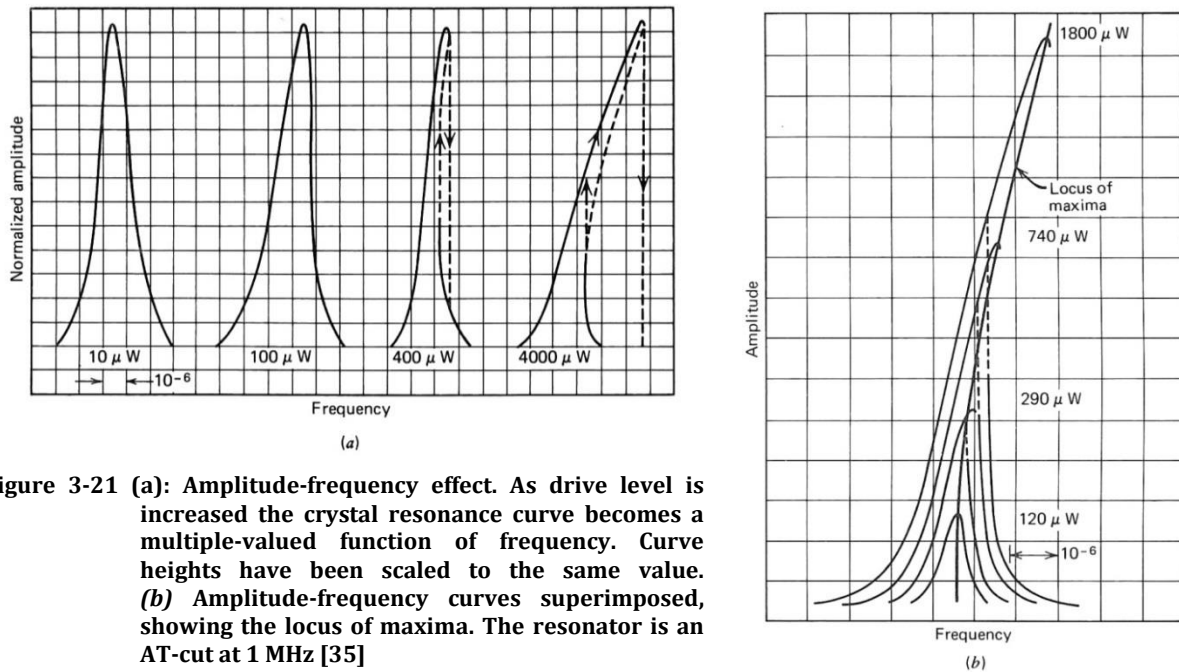


Figure 3-21 (a): Amplitude-frequency effect. As drive level is increased the crystal resonance curve becomes a multiple-valued function of frequency. Curve heights have been scaled to the same value. (b) Amplitude-frequency curves superimposed, showing the locus of maxima. The resonator is an AT-cut at 1 MHz [35]

The AT-cut behaves as a hard spring and bends toward higher frequencies; the BT-cut acts like a soft spring and bends toward lower frequencies. The locus of the maxima of the resonances is given by

$$\frac{\Delta f}{f} = a I_x^2 \quad (3-13)$$

For conventional AT designs at 5 and 100 MHz, 'a' is approximately 0.20 to 0.25/A². Values of a between 0.02/A² and 0.05/A² have been reported, for doubly rotated cuts, with ϕ angles in the range $\pm 2^\circ$ of the SC-cut, at both third and fifth overtones. With planoconvex designs, a decreases with decreasing curvature and is smallest in flat plates. The effect depends upon geometrical design, material, overtone, and mode of motion. The lowest a value measured to date on a BAW resonator is 0.004/A² on a third overtone, doubly rotated plate having $\phi = 20^\circ$. ST-cut SAW devices have even lower values; a value of $a = 0.0011/A^2$ at 110 MHz has been measured.

The amplitude-frequency effect is more correctly characterized by use of current density rather than I_x in Eq. (3-13); when put on this basis the effect becomes perceptible at densities of roughly 50 $\mu A/mm^2$ for AT-cuts. Since in most designs, electrode area decreases with increasing frequency,

keeping I_x constant for units of increasing frequency, would mean increasing the current density. In order to keep the maximum frequency change $\Delta f/f$ constant, I_x should therefore decrease in higher-frequency units [35].

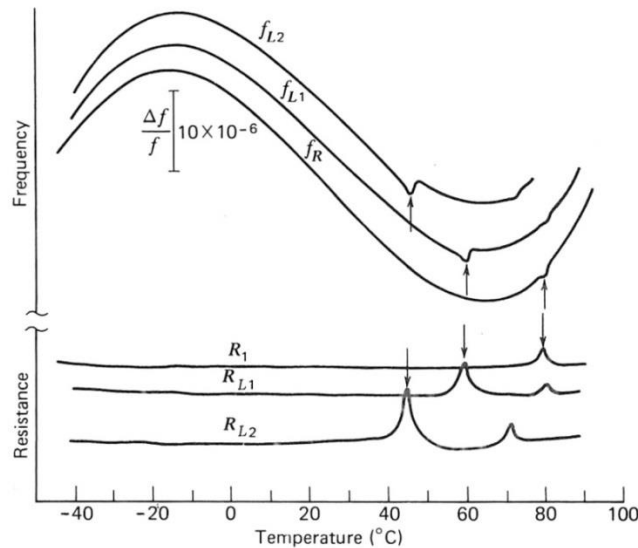


Figure 3-22: Activity dips in the frequency-temperature plots of an AT-cut when operated without and with load capacitors [35]

All curves have been vertically displaced for clarity.

Figure 3-22 shows that the activity dip temperature is a function of CL indicating that the dip is caused by coupling to a flexure mode with a large negative temperature coefficient [35].

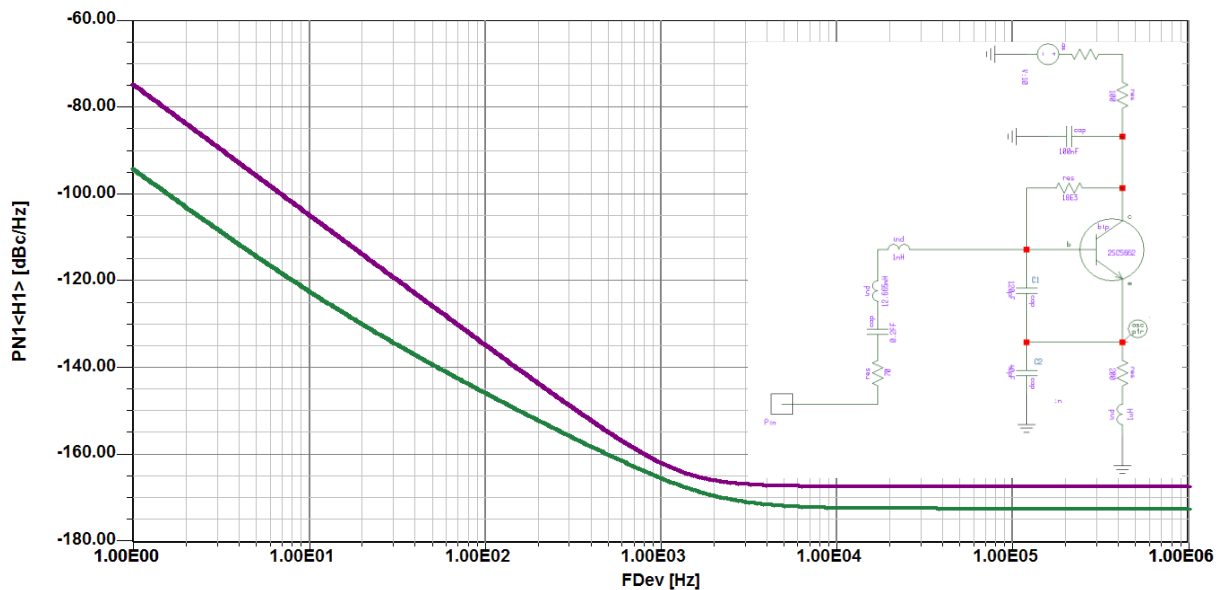


Figure 3-23: Phase noise simulation showing the effect of feedback vs. drive level adjusted by selecting $C1$ and $C2$ values

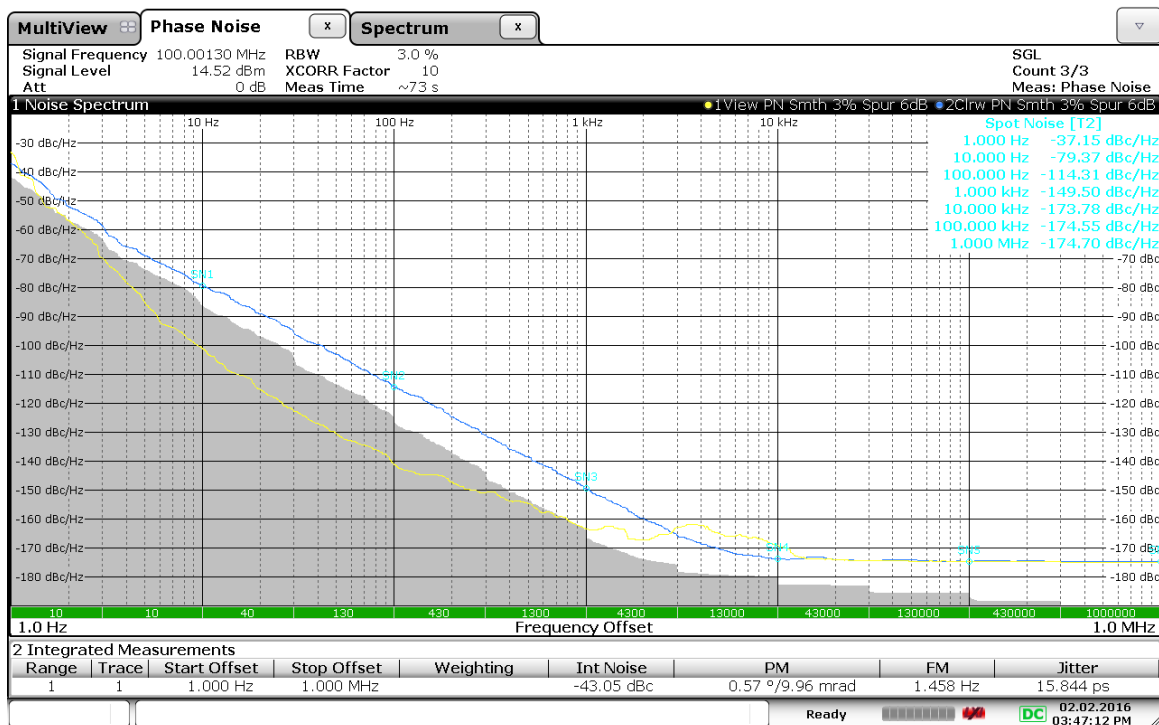
Crystal parameters: $f = 20$ MHz; $C_0 = 2.1$ pF; $R_1 = 3 \ \Omega$; $CL_1 = 35$ pF; $CL_2 = 22$ pF; $I_x = 2$ mA.

The CAD simulated phase noise of crystal oscillator circuit shown here using the equivalent circuit of the crystal, in Figure 3-23 shows the effect of feedback vs. drive level. It was observed that with

higher drive level, the phase noise at close-in improves while the far-off degrades. The opposite takes place with increased feedback. The crossover point is seen at about 5 MHz offset from the carrier. This shows that for optimized design the trade-off between feedback and drive-level has to be considered.

In designing the optimized crystal oscillator circuits, many crystal resonators were considered, operating about the same frequency and quality factor, and observed negligible difference in phase noise. The possible reason for this is that these crystal resonators were pre-selected by the manufacturer.

For validation, CROVEN [39] was requested to supply some crystals which did not meet the selection criteria for a good phase noise. The blue trace shown in the Figure 3-24 shows the measured result of a crystal oscillator using this crystal resonator. The yellow trace superimposed for comparison purposes, is a measured result of another crystal resonator from CROVEN [39] which met the selection criteria. The gray area shows the limit of the dynamic range for the measurement, in this case the measurement of the reject quality crystal. The R&S FSUP was used to carry out this measurement task.



Date: 2.FEB.2016 15:47:12

Figure 3-24: Two different crystal resonators – in same oscillator circuit give different performance

The manufacturers have not been able to identify the reason for such different phase noise results, with crystals with the same equivalent electrical parameters. There is just a certain yield.

3.18 Conclusion:

This chapter gives the necessary information about the crystal resonator which is helpful while making the selection and understanding the behavior of the circuit while using the selected crystal resonators. The physics of quartz crystal is vast and beyond the scope of this work. Nevertheless, an attempt to present the significance and limitations due to various parameters is made using published datasheets, and carried out CAD simulation and measured results.

Chapter 4: Semiconductors Components

This chapter briefly discusses the semiconductors; specifically diodes and transistors, as the selection of these devices in a crystal oscillator design is important and requires some specifications of these devices be considered carefully.

4.1 Diodes:

The following Figure 4-1 shows part of the datasheet of a popular low noise Infineon diode BB555, for a VHF Crystal oscillator application considered for the validation.

Electrical Characteristics at $T_A = 25^\circ\text{C}$, unless otherwise specified					
Parameter	Symbol	Values			Unit
		min.	typ.	max.	
DC Characteristics					
Reverse current $V_R = 30\text{ V}$ $V_R = 30\text{ V}, T_A = 85^\circ\text{C}$	I_R	- -	- -	10 200	nA
AC Characteristics					
Diode capacitance $V_R = 1\text{ V}, f = 1\text{ MHz}$ $V_R = 2\text{ V}, f = 1\text{ MHz}$ $V_R = 25\text{ V}, f = 1\text{ MHz}$ $V_R = 28\text{ V}, f = 1\text{ MHz}$	C_T	17.5 14.01 2.05 1.9	18.7 15 2.24 2.1	20 16.1 2.4 2.3	pF
Capacitance ratio $V_R = 1\text{ V}, V_R = 28\text{ V}, f = 1\text{ MHz}$	C_{T1}/C_{T28}	8.2	8.9	9.8	-
Capacitance ratio $V_R = 2\text{ V}, V_R = 25\text{ V}, f = 1\text{ MHz}$	C_{T2}/C_{T25}	6	6.7	7.5	-
Capacitance matching ¹⁾ $V_R = 1\text{ V to } 28\text{ V}, f = 1\text{ MHz}, 7\text{ diodes sequence, BB535}$ $V_R = 1\text{ V to } 28\text{ V}, f = 1\text{ MHz}, 4\text{ diodes sequence, BB555/-02V}$ $V_R = 1\text{ V to } 28\text{ V}, f = 1\text{ MHz}, 7\text{ diodes sequence, BB555/-02V}$	$\Delta C_T/C_T$	- - -	- 0.15 0.25	2.5 1 2	%
Series resistance $V_R = 3\text{ V}, f = 470\text{ MHz}$	r_S	-	0.58	0.75	Ω
Series inductance	L_S	-	0.6	-	nH

¹For details please refer to Application Note 047

Figure 4-1: Part of the datasheet of Infineon diode BB555 [123]

4.2 AM-to-PM Conversion from tuning diodes operated in reverse bias:

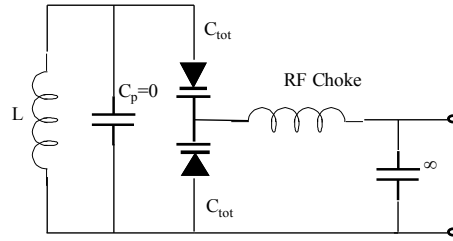


Figure 4-2: Parallel tuned circuit with tuning diodes [20]

Figure 4-2 shows a parallel tuned circuit which is connected to the oscillator. The frequency change is obtained by applying a positive voltage to the + terminal. The parallel capacitor is replaced by the two tuning diodes. Here we will show the influence of the tuning diodes in the voltage-controlled oscillators, the resulting phase noise generated by tuning diodes shown in Figure 4-4.

It is possible to define an equivalent noise R_{aeq} that, inserted in Nyquist's Johnson noise equation,

$$V_n = \sqrt{4kT_0RB} \tag{4-1}$$

where $kT_0=4.2 \times 10^{-21}$ at about 300 K, R is the equivalent noise resistor, and B is the bandwidth, determines an open-circuit noise voltage across the tuning diode. Practical values of R_{aeq} for carefully selected tuning diodes are in the vicinity of 200 Ω to 200 k Ω (high source resistance). If we now determine the noise voltage, $V_n = \sqrt{4 \times 4.2 \times 10^{-21} \times 100000}$ the resulting voltage value is $4 \times 10^{-8}V\sqrt{Hz}$. The 100K value is derived from a typical source resistance driving the tuning diode in the crystal oscillator circuit. (This noise voltage generated from the tuning diode is now multiplied with the VCO gain K_o , resulting in the rms frequency deviation [20].

The typical tuning voltage gain is 50 Hz/V.

AXIOM75ULN-21 Rev.: 3.1 Date: 2012-12-13

Oscillator type: Ultra-Low Phase Noise OCXO

Frequency adjustment range					
Electronic Frequency Control (EFC)	± 2.2	± 2.5		ppm	ref. to nominal frequency
EFC voltage V_c	0		VREF	V	
EFC slope ($\Delta f / \Delta V_c$)	positive				
EFC input impedance	100			k Ω	
Modulation bandwidth	10			kHz	

Figure 4-3: Part of the datasheet of AXTAL AXIOM75ULN-21- Section for Frequency adjustment range [124]

$$(\Delta f_{rms}) = K_o \times (4 \times 10^{-8}V) \text{ in } 1 \text{ Hz bandwidth} \tag{4-2}$$

To translate this into an equivalent peak phase deviation,

$$\theta_d = \frac{K_o\sqrt{2}}{f_m} (4 \times 10^{-8}) \text{ rad in } 1\text{Hz bandwidth} \tag{4-3}$$

or for a typical crystal oscillator gain of 50 Hz/V,

$$\theta_d = \frac{9.164E-7}{f_m} \text{ rad in } 1\text{Hz bandwidth} \tag{4-4}$$

For $f_m = 100$ Hz (typical number of interest for crystal oscillator at 100 Hz offset) for adjacent-channel measurements for FM mobile radios), the $\theta_d = 9.165E-9$. This can be converted now into the SSB signal-to-noise ratio:

$$20 \log\left(\frac{\theta}{2}\right) = -166.8 \qquad Lf(m) = -166.8\text{dBc/Hz} \tag{4-5}$$

The crystal oscillator datasheet at a 100 Hz offset claims -135dBc/Hz. It means that the tuning diode has essentially no influence on the phase noise if this equation holds true.

Another critical number is 10 kHz. At 10 kHz offset the tuning diode contribution is even less, calculated to be approximately -207dBc/Hz.

Unfortunately some diodes for reasons not quite understood are much noisier. The following picture shows the influence of different tuning diodes (part numbers in the simulation results in Figure 4-4 are not known, the results were received in a personal email communication for showing how different tuning diodes exhibit different phase noise), the noisy ones should be avoided.

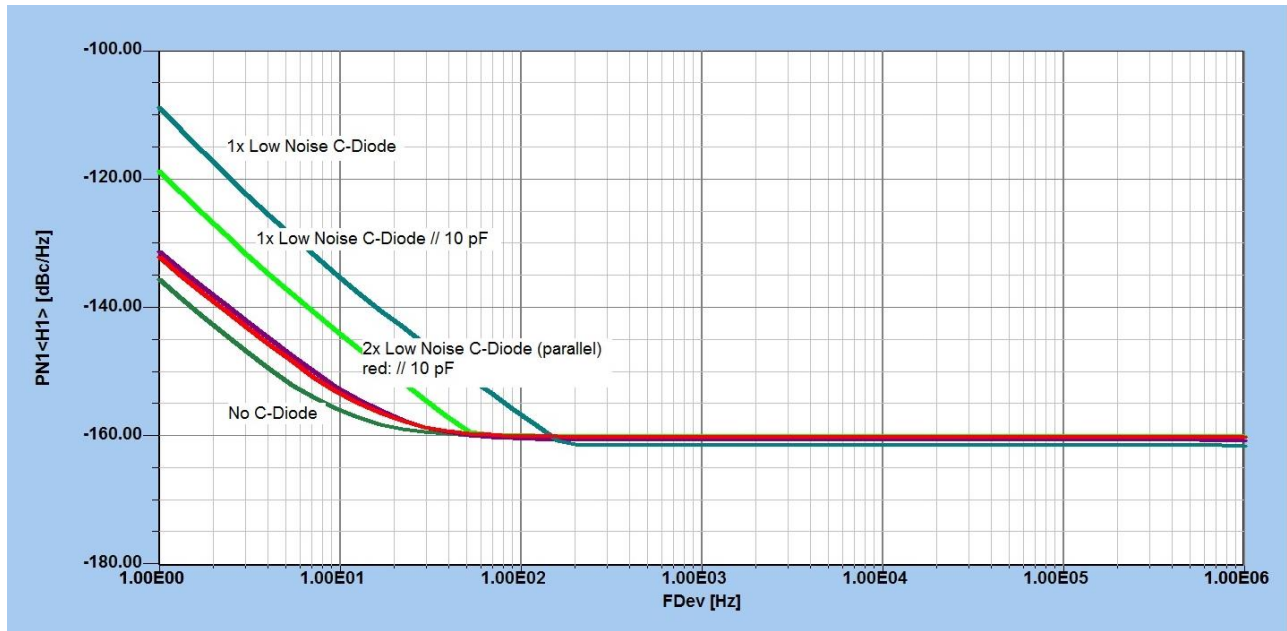


Figure 4-4: CAD Simulation showing influence on phase noise due to different tuning diodes [Courtesy AXTAL, www.axtal.com]

Figure 4-5 shows typical phase noise measurements for a 10 MHz crystal oscillator. Such information can be helpful while selecting the right semiconductor devices for the given frequency of operation.

Typical Phase Noise in dBc/Hz	At offset frequency
-115	@ 1 Hz ($1/f^3$ noise)
-146	@ 10 Hz ($1/f$ noise)
-157	@ 100 Hz (AM Noise)
-160	@ ≥ 1 kHz (Noise Floor)

Figure 4-5: Typical Phase Noise for 10 MHz Crystal oscillator [20]

4.3 Diode Noise Model in forward bias [41, pp-323]:

The noise model for the diodes (Figure 4-6) consists of two contributions: the shot noise and the flicker noise. The shot noise is computed automatically and does not require any parameters. The flicker noise can be specified in two ways:

1. Using the enhanced SPICE noise model by specifying Kf, Af, and FCP in the model\ parameter list (this option is usually sufficient for most applications).

2. Using bias-dependent flicker noise coefficients (specifying Kf and Af at multiple bias points).

Table 4-1: Diode Noise Model Keywords

Keyword	Description	Unit	Default
ID	Required bias current for the data point	Ampere	
Kf	Flicker noise coefficient		0.0
Af	Bias exponent of the flicker noise model		1.0
FCP	Frequency exponent of the flicker noise model		1.0
FC	Flicker noise corner frequency	Hz	

The noise generators in the diode noise model are the series parasitic resistance, R_s , and the intrinsic junction. The figure below illustrates the intrinsic junction noise generator. Let Δf be the bandwidth (usually normalized to 1 Hz). The intrinsic noise generator has a mean-square value of:

$$\langle i_{Dn}^2 \rangle = 2qI_D\Delta f + KF \frac{I_D^{AF}}{f^{FCP}} \Delta f \quad (4-6)$$

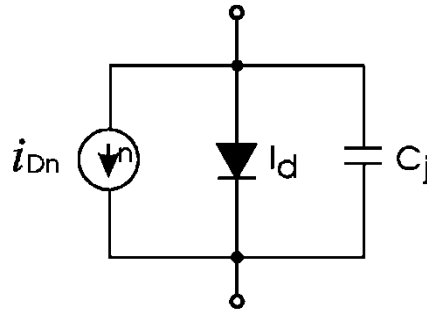


Figure 4-6: Equivalent noise circuit for a diode chip [41]

4.4 Notes on the Diode Noise Model [41]:

1. Shot noise (SN) is always present unless the SN parameter is set to zero. While running a CAD simulation, turning noise off is useful for comparing the total circuit noise that is generated by the nonlinear devices and that generated by the linear circuit components.
2. If the value of Kf (Flicker noise coefficient) is specified as zero, then the flicker noise will not be contributed by the device and only shot noise is considered in the intrinsic model.
3. The corner frequency noise model uses the system noise floor to internally compute the flicker noise coefficient, Kf. The system noise floor is computed by the program using the diode parameters and kT .
4. This noise model of course considers the actual operating temperature, which must be supplied to the model. ([20]-Ch-2)

4.5 Transistors:

Transistors are mostly specified using their small signal equivalent Gummel-Poon model [40]. The Infineon BFP196W NPN Silicon RF transistor offers low noise and low distortions for the

applications up to 1.5 GHz at collector current from 20mA to 80 mA, and is recommended for use [125].

For readers, some relevant parts of the datasheet of this transistor are shown in Figure 4-7(a), (b) and (c).

- For low noise, low distortion broadband amplifiers operate in telecommunications systems up to 1.5 GHz at collector currents from 20 mA to 89 mA
- $f_T = 7.5$ GHz
- $F = 1.5$ dB at 900 MHz

Electrical Characteristics at $T_A = 25^\circ\text{C}$, unless otherwise specified.

Parameter	Symbol	Values			Unit
		min.	typ.	max.	
AC characteristics (verified by random sampling)					
Transition frequency $I_C = 70$ mA, $V_{CE} = 8$ V, $f = 500$ MHz	f_T	5	7.5	-	GHz
Collector-base capacitance $V_{CB} = 10$ V, $f = 1$ MHz	C_{cb}	-	1	1.4	pF
Collector-emitter capacitance $V_{CE} = 10$ V, $f = 1$ MHz	C_{ce}	-	0.36	-	
Emitter-base capacitance $V_{EB} = 0.5$ V, $f = 1$ MHz	C_{eb}	-	3.7	-	
Noise figure $I_C = 20$ mA, $V_{CE} = 8$ V, $Z_S = Z_{Sopt}$, $f = 900$ MHz $f = 1.8$ GHz	F	-	1.5 2.5	-	dB
Power gain, maximum available ¹⁾ $I_C = 50$ mA, $V_{CE} = 8$ V, $Z_S = Z_{Sopt}$, $Z_L = Z_{Lopt}$, $f = 900$ MHz $f = 1.8$ GHz	G_{ma}	-	17.5 11.5	-	
Transducer gain $I_C = 50$ mA, $V_{CE} = 8$ V, $Z_S = Z_L = 50\Omega$, $f = 900$ MHz $f = 1.8$ GHz	$ S_{21e} ^2$	-	12.5 6.5	-	

Figure 4-7(a): Part of Infineon BFP196W NPN Silicon RF transistor datasheet showing Electrical Characteristics [126]

SPICE Parameters (Gummel-Poon Model, Berkley-SPICE 2G.6 Syntax) :

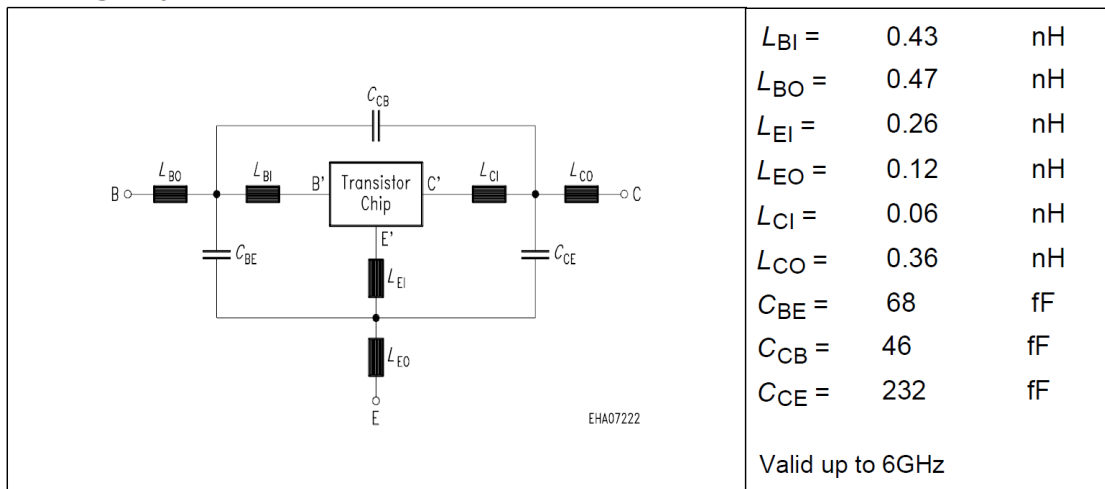
Transistor Chip Data

IS =	1.7264	fA	BF =	125	-	NF =	0.80012	-
VAF =	20	V	IKF =	0.4294	A	ISE =	119.22	fA
NE =	1.1766	-	BR =	10.584	-	NR =	0.94288	-
VAR =	3.8128	V	IKR =	0.019511	A	ISC =	4.8666	fA
NC =	0.88299	-	RB =	1.2907	Ω	IRB =	0.084011	mA
RBM =	1	Ω	RE =	0.75103	Ω	RC =	0.27137	Ω
CJE =	13.325	fF	VJE =	0.7308	V	MJE =	0.33018	-
TF =	23.994	ps	XTF =	0.44322	-	VTF =	0.1	V
ITF =	1.9775	mA	PTF =	0	deg	CJC =	1667	fF
VJC =	0.73057	V	MJC =	0.3289	-	XCJC =	0.29998	-
TR =	2.2413	ns	CJS =	0	fF	VJS =	0.75	V
MJS =	0	-	XTB =	0	-	EG =	1.11	eV
XTI =	3	-	FC =	0.50922	-	TNOM	300	K

All parameters are ready to use, no scaling is necessary.
 Extracted on behalf of Infineon Technologies AG by:
 Institut für Mobil-und Satellitentechnik (IMST)

Figure 4-7(b): Part of Infineon BFP196W NPN Silicon RF transistor datasheet showing Transistor chip data Spice parameters [127]

Package Equivalent Circuit:



For examples and ready to use parameters please contact your local Infineon Technologies distributor or sales office to obtain a Infineon Technologies CD-ROM or see Internet: <http://www.infineon.com/products/discrete/index.htm>

Figure 4-7(c): Part of Infineon BFP196W NPN Silicon RF transistor datasheet showing package equivalent circuit [127]

4.6 BJT Noise Model ([41] pg 326-328)

The noise model for the Gummel-Poon BJT model consists of two contributions: shot noise and the flicker noise. The shot noise is computed automatically and does not require any parameters. The flicker noise can be specified in two ways:

1. Using the enhanced SPICE noise model by specifying Kf, Af, and FCP in the model parameter list (this option is usually sufficient for most applications).
2. Using bias-dependent flicker noise coefficients (specifying Kf and Af at multiple bias points).

Option 1: Specifying the Bias-Independent Flicker Noise Coefficient. This option involves the straightforward specification of Kf, Af, and FCP that are constant with bias, as in the SPICE noise model. Notes on Option 1: The Noise model used in the Harmonic Balance Program follows the syntax of 2G SPICE but has some corrective changes (Pucell/Rohde) and therefore is more accurate.

1. Shot noise is always present unless it is turned off. While running CAD simulation, turning noise off is useful for comparing the total circuit noise that is generated by the nonlinear devices and that generated by the linear circuit components.

2. If the value of Kf is specified as zero, flicker noise will not be contributed by the device and only shot noise is considered in the intrinsic model.

Option 2: Specifying the Bias-Dependent Flicker Noise Coefficient or Flicker Corner Frequency

Option 2 allows a bias-dependent flicker noise coefficient (that is, Kf and Af vary with the bias point).

Table 4-2: BJT Noise Model Keywords [41]

keyword	description	unit	default
IB	Required base bias current for the data point	ampere	
VCE	Required collector-emitter voltage for the data point	volt	
VBS	Base-substrate voltage required for LPNP type when four nodes are used.	volt	
VCS	Collector-substrate voltage required for NPN or PNP type when four nodes are used.	volt-	
Kf	Flicker noise coefficient		0.0
Af	Bias exponent of the flicker noise model		1.0
FCP	Frequency exponent of the flicker noise model		1.0
FC	Flicker noise corner frequency	Hz	

4.7 Notes on the BJT Noise Model:

1. Kf, Af, and FC can be specified as bias dependent. If only one set of noise data is specified, the corresponding bias point is not meaningful because all parameters are considered constant over all bias values. However, the bias point is needed for the program to identify the data as bipolar noise data.

2. The corner frequency noise model option uses the system noise floor to compute the flicker noise coefficient, K_f . The system noise floor is computed by the program using the transistor parameters and kT .

3. This noise model of course considers the actual operating temperature, which must be supplied to the model.

Figure 4-8 shows the BJT noise model. Let Δf be the bandwidth (usually normalized to a 1 Hz bandwidth). The noise generators introduced in the intrinsic device are shown below, and have mean-square values of:

$$\langle i_{bn}^2 \rangle = 2qI_D\Delta f + KF \frac{I_B^{AF}}{f^{FCP}} \Delta f \tag{4-7}$$

$$\langle i_{cn}^2 \rangle = 2qI_C\Delta f \tag{4-8}$$

$$\langle i_{R_{bb}}^2 \rangle = \frac{4kT}{R_{bb}} \Delta f \tag{4-9}$$

$$\langle i_{R_{e1}}^2 \rangle = \frac{4kT}{R_{e1}} \Delta f \tag{4-10}$$

$$\langle i_{R_{c2}}^2 \rangle = \frac{4kT}{R_{c2}} \Delta f \tag{4-11}$$

$$\langle I_B \rangle = \frac{I_{BF}}{BF} + I_{le} \tag{4-12}$$

$$I_C = I_{cf} - I_{cr} \tag{4-13}$$

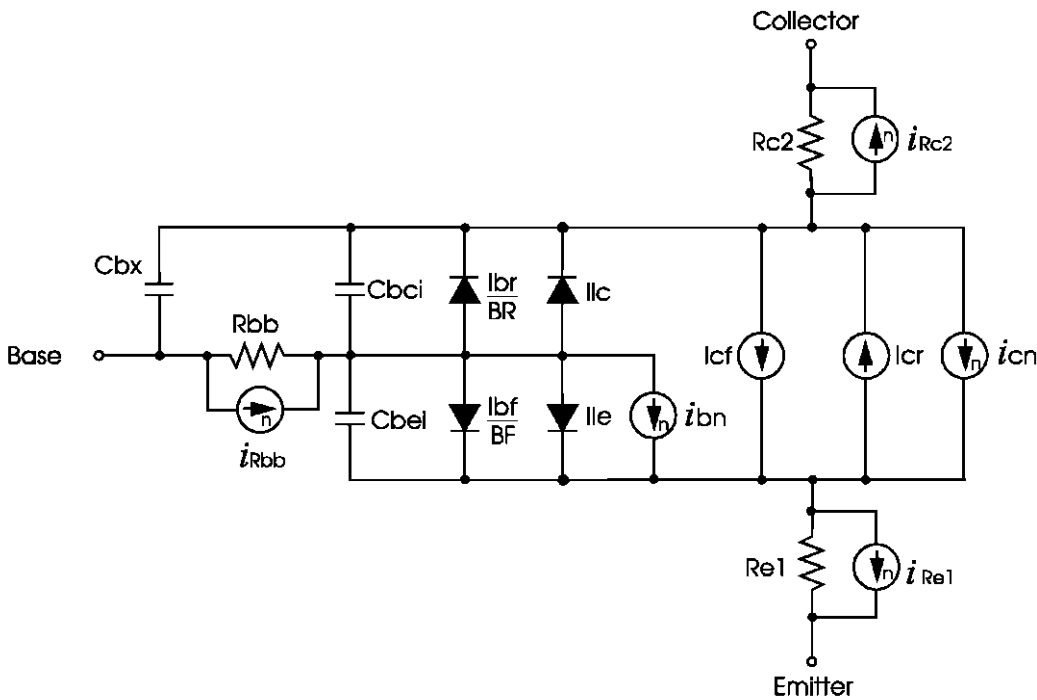


Figure 4-8: BJT noise model (not showing extrinsic parasitics). Current sources with n are noise sources [41]

For the purpose of this dissertation the Ansoft Serenade 7.2 is used.

Interesting enough, based on the diffusion profile of the transistors, not all noise equations are equal. The noise equation above (4-7), uses A_f and K_f factors which are based on DC measurements. The literature is most unspecific what A_f and K_f factor should be used under large signal conditions.

As seen for the diodes, transistors also behave different than expected. The general rule is the higher the f_T , the worse is the phase noise.

The influence of the tuning diode (similar to flicker noise) on the phase noise is shown below:

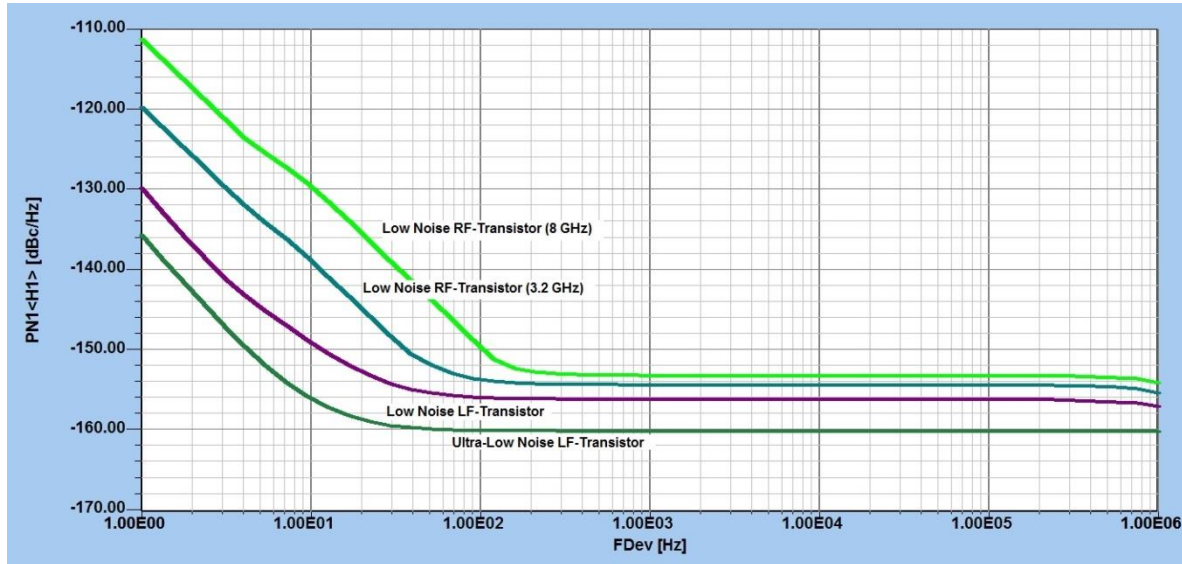


Figure 4-9: A typical CAD Simulated Phase noise plots showing influence of different transistor types (different f_T , operating frequency 100 MHz OCXO, [courtesy AXTAL, www.axtal.com])

4.8 Conclusion

This chapter gives a brief overview of the semiconductor devices and its selection in the design of a crystal oscillator. Various noise models are explained in brief and simulation results of phase noise of different devices is shown.

Chapter 5: Crystal Oscillators

Many of today's electronics circuits need a reference or frequency standard, sometimes also called a clock generator. Any signal generator uses an internal oscillator, and either modulates its amplitude or frequency or a combination of both. Probably the largest application of oscillators is in cell phones. To generate the output frequency and for synchronization of data, a precise oscillator is necessary.

In this dissertation, theoretical basis, CAD simulation and a crystal oscillator circuit built for experimental validation are considered. The results of various CAD simulations that were carried out as part of this research work and the theory that was studied specific to crystal oscillators are presented and discussed in this chapter. The measurements are considered in the next chapter.

In addition, for the benefit of the readers and completeness, following is an early history in brief, of how crystal oscillators evolved [1]-[11].

5.1 Introduction:

Oscillators using electron tubes have been around for quite some time. Initially people tried to build an amplifier but it ended up being an oscillator because of unwanted feedback. Feedback can be caused by many things, though its detailed discussion would be out of the scope of this dissertation.

A nice and early explanation found on oscillators is given by Terman [1] which reads on pg. 480, section 6: A vacuum-tube oscillator is essentially a vacuum-tube amplifier arranged so that an exciting voltage of the proper magnitude and phase to produce the amplified output is obtained from this output. The tube in such an arrangement acts as an inverter that changes d-c plate power into a-c energy.

Figure 5-1 is a reproduction of the various oscillator circuits shown by Terman, considered relevant at the time. Figure 5-1a shows the schematic of a Hartley oscillator. If we exchange L and C it translates into the frequently used Colpitts oscillator as seen in Figure 5-1b. The Hartley Oscillator of Figure 5-1a and electron coupled oscillator of Figure 5-1f are essentially the same.

Terman [1] explains the tube oscillators as follows:

As illustrated in Figure 5-1, the frequency generated by a vacuum-tube oscillator adjusts itself to a value such that the voltage that the oscillations apply to the grid of the tube is of exactly the proper phase, to produce the oscillations that supply this grid-exciting voltage. This frequency approximates the resonant frequency of the tank circuit, but is also influenced by such factors as the voltages acting on the tube, the effective Q of the tank circuit, the harmonics generated, the resistance and reactance coupled into the tank circuit by the load, etc.

All these modifying factors tend to produce small phase shifts between the exciting voltage and the output voltage of the tube, and the oscillator must operate slightly off the resonant frequency of the tank circuit in order to introduce a compensating phase shift.

When there is more than one resonant circuit, as in the tuned-grid tuned-plate arrangement, the frequency tends to be controlled by the circuit in which the circulating reactive volt-amperes are greatest.

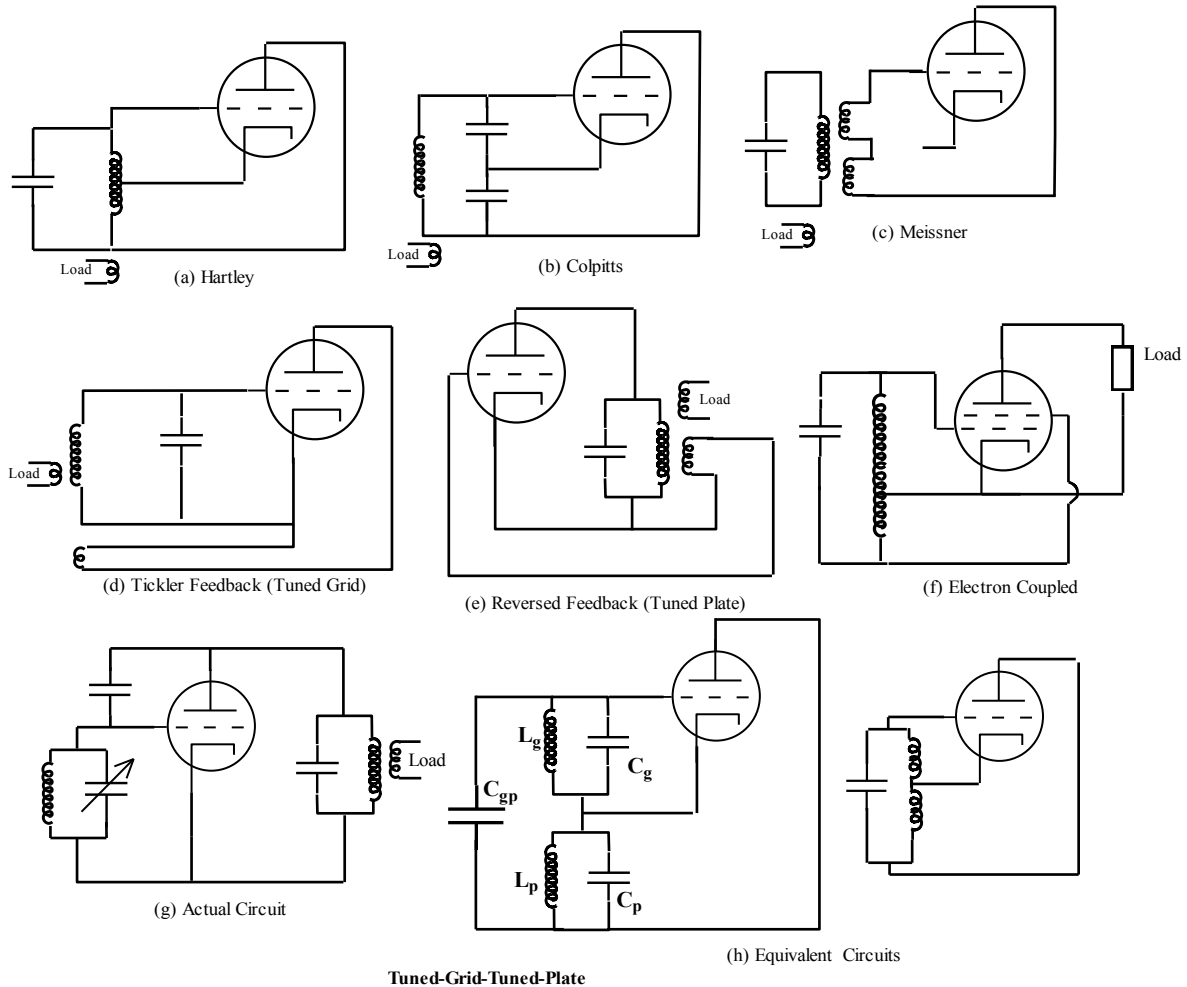


Figure 5-1: Schematic of common types of tube oscillator circuits [1]

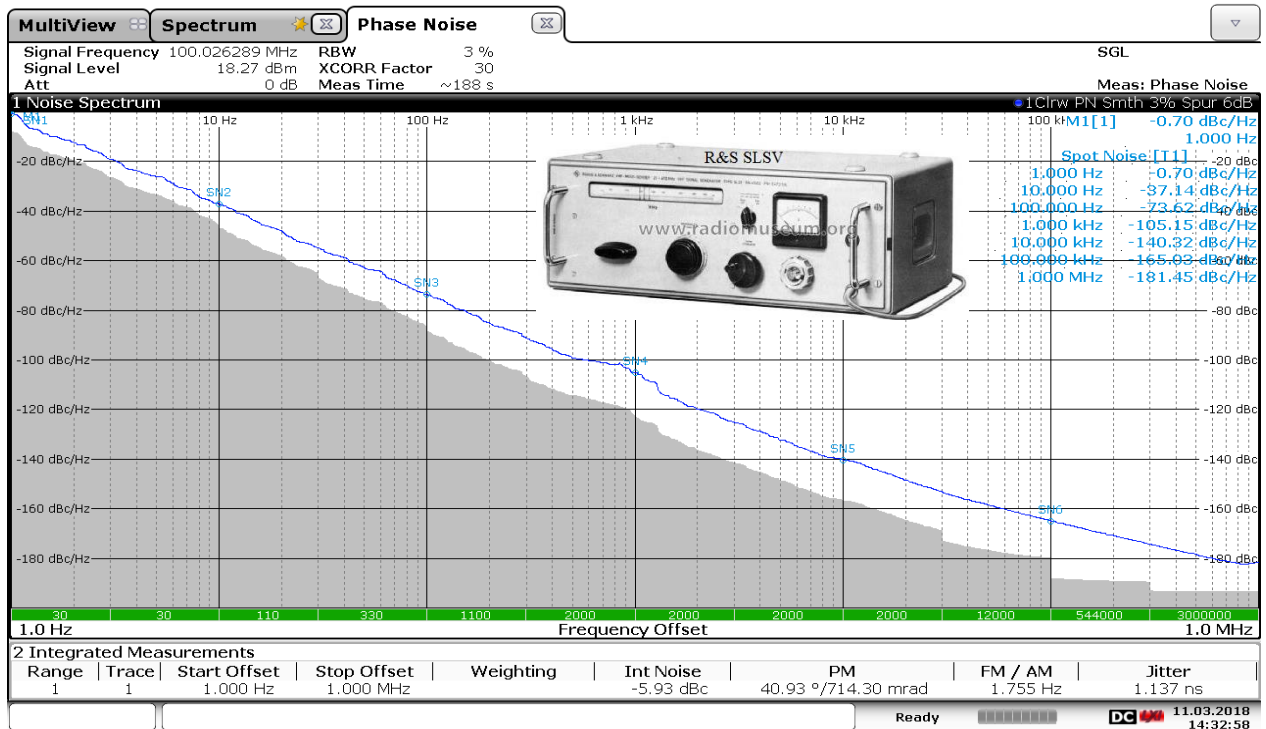
Besides the output power of an oscillator the frequency stability of an oscillator is a priority. This led to the development of crystal oscillators utilizing low noise power efficient semiconductor transistors.

Figure 5-2 shows the typical measured phase noise of a free-running 100 MHz tube LC-oscillator (R&S SLSV) with DC bias 220 Volt, output power is about +18 dBm, and far out noise floor is -182dBc/Hz. As shown in Figure 5-2, the close-in phase noise is -73.62dBc/Hz @ 100 Hz offset. The poor phase noise and high DC voltage operating condition limits the application in modern radio communication systems.

The evident drawbacks of the high DC voltage operating condition of the tube oscillator led to the invention of a semiconductor oscillator with reasonable compromise of reduced output power but improved FOM (Figure of Merit) [10]-[11].

Figure 5-3 shows the CAD simulated phase noise of a typical free-running FET based oscillator with a 2N4416 Siliconix transistor, for higher output power [43] exhibits a similar far-out noise floor but lower close-in phase noise with 5dBm reduced power; which is about 13dBm power output.

The pros are: less than the tube oscillator’s operating DC bias, typically 12 volt; tube oscillator operates at a much higher voltage, typically 250V. Multiple buffer stage high power low noise amplifier gain block can be used as alternative solutions!



14:32:59 11.03.2018

Figure 5-2: Typical measured phase noise of a free-running tube LC-oscillator [R&S SLSV] at about 100 MHz (18.27 dBm output power, operating DC bias 250 volts) [Courtesy Synergy Microwave]

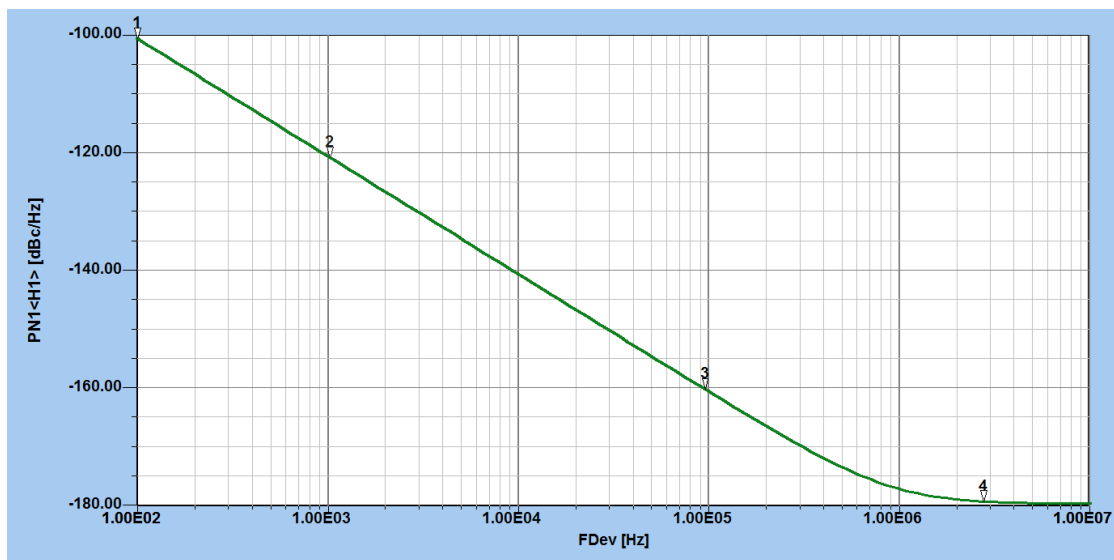


Figure 5-3: Simulated Phase Noise of a typical free-running 100 MHz FET based oscillator with a 2N4416 Siliconix transistor, 13.56 dBm output power, operating DC bias 12 volts [121][Courtesy Synergy Microwave Corporation]

5.2 Cady's Crystal Oscillator:

The crystal oscillator based on the Cady type oscillator circuit topology was already introduced in Chapter 1 (Figure 1-1). To translate this circuit in to a modern approach the circuit schematic is

redrawn by replacing the tube with a semiconductor bipolar transistor, and simulated using a harmonic balance based CAD circuit simulator. Figure 5-4 shows this modern day typical arrangement of Cady's circuit schematic.

Rizzoli et al [44] developed the CAD tool used here, that works on the principle of Harmonic Balance and can correctly simulate phase noise. A variety of validation publications then followed.

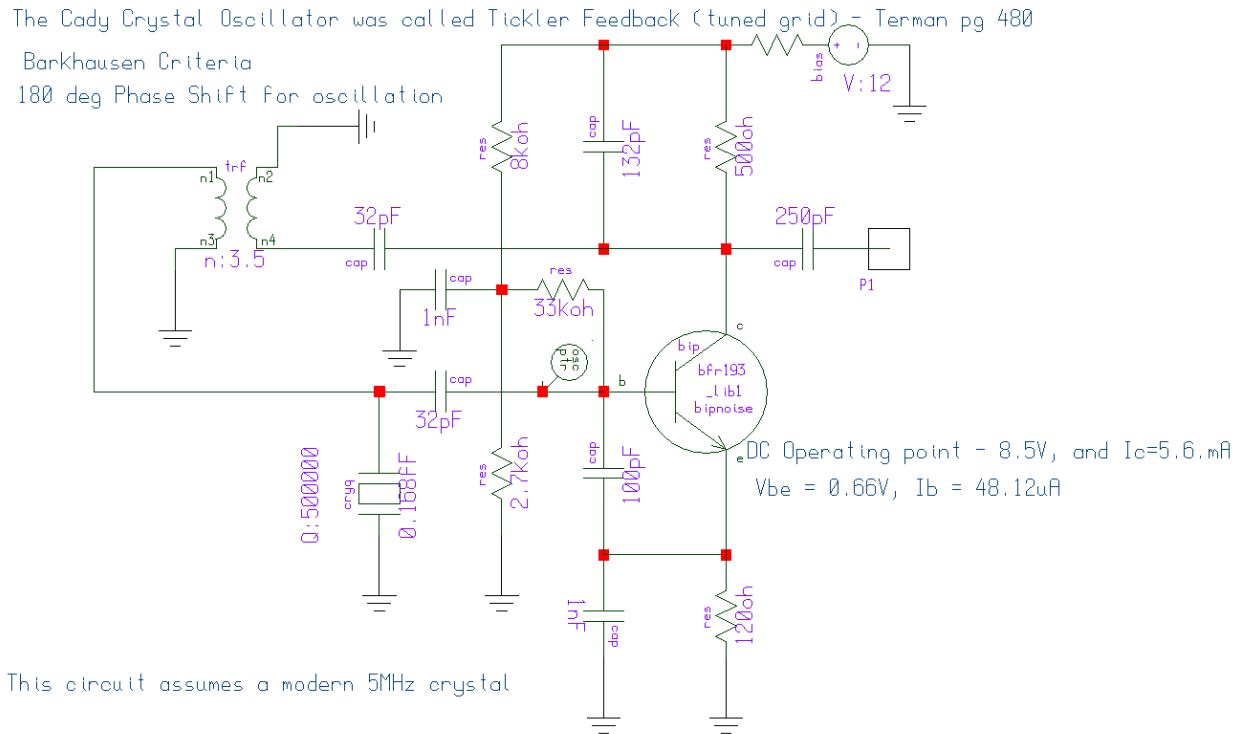


Figure 5-4- Simulation schematic of the Cady circuit

As illustrated in Figure 5-4, which can be considered a redrawn Colpitts oscillator, the emitter is at ground, and the feedback is achieved using a transformer. The turns ratio 'n' is 3.5; therefore the impedance ratio is $(n^2) = 12.25$.

The conventional old tubes had fairly large capacitance values, so the base-emitter capacitance of 100pF and the 32pF from collector to RF ground are practical values to deliver essential negative resistance to compensate the losses of the oscillator resonator tank [9, pp 402]. The fact that this oscillator works is not really surprising and unexpected; but the output power is full of harmonics as shown in Figure 5-5.

In this CAD simulation, a bipolar transistor biased at 6V and operating at $\approx 5\text{ mA}$ is the active device. The old tubes had a transconductance of 2 to 5 mS, while the BJT has a transconductance of 39 mS per 1mA or about 195mS at 5mA. This means that the loop gain with the transistor is much higher (loop gain is directly proportional to transconductance) [9, pp. 401]. The bias circuit is conventional using an emitter resistor of 120 ohms, with a bypass capacitor of 1pF (parasitic value).

The voltage divider of 8k Ω and 3.6k Ω with a supply voltage of 12V produces a base voltage of $\frac{12}{(8000+3600)} \times 3600 = 3.7\text{V}$.

The emitter-resistor voltage drop is $5\text{ mA} \times 120\Omega = 0.6\text{V}$ and the base emitter voltage drop is about 0.7V. From this we can calculate the base current.

The differential voltage across the 50kΩ resistor is $(3.7 - (0.6 + 0.7)) = 2.4V$. Therefore the base current has to be $2.4V/50k\Omega = 48\mu A$.

The CAD simulation shows $I_b = 46.6\mu A$. The reason for the difference is the finite accuracy of the bipolar transistor model.

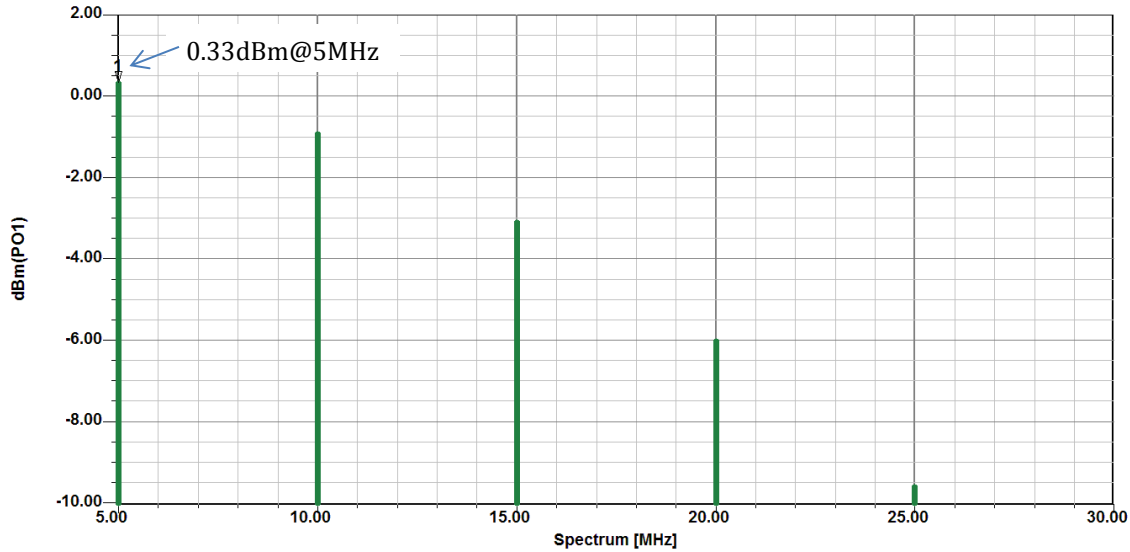


Figure 5-5: Output power spectrum of Cady's simulated circuit of Figure 5-4

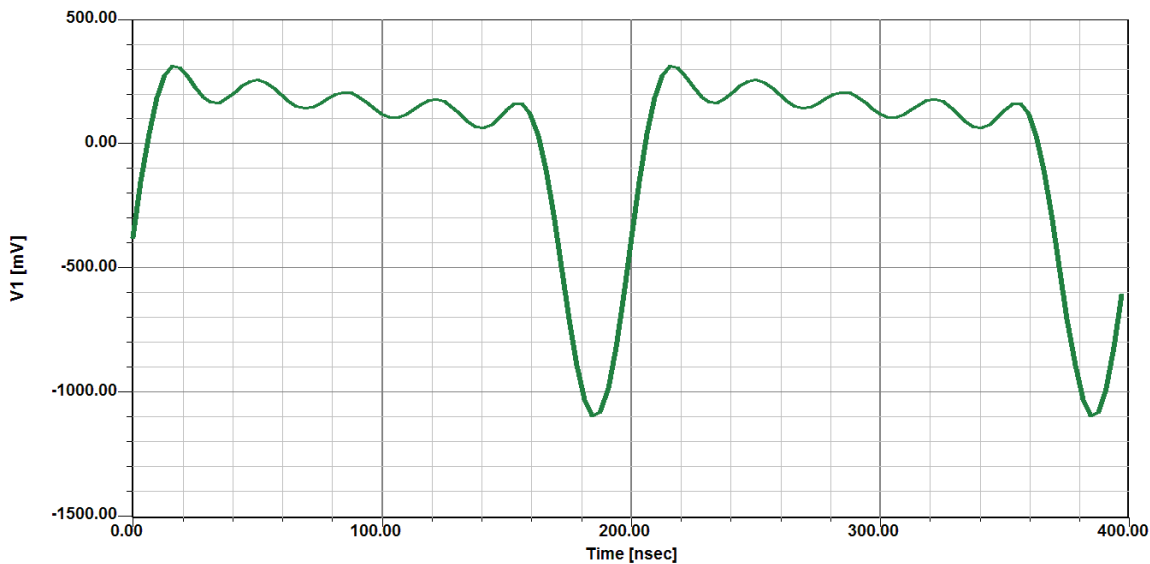


Figure 5-6: Collector Voltage waveform of the Cady's simulated circuit

The harmonic distortion is further seen while analyzing the output voltage at the collector (Figure 5-6).

In the early 1920s, neither the CAD tools to simulate nor a spectrum analyzer were available to display the resulting waveforms. Modern oscillators are evaluated also by its phase noise, besides the output power. Figure 5-7 shows the CAD simulated single sideband phase noise of this Cady based crystal oscillator.

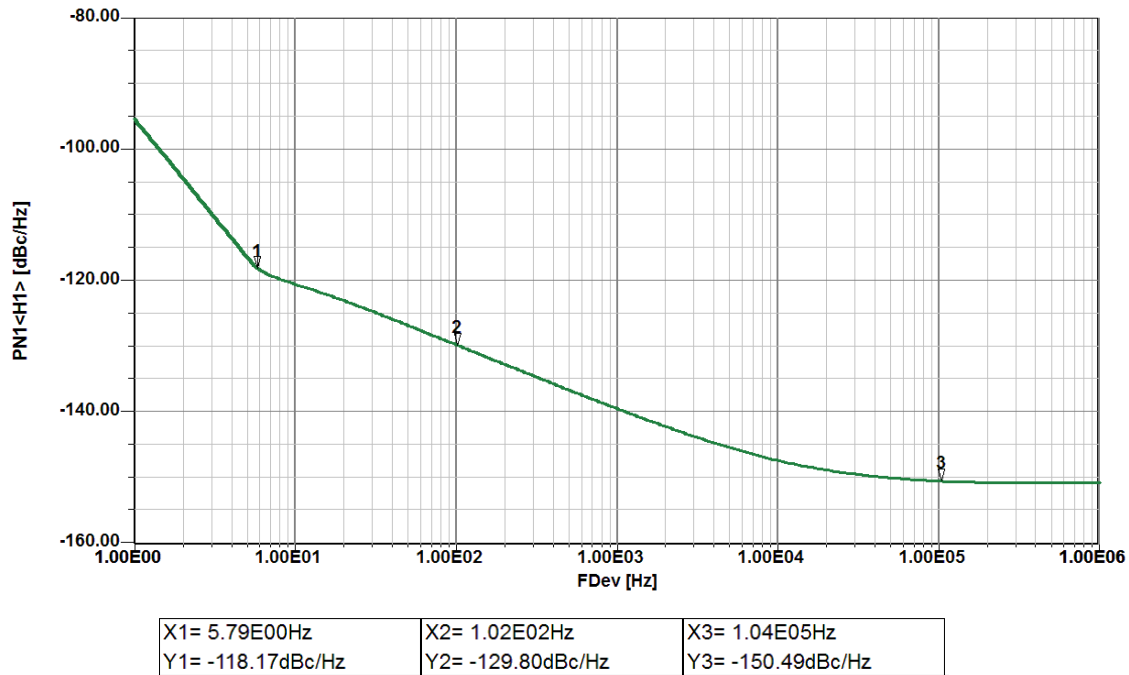


Figure 5-7: Simulated single sideband phase noise of this Cady based crystal oscillator

The phase noise plot shows the signal to noise ratio (dimensionless) in a 1 Hz bandwidth for an offset from the carrier from 1 Hz to 1 MHz.

The ambient SSB (single side band) noise floor is $kT = -177 \text{ dBm/Hz}$ (Johnson noise).

The signal to noise ratio (in dB equals the difference) at 1 MHz offset is $(0.33 \text{ dB} + 152 \text{ dB}) = 152.33 \text{ dB}$.

The dent seen between 1 Hz to 10 Hz is the result of the flicker component. The frequency range from 0.1 Hz to approximately 10 Hz, shows the flicker noise contribution around 4 Hz.

The area upto 10 kHz is proportional to $1/Q^2$ (where Q is the quality factor) and the noise floor settles at -150 dBc/Hz .

This CAD simulation is shown just to look at the functionality of the often quoted Cady circuit.

While the modern tools show a good answer for the circuit, this is nothing remarkable and by far not today's state-of-the-art, but shows that Cady really had all the inventive know-how.

The transistor used for the simulation is made by Infineon, in Germany, a very non-exotic transistor and the crystal used has an unloaded Q of 500000. From the literature it is unclear whether this is a valid assumption. Today's 5 MHz crystals have a Q (Figure of Merit: Stored energy/Dissipated energy) closer to 2000000.

Today's crystal oscillators that are generally built around the Colpitts type configuration, the LC-tuned circuit provides a 180 degrees phase shift between base and collector as does the transistor and therefore the Barkhausen criteria is met.

The Barkhausen criteria stipulate that the phase shift is 360 degree and the steady-state loop gain is slightly greater than one. In the Barkhausen criteria description, it is frequently overlooked that the loop gain to initiate oscillation should be around 3-4. As it was developed for tubes, this was a

voltage gain while for transistors it is more like power gain. The limiting effect needed to provide constant amplitude is due to a voltage or current limiting, sometimes clamping diodes or AGC (Automatic Gain Controlled) circuit may be used.

5.3 Circuit Analysis using the Colpitts Topology:

As pointed out, the majority of crystal oscillators are based on the Colpitts oscillator. The Colpitts oscillator can be recognized by the capacitive voltage divider and a parallel tuned circuit, loosely coupled to the base. A general topology of the Colpitts oscillator is shown in Figure 5-8.

In order for this oscillator to operate, the part on the left of the capacitive divider has to be inductive.

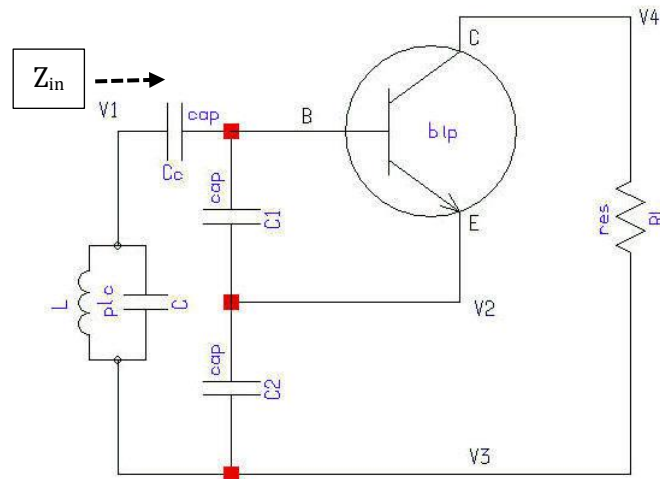


Figure 5-8: General topology of the Colpitts oscillator [9]

The value of the input impedance Z_{in} (looking into the base of the transistor of the Colpitts Oscillator), $Z_{in} = R_n + jX_n$ is given by [4][128],

$$Z_{in}|_{package} = - \left[\frac{Y_{21}}{\omega^2(C_1+C_p)C_2} \frac{1}{(1+\omega^2Y_{21}^2L_p^2)} \right] - j \left[\frac{(C_1+C_p+C_2)}{\omega(C_1+C_p)C_2} - \frac{\omega Y_{21} L_p}{(1+\omega^2 Y_{21}^2 L_p^2)} \frac{Y_{21}}{\omega(C_1+C_p)C_2} \right] = R_n + jX_n \quad (5-1)$$

Where R_n and X_n are the resistance and reactance looking into the base of the transistor.

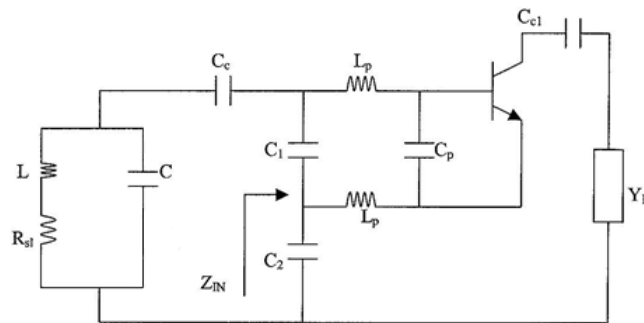


Figure 5-9: Colpitts oscillator circuit [9]

In order to form a simple crystal oscillator, the parallel tuned circuit is replaced with the equivalent circuit of the crystal as shown in Figure 5-9.

A CAD simulation for such a 10 MHz crystal oscillator based on the Colpitts configuration is shown in Figure 5-10.

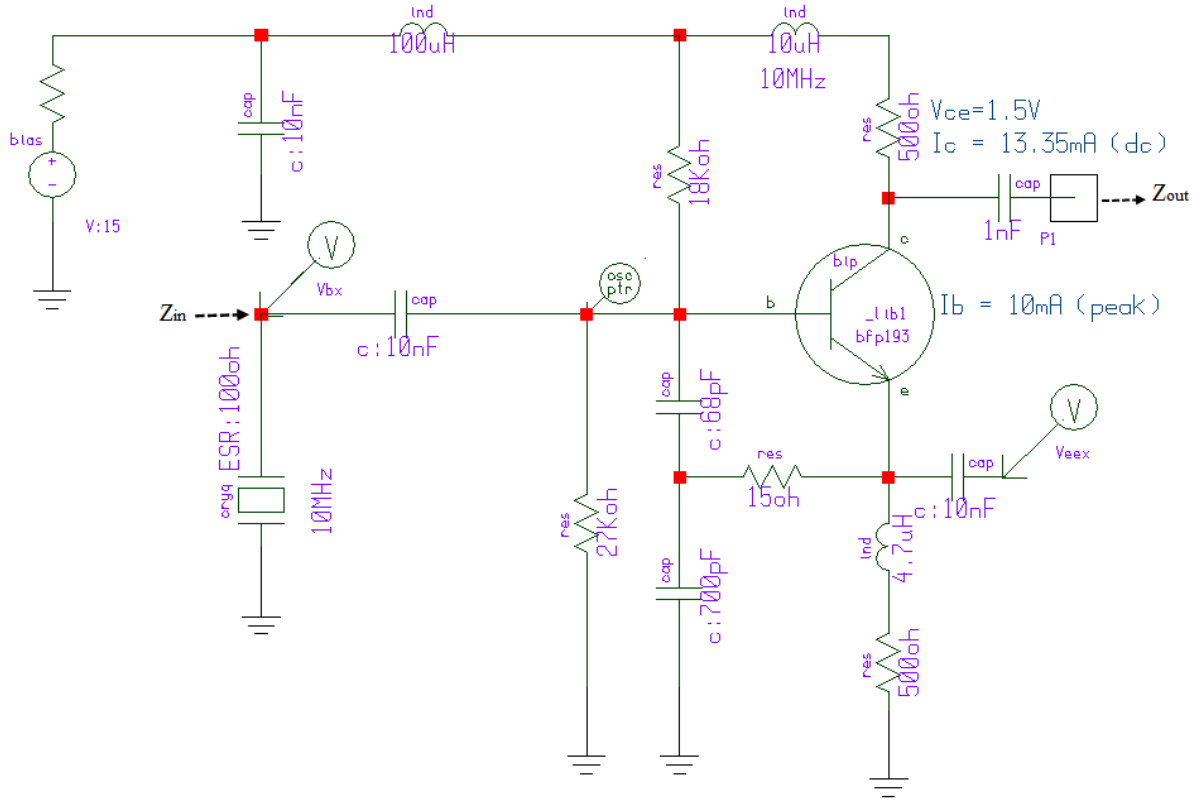


Figure 5-10: Colpitts Oscillator schematic

As an initial starting condition, the capacitor C_1 (base-emitter), is chosen at 68pF, and C_2 (emitter to ground), about twice as much (150pF). The initial assumption is based on approximate calculation of negative resistance ($R_n \approx -\frac{Y_{21}}{\omega^2(C_1C_2)}$) from Equation (5-1) for ideal condition (without package parasitics, this means L_p and C_p are neglected). The resistor (15Ω) from the voltage divider to the emitter linearizes the circuit.

From (5-1), The value of C_2 was gradually increased to find that increasing C_2 changes the negative resistance, the real and imaginary parts shown in Figures 5-11 and 5-12, and at certain value offers the best phase noise for a given FOM (Figure of merit).

The effect of the different values of C_2 on phase noise is shown in Figure 5-13.

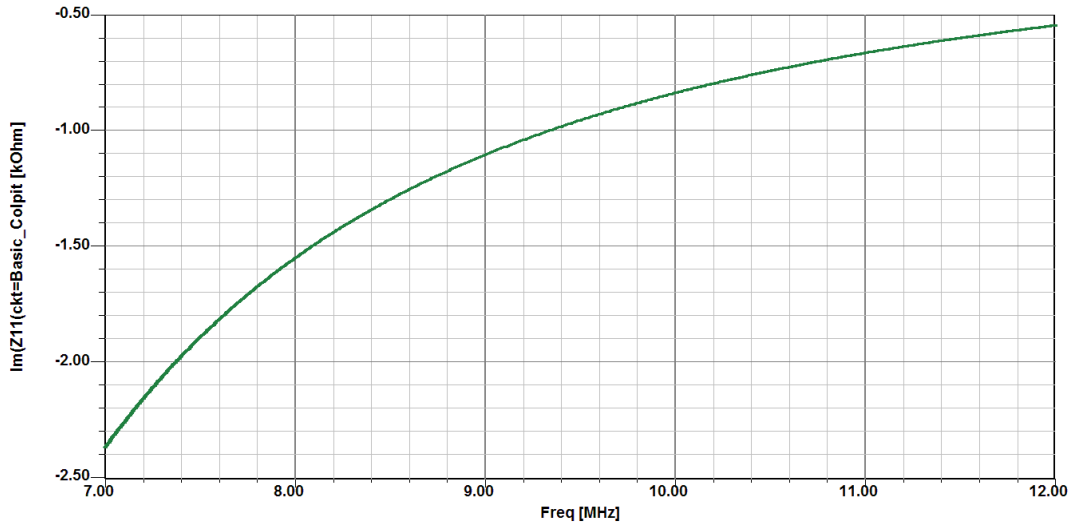


Figure 5-11: Imaginary part of the impedance - $\text{Im}(Z_{in})$

The real and imaginary parts of the impedance were plotted with respect to frequency to show the negative value of the impedance at the frequency of interest, which is 10 MHz in this case.

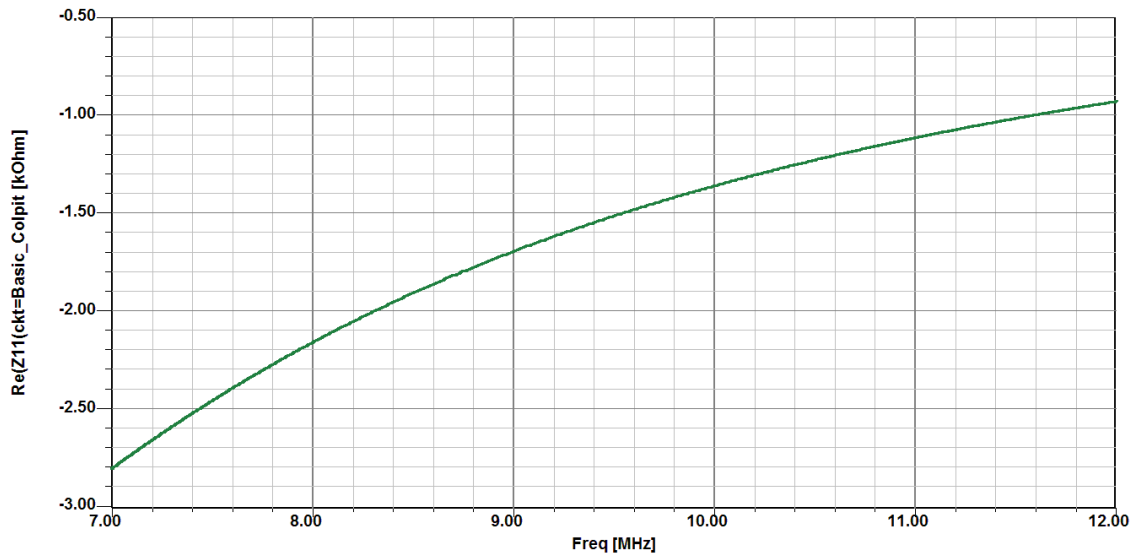


Figure 5-12: Real part of the impedance $\text{Re}(Z_{in})$

The optimized circuit exhibits a negative resistance of 490 Ohms at 10 MHz.

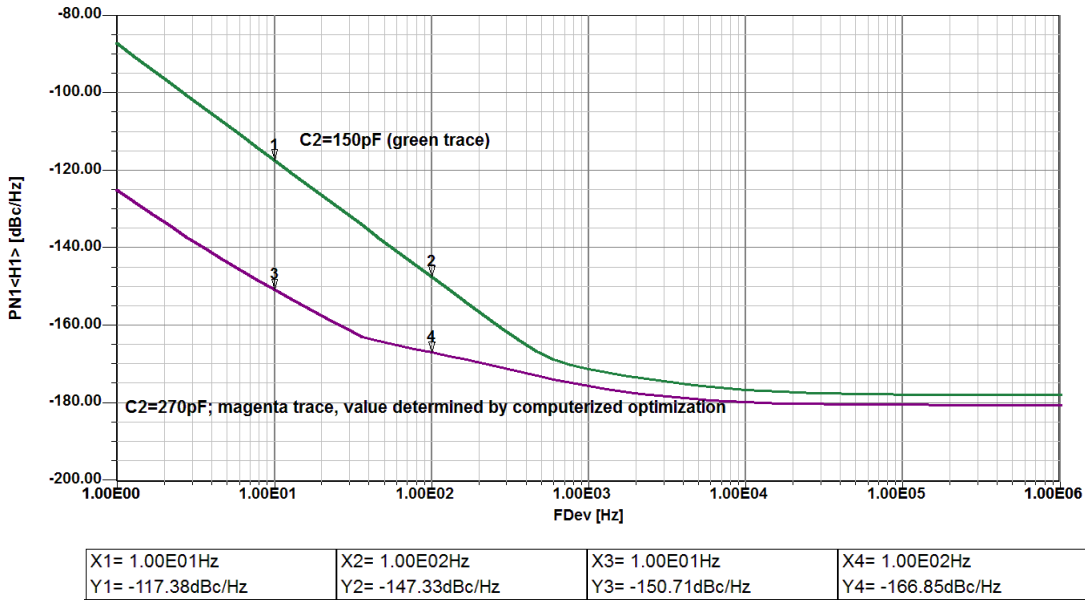


Figure 5-13: Simulated phase noise plot showing the effect of the value of $C_2=150$ pF and $C_2=270$ pF

Another interesting question is how much noise is due to flicker, A_f and K_f ? (These parameters are defined in Chapter 2). This can be tested by setting K_f to $1e-20$. This value of course is not realistic but only the Schottky noise and the Johnson noise are considered, simulation shown in the Figure 5-14.

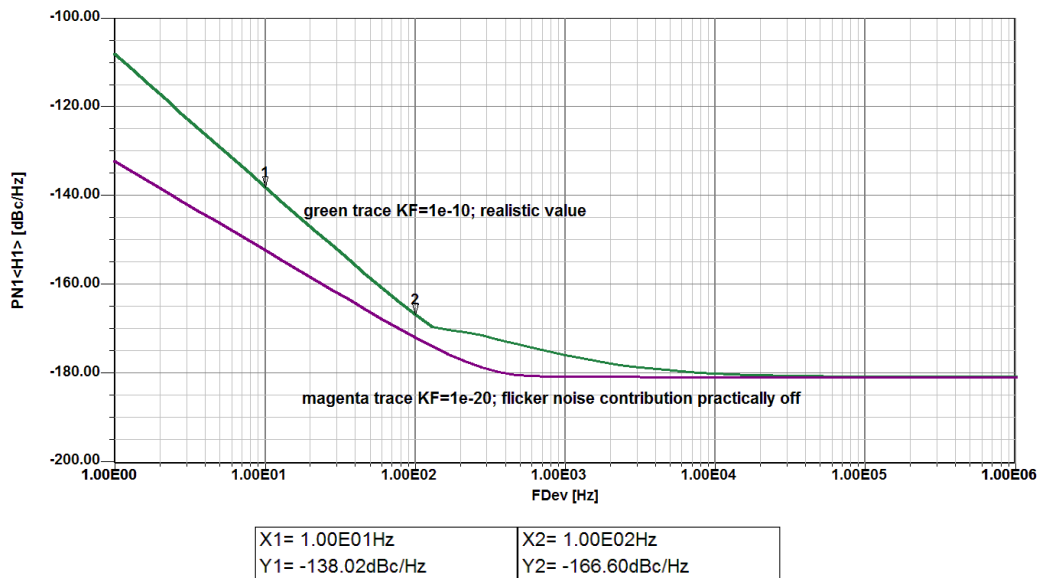


Figure 5-14: Simulated Phase noise plot with and without the effect of flicker

The internal Schottky and Johnson noise contribution are calculated correctly and cannot be shut-off. Therefore this is the best practical case without flicker.

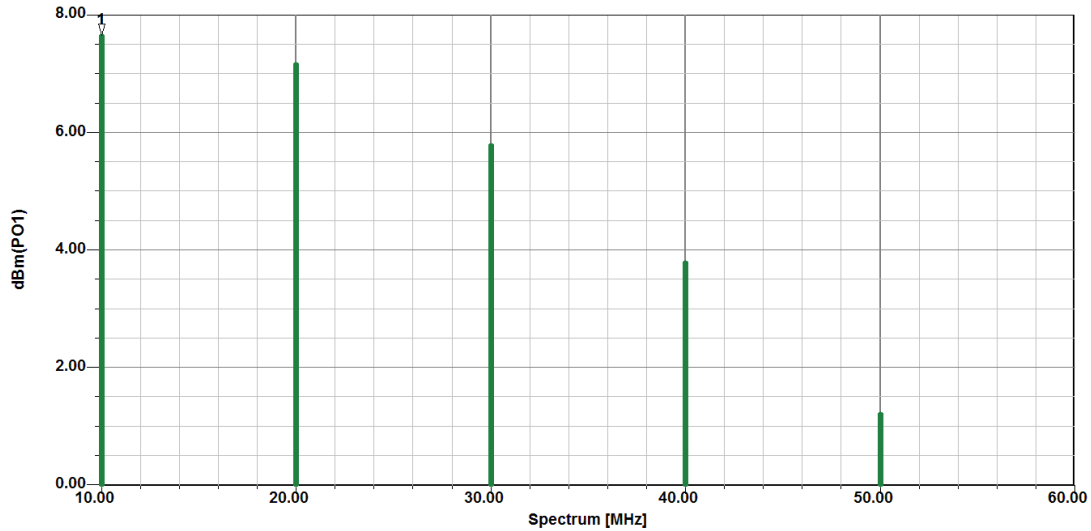


Figure 5-15: Output power for the 10 MHz Colpitts Crystal Oscillator Circuit in Figure 5-11

The output power for the Colpitts Circuit of Figure 5-11 is shown in Figure 5-15.

The following plots shown in Figure 5-16 and Figure 5-17 illustrate the voltage and currents for this optimized crystal oscillator circuit operating at 10 MHz.

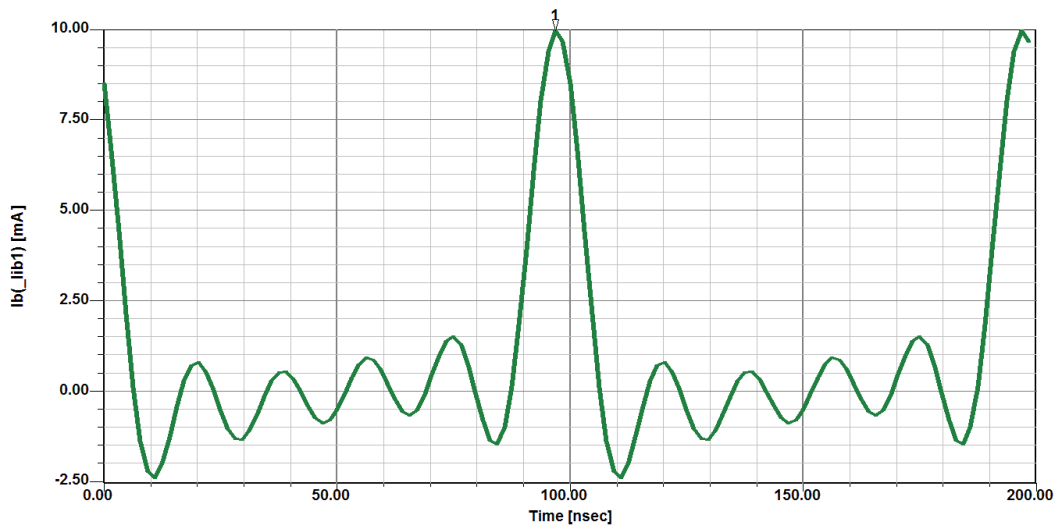


Figure 5-16: Base current of the Transistor of the 10 MHz Colpitts Crystal Oscillator Circuit in Figure 5-11

5.3.1 Important consideration for selection of the transistor found during the course of this work:

The CAD simulated collector current of the oscillator shown in Figure 5-10 exhibits class-C operation, and peaks at approximately 68 mA, as seen in Figure 5-17. This needs to be further explained. The normal cycle is of 180 degrees and in this circuit the cycles occupy only 30 degrees or $1/6^{\text{th}}$ but contain the same energy. Therefore, the peak collector current is about 6 times the dc current. It is therefore important to select a transistor which can handle this peak current of about 70mA.

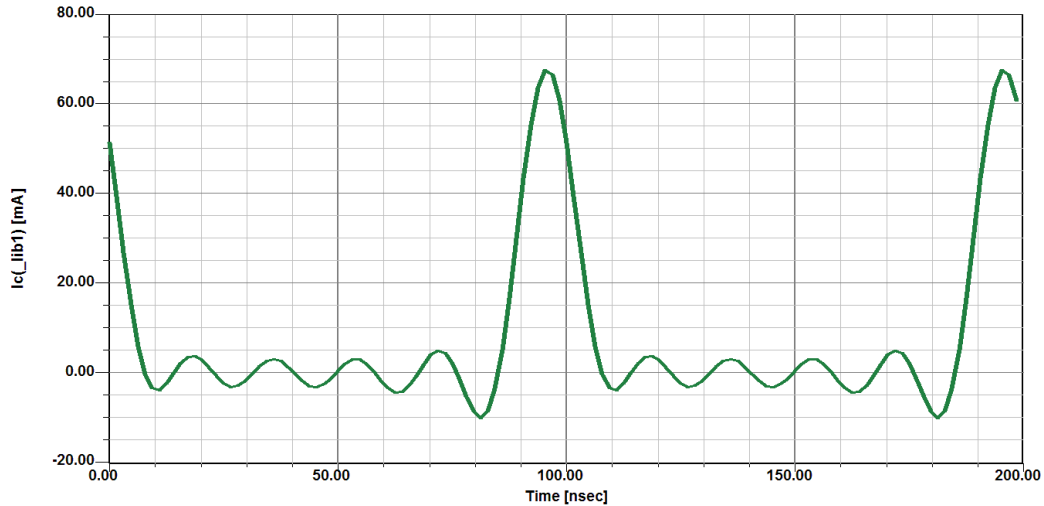


Figure 5-17: Collector current of the transistor for the 10 MHz Colpitts Crystal Oscillator Circuit in Figure 5-11

The maximum current rating for the BFP193 (from Infineon) [45] used in the circuit depicted in Figure 5-10, is 80mA, but the 70mA, as seen in Figure 5-17, are only short pulses, and hence considered safe for operation. Figure 5-18 shows the collector-emitter voltage of this transistor.

The typical energy needed to provide this current is based on the flywheel effect of the tuned circuit or the energy stored in the crystal acting as an inductor and the external capacitors.

From a DC point of view, the maximum current would be $15V / (250\Omega + 500\Omega) = 20 \text{ mA}$, the actual dc current was 13.35 mA, therefore the ratio (the peak value of the collector RF current to the actual dc current = $70/13.35=5.24$) is 5.24, indicating that the conducting angle was $180/5.24 = 34.3^\circ$ (with reasonable accuracy, since a 30° duty cycle is generally considered an optimum choice) [9, Chapter 6].

The assumption of 30° duty cycle is evaluated on an empirical basis for Colpitts oscillator topology, that is based on developing several thousands of Colpitts oscillator circuits utilizing different resonator topology (high q factor resonator such a quartz crystal resonator, ceramic resonator, SAW resonator, Dielectric resonator) depending upon the frequency of operations.

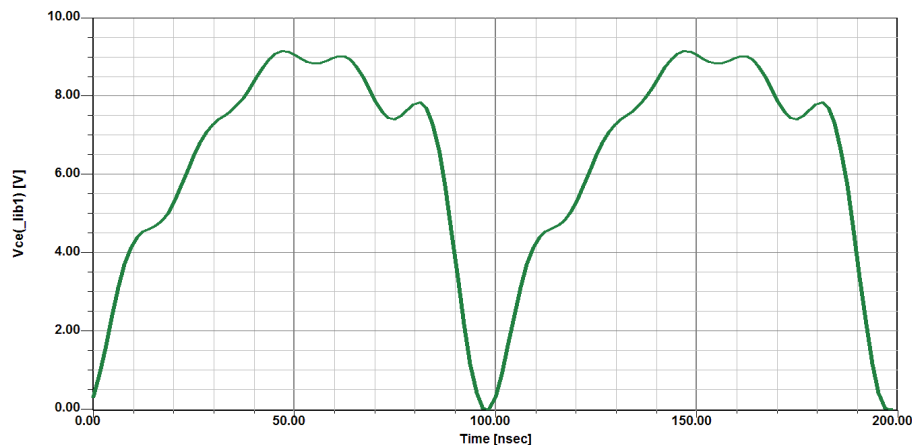


Figure 5-18: Collector-Emitter voltage of the transistor of the 10 MHz Colpitts Crystal Oscillator Circuit in Figure 5-11

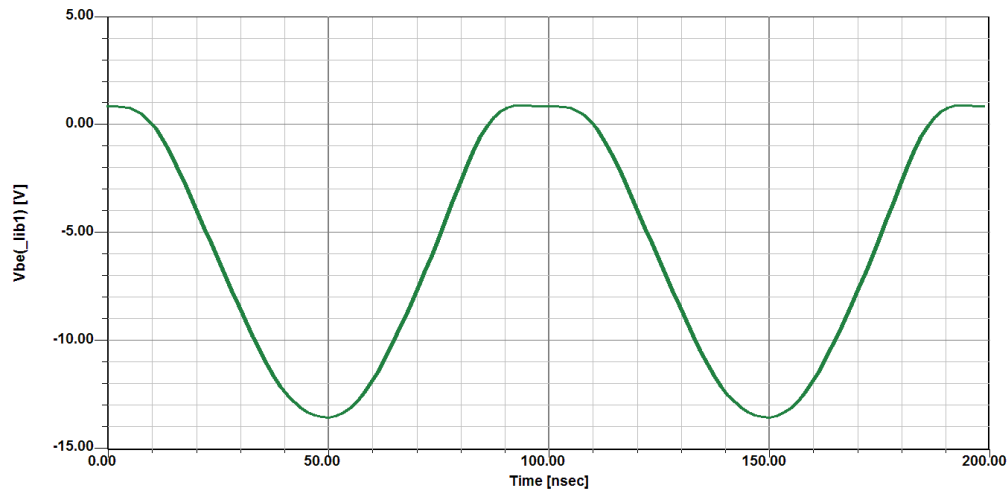


Figure 5-19: Base-Emitter voltage of the transistor of the 10 MHz Colpitts Crystal Oscillator Circuit in Figure 5-11

As the collector is electrically at RF ground, this is the base to ground RF voltage as shown in Figure 5-19. The base-emitter junction for positive voltages clips the value for negative voltages; the transistor is effectively shut off. This was a first and simple approach.

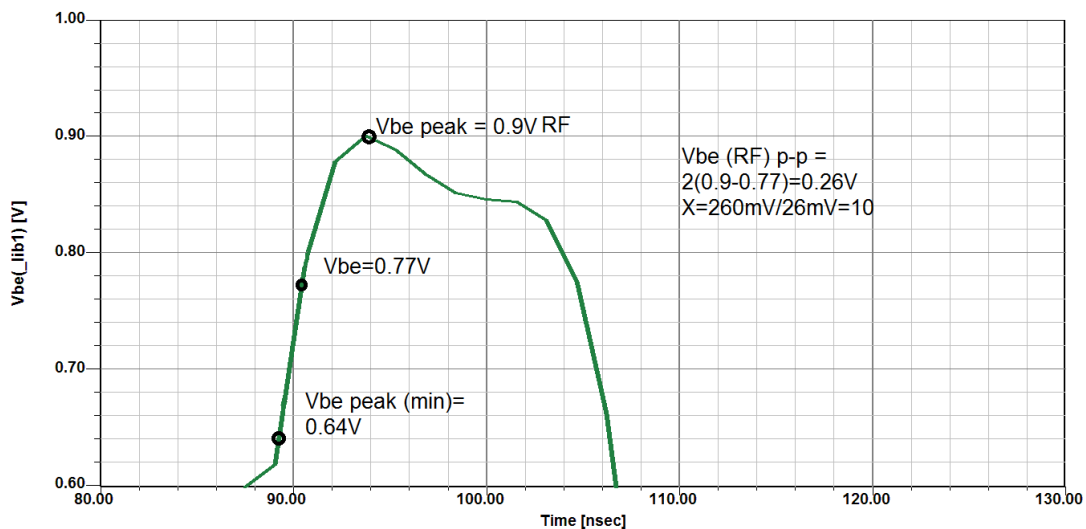


Figure 5-20: A closer look at the base-emitter voltage – RF swing over the DC bias (0.77V \approx 100mV)

Some further explanations are necessary for better understanding.

A drive level is defined in the next analysis, which is normalized to V_1 (RF drive voltage at the base).

This V_1 divided by 26 mV = q/kT .

If we analyze V_{be} as shown in the plot of Figure 5-20, compared to the V_{be} (dc), which is 0.77V, the peak RF voltage, is 0.9. The peak-to-peak value is calculated as $2 \times (0.9 - 0.77) = 0.26$ V.

The RF peak-to-peak voltage then is 260mV; we get the normalized drive level by dividing this with 26mV, to obtain $x=10$ [9, pp. 104].

For example, 10 MHz Crystal oscillator is designed, from Table 5-1, for $x=10$, it is not a good approach to drive a Quartz crystal resonator at this power level realistically because of reliability

issues. Moreover, it would defeat its purpose as a frequency standard, but for a better understanding, it is a useful introduction in designing a crystal oscillator quickly and analyzing it.

The crystal itself can be obtained at 10 MHz fundamental frequency but if higher performance is required, a third or 5th overtone crystal should be used.

If this is done, mode suppression is required and the concept is introduced in section 5.5.

Some typical crystal datasheets are shown in Chapter 3, Figure 3-1a and Figure 3-1b for quick reference.

The relevant parts of a typical datasheet of a 100 MHz crystal oscillator are shown in Figure 5-21a and Figure 5-21b.



Specification	AXIOM75ULN	Rev.: 3	Date: 2014-05-08
---------------	------------	---------	------------------

Oscillator type: Ultra-Low Phase Noise OCXO with Sine Wave Output

Parameter	min.	typ.	max.	Unit	Condition
Frequency Range	80		125	MHz	
Standard frequencies	100.000/120.000			MHz	
Frequency stability					
Initial tolerance @ +25°C			±300	ppb	V _C @ VREF/2
vs. operating temperature range	Option 2 & 3 See tables 2 & 3				steady state
vs. supply voltage variation (pushing)			±10	ppb	V _S ±5%
vs. load change (pulling)			±5	ppb	R _L ±5%
Long term (aging) per day		±1	±2	ppb	after 30 days operation
Long term (aging) 1 st year		±100	±200	ppb	after 30 days operation
Frequency adjustment range					
Electronic Frequency Control (EFC)	±1	±2		ppm	
EFC voltage V _C	0	VREF/2	VREF	V	
EFC slope (Δf / ΔV _C)	Positive				
EFC input impedance	100			kΩ	
RF output					
Signal waveform	Sine wave				
Load R _L	50			Ω	±5%
Output level (Note 2)	+7			dBm	
Harmonics			-30	dBc	
Spurious			-90	dBc	
Warm-up time		3	5	min	Δf _{final} /f ₀ < ±0.1 ppm
Phase noise @ 100 MHz and 120 MHz	See table 1				Option 1
G-Sensitivity			1.0	ppb/g	per axis
Reference voltage VREF output (Note 3)		10.0		V	
Supply voltage V _S (Note 3)	11.4	12.0	12.6	V	
Current consumption (steady state)			150	mA	@ +25°C (Note 4)
Current consumption (warm-up)			350	mA	(Note 4)
Enclosure (see drawing) (LxWxH)	25.8x25.8x12.7 max.			mm	IEC 60679-3 CO 43
Weight			20	g	
Packing	Palette				

Notes:

1. Terminology and test conditions are according to IEC60679-1 and MIL-PRF-55310, unless otherwise stated
2. Other output level on request
3. Other supply and reference voltage on request
4. May be higher for wide operating temperature range

Absolute Maximum Ratings

Parameter	min.	max.	Unit	Condition
Supply Voltage V _S	-0.5	V _S + 10%	V	V _S to GND
Control Voltage V _C	-0.5	15	V	V _C to GND
Storage Temperature	-55	+125	°C	

Figure 5-21a: Part of 100 MHz Crystal oscillator datasheet (Courtesy: AXTAL- www.axtal.com)



Phase Noise – Option 1:

Offset	100 MHz					120 MHz					Unit
	A	B	C	D	E	A	B	C	D	E	
10 Hz	-90	-95	-97	-100	-105	-85	-90	-95	-97	-100	dBc/Hz
100 Hz	-125	-130	-132	-135	-137	-118	-122	-125	-127	-130	dBc/Hz
1 kHz	-155	-158	-160	-162	-164	-148	-150	-153	-155	-157	dBc/Hz
10 kHz	-165	-168	-170	-172	-174	-160	-165	-168	-170	-172	dBc/Hz
≥100 kHz	-175	-175	-175	-175	-175	-175	-175	-175	-175	-175	dBc/Hz

Table 1

Frequency stability vs. temperature

Option 2	Stability [ppb]
05	±5
10	±10
25	±25
50	±50
100	±100
200	±200

Table 2

Lower Temperature		Upper Temperature	
Option 3	T [°C]	Option 3	T [°C]
0	0	A	+50
1	-10	B	+60
2	-20	C	+70
3	-30	D	+75
4	-40	E	+80
5	-55	F	+85

Table 3

Standard: "1B" = -10°C to +60°C

Temperature range [°C]	Frequency stability [Option 2]					
	05	10	25	50	100	200
0 ~ +50	O	X	X	X	X	X
-10 ~ +60	O	X	X	X	X	X
-20 ~ +70	O	X	X	X	X	X
-30 ~ +70	O	O	X	X	X	X
-40 ~ +75	-	O	X	X	X	X
-40 ~ +85	-	-	O	X	X	X
-55 ~ +85	-	-	O	X	X	X

Table 4 "Availability"

X = available, O = available on request, - not available

Figure 5-21b: Part of 100 MHz Crystal oscillator datasheet (Courtesy: AXTAL, www.axtal.com)

5.4 Derivation of the Bessel functions [9]:

The synthesis approach based on Bessel functions, derivation shown in this section 5.4, is also discussed for comparative analysis.

The definition of drive level

$$x = \frac{V_1}{(kT/q)} = \frac{qV_1}{kT} \tag{5-3}$$

$i_e(t)$ is the emitter current and x is the drive level which is normalized to kT/q .

From the Fourier series expansion, $e^{xcos(\omega t)}$ is expressed as

$$e^{xcos(\omega t)} = \sum_n a_n(x) \cos(n\omega t) \tag{5-4}$$

$a_n(x)$ is a Fourier coefficient and given as

$$a_0(x)|_{n=0} = \frac{1}{2\pi} \int_0^{2\pi} e^{xcos(\omega t)} d(\omega t) = I_0(x) \quad (5-5)$$

$$a_n(x)|_{n>0} = \frac{1}{2\pi} \int_0^{2\pi} e^{xcos(\omega t)} \cos(n\omega t) d(\omega t) = I_n(x) \quad (5-6)$$

$$e^{xcos(\omega t)} = \sum_n a_n(x) \cos(n\omega t) = I_0(x) + \sum_1^\infty I_n(x) \cos(n\omega t) \quad (5-7)$$

$I_n(x)$ is the modified Bessel function.

$$\text{As } x \rightarrow 0 \Rightarrow I_n(x) \rightarrow \frac{(x/2)^n}{n!} \quad (5-8)$$

$I_0(x)$ are monotonic functions having positive values for $x \geq 0$ and $n \geq 0$; $I_0(0)$ is unity, whereas all higher order functions start at zero.

The short current pulses are generated from the growing large-signal drive level across the base-emitter junction, which leads to strong harmonic generation. The emitter current represented above can be expressed in terms of harmonics as

$$i_e(t) = I_s e^{\frac{qV_{dc}}{kT}} I_0(x) \left[1 + 2 \sum_1^\infty \frac{I_n(x)}{I_0(x)} \cos(n\omega t) \right] \quad (5-9)$$

$$I_{dc} = I_s e^{\frac{qV_{dc}}{kT}} I_0(x) \quad (5-10)$$

$$V_{dc} = \frac{kT}{q} \ln \left[\frac{I_{dc}}{I_s I_0(x)} \right] \Rightarrow \frac{kT}{q} \ln \left[\frac{I_{dc}}{I_s} \right] + \frac{kT}{q} \ln \left[\frac{1}{I_0(x)} \right] \quad (5-11)$$

I_s = collector saturation current

$$V_{dc} = V_{dq} - \frac{kT}{q} \ln I_0(x) \quad (5-12)$$

$$i_e(t) = I_{dc} \left[1 + 2 \sum_1^\infty \frac{I_n(x)}{I_0(x)} \cos(n\omega t) \right] \quad (5-13)$$

V_{dc} and I_{dc} are the operating DC bias voltage and the DC value of the emitter current. Furthermore, the Fourier transform of $i_e(t)$, a current pulse or series of pulses in the time domain yields a number of frequency harmonics common in oscillator circuit designs using nonlinear devices.

The peak amplitude of the output current, the harmonic content defined as $\frac{I_n(x)}{I_1(x)}$ and the DC offset voltage are calculated analytically in terms of the drive level, as shown in Table 5-1. It gives good insight of the nonlinearities involved in the oscillator design.

From the table 5-1, the peak current $2[I_1(x)/I_0(x)]$ in column 5 approaches $1.897I_{dc}$ for a drive level ratio $x=10$.

$$\text{for } T=300K, \frac{kT}{q} = 26mV \quad (5-14)$$

$$\text{and } V_1 = 260mV \text{ for } x=10 \quad (5-15)$$

The second harmonic-distortion [56] $\frac{I_2(x)}{I_1(x)}$ is 85% for a normalized drive level of $x=10$ and the corresponding DC offset is 205.518mV. When referring to the amplitude, x is always meant as normalized to $\frac{kT}{q}$.

Again it needs to be pointed out that the actual peak current as displayed above, follows the ratio of 180° /conducting cycle; in our example, about 35° . (See Figure 5-17).

Table 5-1 For T=300 K, data are generated at a different drive-level

Drive level [x]	Drive-Voltage $[\frac{kT}{q} * x]$ mV	Offset-Coefficient $\ln[I_0(x)]$	DC-Offset $\frac{kT}{q} [\ln I_0(x)]$ mV	Fundamental Current $2[I_1(x)/I_0(x)]$	Second-Harmonic $[I_2(x)/I_1(x)]$
0.00	0.000	0.000	0.000	0.000	0.000
0.50	13.00	0.062	1.612	0.485	0.124
1.00	26.00	0.236	6.136	0.893	0.240
2.00	52.00	0.823	21.398	1.396	0.433
3.00	78.00	1.585	41.210	1.620	0.568
4.00	104.00	2.425	63.050	1.737	0.658
5.00	130.00	3.305	85.800	1.787	0.719
6.00	156.00	4.208	206.180	1.825	0.762
7.00	182.00	5.127	330.980	1.851	0.794
8.00	208.00	6.058	459.600	1.870	0.819
9.00	234.00	6.997	181.922	1.885	0.835
10.00	260.00	7.943	206.518	1.897	0.854
15.00	390.00	12.736	331.136	1.932	0.902
20.00	520.00	17.590	457.340	1.949	0.926

In the next section, a part of the commonly available (HP10811A/B) circuit of the 10 MHz crystal oscillator is used for simulation and is then scaled to 100 MHz.

5.5 A Simulation exercise using the available HP10811A/B circuit - a 10 MHz crystal oscillator:

The following test circuits shown in Figure 5-22a and Figure 5-22b are simplified versions of the HP 10811A/B oscillator [17].

The main difference between the actual circuit and the circuit simulations shown below is that the output buffer stages are not being considered. The output stage is added in the next circuit simulation shown in Figure 5-22b.

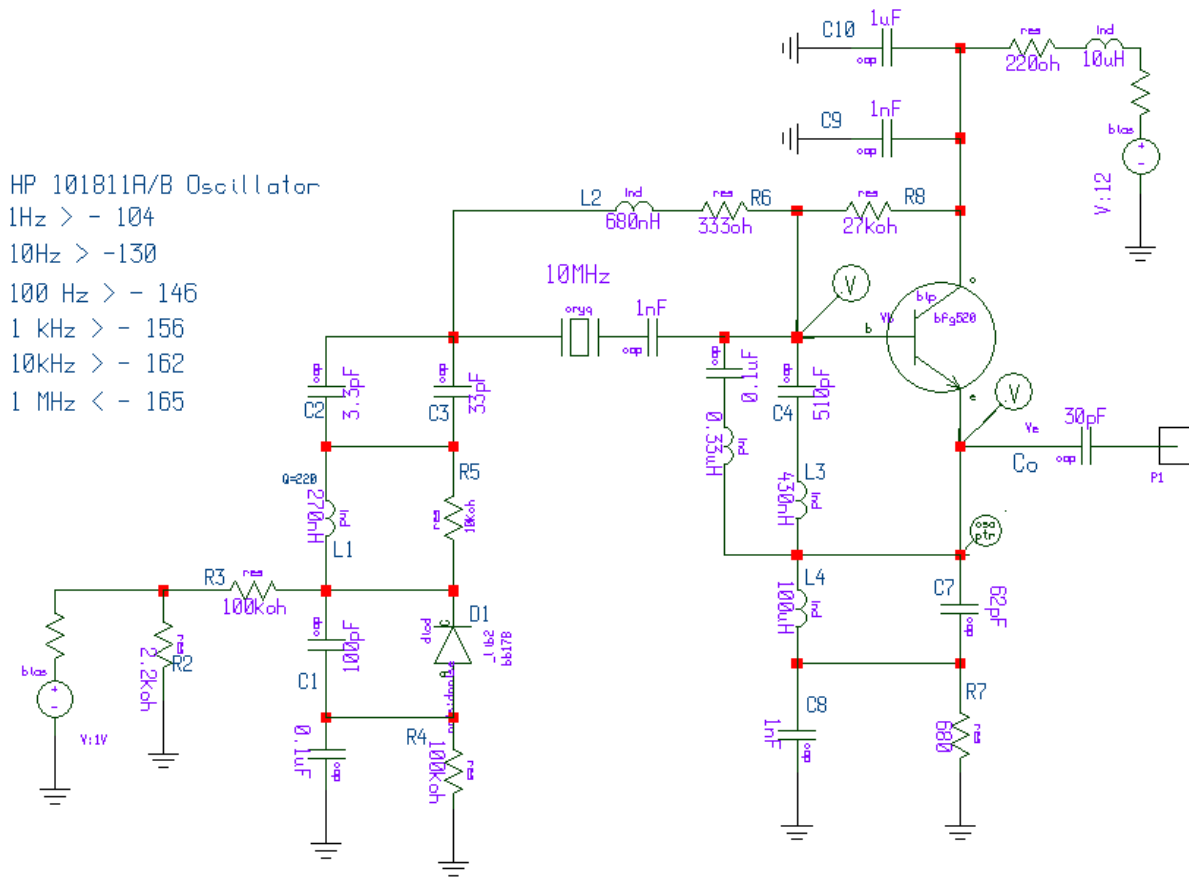


Figure 5-22a: Part of the actual circuit schematic of the HP10811A [53]

Based on the circuit shown in Figure 5-22a, and removing the tuning part, the following modified circuit shown in Figure 5-22b, which represents the total RF chain.

The two-stage 10 MHz crystal oscillator is derived from the HP 10811A [53].

The concept of grounded base oscillator shown in Figure 5-22b, will be used later in the 100 MHz crystal oscillator design.

The oscillator circuit shown in Figure 5-22b, illustrates the tuning and the DC feedback system that stabilizes the collector current. The DC feedback circuit consists of the collector resistor of 220 ohms and the base-collector resistor of 27kohms,. It turns out that this circuit actually lowers the phase noise, within its loop bandwidth.

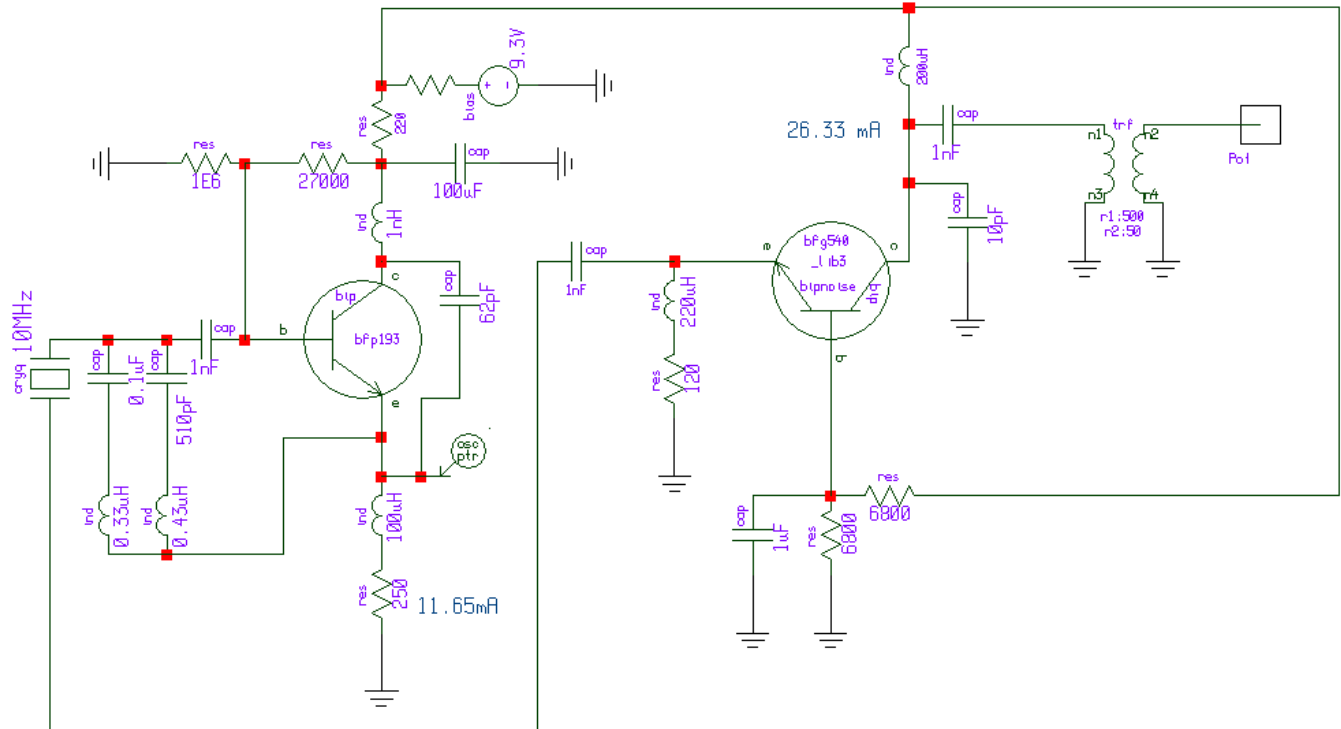


Figure 5-22b: Modified Part of the actual circuit schematic of the HP10811A [53]

The bias circuit:

It consists of a base-collector 27 kΩ resistor; the high impedance value ($\cong 1 \text{ M}\Omega$) resistor is assumed just as a place holder.

The 1nH inductor between collector and RF ground is generated by the printed circuit board.

The collector DC feedback-resistor is 220 Ohms and the emitter dc resistor is 250ohms.

The resulting collector current is 11.65 mA. The fractional numbers result from the base-emitter voltage of 0.77V and integer numbers from the resistors.

The energy is filtered through the 10 MHz crystal, a concept published by Rohde [14].

The crystal is then terminated into the grounded base circuit, which using a transformer provides about 13 dBm output powers. In the reference [[9] – pp 101 to Appendix D] examples are given for microwave circuits with essentially no limitation of the power dissipation of the resonator.

However, a typical crystal oscillator, especially if designed for low aging, cannot tolerate high dissipation. This means applying the Bessel function approach, the normalized drive level should not exceed 6.

We calculate the normalized drive level X from: $X = \frac{V_1}{(kT/q)} = \frac{qV_1}{kT}$ though determination of V_1 is tricky.

The results of the simulation are shown below:

Figure 5-23 shows the base-emitter voltage of the transistor in circuit of Figure 5-22b.

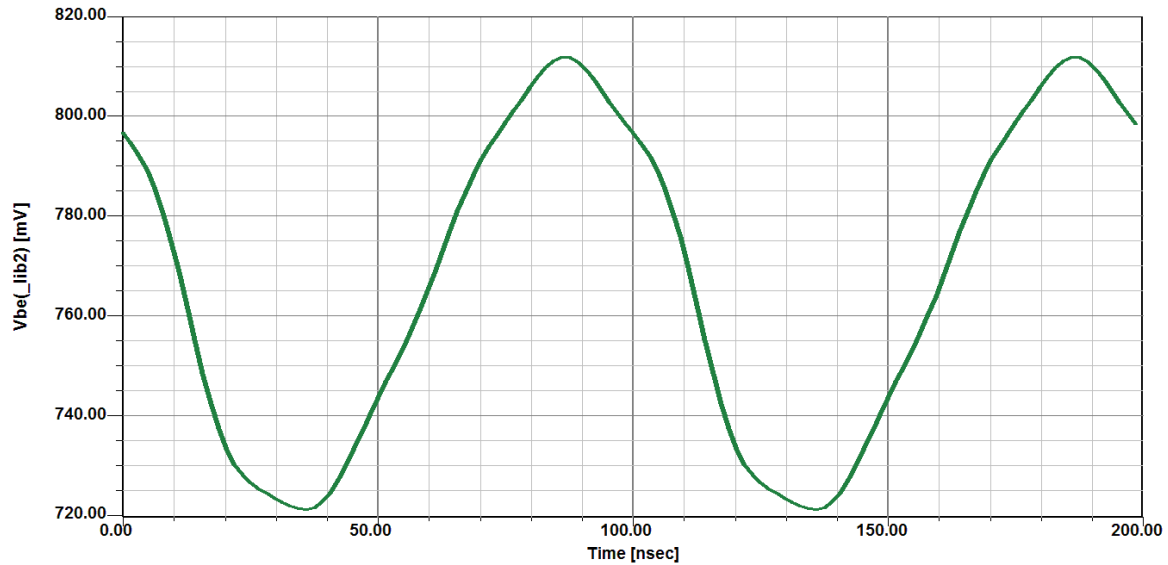


Figure 5-23: Base-Emitter voltage of the transistor in circuit of Figure 5-22b

The dc bias V_{be} is 0.77V. The RF p-p is about 90mV.

From the Table 5-1 which shows drive level and DC offset, we learn that value of x is a little above 5.

The fundamental frequency current is approx. $1.8 \times I_{dc} = 1.8 \times 11.65 = 21\text{mA}$.

This oscillator operates close to linear range, that is why the simulated peak current is close to the calculated peak current as seen in the (I_c) plot shown below in Figure 5-24.

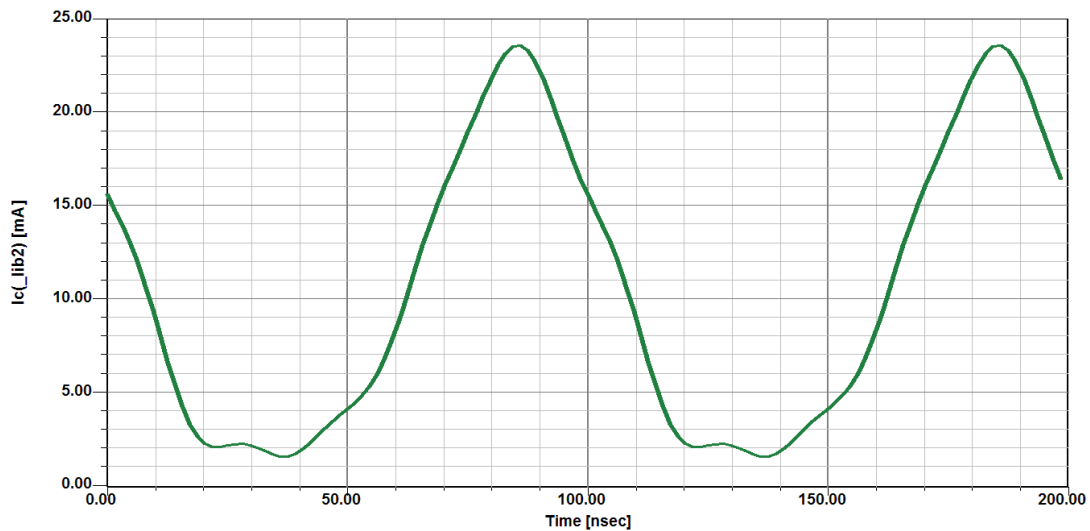


Figure 5-24: Collector current of the transistor in circuit of Figure 5-22b

The large signal transconductance is given by:

$$Y_{21} = \left. \frac{I_1}{V_1} \right|_{\text{fundamental-freq}} = \frac{1.81 I_{dc}}{90\text{mV}} = \frac{20.97\text{mA}}{90\text{mV}} \cong 230\text{mS} \quad (5-2a)$$

Next is the calculation of the feedback circuit and the loop gain.

$$\text{Loop gain} = \frac{Y_{21} R_p}{n} > 1 \quad (8, \text{ in this case}) \quad (5-2b)$$

The value of R_p is the loss resistor of the crystal, typically $< 100 \text{ Ohm}$ (see crystal datasheet), for this example 65 Ohm .

The large signal transconductance $Y_{21(\text{RF})}=200\text{mS}$, calculated (Collector RF current/RF voltage swing) from Figures 5-23 and 5-24, this would be the steady state.

However, because of the high Q , more than $1\text{E}6$, a starting loop gain >5 is preferred, here selected 8 for the theoretical evaluation and study purpose.

The resulting n from Equation (5-2) is $n=1.6$ $[(200 \times 10^{-3} \times 65)/8 \cong 1.6]$

From the definition,

$$\frac{V_{eb}}{V_{cb}} = \frac{C_2}{C_1 + C_2} = \frac{1}{n} \text{ and knowing } n, \text{ we obtain } C_1/C_2 = (n-1) = 0.6$$

$C_1=40\text{pF}$ (from the mode suppression circuit) and $C_2=62\text{pF}$ (capacitor from the emitter to the collector, which is at RF ground).

A typical example of the dc shift as shown in Figure 5-25, is a SPICE based example [9]. Here the starting value is the familiar 0.77V , and after steady state condition, the base-emitter junction rectifies the RF and produces a DC-shift, the average RF voltage at the emitter now is 100mV . This case clearly shows an oscillator operating in class C.

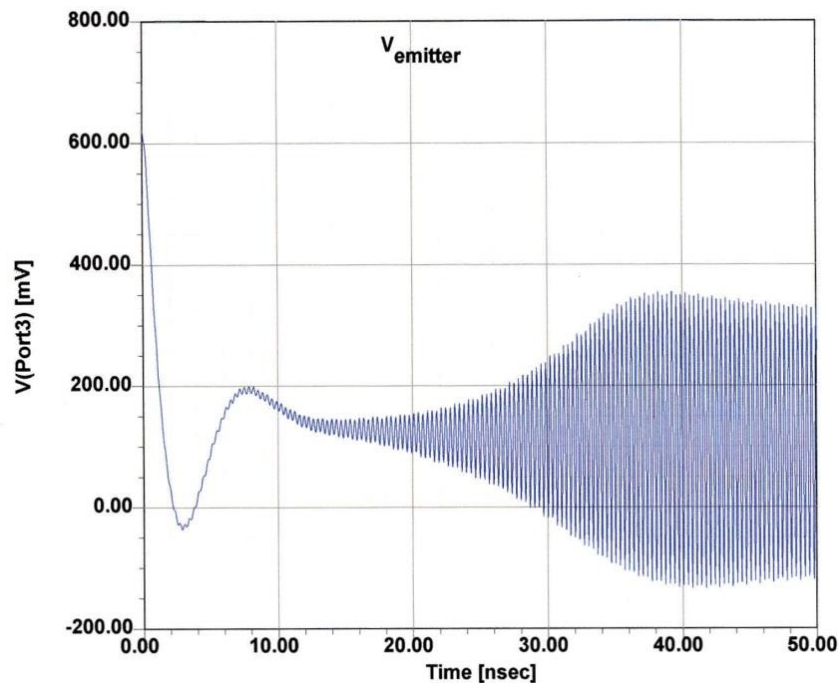


Figure 5-25: Example of the transient simulation of a high- Q crystal oscillator showing the DC-offset [9]

The next two plots Figure 5-26 and Figure 5-27 show the simulated I_b (base current) and V_{ce} collector-emitter voltage. As the collector is electrically at RF ground, in reality it is the emitter to ground voltage.

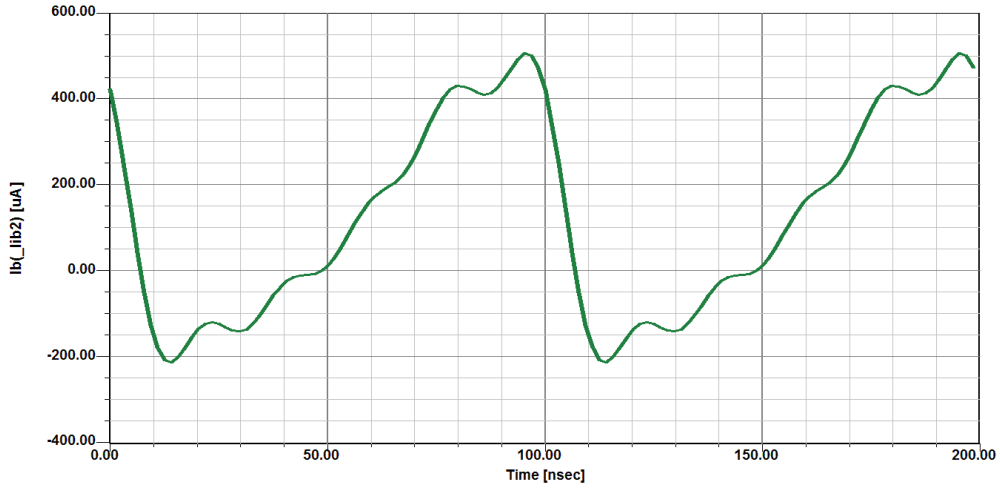


Figure 5-26: Simulated base current of the first transistor in Figure 5-22

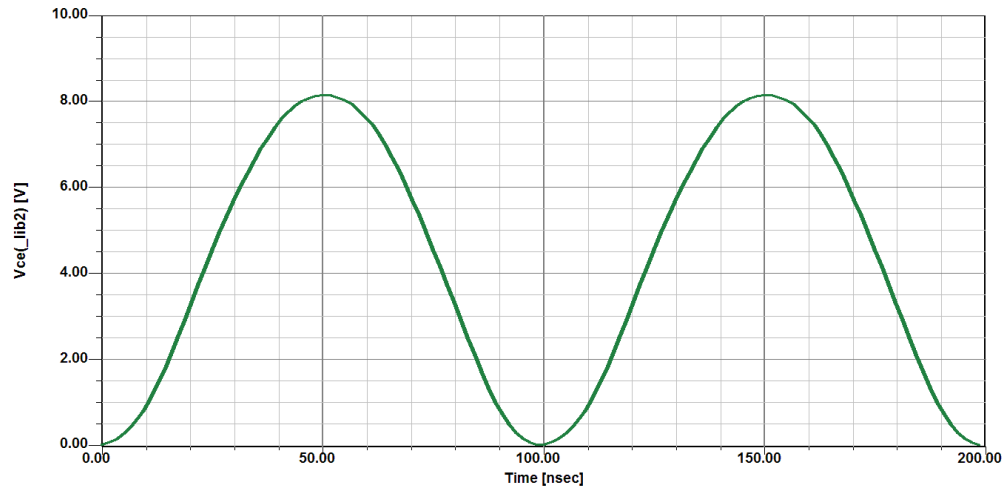


Figure 5-27: Simulated Collector-Emitter voltage (V_{ce}) of the first transistor in Figure 5-22

The output power as can be seen in Figure 5-28 is 12.3 dBm and the resulting phase noise plot is shown after this in Figure 5-29.

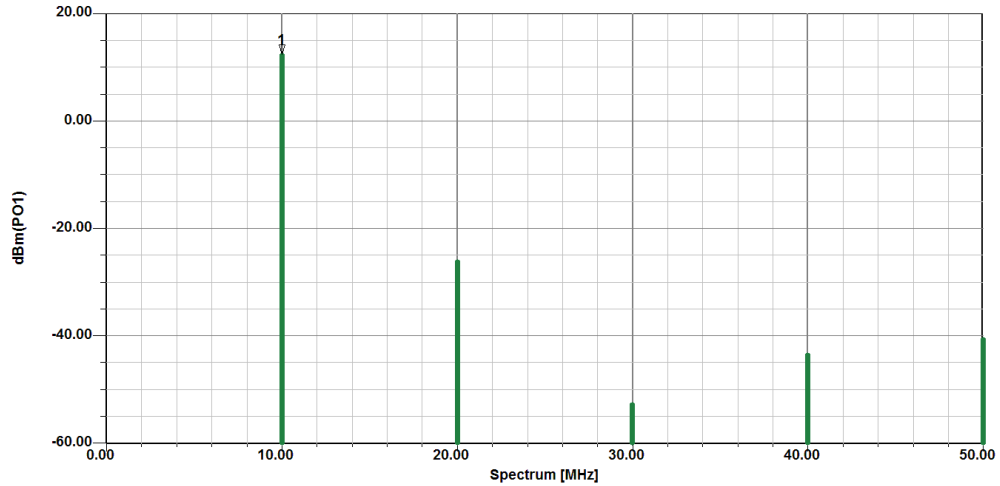


Figure 5-28: Simulated Output power of the circuit in Figure 5-22

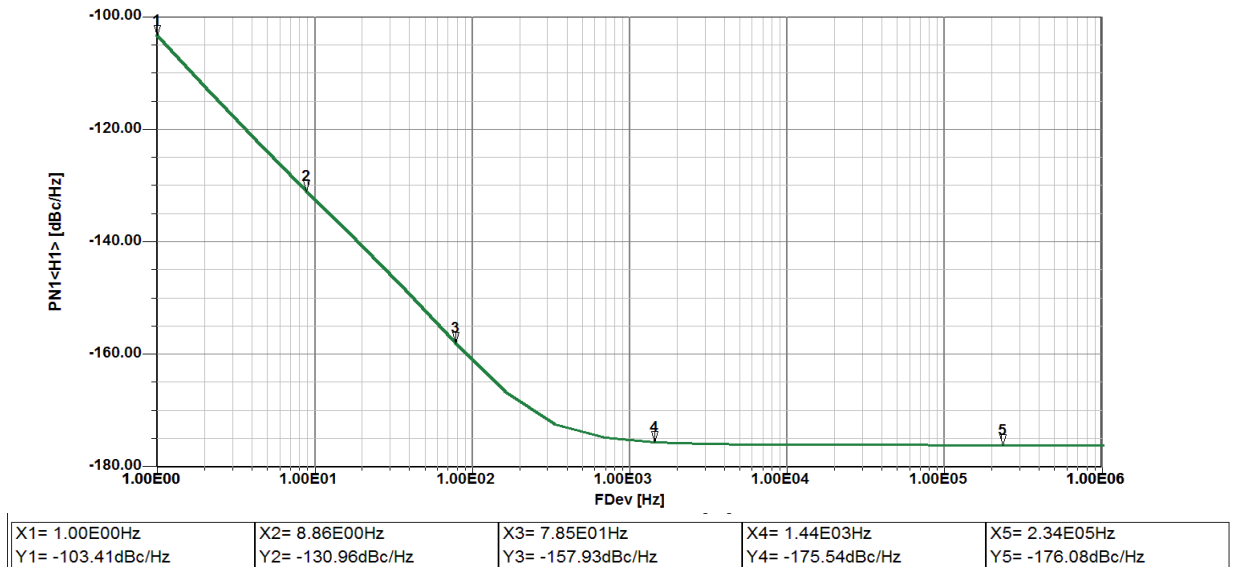


Figure 5-29: Simulated phase noise of the circuit in Figure 5-22

5.6 Mode-Suppression circuit:

The typical Colpitts based circuit of the crystal oscillator has a network which suppresses sub-harmonic resonances. At 10 MHz the network generates a 40pF capacitor between base and emitter, the collector is at RF-ground and the emitter to RF-ground capacitor is 62pF. Figure 5-30 shows the typical mode-suppression circuit.

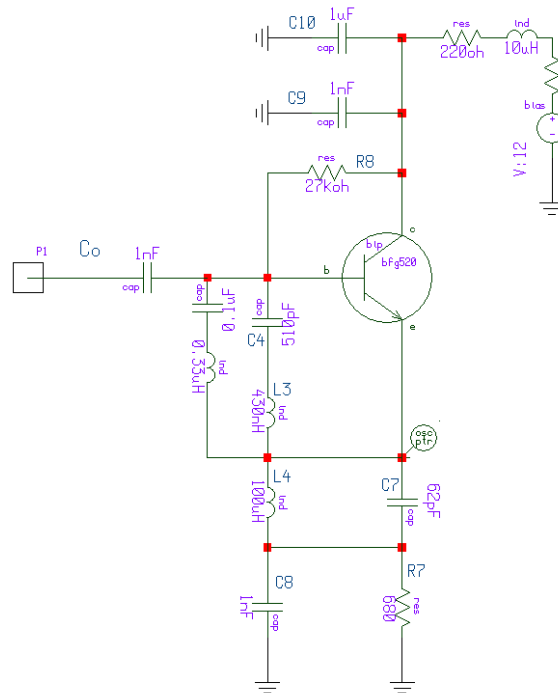


Figure 5-30: Sub-harmonics suppression circuit

The L-C harmonically tuned circuit across the Base-Emitter as illustrated in Figure 5-30 helps in reduction of the undesired modes. The test circuit contains the oscillator portion minus the crystal. The input impedance has to be real and negative around 10 MHz and the imaginary part has to be capacitive. Figure 5-31 shows the linear analysis (of the circuit in Figure 5-22) showing the real part of the negative impedance.

Table 5-2: The measured crystal parameters of HP 10811A

R1 [Ohm]	C1 [fF]	C0 [pF]	CL [pF]	Q
13.8	0.479	4.44	6.40	2.48E6
<100	0.19	3.8	20	1.2E6

The second row shows the typical parameters of a modern 10 MHz crystal. The old HP crystal had about twice the unloaded Q. A crystal with these parameters is no longer manufactured. On the other hand modern oscillators compete well with this HP oscillator, by using a novel circuit [10]-[11].

Table 5-3: Measured and simulated data of modern day and older crystal oscillators

Phase Noise of various designs	Axtal 10 MHz XO Measured Data	HP10811A 10 MHz XO Measured Data	HP10811A - Optimized with Simulator
Offset frequency	dBc/Hz	dBc/Hz	dBc/Hz
@ 1 Hz	-115	-100	-103
@ 10 Hz	-146	-128	-130
@ 100 Hz	-157	-147	-158
@ ≥ 1 kHz	-160	-161	-175

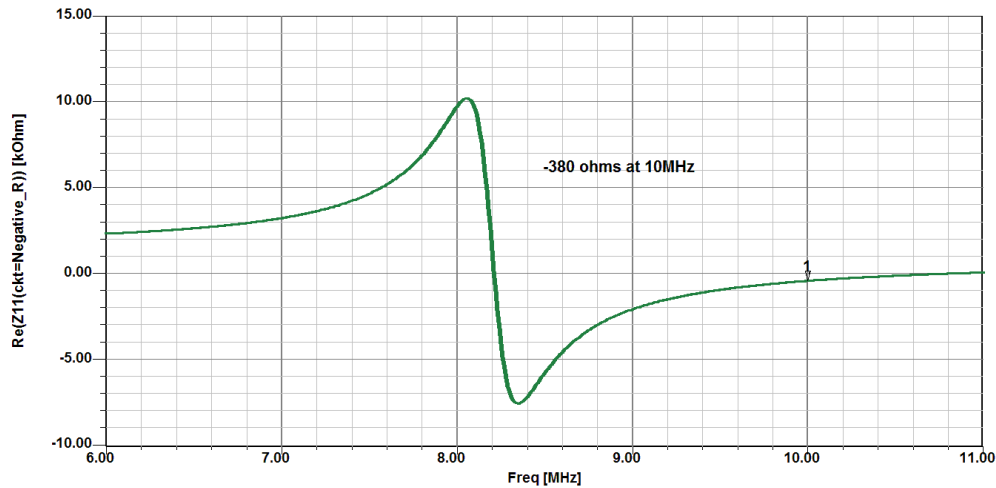


Figure 5-31: Linear analysis (of the circuit in Figure 5-22) showing the Real part of the negative impedance

5.7 A Discussion on some of the findings in this work - considering the 100 MHz case:

The 10 MHz crystal oscillators discussed so far are really secondary frequency standards. Other secondary frequency standards are Rubidium frequency standards synchronizing a 5 MHz or a 10 MHz crystal oscillator. Their frequency stability depends on parameters like temperature, air pressure and power supply variations.

Primary or absolute frequency standards are Cesium atomic frequency standard or Hydrogen masers. In the USA, NIST, Boulder Colorado has these [54].

The 100 MHz crystal oscillators are driven upto several mW dissipation and phase locked against the higher stability 10 MHz standard. The following block diagram (Figure 5-32) shows how this is done.

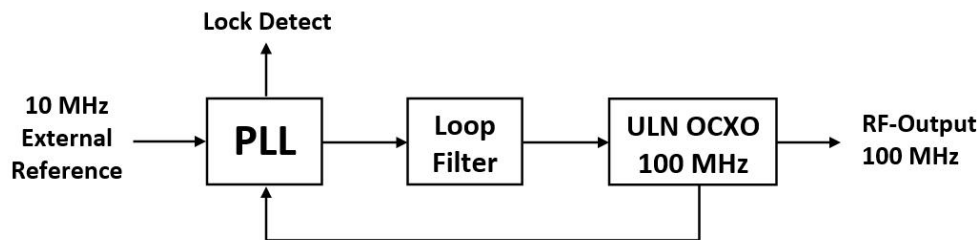


Figure 5-32: A simple Block Diagram showing the configuration to implement aging of the 100MHz and get phase noise of the 10 MHz [19]

The purpose of this dissertation is to design a very low noise 100 MHz crystal oscillator which can tolerate much higher crystal current. As a starting condition we consider the 10 MHz design and mathematically scale the mode-suppression circuit to 100 MHz. This again is based on the Colpitts approach and results in the following circuit (Figure 5-33a).

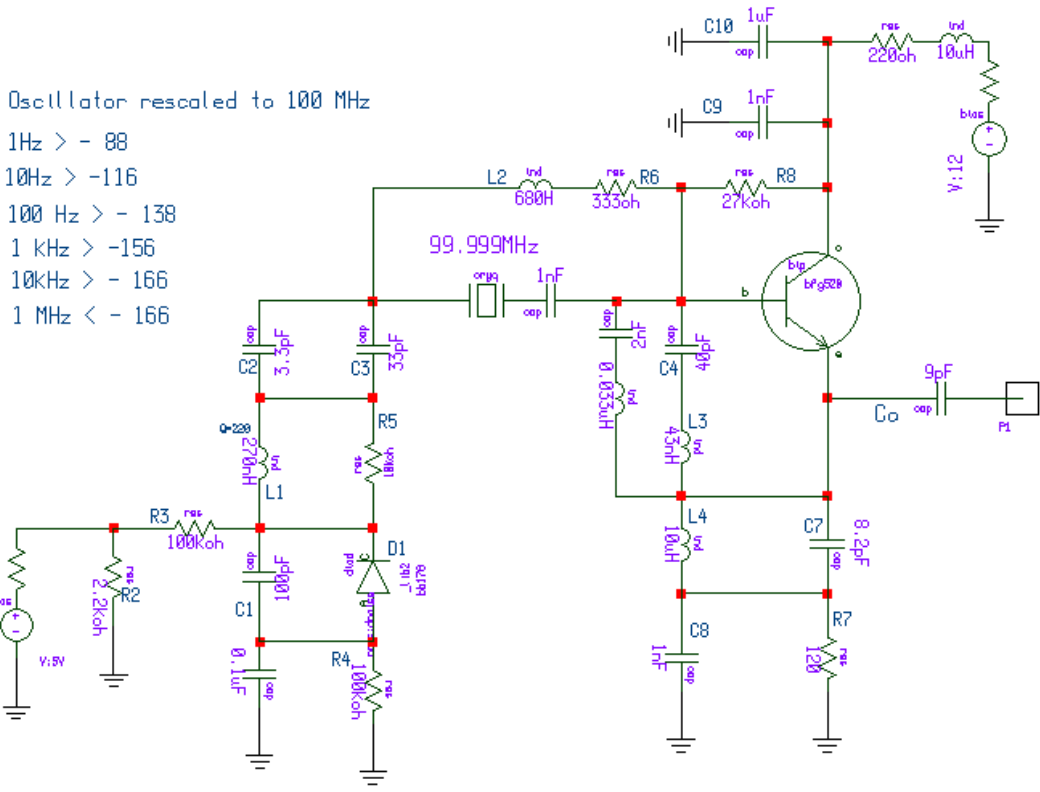


Figure 5-33a: Scaled to 100 MHz based on the 10 MHz HP10811A circuit [17]

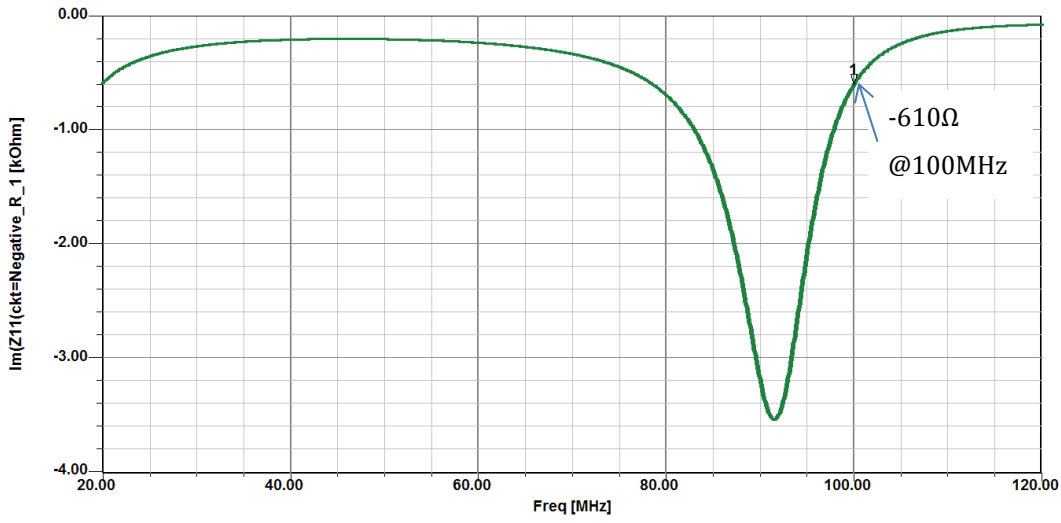


Figure 5-33b: Simulated imaginary part of the negative impedance $Im(Z_{11})$ of the circuit in Figure 5-33a

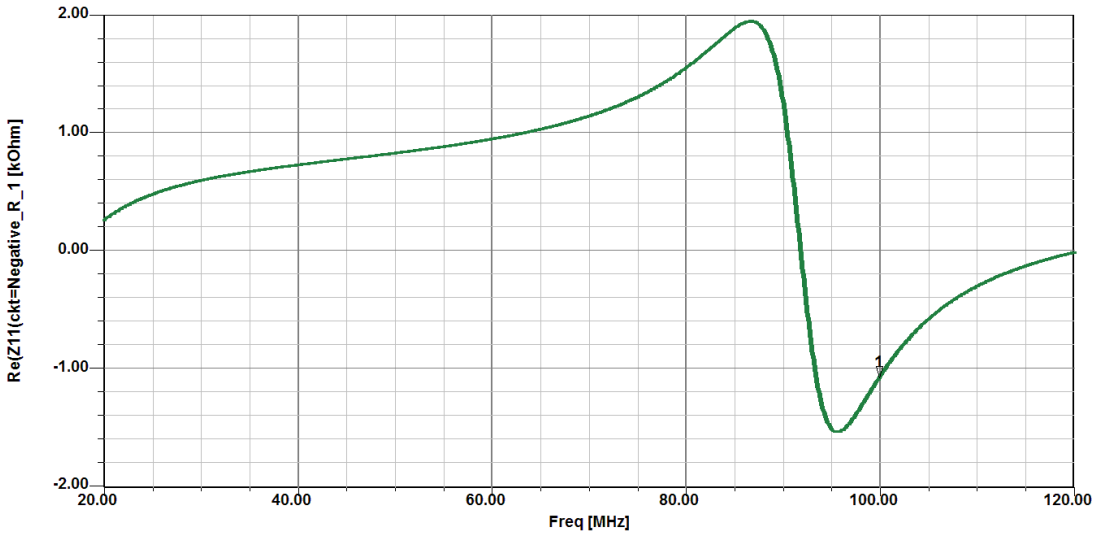


Figure 5-33c: Simulated real part of the negative impedance $Re(Z_{11})$ of the circuit in Figure 5-33a

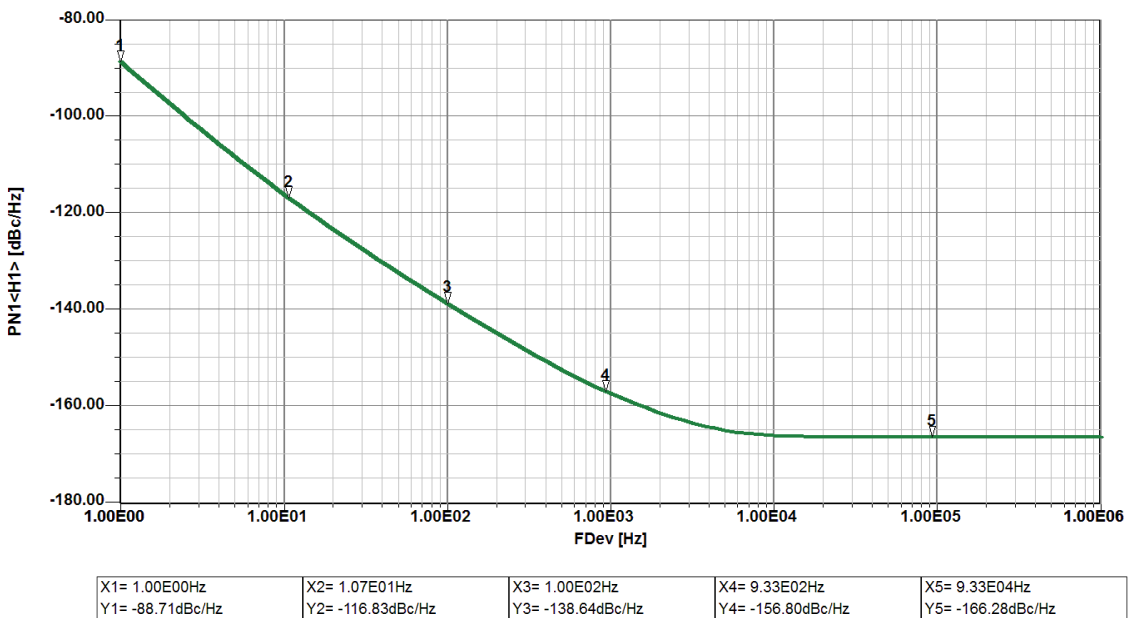


Figure 5-33d: Simulated phase noise of the circuit in Figure 5-33a

The CAD Simulation results are shown in Figure 5-33b, Figure 5-33c, and Figure 5-33d. Figure 5-34 shows the simulated results of the effect of different drive levels on the phase noise.

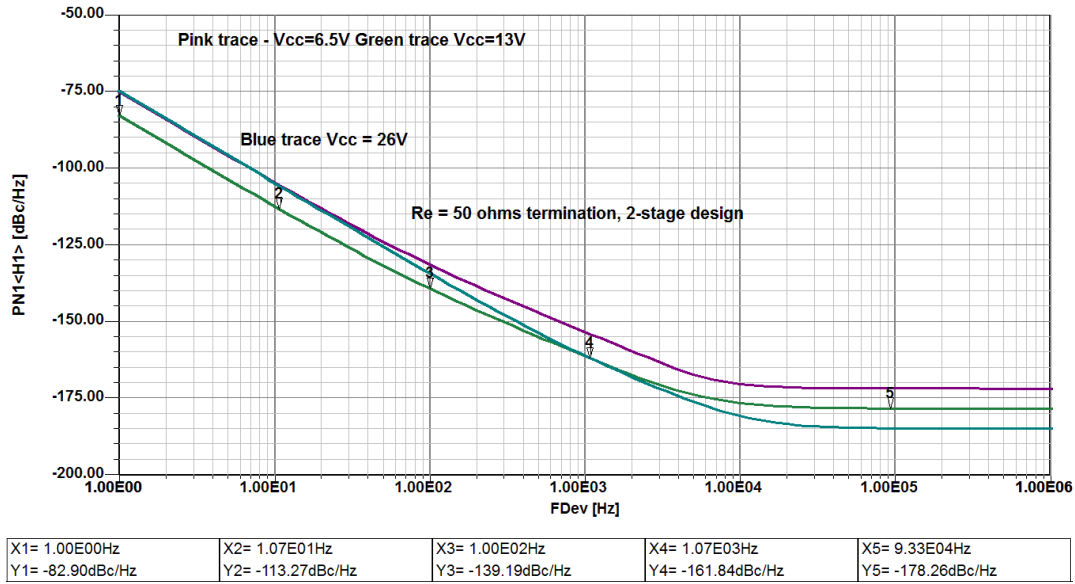


Figure 5-34: Effect of different drive levels on phase noise

This oscillator circuit (Figure 5-33a) is not the best or the state-of-the-art. The oscillator circuit discussed below in Figure 5-35 shows that, by adding another transistor, better results and more flexibility becomes possible. The CAD simulated phase noise is shown in Figure 5-36.

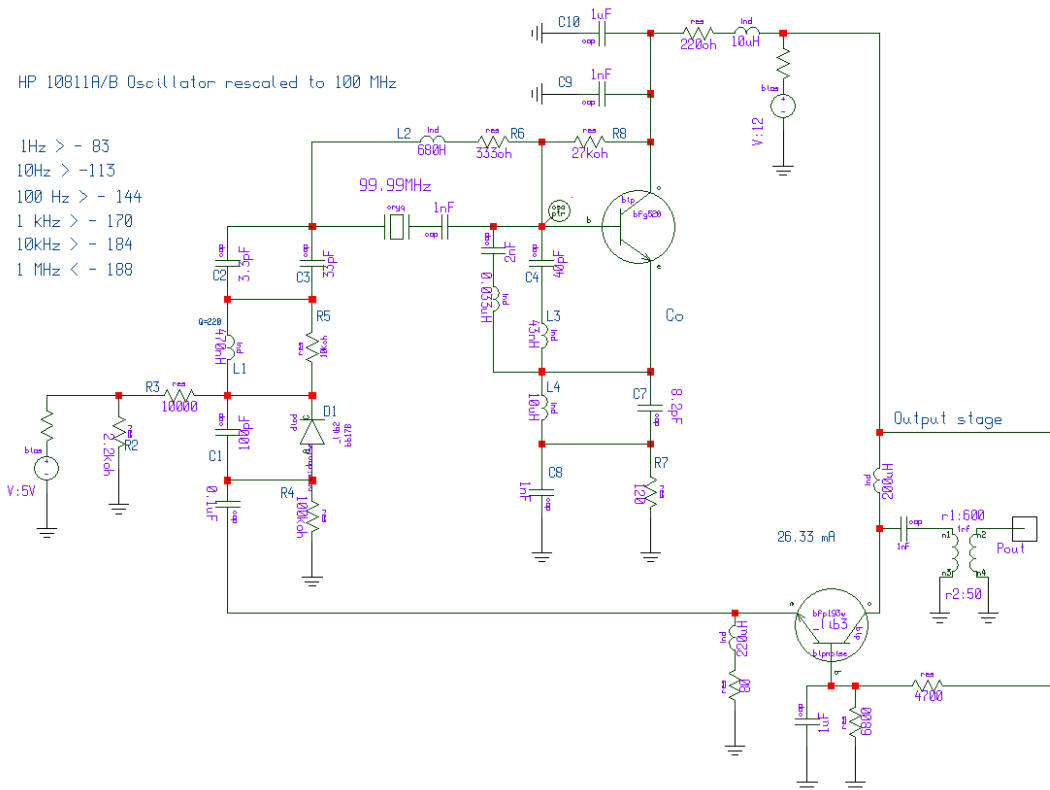


Figure 5-35: Schematic of the modified circuit based on Figure 5-33a for better phase noise performance

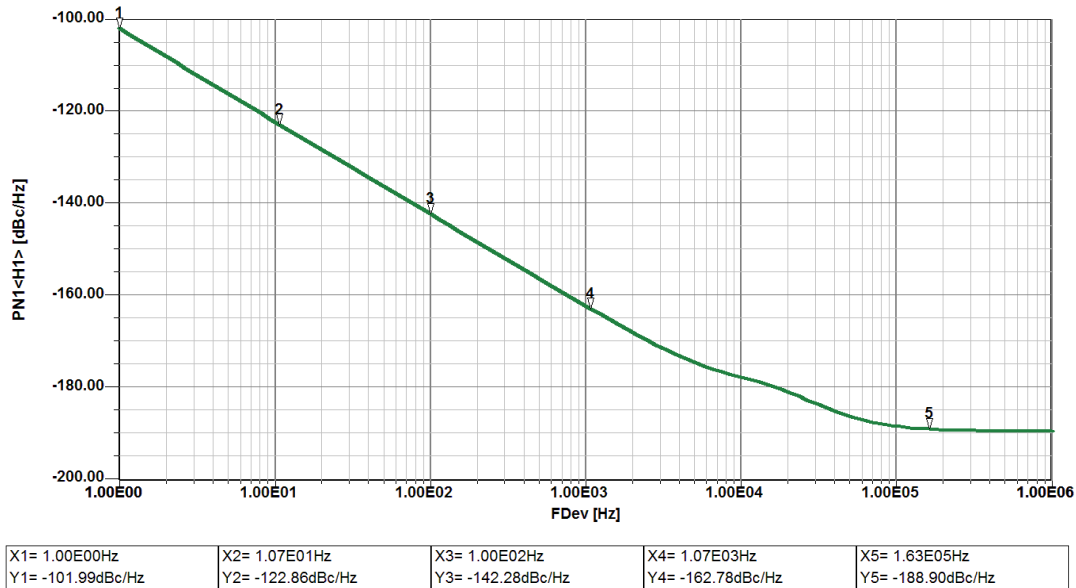


Figure 5-36: Simulated phase noise of the circuit in Figure 5-35

5.8 The Meissner circuit approach:

The Meissner oscillator can be derived by rotating the Colpitts oscillator.

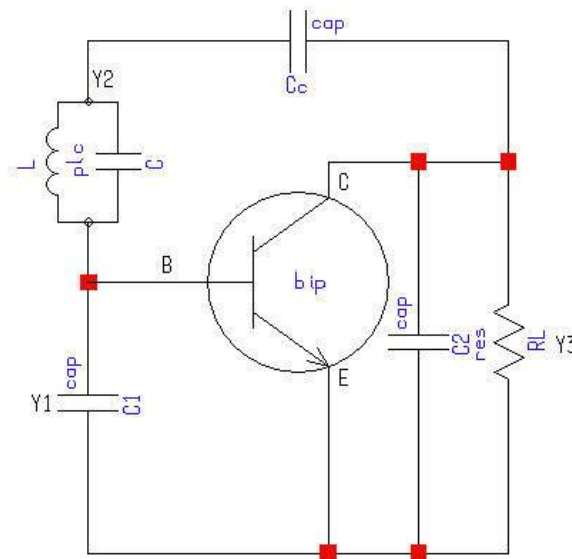


Figure 5-37: Meissner oscillator [9]

The Colpitts oscillator circuit shown in Figure 5-8 [9, Fig. 2-23] can be rotated to achieve what is seen in Figure 5-37 [9, Fig. 2-24], typically called as the Meissner oscillator in the literature. This means the emitter is at RF ground. C_1 is the familiar base-to-emitter capacitor and C_2 is the emitter-to-collector capacitor, where the collector now is RF-wise hot. In this case, the crystal again acts as an inductor. This circuit is also called as Clapp oscillator. It is defined that the inductor has a capacitor in series. The base-collector parallel circuit is now a series tuned circuit. The design

guidelines are the same as for the Colpitts oscillator. The advantage of this circuit is that the collector RF voltage is much higher and more output power is available.

By adding an additional transistor [7, Ch. 4], a larger degree of freedom is possible, as gain and phase can be adjusted independently. An example of such an oscillator showing the two-transistor design, for low frequency application is shown in Figure 5-38.

5.9 Two Transistor Design:

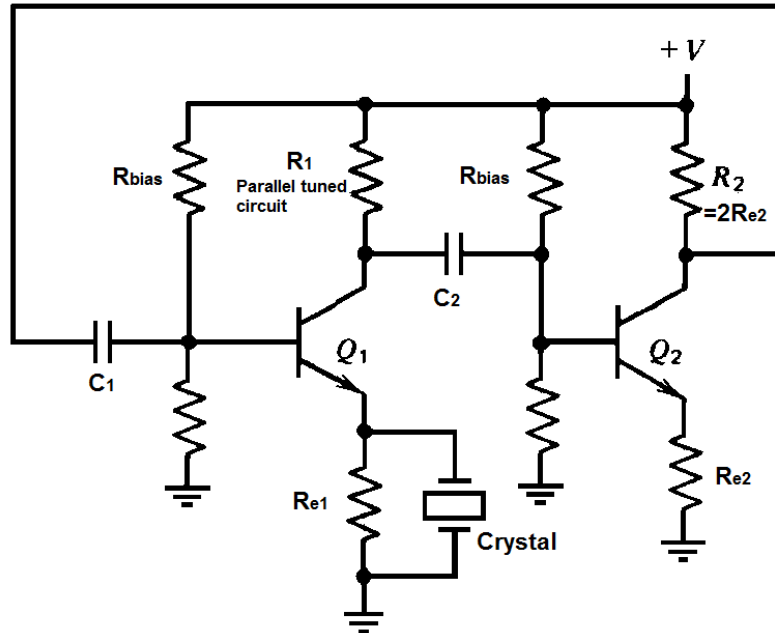


Figure 5-38: A typical representation of 2- transistor design topology for high performance crystal oscillator circuit [7]

The topology shown in Figure 5-38 is similar to the Driscoll circuit [2] where the output of the second transistor is fed to the base of the first transistor by 180° phase-shift. The second transistor automatically produces the feedback and phase shift [7].

The emitter-coupled series-resonant oscillator circuit based on [7] is modified to suit our 100 MHz crystal oscillator design. The bias resistor R_1 in the original circuit was $0.8 \times R_{e1}$.

From [7], the disadvantage of the circuit is that the waveforms vary with the circuit's stray capacitance, because loop gain is almost high enough to oscillate at any frequency. The modified circuit discussed here addresses this drawback using a mode-suppression mechanism circuit [3]-[4].

For low frequencies no tuned circuit is required. The advantage of this two-stage circuit is that the voltage gain can be determined by the ratio of the collector/emitter resistor of both the first and second transistor. Gain for the first transistor is R_1/R_{e1} and R_2/R_{e2} for the second transistor. This results in a voltage gain of 2 for both cases. The actual feedback can be set by the two coupling capacitors.

For high frequencies both the collector resistors have to be replaced by a parallel tuned circuit; at resonance the values have to be R_1 and R_2 .

As previously shown the RF energy is taken out via the crystal to the grounded base circuit, as seen in the simulation Figure 5-41.

5.9.1 Transistor Selection Criteria:

This circuit (Figure 5-38) is intended to be the final effort to build an ultra-low noise 100 MHz crystal oscillator and therefore the transistor selection is critical.

The transistor affects the noise from below 1 Hz of the carrier to about a 100 Hz. A good candidate is the BFG540 from Infineon. Figure 5-39 and Figure 5-40 show some relevant portions of the datasheet.

NXP Semiconductors			Product specification			
NPN 9 GHz wideband transistor			BFG540W BFG540W/X; BFG540W/XR			
QUICK REFERENCE DATA						
SYMBOL	PARAMETER	CONDITIONS	MIN.	TYP.	MAX.	UNIT
V_{CBO}	collector-base voltage	open emitter	–	–	20	V
V_{CES}	collector-emitter voltage	$R_{BE} = 0$	–	–	15	V
I_C	collector current (DC)		–	–	120	mA
P_{tot}	total power dissipation	$T_s \leq 85^\circ\text{C}$	–	–	500	mW
h_{FE}	DC current gain	$I_C = 40\text{ mA}; V_{CE} = 8\text{ V}$	100	120	250	
C_{re}	feedback capacitance	$I_C = 0; V_{CB} = 8\text{ V}; f = 1\text{ MHz}$	–	0.5	–	pF
f_T	transition frequency	$I_C = 40\text{ mA}; V_{CE} = 8\text{ V}; f = 1\text{ GHz}; T_{amb} = 25^\circ\text{C}$	–	9	–	GHz
G_{UM}	maximum unilateral power gain	$I_C = 40\text{ mA}; V_{CE} = 8\text{ V}; f = 900\text{ MHz}; T_{amb} = 25^\circ\text{C}$	–	16	–	dB
		$I_C = 40\text{ mA}; V_{CE} = 8\text{ V}; f = 2\text{ GHz}; T_{amb} = 25^\circ\text{C}$	–	10	–	dB
$ S_{21} ^2$	insertion power gain	$I_C = 40\text{ mA}; V_{CE} = 8\text{ V}; f = 900\text{ MHz}; T_{amb} = 25^\circ\text{C}$	14	15	–	dB
F	noise figure	$\Gamma_s = \Gamma_{opt}; I_C = 10\text{ mA}; V_{CE} = 8\text{ V}; f = 2\text{ GHz}$	–	2.1	–	dB
F	noise figure	$\Gamma_s = \Gamma_{opt}; I_C = 10\text{ mA}; V_{CE} = 8\text{ V}; f = 900\text{ MHz}$	–	1.3	1.8	dB
		$\Gamma_s = \Gamma_{opt}; I_C = 40\text{ mA}; V_{CE} = 8\text{ V}; f = 900\text{ MHz}$	–	1.9	2.4	dB
		$\Gamma_s = \Gamma_{opt}; I_C = 10\text{ mA}; V_{CE} = 8\text{ V}; f = 2\text{ GHz}$	–	2.1	–	dB

Figure 5-39: Portions of the datasheet of the transistor BFG540 [www.nxp.com]

This transistor is a good choice as the noise figure between 1mA and 20mA barely moves and it has enough gain. The I_{Cmax} is 120mA, which means the transistor is operating in a safe region.

Now, the chosen circuit is modified to fit the RF requirements, the new circuit is shown in Figure 5-41. The gain of the second stage is the $560\Omega/270\Omega \approx 2$, as already pointed out, and the RF choke parallel to the 560Ω provides the DC path. This second stage is a feedback arrangement and highly linear.

The intermodulation distortion information on the datasheet is not valid because of the emitter feedback.

The emitter resistor linearizes the circuit and reduces the AM-to-PM conversion associated with modulating flicker noise components on the carrier.

The first stage has a tuned circuit in the collector, which is necessary to suppress the lower modes of the 100 MHz crystal.

The feedback of the first stage is the collector resistor $150\Omega/70\Omega \approx 2$.

The open loop gain of the circuit therefore is 4. The advantage of this is that the DC operating point of the transistor does not affect the gain, **as the gain is due to the ratio of the 2 resistors.**

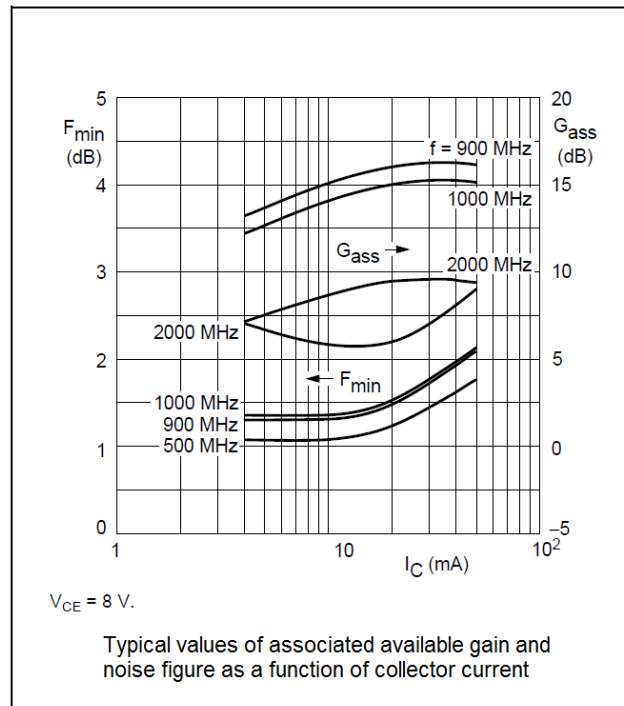


Figure 5-40: Portions of the datasheet of the transistor BFG540 showing typical values of associated available gain and noise figure as a function of collector current [www.nxp.com]

Using the circuit diagram proposed by Matthys [7], which was really a low frequency approach, operating in the few MHz range, and re-designing it for VHF, a 100 MHz design, the following is a proposed circuit shown in Figure 5-41.

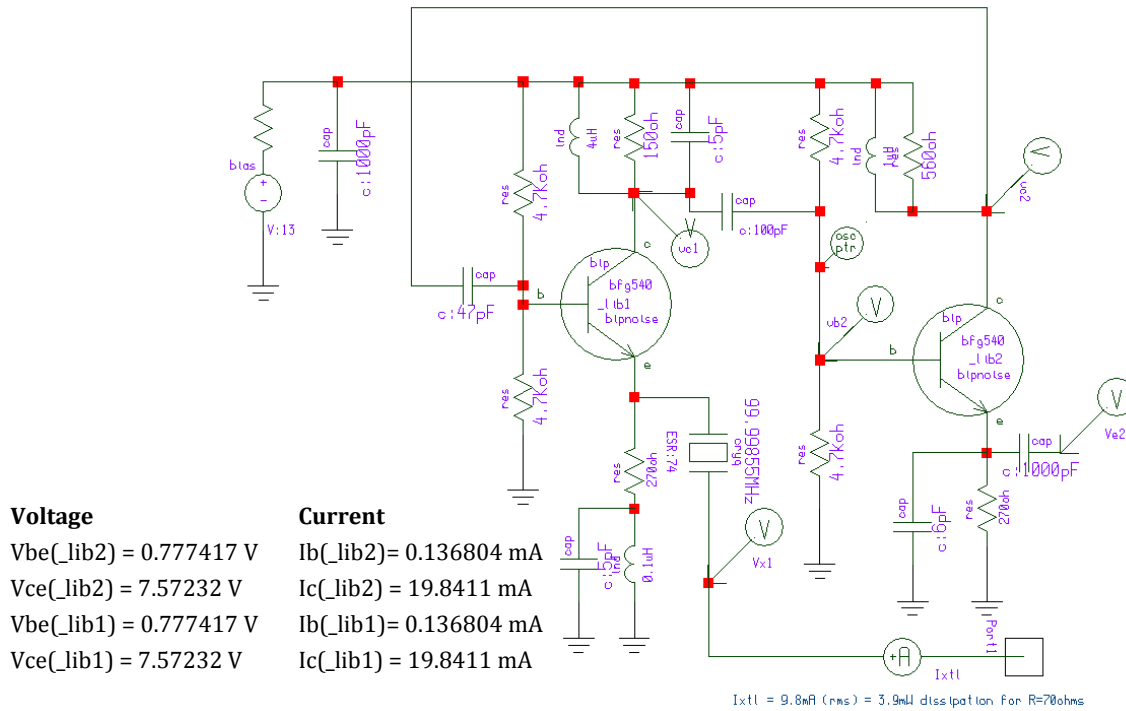


Figure 5-41: Schematic for simulation of the modified 100 MHz XO [7, Fig. 5.23]

5.10 What's new?

New is the concept that the transistor parameters which are typically bias dependent, have no more influence as the system gain is essentially determined by the ratio of two resistors. The degree of design freedom is definitely higher than the single transistor design. It was observed during measurement on the R&S FSWP, (that has the capability to show AM noise) that the AM-PM conversion (frequency modulation) is much improved because of the RF feedback.

The key requirements from the circuit are the phase noise which itself depends on the amplitude stabilization (transistor limiting) and the DC operating point.

The DC operating point for both the transistors was chosen to be $\approx 20\text{mA}$. The reason for this bias is that the noise figure is fairly constant upto this point (see Figure 5-40). The maximum DC current for this device from the datasheet, is 120mA, therefore the circuit is running in a safe operation mode.

When compared to the circuit of Matthys [7], the left transistor has a parallel tuned circuit and the second transistor has a phase shift circuit in the emitter, to meet the oscillation criteria.

The gain of this transistor is 520Ω (collector resistor)/ 270Ω (emitter resistor) ≈ 2 .

The left transistor circuit gain is 150Ω (collector resistor)/ 70Ω (crystal resistor) ≈ 2 . Therefore the loop gain is 4, voltage gain, or 12dB.

The power supply voltage was selected to be 13V, as this gave the best phase noise.

DC Bias:

$$19.8\text{mA} \times 270\Omega = 5.35\text{V} \text{ (} V_{e0} = \text{emitter to ground),}$$

$$5.35 + 0.77 = 6.1\text{V} \text{ (} V_b = \text{base to ground),}$$

$$V_b = 13 \times 4.7\text{k}\Omega / (4.7\text{k}\Omega + 4.7\text{k}\Omega) = 6.5\text{V}$$

The difference of about 400mV is due the DC-Offset

$$\frac{kT}{q} [\ln I_0(x)] mV \quad (\text{See table 5-1})$$

5.11 Limiting action:

An oscillator must include nonlinearity, for RF power limiting also called limiting action, which maintains the oscillation amplitude in stable equilibrium. Limiting means to reduce the effective transconductance or loop gain of an oscillator as the amplitude increases [35].

The following basic forms of limiting as given by Parzen [35] are as follows:

Self-limiting: amplifier producing the oscillations limits its gain by its own nonlinear action. Most oscillators that use a single transistor as the amplifier and limiter are then the self-limiting ones. This type of limiting does not provide as good short-term performance as oscillators with other limiter types, but surprisingly good performance is obtainable even with crystals operating at very low drive level.

External limiting: The limiting that is performed by auxiliary devices or circuits such as diodes, symmetrical clippers, and transistors. In two-transistor oscillators, one transistor is used specifically for limiting purposes, not applied here.

Automatic Level Control Limiting: The rectified output voltage is compared to a dc reference voltage. The difference voltage is then used to adjust the amplifier gain to the value demanded by the oscillator circuit. This is mostly used in crystal oscillators where the crystal power dissipation is limited to about 25 μ W for very low aging.

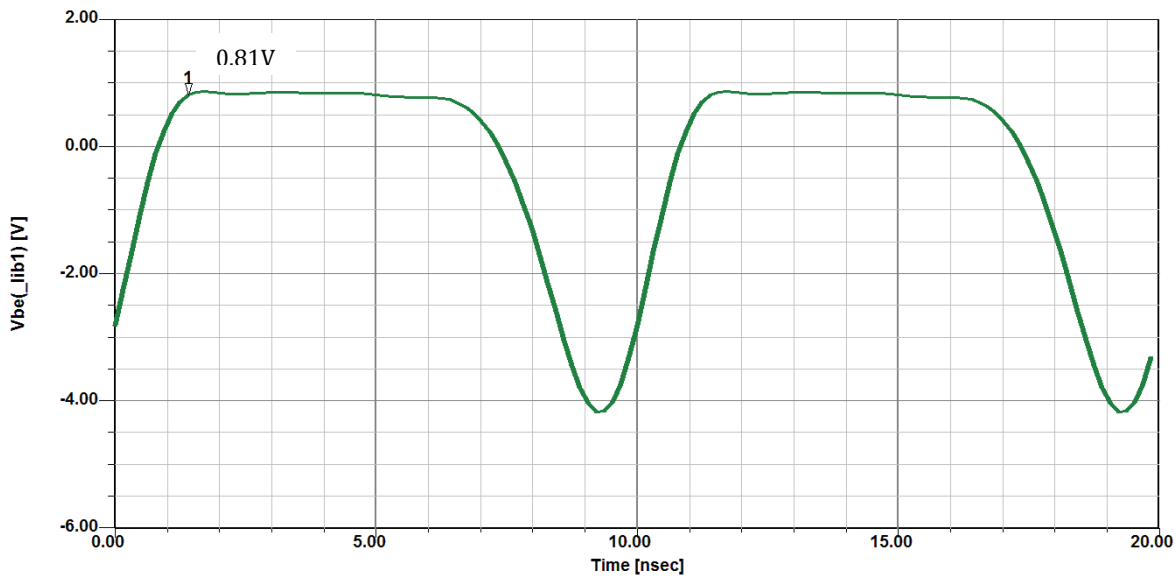


Figure 5-42: Shows the base-emitter junction of the first transistor limits the RF voltage

The biasing limits the RF voltage as seen the Figure 5-42 above. This results in a voltage clipping at the collector as seen in Figure 5-43.

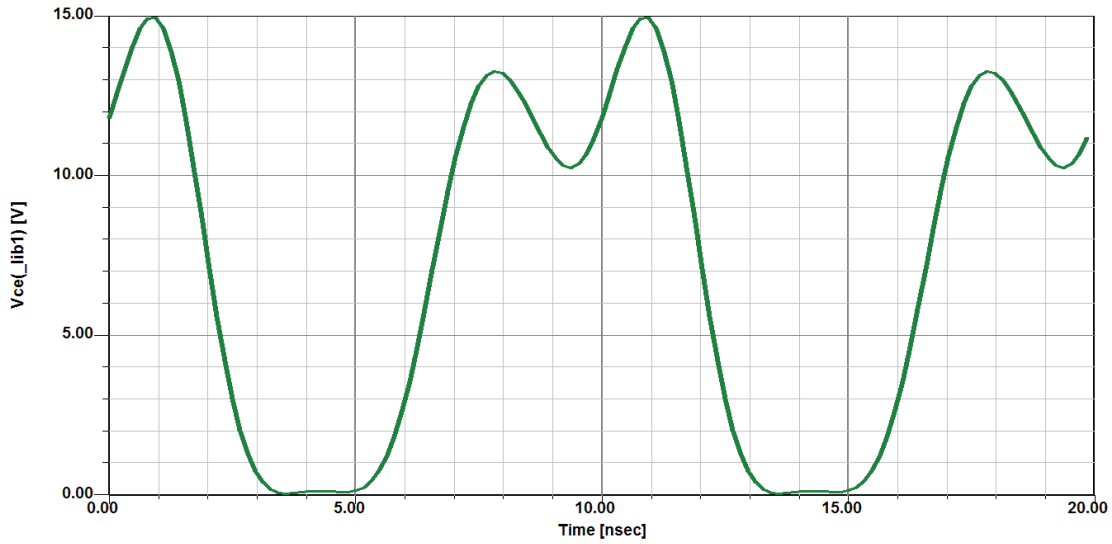


Figure 5-43: Collector voltage clipping

The second transistor mimics this as seen in Figure 5-44:

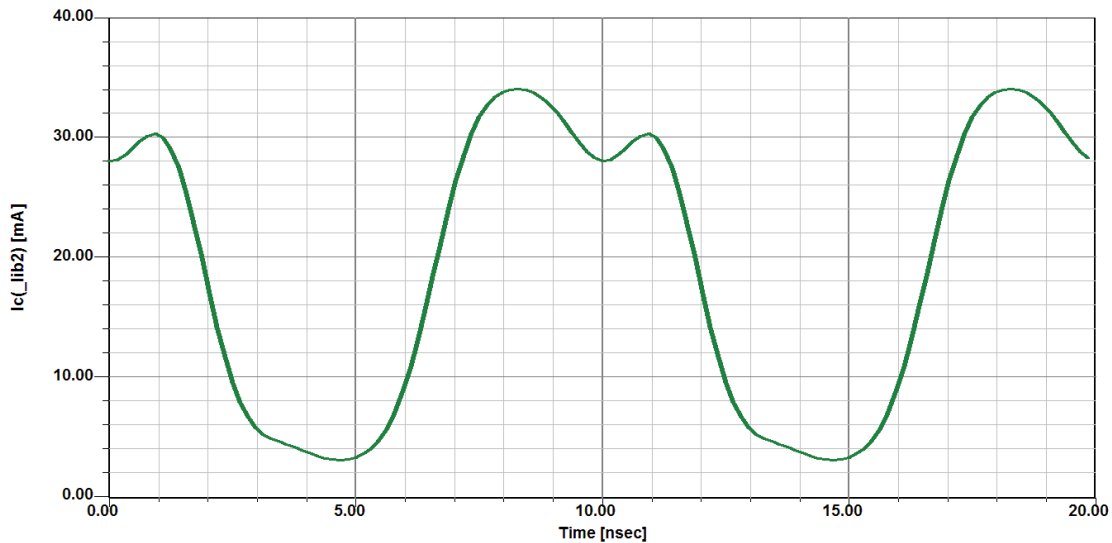


Figure 5-44: Collector current of the second transistor indicates the voltage limiting/clipping

It is important to note the 180° phase shift between the two transistors.

The output power is about 8dBm, as seen in Figure 5-45. The output power and isolation stage has not been added. The crystal, as wanted, acts as an excellent filter, and suppresses harmonics by almost 70dB.

The crystal holder is responsible for the small RF leakage,

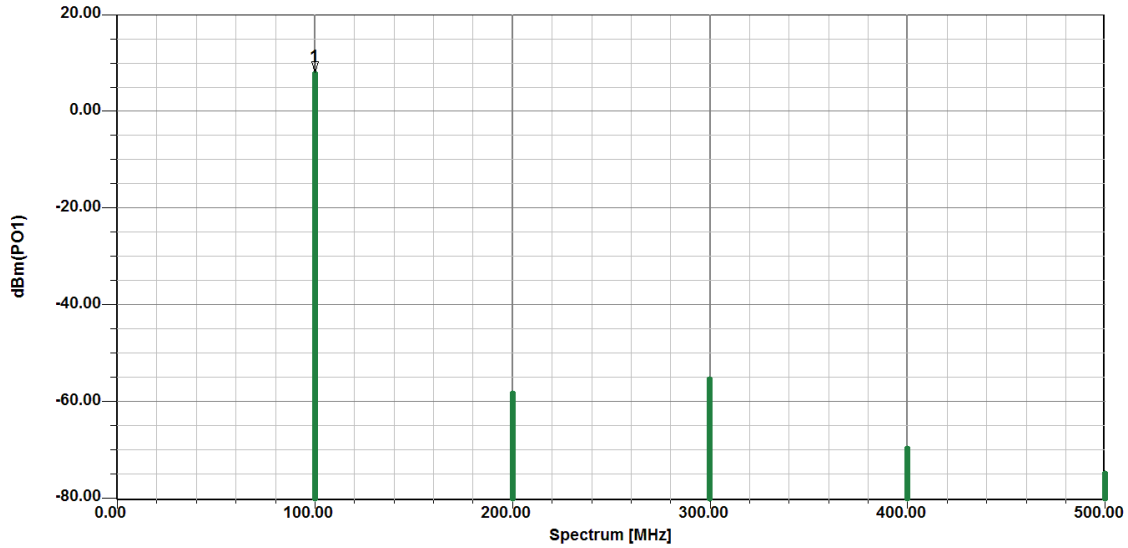


Figure 5-45: Simulated Output power

Final information needed is the phase noise, shown in Figure 5-46.

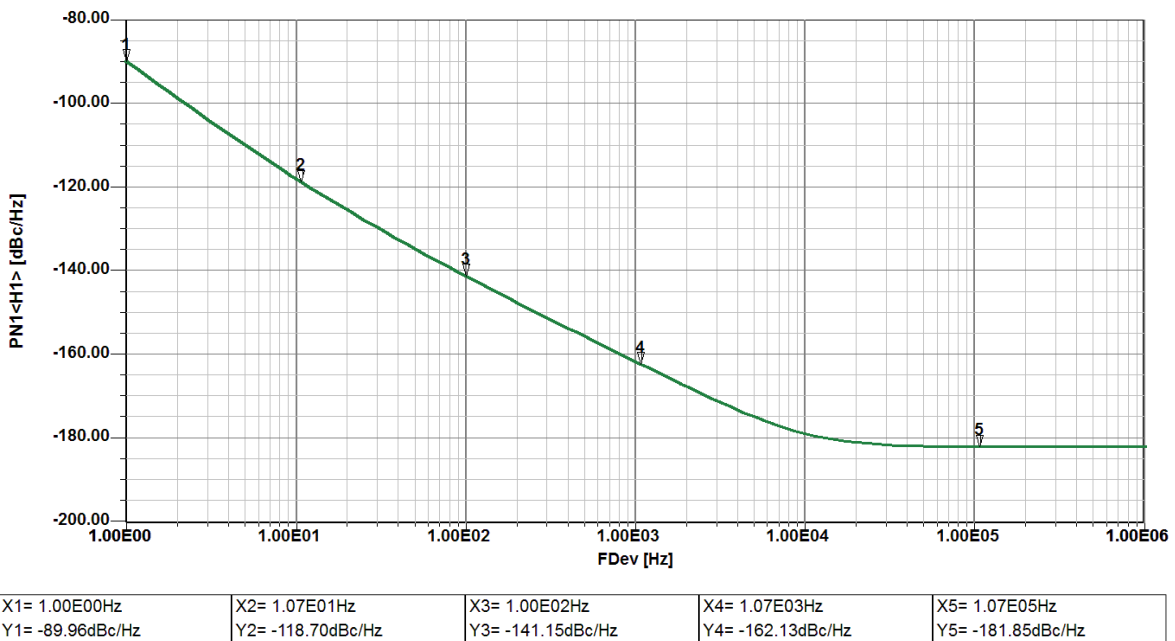


Figure 5-46: Simulated phase noise of the crystal oscillator of Figure 5-41

The Figure-of-merit points are the 100 Hz value for being -141dBc/Hz and the far out at 1 MHz offset is -182dBc/Hz. Another FoM for the crystal oscillator is the power consumption and the RF output power for which this phase noise is achieved.

As an example, the Wenzel golden citrine required 18dBm for about the same phase noise, a difference of about 10dBm, thus making this design far superior.

The complete two transistor design, with the grounded base amplifier is shown in the Figure 5-47. The circuit is optimized for phase noise performance and with the addition of the amplifier, gives

more output power without any significant effect on the phase noise performance. Figure 5-48a shows the CAD simulated phase noise performance and Figure 5-48b the simulated output power. Measured phase noise of the 100 MHz crystal oscillator is seen in Figure 5-49.

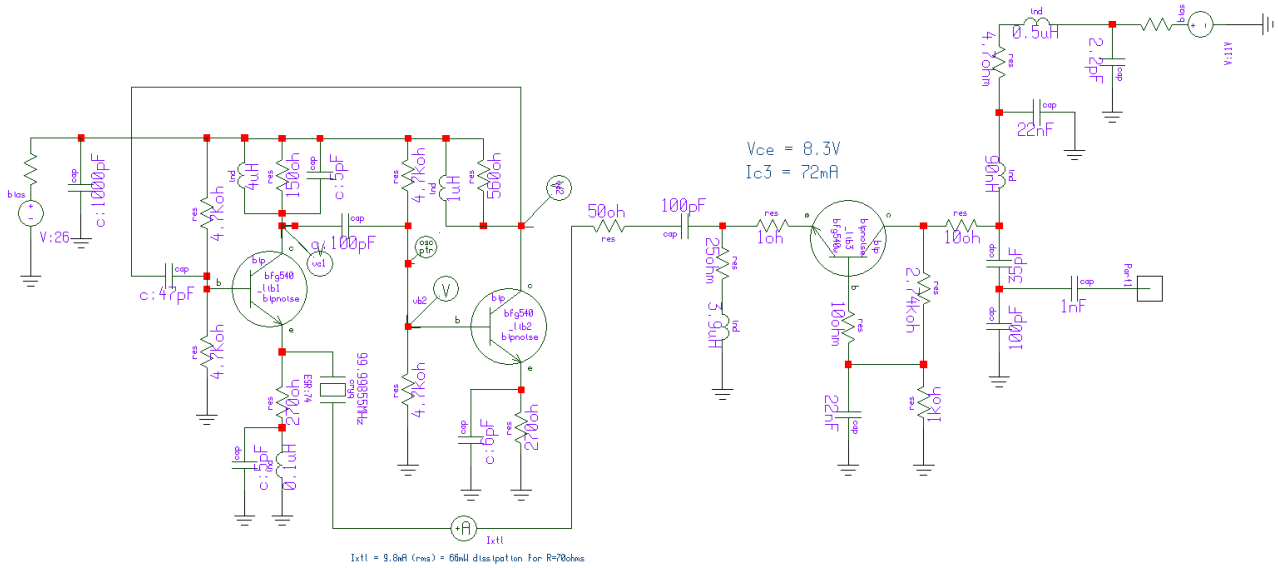


Figure 5-47: Two transistor design with grounded base amplifier

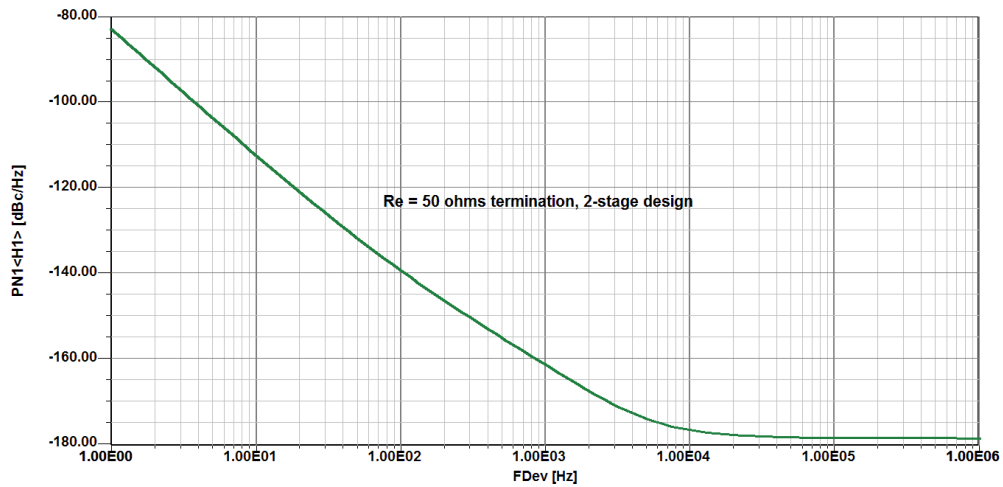


Figure 5-48a: Simulated phase noise performance of the circuit of Figure 5-47

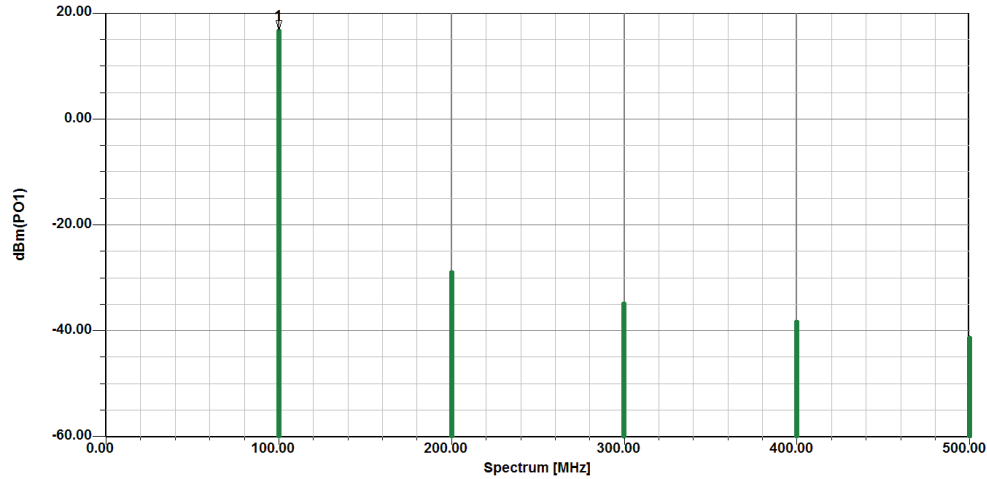


Figure 5-48b: Simulated output power of the circuit of Figure 5-47

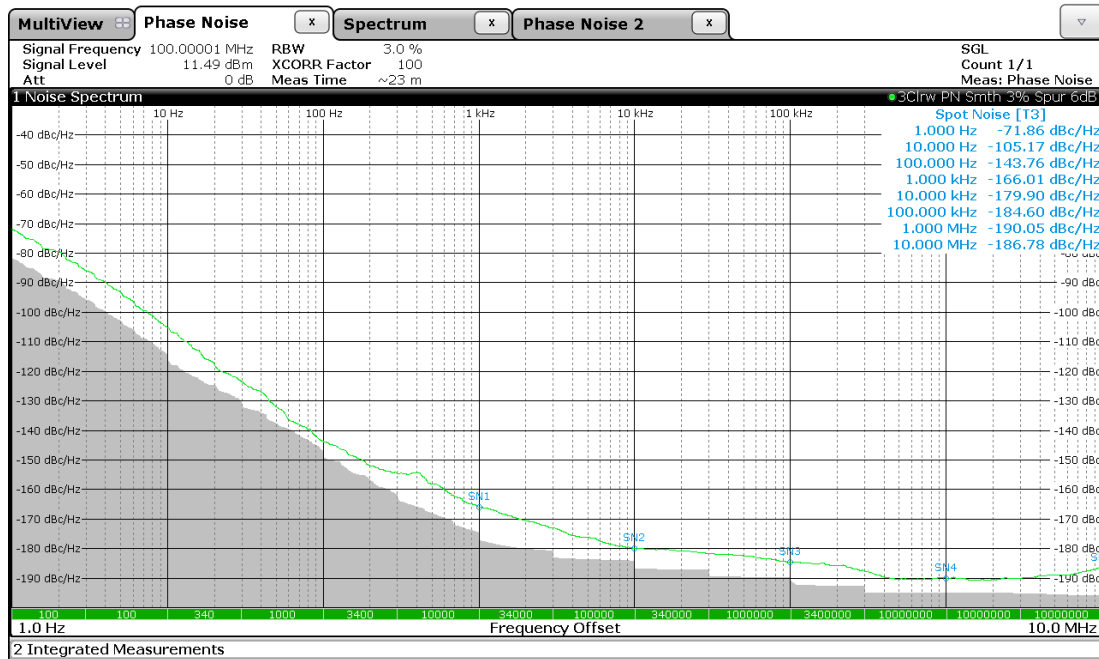


Figure 5-49: Measured phase noise of the 100 MHz crystal oscillator

5.12 Conclusion

This chapter started with a look into the past showing the beginning of crystal oscillators with Cady’s circuit. The general topology of the Colpitts oscillator and its simulation and theoretical analysis was presented. Factors that influence the selection of the transistor for such circuits, is an important aspect of the design and has been addressed in this chapter.

A finding that is unique to the best of author’s knowledge, and an outcome from this work is the relation between the ratio of the duty cycle and the conducting angle is within reasonable accuracy, as explained in section 5.3.1.

A CAD simulation and its results for the relevant parts of the prevalent HP10811A 10 MHz crystal oscillator circuit are shown and then the circuit is scaled for 100 MHz and simulation results are shown.

Improvement in phase noise may be possible with the use of the mode suppression circuit discussed in this chapter.

The two-transistor design which is the main circuit on which the final design is based is simulated and then the grounded base amplifier is used, with the crystal also serving as the filter in the emitter is then simulated. The measured results of the actual circuit measured on the R&S FSWP are shown. The simulation and measured show a close match. The improvement in the noise floor below kT is achieved due to the crystal filter, at the cost of 3-4 dBm of output power.

Table 5-4: This work so far as compared with a typical crystal oscillator on the market

Measured Data	Axtal 100M Hz XO (Fig. 5-21b)	This Work so far
Offset frequency	dBc/Hz	dBc/Hz
@ 1 Hz	-	-101
@ 10 Hz	-105	-122
@ 100 Hz	-137	-142
@ 1 kHz	-164	-163
@ 10 kHz	-174	-178
@ \geq 100 kHz	-175	-188

The table 5-4 summarizes the measured results compared with a sample unit of similar specification currently available on the market, with this work so far.

The reported experimental results were published as a part of this research work, and participated in the student design contest IMS 2016 [31], that was the recipient of the 1st place student project award. This is discussed in Chapter 7 and the measured results are presented.

Chapter 6: Phase Noise Measurement

This chapter is based on a research study of various methods of phase noise measurement done as a part of this work, and co-authored the “Focused Issue Feature” published in the Sept/Oct 2013 IEEE Microwave Magazine [24].

The customary goal for measuring phase noise in an R&D environment is to achieve the lowest measurement noise floor possible. As we shall see, this is not necessarily the best choice, depending on the signal source being measured. In a production environment, the objective is fast throughput for product phase noise performance testing. Again, this is best achieved by using a method that is appropriate for the source being measured [1]-[23].

There are some very capable general-purpose phase noise measurement instruments available on the market, including the Agilent-E5052B, Rohde & Schwarz-FSUP and FSWP, Holzworth-HA7402A, Noise XT-DCNTS, Anapico-APPH6000-IS, and OE Wave-PHENOM™. With the growing demand for improved dynamic range and lower noise floor, equipment companies are introducing general purpose phase noise analysis software driven tools for extracting far out (offset frequency > 1MHz) noise below the kT floor even though claims of -195 dBc/Hz or lower lack the practical utility.

Modern phase noise test equipment addresses these issues, but one must understand the limitations of measurement techniques so that a suitable method can be chosen. The Direct Spectrum Method, PLL method, delay line discriminator method, and cross-correlation method are frequently used to measure the oscillator phase noise. The first one is the simplest and has the biggest limitation. The last one requires the most complex measurement system but useful and can measure oscillator phase noise performance better than that of its reference oscillator [24].

6.1 Primary phase noise measurement techniques

Here we present the following primary phase noise measurement techniques, listed in the order of increasing precision based on [21][24][90]-[93]:

- 6.1.1 Direct Spectrum Technique
- 6.1.2 Frequency discriminator method
 - Heterodyne (digital) discriminator method
- 6.1.3 Phase detector techniques
 - (Reference source/PLL method)
- 6.1.4 Residual Method
- 6.1.5 Two channel cross-correlation technique

6.1.1 Direct Spectrum Technique

This is the simplest technique for making phase noise measurements. Using this technique, measurements are valid as long as the analyzer's phase noise is significantly lower than that of the device under test (DUT). Figure 6-1 shows the basic block diagram of a Direct Spectrum Measurement Technique. As shown in Figure 6-1, the signal from the device under test (DUT) is input into a spectrum/signal analyzer tuned to the DUT frequency, directly measuring the power spectral density of the oscillator in terms of $\mathcal{E}(f_m)$. Because the spectral density is measured with the carrier present, this method is limited by the spectrum/signal analyzer's dynamic range. Though this method may not be useful for measuring very close-in phase noise to a drifting carrier, it is convenient for qualitative quick evaluation on sources with relatively high noise. For practical application, the measurement is valid if the internal single sideband (SSB) phase noise of the

Spectrum/Signal analyzer at the offset of interest is lower than the noise of the DUT. It is therefore essential to know the internal phase noise of the analyzer we are using.

Because the spectrum/signal analyzer measures total noise power without differentiating amplitude noise from phase noise, the amplitude noise of the DUT must be significantly below its phase noise (typically 10 dB will suffice). This can be assured by first passing the DUT signal through a limiter. The presence of amplitude noise is suggested if the sidebands of the signal are not symmetrical. It is very important to adjust the noise measurement from the spectrum analyzer.

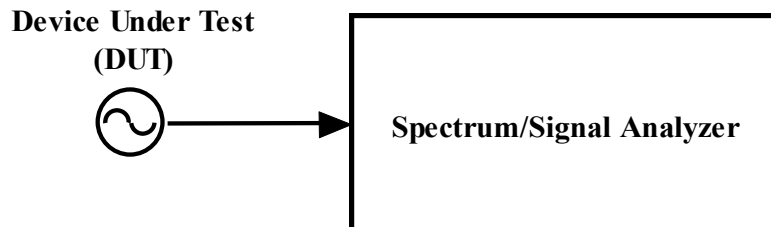


Figure 6-1: Direct Spectrum Measurement Technique [24]

All spectrum analyzers pass signals through a logarithmic amplifier (logamp) before detection and averaging. This distorts the noise waveform, essentially clipping it somewhat from the logarithmic transfer function. A 2.5dB error on the low side results from this average-of-log process. The details of this measurement techniques can be found in Agilent application note AN1303, "Spectrum and Signal Analyzer Measurements and Noise" for more details [21][24].

Advantages:

- Simple, frequency based measurement
- Fast measurement, for relatively noisy sources
- Relatively low cost
- Suitable for measurements of oscillators that drift slightly (less than the resolution filter bandwidth) during measurement.

Drawbacks:

- Not suitable for measuring oscillators with ultra-low phase noise performance, because the noise floor of the instrument is comparatively high.
- Not suitable for measuring the phase noise within 1 kHz of the carrier frequency, mostly because spectrum analyzers have their own noise properties that can degrade the measurement results.
- Limited measurement dynamic range
- One of the major drawbacks of the Direct Spectrum technique is its dynamic range limitation due to the presence of the carrier power. All of the following measurement techniques eliminate this limitation by separating the sideband noise from the carrier power, using a variety of techniques.

6.1.2 Frequency Discriminator Method

In the frequency discriminator method, the frequency fluctuations of the source are translated to low frequency voltage fluctuations, which can then be measured by a baseband analyzer. There are several common implementations of frequency discriminators including cavity resonators, RF bridges and a delay line.

Delay Line Frequency Discriminator:

The delay-line measurement system is often chosen for the flexibility in measuring a free-running oscillator between 1 GHz and 10 GHz. The delay-line technique has sufficient sensitivity to measure most microwave oscillators with loaded Q-factors of several hundred and does not require a second reference oscillator.

The expression of delay can be calculated as

$$t_{delay} = \sqrt{\epsilon_r} \left(\frac{l_{cable}}{c} \right) \quad (6-1)$$

Where ϵ_r is the relative dielectric constant in a coaxial cable.

The primary advantage of this method is that it can be used to measure noisy sources but on the other hand, it does not work with low noise sources, because the noise performance of this method is the limiting factor. Delay-line discriminators are limited by the loss of the delay-line due to the power requirements for the mixer. Using lower power than required will lead to degraded performance of the system. The noise floor depends on the length of the cable (delay), the longer the delay the lower the noise floor, but it will also mean higher losses and lower offset frequency. The highest usable offset frequency depends mostly on the length of the delay. There is a null at $f=1/t_{delay}$ offset frequency, and the recommendation is to use offset frequencies up to $f=1/(4t_{delay})$. With a 500ns delay, the usable offset frequency range is from 0 to 500 kHz.

As shown in Figure 6-2, the signal power from the DUT is split into two channels. The signal in one path is delayed relative to the signal in the other path. The delay line converts the frequency fluctuation to phase fluctuation. The mixer requires phase quadrature at its two inputs at the carrier frequency, which is achieved by either adjusting the delay line (not likely) or using a small phase shifter in the through-path. As shown in Figure 6-2, the mixer (acting as phase detector) converts the phase difference between the delayed and undelayed paths into a DC voltage related by the phase discriminator constant K_ϕ . The output of this frequency discriminator is then read on the baseband spectrum analyzer as frequency noise. This frequency noise is converted to phase noise using the well-known relationship between FM and PM, and reported as phase noise measurement [21][24].

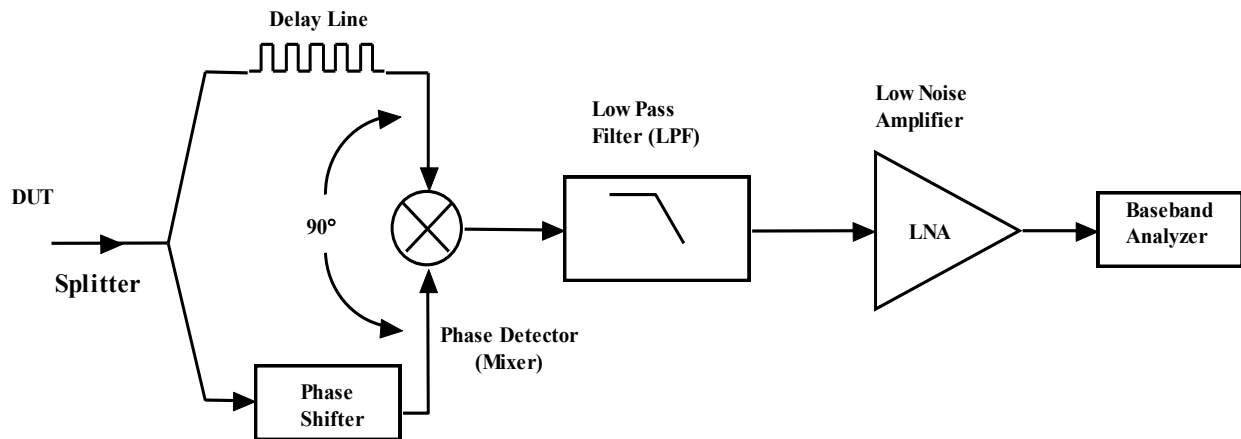


Figure 6-2: Shows the basic block diagram of frequency discriminator method (Courtesy: Agilent Company) [21]

The frequency fluctuations of the oscillator in terms of offset frequency f_m are related to the phase detector constant K_ϕ and the delay τ_d by [20]-[24]:

$$\Delta V(f_m) = [K_\phi 2\pi\tau_d] \Delta f(f_m) = K_d \Delta f(f_m) \quad (6-2)$$

Since frequency is the time rate change of phase we have:

$$S_{\phi}(f_m) = \frac{S_{\Delta f}(f_m)}{f_m^2} = \frac{\Delta f^2(f_m)}{f_m^2} \quad (6-3)$$

The voltage output is measured as a double sideband voltage spectral density $S_v(f_m)$.

From (6-2) and (6-3), phase noise $S_{\phi}(f_m)$ is related to the measured $S_v(f_m)$ by:

$$S_{\phi}(f_m) = \frac{\Delta V^2(f_m)}{K_d^2 f_m^2} = \frac{S_v(f_m)}{K_d^2 f_m^2} \quad (6-4)$$

The single sideband phase noise is given by

$$\mathcal{L}_{\phi}(f_m) = \frac{S_v(f_m)}{2K_d^2 f_m^2} \quad (6-5)$$

$$\mathcal{L}_{\phi}(f_m)[dBc/Hz] = S_v(f_m) - 3 - 20 \log(K_d) - 20 \log(f_m) \quad (6-6)$$

With a single calibration of the mixer as a phase detector, K_{ϕ} and known delay τ_d , the phase noise of an oscillator can be measured using FFT (baseband) analyzer. The phase discriminator constant K_{ϕ} is in V/rad and is determined by measuring the DC output voltage change of a mixer while in quadrature (nominally 0V DC) for a known phase change in one branch of discriminator. The value of K_d is dependent upon the RF input power of the mixer that in turn is directly proportional to the noise floor shown in Figure 6-3 [20]-[24].

Using Z-parameters the sensitivity of the delay line discriminator can be determined first by introducing the Q-factor defined with respect to the phase of the open-loop transfer function $\phi(\omega)$ at the resonance of parallel RLC circuit [21][24][90]-[93]:

$$\phi(j\omega) = \tan^{-1} \frac{\text{Imag}(Z(j\omega))}{\text{Real}(Z(j\omega))} \quad (6-7)$$

$$Q = \frac{1}{R} \sqrt{\frac{L}{C}} = \frac{\omega \delta_{\phi}}{2\delta\omega} \quad (6-8)$$

A typical coaxial delay-line exhibits a linear phase relation with frequency across the usable bandwidth of the transmission line.

The linear phase relationship in a coaxial line to the derivative of the phase change in a resonator results in an effective Q, Q_E for a transmission line with time delay τ_d :

$$Q_E = \pi f_0 \tau_d \quad (6-9)$$

From (6-8), the effective Q-factor increases linearly with both delay line length and frequency of operation. Using Q_E as the Q-factor in the Leeson's equation and using an approximate mixer noise floor of -175 dBc.

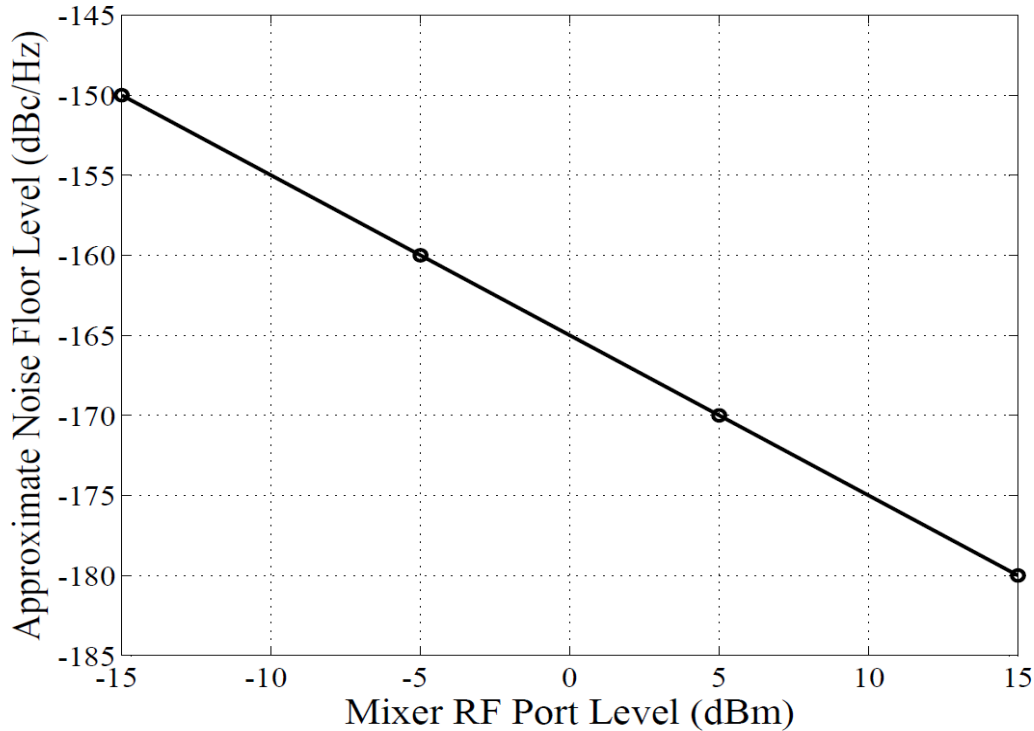


Figure 6-3: The ideal phase detector sensitivity in terms of RF power (assuming LO power is great than RF) and phase detector constant K_{ϕ} . The noise floor sensitivity is 1:1 to mixer power input [90]

Advantages:

- Better Sensitivity than Direct Spectrum Methods
- Good for free running sources such as LC oscillators or cavity oscillators
- Appropriate when the DUT is a relatively noisy source with high-level, low rate phase noise or high close-in spurious sideband

Drawbacks:

- Significantly less sensitivity than phase detector methods
- A longer delay line will improve the sensitivity but the insertion loss of the delay line may exceed the source power available and cancel any further improvement.
- In addition, longer delay lines limit the maximum offset frequency that can be measured. This method is best used for free running sources such as LC oscillators or cavity oscillators, although the frequency discriminator method degrades the measurement sensitivity, particularly at close to the carrier frequency.

Heterodyne (Digital) Discriminator method

As shown in Figure 6-4, the heterodyne (digital) discriminator method is a modified version of the analog delay line discriminator method and can measure the relatively large phase noise of unstable signal sources and oscillators.

Unlike the analog discriminator method, here the input signal is down-converted to a fixed intermediate frequency f_{if} using a separate local oscillator. The local oscillator is frequency locked to the input signal. Working at a fixed frequency, the frequency discriminator does not need re-connection of various analog delay lines at any frequency. This method allows wider phase noise

measurement ranges as compared to the PLL method. This option is available in in latest commercial phase noise measurement equipments (Agilent E5052B, R&S FSUP).

Advantages:

- Offers easy and accurate AM noise measurements (by setting the delay time to zero) with the same setup and RF port connection as the phase noise measurement
- Frequency demodulation can be implemented digitally

Drawbacks:

- Dynamic range of Phase Noise measurement is further limited by the additional scaling amplifier and ADCs.

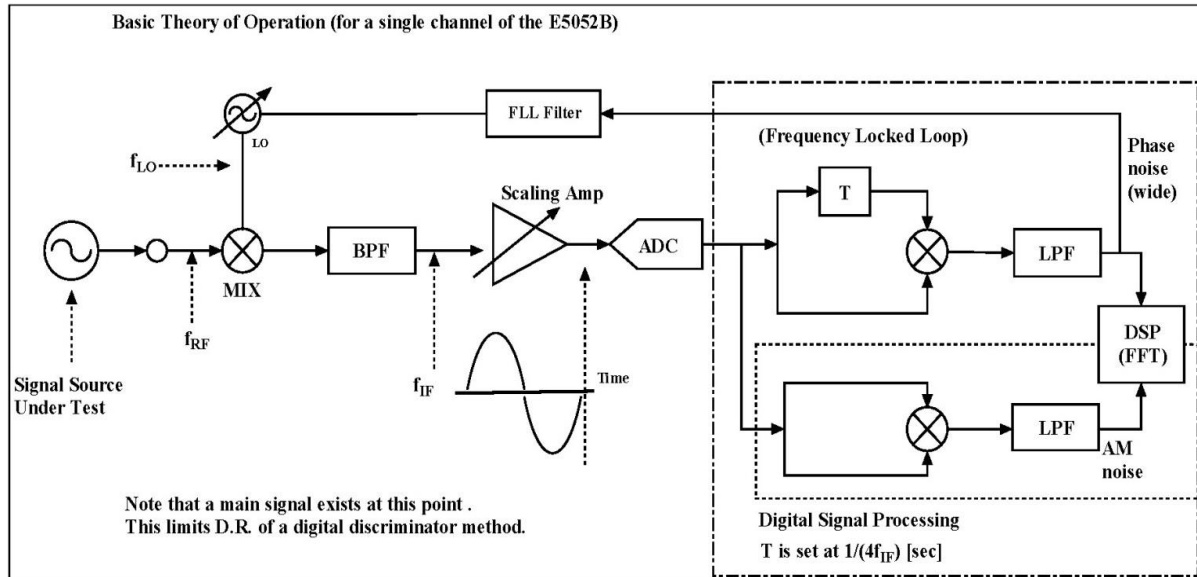


Figure 6-4: Basic block diagram of heterodyne (digital) discriminator method (Courtesy: Agilent) [91]

6.1.3 Phase Detector Technique

Figure 6-5 shows the basic concept for the phase detector technique. The phase detector method measures voltage fluctuations directly proportional to the combined phase fluctuations of the two input sources. To separate phase noise from amplitude noise, a phase detector (PD) is required. The (PD) converts the phase difference of the two input signals into a voltage at the output of the detector. When the phase difference between the two input signals is set to 90° (e.g. at quadrature), the nominal output voltage is zero volts and sensitivity to AM noise is minimized. Any phase fluctuation from quadrature results in voltage fluctuation at the output. This method has a very low noise floor and therefore has a very good measurement dynamic range.

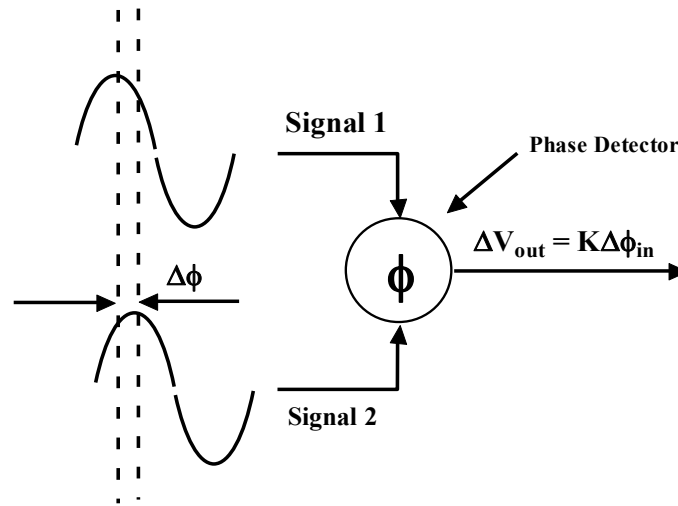


Figure 6-5: Basic concept of Phase detector techniques [21]

Reference Source/PLL Method

Figure 6-6 shows the basic block diagram of the phase detector method using reference source/PLL techniques. The basis of this method is to use a phase lock loop (PLL) in conjunction with a double balanced mixer (DBM) used for the phase detector. The PLL compares the phases of two input signals and generates a third signal which is used to steer one of the input signals into phase quadrature with the other. When the phase of the input signals are aligned, the loop is said to be locked and the nominal output from the phase detector is zero. This voltage varies a little due to phase noise on the input signals. The noise present at the output of the mixer includes phase noise of both signals. If the noise from the reference oscillator is more than 20 dB lower than the noise from DUT, the main contributor for phase noise is the DUT.

As shown in Figure 6-6, two sources, one from the DUT and the other from the reference source, provide inputs to the mixer. Again the reference source is controlled such that it follows the DUT at the same carrier frequency (f_c) and in phase quadrature (90° out of phase) to null out the carrier power. The mixer sum frequency ($2f_c$) is filtered out by the low pass filter (LPF), and the mixer difference frequency is 0 Hz (dc) with an average voltage output of 0 V when locked. The DC voltage fluctuations are directly proportional to the combined phase noise of the two sources. The noise signal is amplified using a low noise amplifier (LNA) and measured using a spectrum analyzer.

The advantage of this method is broadband measurement capability for both fixed frequency and tunable oscillators. With only a few different double balanced mixers and suitable reference oscillators, noise on signals from 1 MHz to several tens of GHz can be measured. If the DUT is a tunable oscillator, the reference oscillator will then be a free running one and the DUT would be controlled with the PLL, and need a suitable PLL amplifier after the low pass filter (LPF). The limitation of this method is that it is difficult to determine the contribution of noise, i.e. which part of the noise comes from the reference and which from the DUT. Nevertheless, this problem is true for most measurement systems.

Usually, if the phase noise levels of the two signals are not that far from each other, a correction factor ($P_{correction}$) from 0 to 3dB is subtracted from the measured result, where the highest number is used when the noise levels are equal [83]-[86]. The expression of the correction factor is given by [91]

$$P_{correction} = 10 \log_{10} \left(1 + 10^{-\frac{\Delta P}{10}} \right) \quad (6-10)$$

Where ΔP is the difference between the noises of the reference and the DUT in dB, Table 6-1 shows the correction factors for different noise level differences.

Table 6-1: Correction factor if the phase noise of the reference oscillator is near the phase noise of DUT

$\Delta P/\text{Db}$	0	2	4	6	8	10	15	20
$P_{\text{Correction}}/\text{dB}$	3	2.12	1.46	0.97	0.64	0.4	0.14	0.04

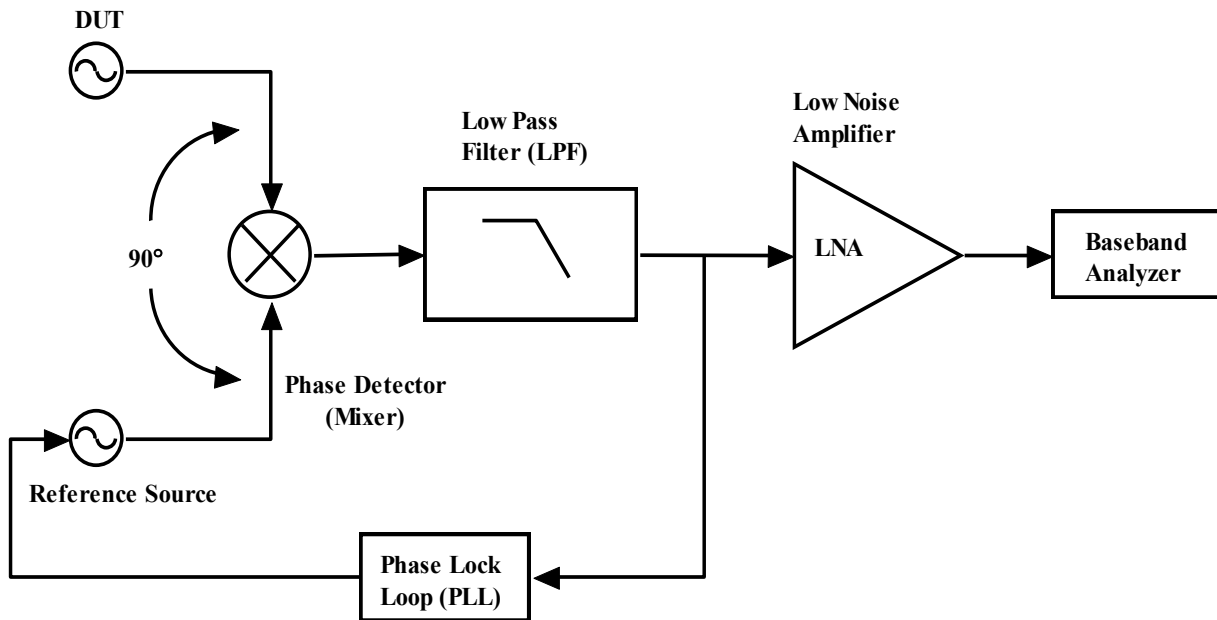


Figure 6-6: Shows the basic block diagram Phase Detector Method using reference source/PLL techniques). Small fluctuations from nominal voltages are equivalent to phase variations. The phase lock loop keeps two signals in quadrature, which cancels carriers and converts phase noise to fluctuating DC voltage (Courtesy of Agilent Technologies) [21][24]

This method exhibits promising noise floor but the performance is dependent on DBM and reference source characteristics. The selection of a mixer as a phase detector is critical to the overall system performance.

Choice of DBM as Phase Detector:

Figure 6-7 exhibits typical DBM phase detector response curve, where V_{IF} varies as the cosine of the phase difference $\Delta\phi$ between LO and RF signals [90].

As shown in Figure 6-7, phase detector response (V_{IF}) is reasonably linear in the region $\Delta\phi$ where phase detector sensitivity ($\frac{\partial V_{IF}}{\partial \phi}$) is maximum, represented by

$$\Delta\phi = (\phi_{LO} - \phi_{RF}) = \left(\frac{\pi}{2} + \delta\phi\right) \tag{6-11}$$

The phase detector output $V_{IF}(t)$ is given by [89][90]

$$V_{IF}(t) = \pm V \cos[(\omega_R - \omega_L)t + \Delta\phi(t) + \pi] \tag{6-12}$$

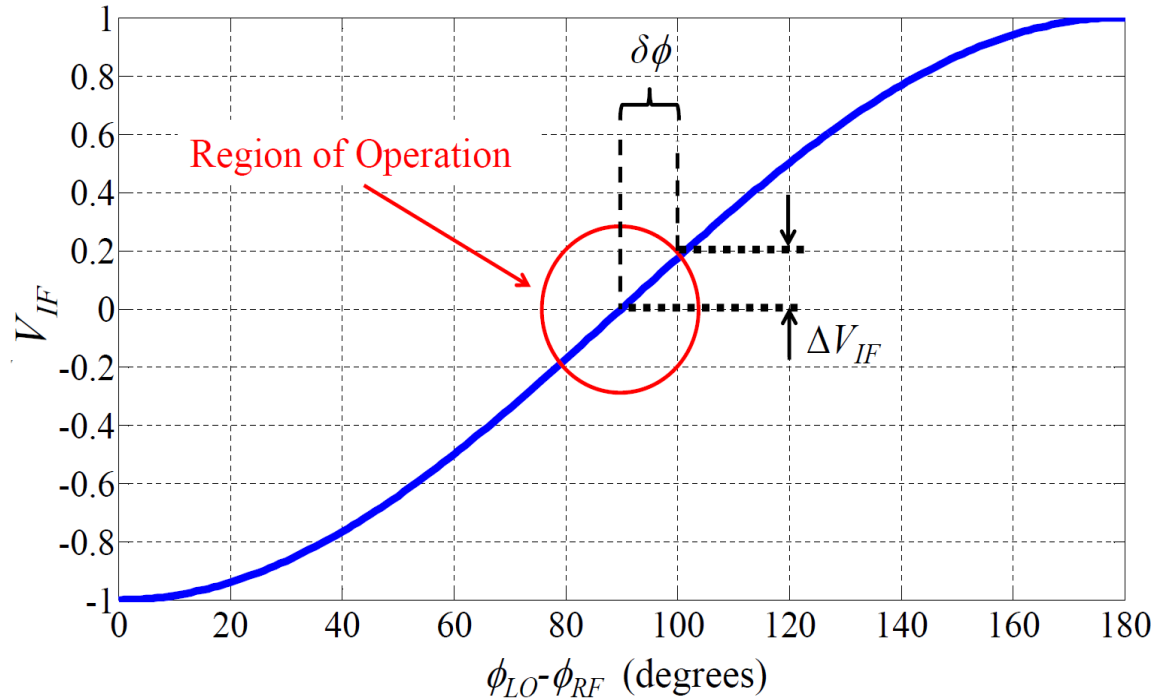


Figure 6-7: Shows the response of DBM as a phase detector varies as $\text{Cos}(\Delta\theta + \pi)$, (V_{IF}) is reasonably linear in the region ($\Delta\theta = \frac{\pi}{2} + \delta\theta$) [90]

For mixer's two input signals are at the same frequency, $\omega_R = \omega_L$ and 90° out of phase, $V_{IF}(t)$ is

$$\Delta V_{IF}(t) = \pm V \sin \delta\theta(t) \quad (6-13)$$

where V is the peak amplitude (at $\Delta\theta = 0$ or π), $\Delta V_{IF}(t)$ is the instantaneous voltage fluctuations around DC, and $\delta\theta(t)$ is the instantaneous phase fluctuation.

For $\delta\theta(t) \ll 1 \text{ rad}$, $\sin(\delta\theta(t)) \simeq \delta\theta(t)$, which describes a linear response region, the phase detector sensitivity varies linearly with maximum output voltage as

$$\Delta V_{IF}(t) = V \delta\theta = K_{\theta} \delta\theta \quad (6-14)$$

where, K_{θ} is the phase detector gain constant (volts/radian), equal to the slope of the mixer sine wave output at the zero crossing.

Choice of Reference Sources:

The other critical component of the phase detector method is the reference source. As discussed in the Direct Spectrum technique section, a spectrum analyzer measures the sum of noise from both sources. Therefore, the reference source must have lower phase noise than device under test, DUT. For practical purposes 10 dB margin is sufficient to ensure correct measurements within reasonable degree of accuracy. When a reference source with lower phase noise is unavailable then it is appropriate to use a source with comparable phase noise to the DUT. In this case, each source contributes equally to the total noise and 3-dB subtracted from the measured value.

Advantages:

- Excellent sensitivity for measuring low phase noise levels
- Wide signal frequency range
- Wide offset frequency range (0.01 Hz to 100 MHz)
- Rejects AM noise
- Frequency tracks slowly drifting sources.

Drawbacks:

- Requires a very clean reference source that is electronically tunable,
- Measurement frequency bandwidth matched to the tuning range of the reference sources.
- Locking PLL bandwidth is very narrow, < 10% of the minimum offset frequency used in the measurement.
- Narrow PLL bandwidth cannot track a noisy source.
- Expensive and complex

In conclusion, the phase detector method has excellent system sensitivity, but on the other hand its complexity (PLL and two oscillators are required) must be handled with care.

6.1.4 Residual method

The methods shown thus far can be used to measure only oscillators. There are some methods for measuring 2-port devices, and the residual method is one of them. It can be used for example to measure amplifiers, mixers, cables, and filters.

As shown in Figure 6-8, the output of a reference source is split with a power splitter. One branch is connected through the DUT to the mixer and the other branch through a phase shifter to the mixer. The phase shifter is adjusted until the phases are in quadrature, and the output of the mixer is measured with a spectrum analyzer. Because the noise from the reference source is coherent at the mixer input and the signals are in quadrature, it will be subject to some degree of cancellation.

The degree of cancellation improves as the signal path delay in the two arms of the bridge is minimized. The remaining phase noise at the mixer output is thus added by the DUT. When the DUT is relatively broadband (i.e. low delay) device having equal input and output frequencies, the need for a second device in the other bridge arm is eliminated. When the device is either narrowband, or is one with unequal input and output frequencies (a mixer frequency multiplier or divider etc.) identical devices must be used in both arms of the phase bridge.

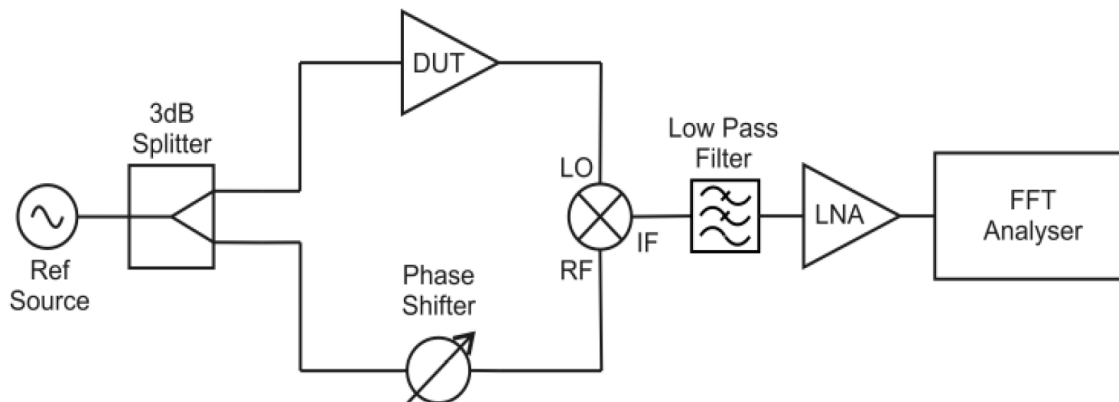


Figure 6-8: Residual method set-up (Simplified single channel residual phase noise measurement system) [24]

The noise floor of a system utilizing this single channel measurement technique is highly dependent on and limited by the noise floors of the mixer, filters and low noise amplifier. This type of system can have a residual phase noise floor in the region of -180dBc/Hz at high offset frequencies.

In residual noise measurement system, the noise of the common source might be insufficiently canceled due to improperly high delay-time differences between the two branches. It is therefore vitally important to match the delay times very closely [20]-[24][99].

A Residual Phase Noise Measurement System

Figure 6-9 shows a system that automatically measures the residual phase noise of the 8662A synthesizer. It is a residual test, since both instruments use one common 10 MHz referenced oscillator. Quadrature setting is conveniently controlled by first offsetting the tuning of one synthesizer by a small amount, usually 0.1 Hz. The beat signal is then probed with a digital voltmeter and when the beat signal voltage is sufficiently close to zero, matching the synthesizer tuning commands to stop the phase slide between the synthesizers [21].

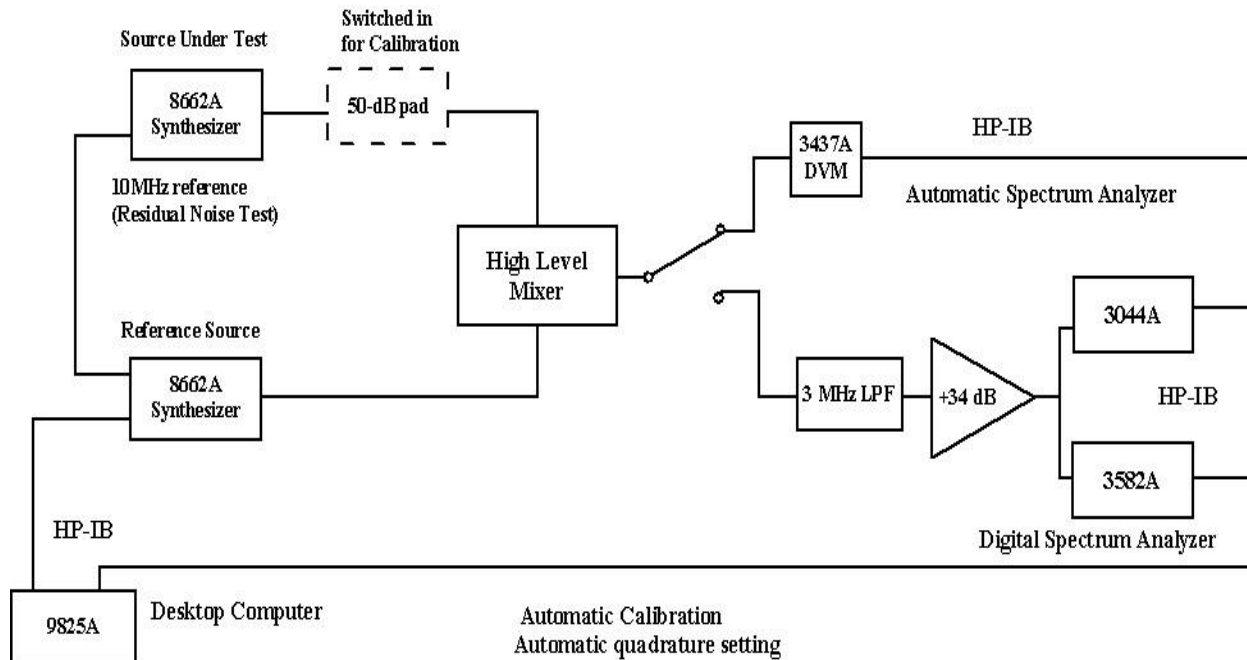


Figure 6-9: Automatic system to measure residual phase noise of two 8662A synthesizers (Courtesy of Hewlett-Packard Company) [21]

6.1.5 Two-Channel Cross-Correlation Technique

Figure 6-10 shows the diagram of the 2-channel cross-correlation technique from Agilent [21]; built around a similar measurement set-up as the PLL method except that there are three oscillators and the measurement involves performing cross-correlation operations among the outputs from each channel. It can be seen that there are two reference oscillators, one power splitter, two mixer/amplifier/PLL circuits and a cross-correlation FFT analyzer. The cross-correlation technique is used to minimize the noise contribution from mixer, filter and LNA from the measurement results. This works because the noise from the DUT is common between both paths, but the noise contributed from each internal reference oscillator is independent. Thus over time, the noise contributions from the independent sources will show a zero cross-correlation. However, the noise from the DUT will correlate, and ultimately dominate the output measurement (as desired).

The noise from the first reference feeds into the first phase noise detector and ends up on channel 1 of the cross-correlation FFT analyzer. The noise from the second reference passes through in the second phase noise detector and appears on channel 2 of the cross-correlation FFT analyzer. The output of the DUT is connected through a high isolation inductive power splitter to two mixer circuits where it is mixed with the signal from these two reference oscillators. The outputs of the mixer circuits are used for PLL circuits to lock the internal references in phase quadrature to the

DUT input signal, as in the PLL method. The mixer output signals are then amplified, the DC is filtered away and finally the signals are fed to two channels of the FFT analyzer to perform a cross-correlation measurement between the two output signals.

The noise from output of each mixer can be modeled using two noisy signals [21]-[28]

$$x(t) = a(t) + c(t) \overrightarrow{FFT} X(f) = A(f) + C(f) \quad (6-15)$$

$$y(t) = b(t) + c(t) \overrightarrow{FFT} Y(f) = B(f) + C(f) \quad (6-16)$$

Where $a(t)$ and $b(t)$ are uncorrelated equipment noise present in each channel and $c(t)$ represents the correlated DUT noise. The cross-spectrum of these two signals after averaging over M samples is described by

$$\overline{S_{XY}} = \frac{1}{M} \sum_{m=1}^{m=M} [X_m \times Y_m^*] \quad (6-17)$$

Where 'm' represents the sample index and (*) implies the conjugate function.

From (6-15), (6-16) and (6-17) into (6-18) and (6-19),

$$\overline{S_{XY}} = \frac{1}{M} \sum_{m=1}^{m=M} [(A_m + C_m) \times (B_m + C_m)^*] \quad (6-18)$$

$$\overline{S_{XY}} = \frac{1}{M} \sum_{m=1}^{m=M} [(A_m B_m^*) + (A_m C_m^*) + (C_m B_m^*) + (C_m C_m^*)] \quad (6-19)$$

Considering that there is no correlation between the noisy signals $a(t)$, $b(t)$ or $c(t)$ then as the number of averages increases the uncorrelated terms in the cross spectrum (AB , AC and CB) will tend toward zero. The only remaining term CC represents the power spectral density of the correlated DUT noise. When the analyzer is set to average, the common noise is kept, and the noise not common to both channels is attenuated and averaged away.

From (6-19) the DUT noise through each channel is coherent and is therefore not affected by the cross-correlation, whereas, the internal noises generated by each channel are incoherent and diminish through the cross-correlation operation at the rate of \sqrt{M} (M =number of correlations)

$$[Noise]_{meas} = [Noise]_{DUT} + \left(\frac{[Noise]_{channel\#1} + [Noise]_{channel\#2}}{\sqrt{M}} \right) \quad (6-20)$$

Where $[Noise]_{meas}$ is the total measured noise at the display; $[Noise]_{DUT}$ the DUT noise; $[Noise]_{channel\#1}$ and $[Noise]_{channel\#2}$ are the internal noise from channels 1 and 2, respectively; and M the number of correlations.

From (6-20), 2-channel cross-correlation technique achieves superior phase noise measurement capability but the measurement speed suffers, when increasing the number of cross-correlations. This method offers 15 to 20 dB improved phase noise measurement sensitivity when compared to the Reference source/PLL method described above, so it can be used to measure oscillators with ultra-low phase noise. It is even possible to measure oscillators with better noise performance than the reference oscillators, because phase noises from the reference oscillators are suppressed considerably.

The improved dynamic range and noise floor of the cross-correlation phase noise measurement technique comes at price. Usually many samples are needed in order to average out the uncorrelated noise. The measuring yardstick of the confidence interval of a phase noise detector is expressed by [20]-[24][71][80-85]:

$$S_{\phi}^s(f) = S_{\phi}^m(f) \left(1 \pm \frac{1}{\sqrt{n}} \right) = \mp 10\% \text{ (for } n = 100) \rightarrow \text{ For single-channel} \quad (6-21)$$

$$S_{\phi}^x(f) = S_{\phi}^m(f) \left(1 \pm \frac{2S_{\phi}^s}{\sqrt{n}} \right) = \mp 10\% \text{ (for } n = 20,000) \rightarrow \text{ For dual-channel} \quad (6-22)$$

Where

x = cross -correlation

m = measured (noise)

s = single channel

n = number of samples

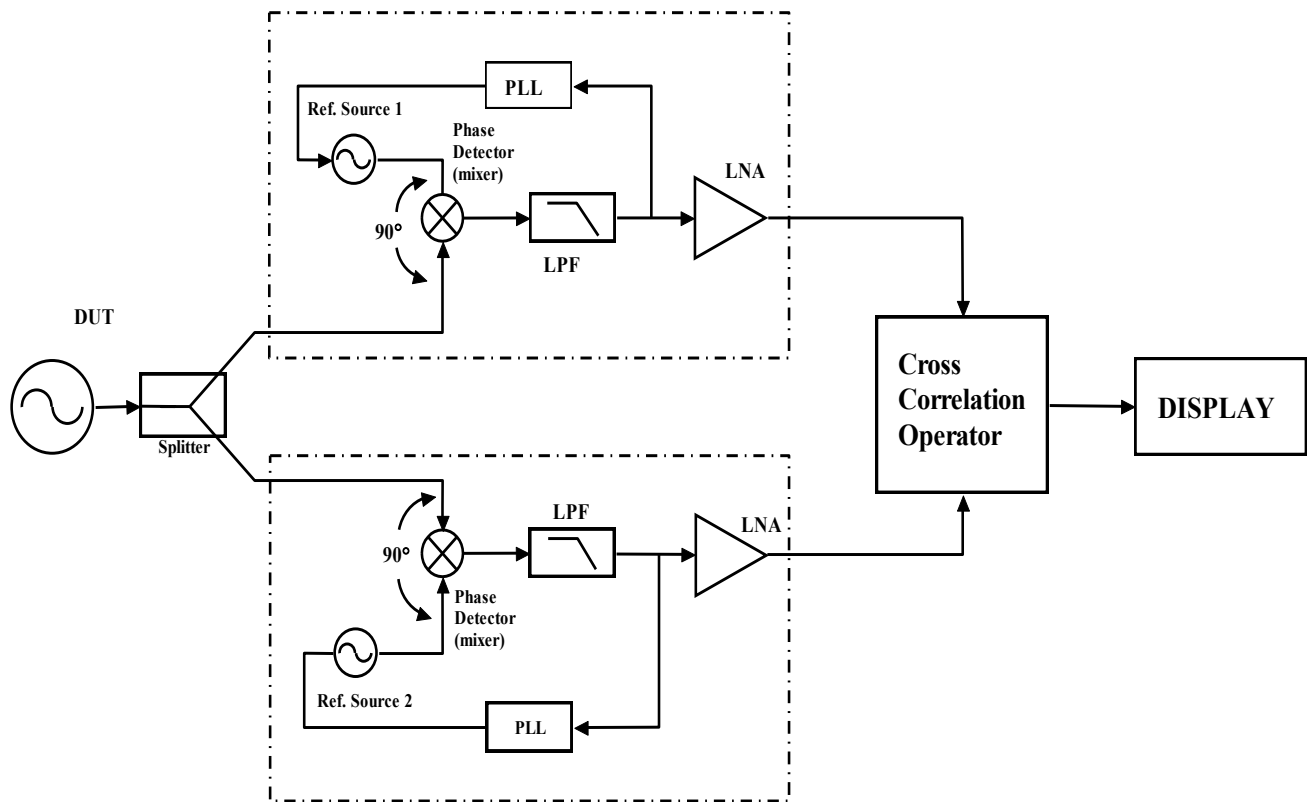


Figure 6-10: Shows the basic block diagram of 2-channel cross-correlation technique (Courtesy: Agilent) [21][24]

Equation (6-21) shows that for a single channel the confidence interval is $\pm 10\%$ for 100 samples. Equation (6-22) shows that to obtain the same confidence interval for a phase noise measurement 10 dB below the single channel noise floor 20,000 samples are required. Indeed, the dual channel or cross-correlation method of phase noise results in a lower floor than the standard single channel method but there is a cost of measurement speed. From (6-21) and (6-22), more averages are required to achieve the same level of confidence in a measurement for dual-channel cross-correlation method. The advantage of lower noise floor using the cross-correlation method provides a level of characterization of extremely low noise Crystal oscillators, which was not possible using the single channel method. The practical value of the noise floor is [24]:

$$[L(f)]_{SSB} = -177 + N_a - P_i \quad (6-23)$$

Where N_a is the noise figure and P_i is the power available.

Today, the cross-correlation process is the only technique that allows close to thermal noise floor measurements below -177dBc/Hz at far offset from the carrier, and with 20dB of DUT output power can provide a noise floor better than -195dBc/Hz provided the DUT output buffer stage is low noise amplifier and can handle the 20dBm power. However, this improvement of 20 dB is based on 100,000 correlations, which results in a long measurement time [18]-[24][71][80-85] [105]-[111].

Advantages:

- Best sensitivity for measuring low phase noise levels
- Wide signal frequency range

- Wide offset frequency range (0.01 Hz to 100 MHz)
- Frequency tracks slowly drifting sources
- Rejects AM noise

Drawbacks:

- Complexity: Requires two very clean reference sources that are electronically tunable
- Long measurement times when very low noise is being measured
- Measurement frequency bandwidth matched to the tuning range of the reference sources
- Phase Inversion and collapse of the cross-spectral function (condition when the detection of the desired signal using cross-spectral techniques collapses partially or entirely in the presence of second uncorrelated interfering signal).

6.2 Conventional Phase Noise Measurement System (Hewlett-Packard)

This section is based on published Hewlett-Packard material [21], described here to give brief insights about the working principle of the early, very low phase noise measurement equipment (during the 1980s) and subsequently the development of modern automated test systems [19]-[21][24].

The most sensitive method to measure the spectral density of phase noise $S_{\Delta\theta}(f_m)$ requires two sources – one or both of them may be the device(s) under test – and a double balanced mixer used as a phase detector. The RF and LO input to the mixer must be in phase quadrature, indicated by 0 Vdc at the mixer IF port. Good phase quadrature assures maximum phase sensitivity K_θ and minimum AM sensitivity. With a linearly operating mixer, K_θ equals the peak voltage of the sinusoidal beat signal produced when both sources are frequency offset (Figure 6-11). When both signals are set in quadrature, the voltage ΔV at the IF port is proportional to the fluctuating phase difference between the two signals.

$$\Delta\theta_{rms} = \frac{1}{K_\theta V_{rms}} \quad (6-24)$$

$$S_{\Delta\theta}(f_m) = \frac{(\Delta V_{rms})^2(1Hz)}{V_{B peak}^2} \frac{1}{2} \frac{(\Delta V_{rms})^2(1Hz)}{V_{B rms}^2} \quad (6-25)$$

$$\mathcal{L}(f_m) = \frac{1}{2} S_{\Delta\theta}(f_m) = \frac{1}{4} \frac{(\Delta V_{rms})^2(1Hz)}{V_{B rms}^2} \quad (6-26)$$

where K_θ is phase detector constant and $V_{B peak}$ for sinusoidal beat signal

Calibrations required of the wave analyzer or spectrum analyzer can be read from the equations above. For a plot of $\mathcal{L}(f_m)$ the 0-dB reference level is to be set 6 dB above the level of the beat signal. The -6-dB offset has to be corrected by + 1.0 dB for a wave analyzer and by +2.5 dB for a spectrum analyzer with log amplifier followed by an averaging detector. In addition, noise bandwidth corrections likely have to be applied to normalize to 1 Hz bandwidth.

Since the phase noise of both sources is summed together in this system, the phase noise performance of one of them needs to be known for definite data on the other source. Frequently, it is sufficient to know that the actual phase noise of the dominant source cannot deviate from the measured data by more than 3 dB. If three unknown sources are available, three measurements with three different source combinations yield sufficient data to calculate accurately each individual performance.

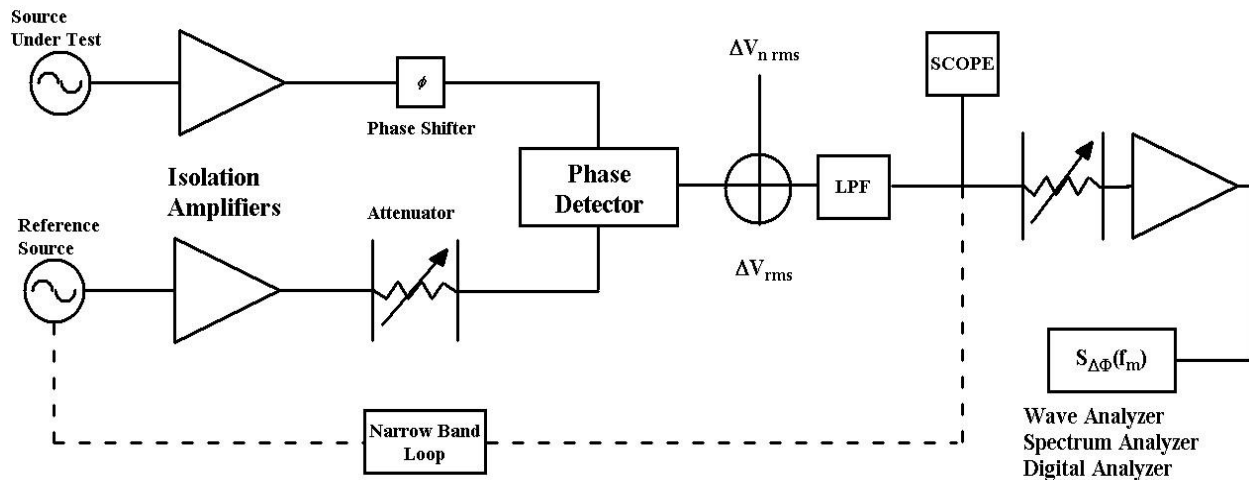


Figure 6-11: Phase Noise system with two sources maintaining phase quadrature [21][24]

Figure 6-11 indicates a narrowband phase-locked loop that maintains phase quadrature for sources that are not sufficiently phase stable over the period of the measurement. The two isolation amplifiers are to prevent injection locking of the sources to each other. The noise floor of the system is established by the equivalent noise voltage ΔV_n at the mixer output. It represents mixer noise as well as the equivalent noise voltage of the following amplifier:

$$\mathcal{L}_{system}(f_m) = \frac{1}{4} \frac{(\Delta V_{n\ rms})^2 (1\text{Hz})}{V_B^2\ rms} \quad (6-27)$$

Wideband noise floors close to -180 dBc can be achieved with a high-level mixer and a low-noise amplifier. The noise floor increases with f_m^{-1} due to the flicker characteristic of ΔV_n . System noise floors of -166dBc/Hz at 1 kHz have been realized.

To get this excellent performance, the phase detector/PLL method is complex and requires significant calibration. In measuring low-phase-noise sources, a number of potential problems have to be understood to avoid erroneous data. These include:

When two sources are phase locked to maintain phase quadrature, it has to be ensured that the lock bandwidth is significantly lower than the lowest Fourier frequency f_m of interest, unless the test set takes into account (as many do) the loop suppression response

Even with no apparent phase feedback, two sources can be phase locked through injection locking, resulting in suppressed close-in phase noise and causing a measurement error. This can normally be avoided with the use of high isolation buffer amplifiers or frequency multipliers.

- AM noise of the RF signal can come through if the quadrature setting is not maintained accurately.
- Deviation from the quadrature setting also lowers the effective phase detector constant.
- Nonlinear operation of the mixer results in a calibration error.
- Need for low harmonic content: A non-sinusoidal RF signal causes K_θ to deviate from V_{Bpeak}
- The amplifier or spectrum analyzer input can be saturated during calibration or by high spurious signals such as line frequency multiples.
- Closely spaced spurious signals such as multiples of 60 Hz may give the appearance of continuous phase noise when insufficient resolution bandwidth and averaging are used on the spectrum analyzer.
- Impedance interfaces must remain unchanged when transitioning from calibration to measurement.

- Noise from power supplies for devices under test can be a dominant contributor of error in the measured phase noise.
- Peripheral instrumentation such as an oscilloscope, analyzer, counter, or DVM can inject noise.
- Microphonic effects may excite significant phase noise in devices.

Despite all these hazards, automatic test systems now exist and operate successfully [6]. Oscillator manufacturers and users who frequently need to evaluate the performance of ultra low phase noise oscillators, at some point, recognize that their phase noise test systems could be primarily improved in the following aspects:

- Accuracy
- Speed of test
- Large dynamic range and lower noise floor
- Reliability and repeatability of test data
- Range, ease of use and data retrieval
- Cost (though high performance test systems will never be cheap!)

6.3 General Discussion on Phase Noise:

Characterizing the phase noise of a system or component is not necessarily very easy. Many different approaches are possible, but the key is to find the best approach for the measurement requirements at hand. Practically, it is advisable to use the cross-correlation approach for the best sources so that keeping them locked is easy during measurement cycle. In principle, each reference is locked to track the DUT, therefore PLL bandwidth needs to be monitored for reliable and accurate measurement. Usually, corrections for PLL bandwidth works to some degree, but corrections beyond certain limit have more errors, leading to inaccurate phase noise measurement of the DUT. One of the weaknesses, with the cross-correlation method is that, many measurements must be made and the average calculated between them. Thus, the measurement takes longer, and the DUT must be kept locked for a longer time. Usually, 1-sweep takes approximately 10 seconds, and the required amount of sweep is 2^m where $m > 2$ but for a noisy source this may not be easy. Hence, this method is most suitable for measuring low noise oscillators having a small frequency drift. A survey of some of the more common topologies along with some possible trouble spots helps one to review and keep in mind the advantages and limitations of each approach. Figure 6-12 Shows phase noise plots and noise floor for 3-phase noise measurement techniques (Delay line, PLL and cross-correlation) [21][24][90].

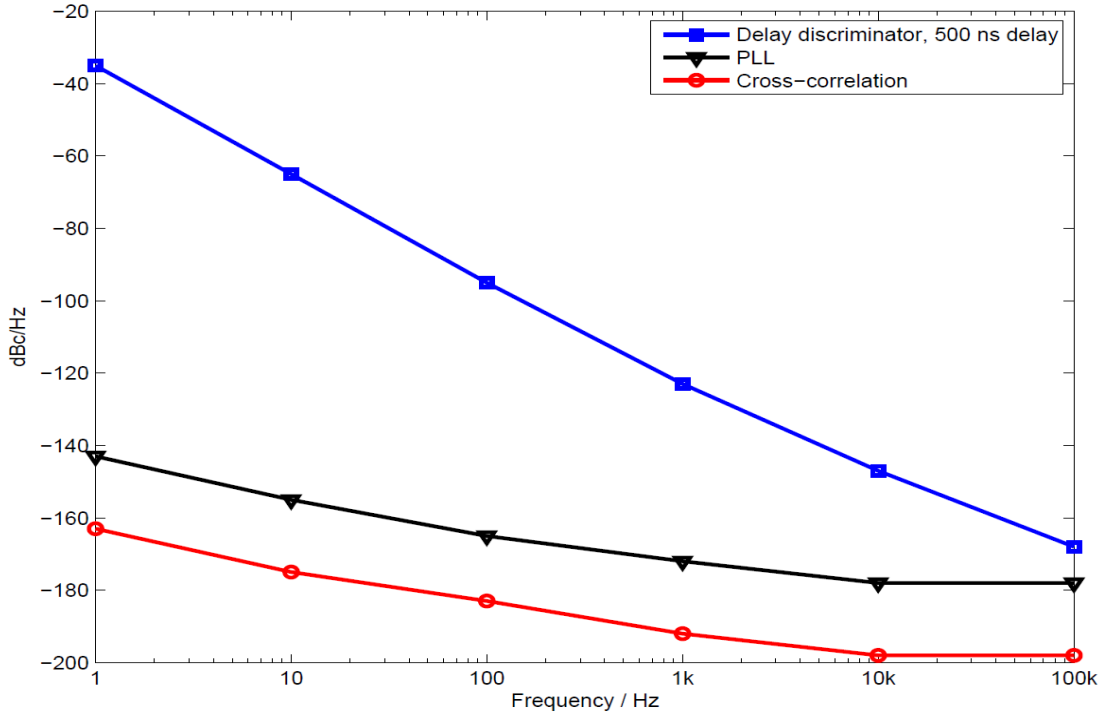


Figure 6-12: Shows phase noise plots and noise floor for 3-techniques (PLL, Delay line, and cross-correlation)[24]

6.4 Prediction and Validation of Oscillator Phase Noise Measured on Different Equipments

The phase noise equation for a Colpitts based oscillator circuit can be expressed as [9]

$$\mathcal{L}(\omega) = 10 \log \left\{ \left[4kTR + \frac{4qI_c g_m^2 + \frac{4K_f I_b^{AF}}{\omega} g_m^2}{\omega_0^2 C_1^2 (\omega_0^2 (\beta^+)^2 C_2^2 + g_m^2 \frac{C_2^2}{C_1^2})} \right] \left[\frac{\omega_0^2}{4\omega^2 V_{cc}^2} \right] \left[\frac{Q_0^2}{Q_L^2} + \frac{[C_1 + C_2]^2}{C_1^2 C_2^2 \omega_0^4 L^2 Q_L^2} \right] \right\} \quad (6-28)$$

where

$$\beta^+ = \left[\frac{Y_{21}^+}{Y_{11}^+} \right] \left[\frac{C_1}{C_2} \right]^p \quad g_m = [Y_{21}^+] \left[\frac{C_1}{C_2} \right]^q; \text{ Values of } p \text{ and } q \text{ depends upon the drive level}$$

Y_{21}^+, Y_{11}^+ = large signal [Y] parameter of the active device

K_f = flicker noise coefficient

AF = flicker noise exponent

$\mathcal{L}(\omega)$ = ratio of sideband power in a 1 Hz BW at ω to total power in dB

ω = frequency offset from the carrier

ω_0 = center frequency

Q_L = loaded Q of the tuned circuit

Q_0 = unloaded Q of the tuned circuit

kT = 4.1×10^{-21} at 300 K (room temperature)

R = equivalent loss resistance of the tuned resonator circuit

I_c = RF collector current

I_b = RF base current

V_{cc} = RF collector voltage

C_1, C_2 = feedback capacitor as shown in Figure (6-13)

6.5 Verification of 100 MHz Crystal Oscillator using CAD simulation Tool (Ansoft Designer from Ansys)

Figures 6-13 shows the typical simplified 100 MHz Colpitts Crystal oscillator circuit, grounded base buffer circuit, and Figures 6-14, 6-15, 6-16 and 6-17 show CAD simulation results for the Noise Figure, polar plot of noise, phase noise, and output power respectively.

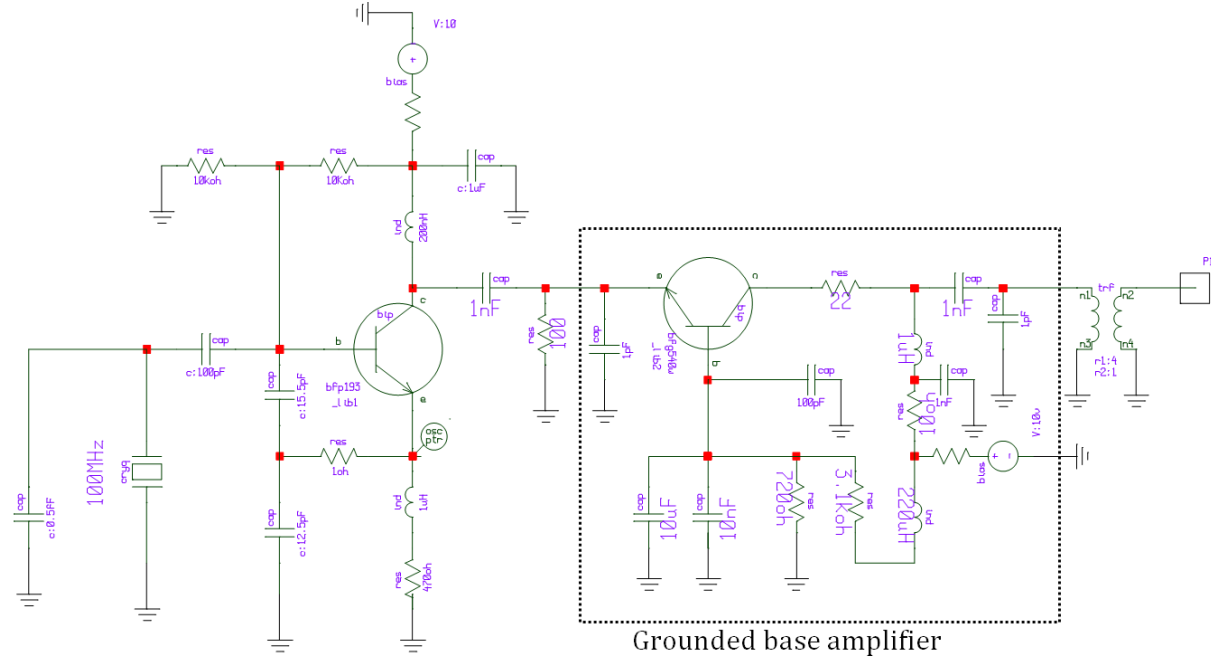


Figure 6-13: 100 MHz Colpitts Crystal Oscillator with the Grounded-Base low noise Amplifier [24]

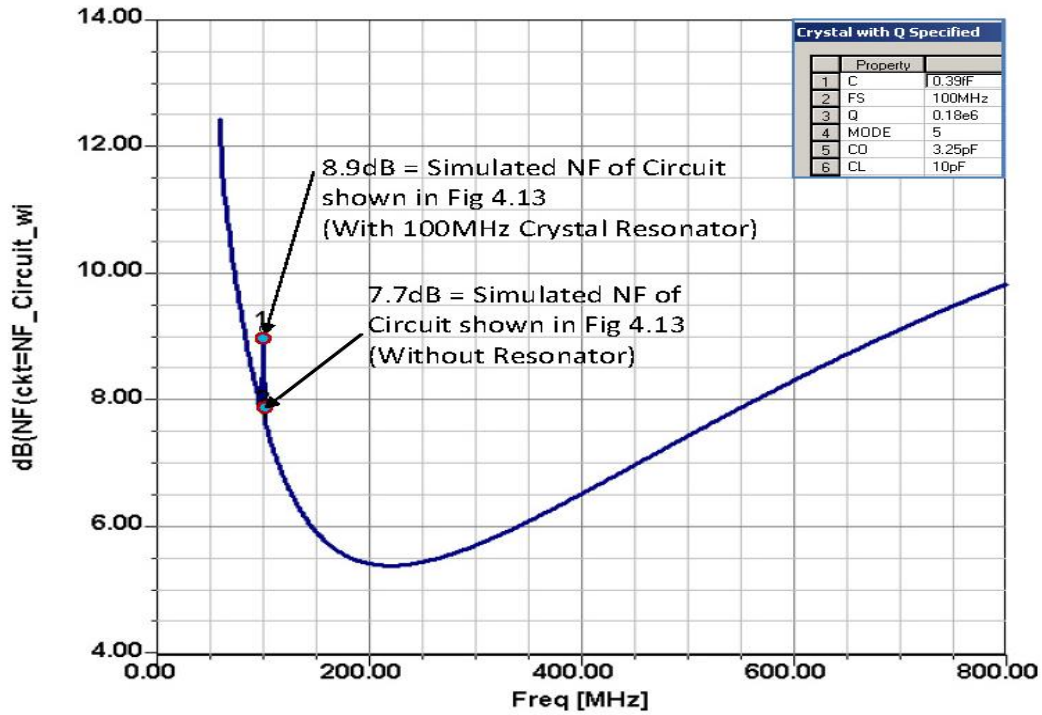


Figure 6-14: Simulated plot showing NF of 100 MHz Oscillator shown in Fig 6-13 [63, Fig 4.145]

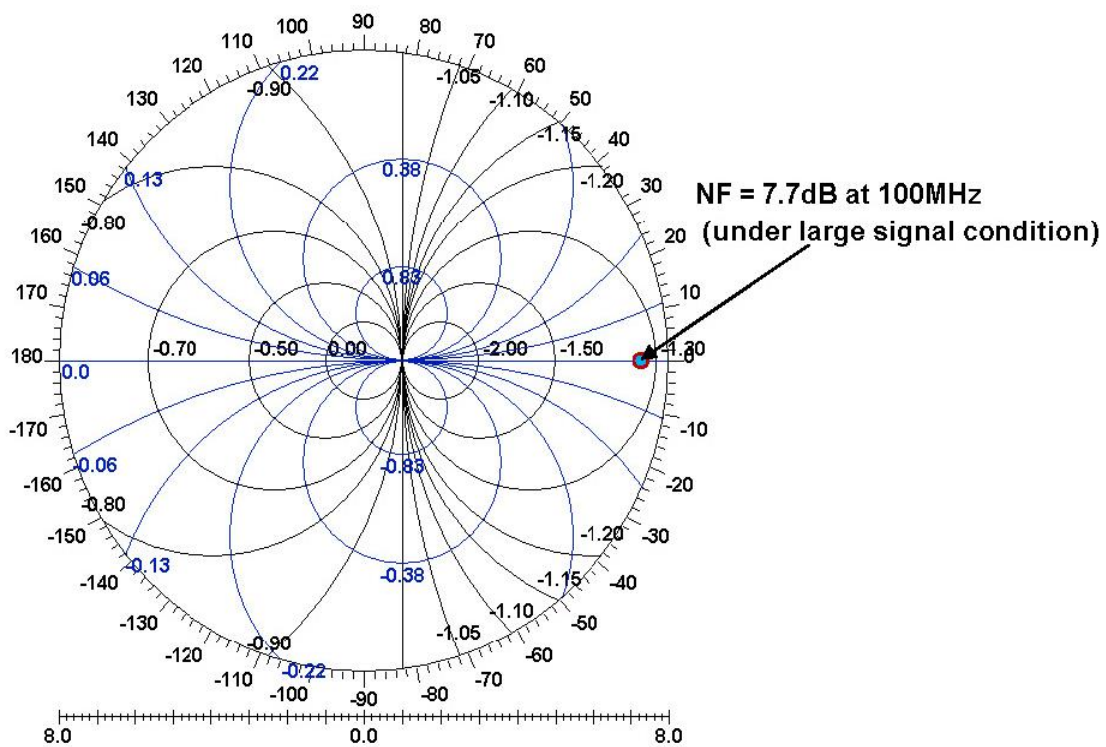


Figure 6-15: CAD simulated Polar Plot of Noise of the Oscillator Circuit shown in Figure 6-13 [63, Fig 4.15]

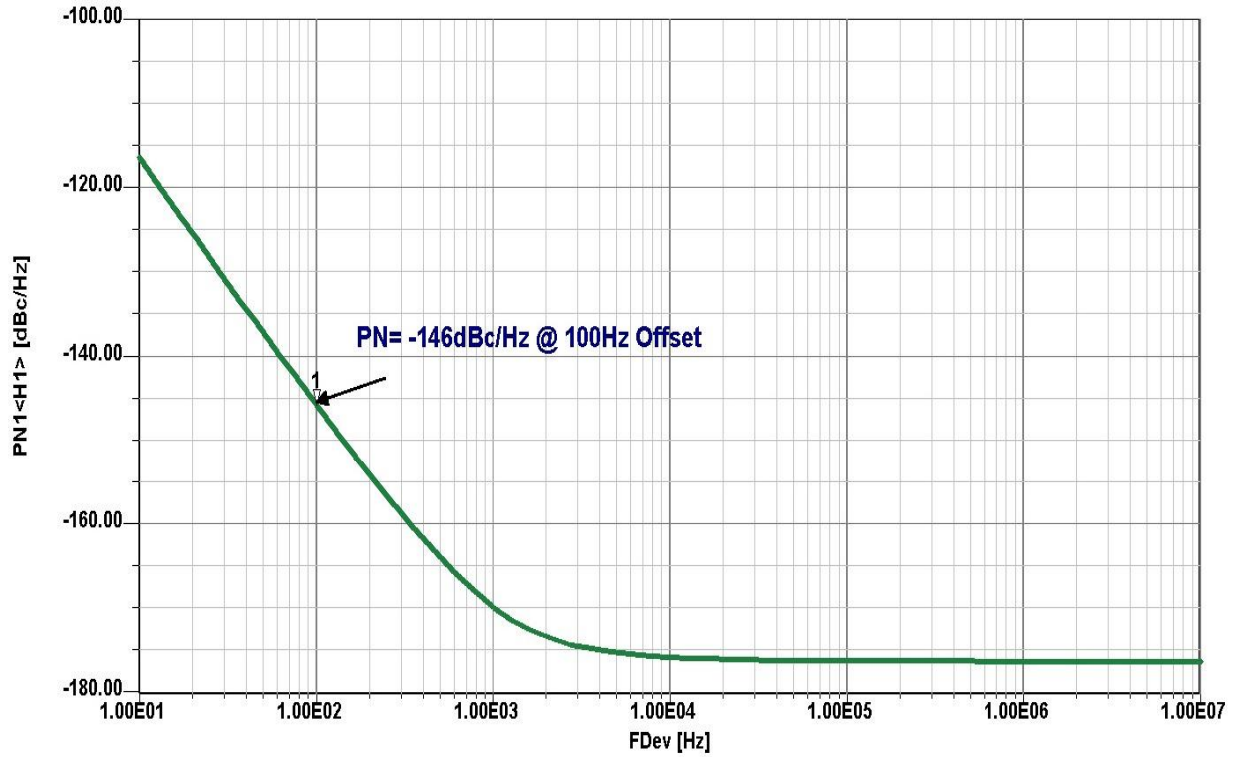
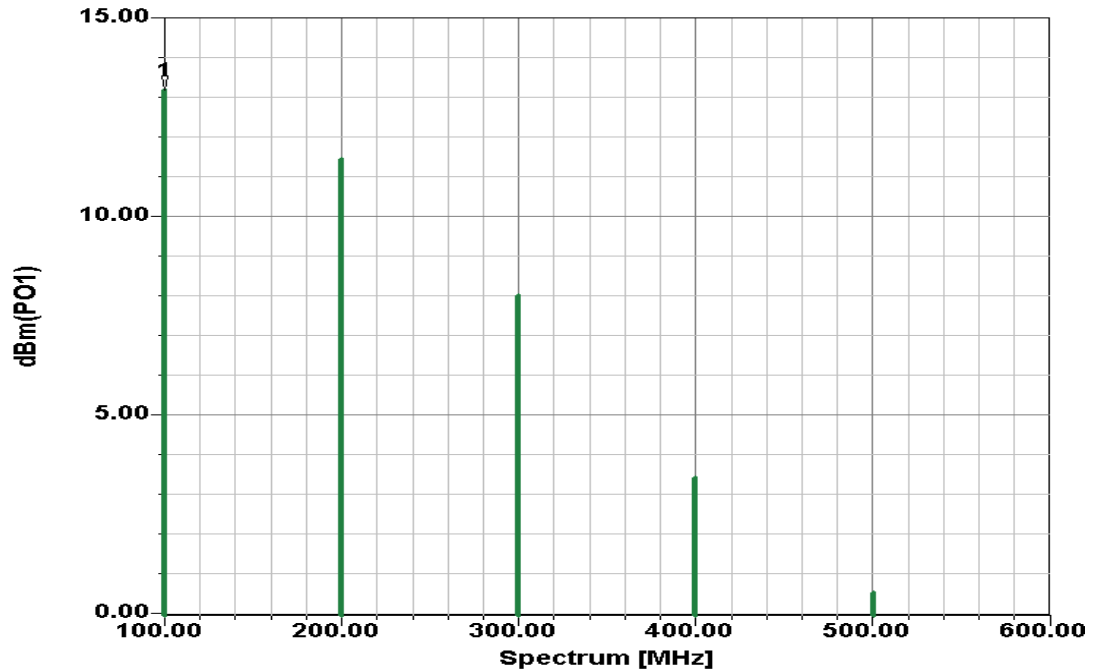


Figure 6-16: CAD simulated Phase Noise Plot of 100 MHz Crystal Oscillator with Buffer Stage [63, Fig 4.16]



X1= 100.00MH;
Y1= 13.20

Figure 6-17: Simulated Power Output Plot of 100 MHz Crystal Oscillator with Buffer Stage [63, Fig 4.17]

The basic equation needed to predict the phase noise using CAD simulation for the circuit shown in Figures 6-13 and 6-14 is found in [9].

$$\mathcal{L}(f_m) = 10 \log \left\{ \left[1 + \frac{f_0^2}{[2f_m Q_o m(1-m)]^2} \right] \left(1 + \frac{f_c}{f_m} \right) \frac{FkT}{2P_o} + \frac{2kTRK_o^2}{f_m^2} \right\} \quad (6-29)$$

where $\mathcal{L}(f_m)$, f_m , f_0 , f_c , Q_L , Q_o , F , k , T , P_o , R , K_o and m are the ratio of the sideband power in a 1 Hz bandwidth at f_m to total power in dB, offset frequency, flicker corner frequency, loaded Q , unloaded Q , noise factor, Boltzmann's constant, temperature in degree Kelvin, average output power, equivalent noise resistance of tuning diode, voltage gain and ratio of the loaded Q -factor (Q_o) and unloaded Q -factor (Q_L).

In the past this was done with the Leeson formula, which contains several estimates, those being output power (P_o), flicker corner frequency (f_c), oscillator noise factor (F), and the operating (or loaded) Q . Now, one can assume that the small signal linear estimation of noise factor (F) can give wrong estimation of phase noise when oscillator operates under large signal condition.

The approximate formulae (considering quasi-nonlinear analysis) of the noise factor under the large signal condition can be given by the following equation [9, pp. 135].

$$F \cong 1 + \frac{Y_{21}^+ C_2 C_c}{(C_1 + C_2) C_1} \left[r_b + \frac{1}{2r_e} \left(r_b + \frac{(C_1 + C_2) C_1}{Y_{21}^+ C_2 C_c} \right)^2 \left(\frac{1}{\beta^+} + \frac{f^2}{f_T^2} \right) + \frac{r_e}{2} \right] \quad (6-30)$$

where Y_{21}^+ = large signal [Y] parameter of the active device.

Table 6-2: shows the calculated Noise Figure and Phase Noise for 100 MHz Crystal Oscillator using (6-28), (6-29) and (6-30) for unloaded $Q_o = 180000$, and time average loaded Q ($Q < Q_o/4$) under large signal drive level condition is 25000.

Table 6-2: Calculated Noise Figure and Phase Noise for 100 MHz Crystal Oscillator

Oscillator Frequency	Simulated Large Signal Noise Figure	Calculated Phase Noise at 100 Hz offset
100 MHz	7.7 dB	-146 dBc/Hz

6.6 Verification of 100 MHz Crystal Oscillator (LN XO 100) using Analytical Model

The theoretical calculated parameters of 100 MHz crystal oscillator circuit is given below [ref. 9, pp.181], after defining all the values, the phase noise can be predicted for comparative analysis.

Theoretical calculated parameters of 100 MHz crystal oscillator circuit using MathCad is shown in Figure 6-18 below and the phase noise plot is shown in Figure 6-19.

$$\begin{aligned}
 C1 &:= 15.6\text{pF} & C2 &:= 12.5\text{pF} & kT &:= 4.143 \cdot 10^{-21} \cdot \text{J} & R &:= 0.2 \cdot \Omega \\
 q\text{charge} &:= 1.602 \cdot 10^{-19} \cdot \text{coul} & I_c &:= 8.2 \cdot \text{mA} & I_b &:= 220 \cdot \mu\text{A} \\
 y11 &:= (0.000884 - 0.0000158j) \cdot \text{mho} \\
 y21 &:= (0.0105 - 0.00084j) \cdot \text{mho} \\
 L &:= 6.4949 \cdot 10^{-3} \cdot \text{henry} & a_f &:= 2 & k_f &:= 1 \cdot 10^{-10} & y &:= \frac{C1}{C2} \\
 V_{cc} &:= 10\text{V} & i &:= 0.7 & p &:= 1.45 & q &:= 1.05 \\
 Q &:= 25000 & Q_0 &:= 180000 & n\text{fdB} &:= 4.747 & P_{\text{outdB}} &:= 13 \\
 f_c &:= 100 \text{ MHz} & \omega_c &:= 2\pi \cdot f_c & g_m &:= |y21| \cdot y^q \\
 f_{o_i} &:= 10^i \cdot \text{Hz} & \omega_{o_i} &:= 2\pi \cdot f_{o_i} & B1_i &:= (\omega_{o_i})^2 \cdot L^2 \cdot V_{cc}^2 \\
 k\text{constant} &:= \frac{KT \cdot R}{\omega_c^2 \cdot C2^2} & k_{0_i} &:= \frac{k\text{constant}}{B1_i} & b &:= \frac{|y21| \cdot y^p}{|y11|} \\
 k1\text{constant}_i &:= q\text{charge} \cdot I_c \cdot \text{gm}^2 + \frac{k_f \cdot I_b^{a_f} \cdot \text{gm}^2}{\omega_{o_i}} \\
 k1_i &:= \frac{k1\text{constant}_i}{\omega_c^2 \cdot B1_i} & k3_i &:= \omega_c^2 \cdot \text{gm}^2 & k2_i &:= \omega_c^4 \cdot b^2 & k_i &:= \frac{k3_i}{k2_i \cdot C2^2} \\
 t2_i &:= k_{0_i} \frac{(1+y)^2}{y^2} & t1_i &:= \left[\left(\frac{b^2}{\text{gm}^3} \right)^2 \cdot \frac{k_i^3 \cdot k1_i \cdot (\omega_c)^2}{y^2 + k_i} \right] \cdot \frac{(1+y)^2}{y^2} & 1_i &:= t1_i + t2_i \\
 m_i &:= 10 \cdot \log \left[1_i \cdot (\text{kg}^{-2} \cdot \text{m}^{-4} \cdot \text{s}^5 \cdot \text{A}^2) \cdot \frac{Q_0^2}{Q^2} \right] \\
 L_i &:= \text{if}[m_i < (-177 + P_{\text{out}}(\text{dBm}) - n\text{fdB}), (-177 + P_{\text{outdB}} - n\text{fdB}), m_i]
 \end{aligned}$$

m_i	f_{o_i}	L_i
-88.581	$1 \cdot \text{s}^{-1}$	-88.581
-118.515	$10 \cdot \text{s}^{-1}$	-118.515
-147.901	$100 \cdot \text{s}^{-1}$	-147.901
-174.251	$1 \cdot 10^3 \cdot \text{s}^{-1}$	-174.251
-195.999	$1 \cdot 10^4 \cdot \text{s}^{-1}$	-185.253
-216.22	$1 \cdot 10^5 \cdot \text{s}^{-1}$	-185.253
-236.243	$1 \cdot 10^6 \cdot \text{s}^{-1}$	-185.253
-256.245	$1 \cdot 10^7 \cdot \text{s}^{-1}$	-185.253

Figure 6-18: Shows the theoretical phase noise model expressed in (6-29) [3]

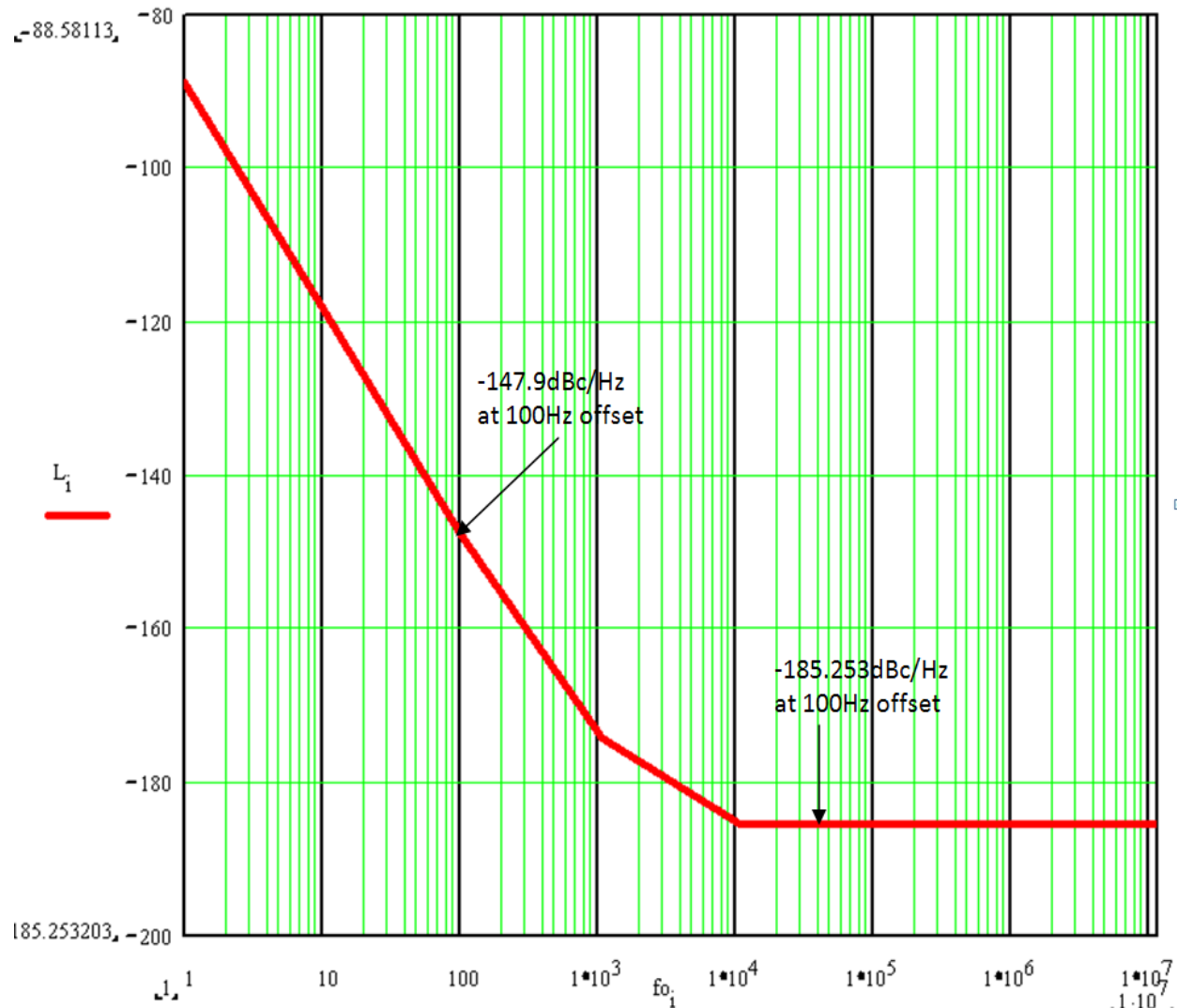


Figure 6-19: Theoretically calculated Phase Noise Plot for 100 MHz Crystal Oscillator (LNXO 100) [3]

6.7 Verification of 100 MHz Crystal Oscillator using Phase Noise Measurement Equipments [3]

For validation of the theoretical model described earlier, 100 MHz Crystal oscillator was built and tested on different Phase Noise Measurement Equipments (Agilent E5052B, R&S FSUP, Holzworth, Noise XT, and Anapico APPH6000-IS) available on the market.

6.7.1 Experimental Verification of 100 MHz Crystal Oscillator using Agilent E5052B

The feature of cross-correlation techniques in Agilent E5052B satisfies the established criteria without additional references, nor calibration of the device under test (DUT) on exact frequency.

Figure 6-20 and Figure 6-21 show the picture of Agilent E5052B equipment and measured phase noise plot of 100 MHz crystal oscillator circuit for the purpose of the verification of measurement uncertainty.

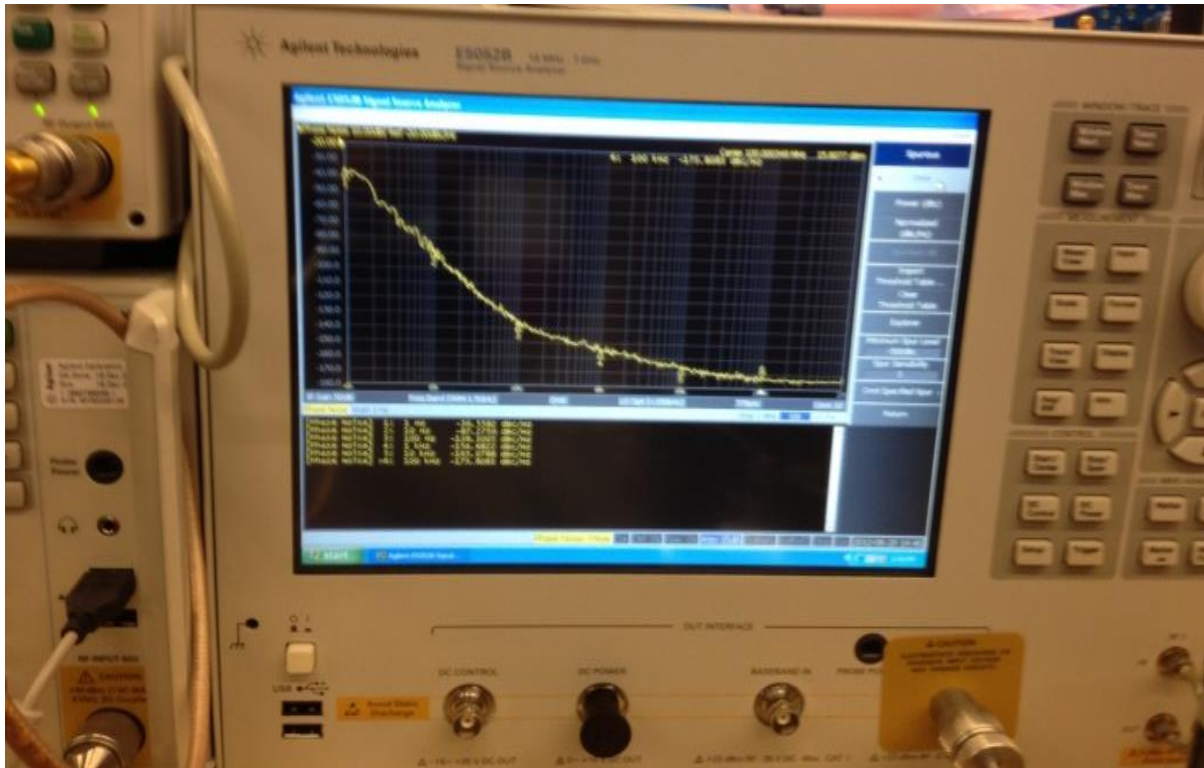


Figure 6-20 shows the picture of E5052B (Courtesy: Agilent) with the phase noise plot of 100 MHz crystal oscillator circuit for the purpose of the verification of measurement uncertainty (IMS show 2012, Montreal, Canada) [3]

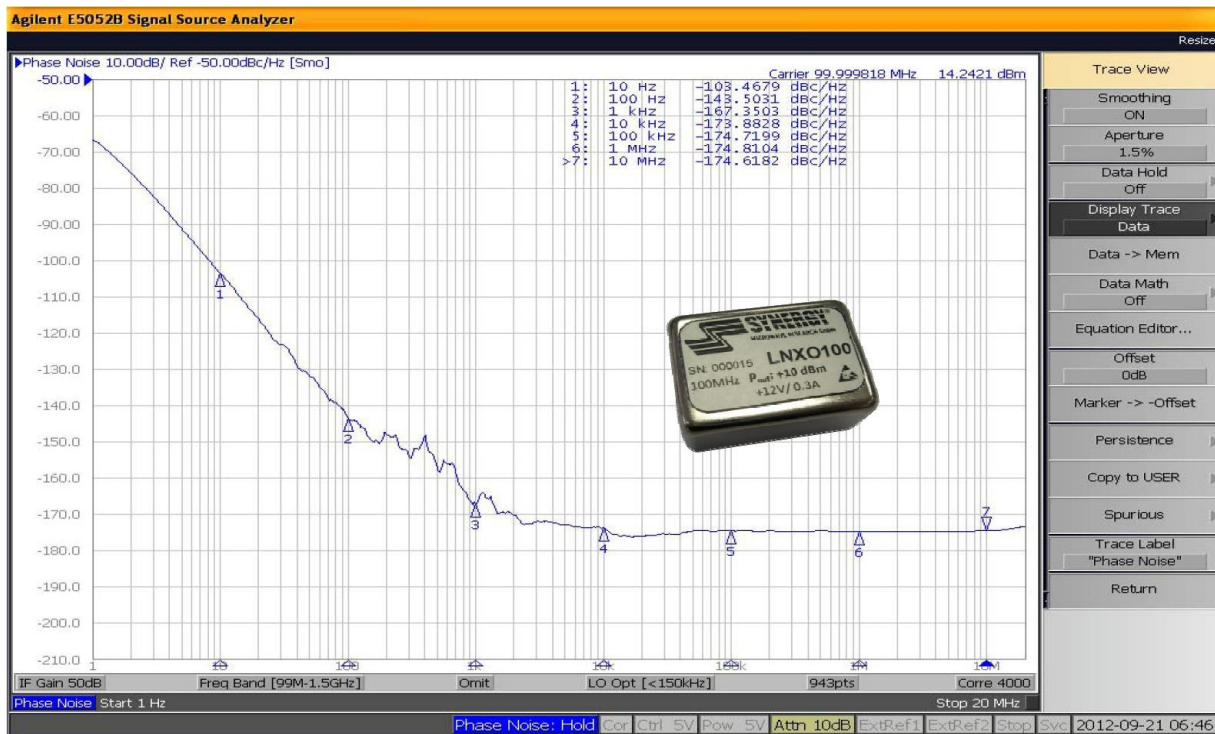


Figure 6-21: 100 MHz Crystal Oscillator Measured on Agilent E5052B (Corr_4000) (measurement performed in IMS show 2012, Montreal, Canada) [3]

The measured phase noise at 100 Hz offset is -143 dBc/Hz for LNXO 100 (100 MHz carrier frequency), this shows the capability of close-in measurement. The main concern is the dynamic range and noise floor of the equipment measured at large offsets from the carrier, the far offset noise floor is -174dBc/Hz at offsets greater than 100 KHz.

The theoretical expectations were closer to -191dBc/Hz at 10 KHz offsets and beyond for 14 dBm output power. The other problem is that the mixer and the post amplifier can easily get into compression, which raises the noise floor [3].

6.7.2 Experimental Verification of 100 MHz Crystal Oscillator using R&S (FSUP 26)[3]

The feature of cross-correlation techniques in R&S (FSUP 26) satisfies the established criteria, and requires neither additional references, nor calibration of the device under test (DUT) on exact frequency.

Figure 6-22 and Figure 6-23 show the pictures of R&S (FSUP 26) equipment and measured phase noise plot of 100 MHz crystal oscillator for the purpose of the verification of measurement uncertainty. The measured phase noise at 100 Hz offset is -140 dBc/Hz for LNXO 100 (100 MHz carrier frequency), and the far offset noise floor is -174 dBc/Hz at offsets greater than 100 KHz.

The theoretical expectations were closer to -191dBc/Hz at 100 KHz offsets and beyond for 14 dBm output power.

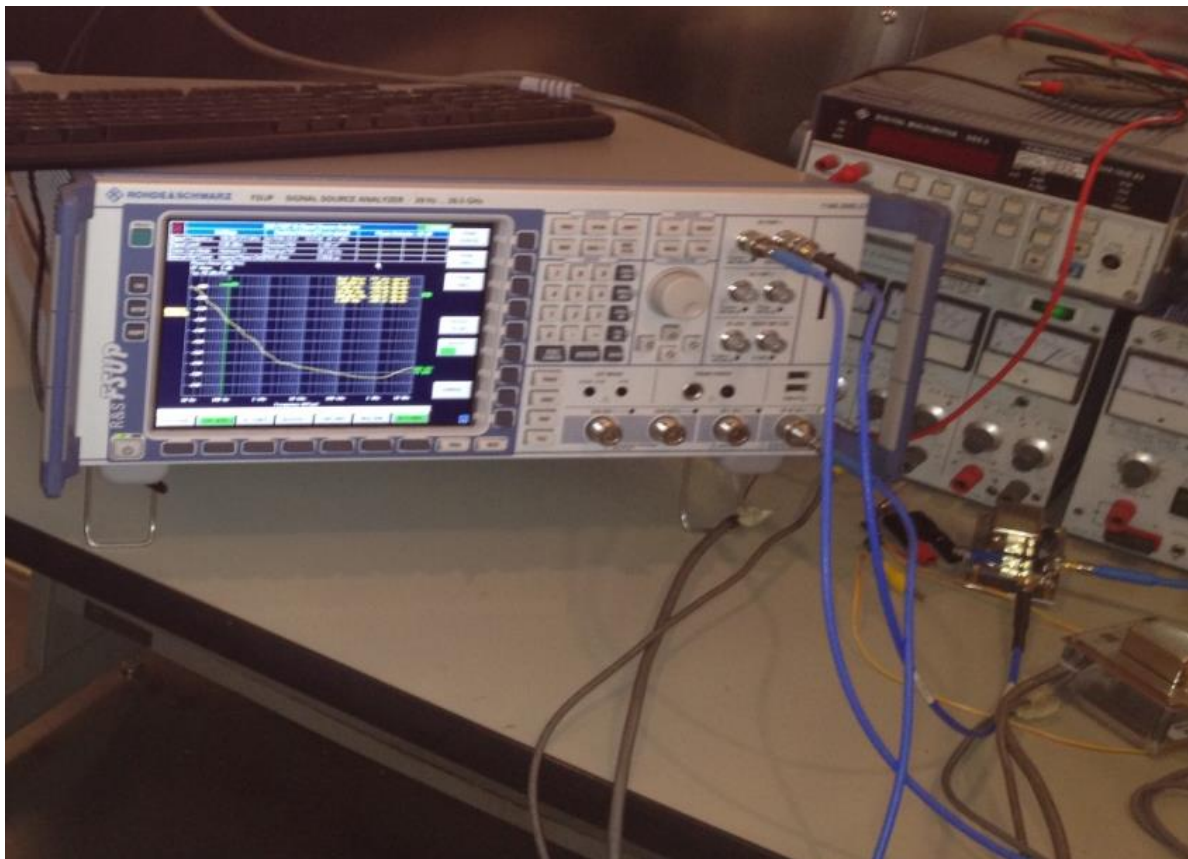


Figure 6-22: Shows the picture of R&S FSUP 26 (Courtesy: R&S) while taking measurement [3]

Design Validation: Low Noise Crystal Oscillator (LNXO)

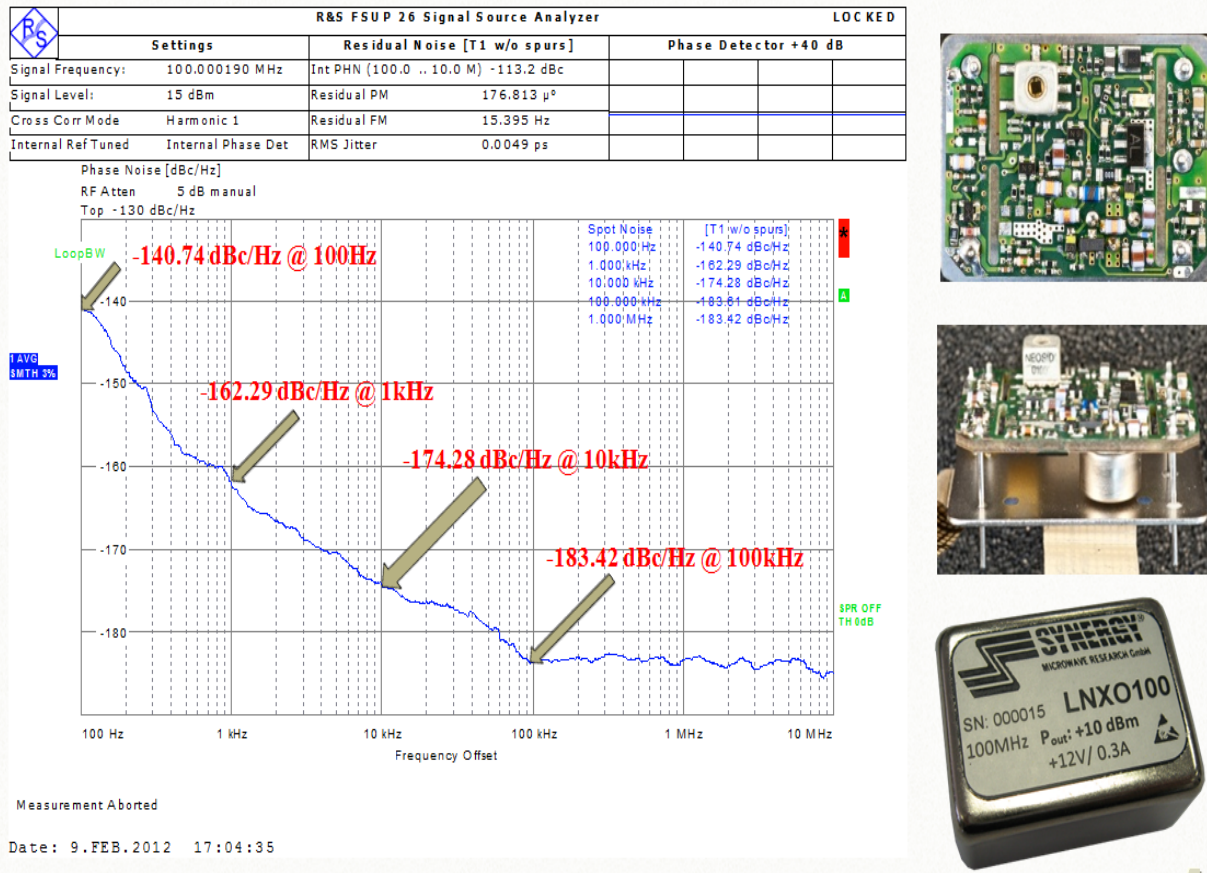


Figure 6-23: 100MHz Crystal Oscillator Measured on R&S FSUP [3]

6.7.3 Experimental Verification of 100 MHz Crystal Oscillator using Anapico (APPH6000-IS)[3]

The feature of cross-correlation techniques in APPH 6000 (Anapico) satisfies the established criteria, but require 2-additional references at exact frequency. Figures 6-24 shows the measured phase noise plot of 100 MHz crystal oscillator for the purpose of the verification of measurement uncertainty.

The measured phase noise at 100 Hz offset is -146dBc/Hz for LNXO 100 (100 MHz carrier frequency), this shows the capability of close-in measurement. The instrument’s specification calls for -184dBc/Hz floor at offsets greater than 100 KHz. The theoretical expectations were closer to -191dBc/Hz at 100 KHz offsets and beyond for 14dBm output power. The main concern is the additional references at exact frequency of DUT.

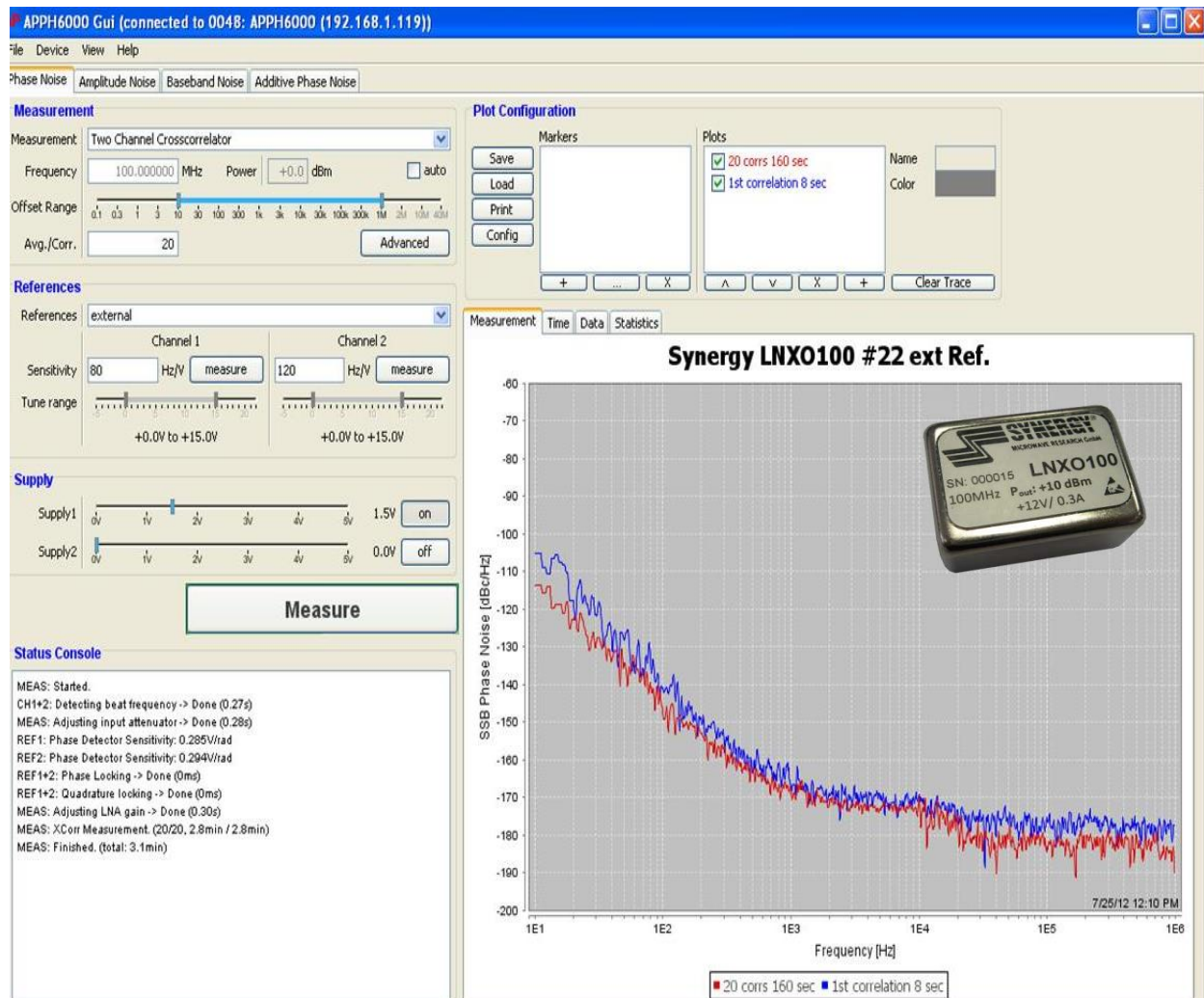


Figure 6-24: Shows the picture of phase noise plots and equipment setting (Courtesy: Anapico APPH6000-IS) 100 MHz Crystal Oscillator Measured on Anapico phase noise engine [3]

6.7.4 Experimental Verification of 100 MHz Crystal Oscillator using Holzworth (HA7402A)[3]

The feature of cross-correlation techniques in Holzworth satisfies the established criteria; require 2-additional references at exact frequency. Figure 6-25 shows the picture of Holzworth phase noise measurement equipment, including the measured phase noise plot of 100 MHz crystal oscillator for the purpose of the verification of measurement uncertainty.

The measured phase noise at 100 Hz offset is -147dBc/Hz for LNXO 100 (100 MHz carrier frequency), this shows the capability of close-in measurement. The instrument's specification calls (conservatively) for -178dBc/Hz floor at offsets greater than 100 KHz. The theoretical expectations were closer to -191dBc/Hz at 100 KHz offsets and beyond for 14dBm output power. The main concern is the additional references at exact frequency of DUT.

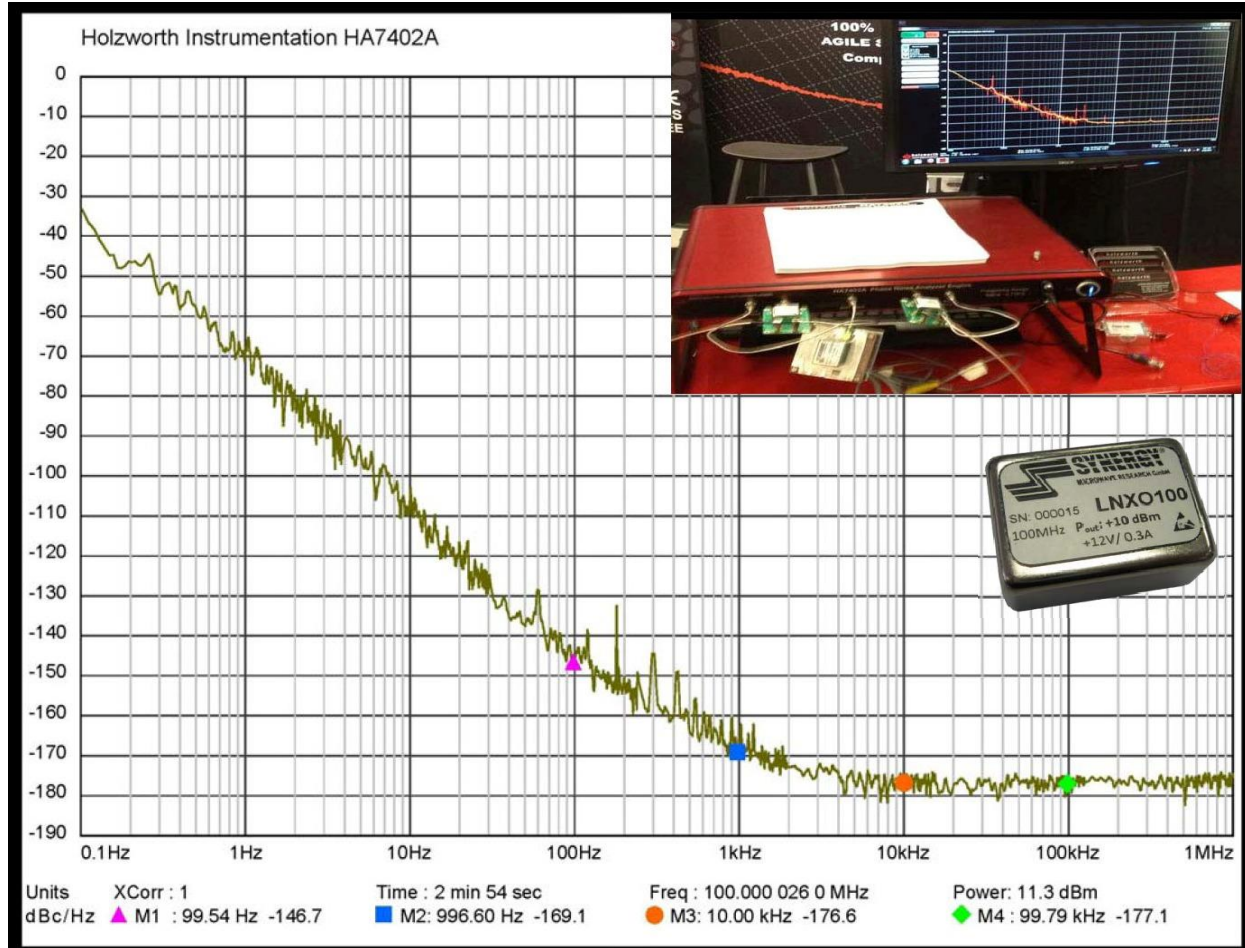


Figure 6-25: shows the picture of phase noise plots and equipment setting (Courtesy: Holzworth) 100MHz Crystal Oscillator Measured on Holzworth Phase Noise Engine (measurement performed in IMS show 2012, Montreal, Canada) [3]

6.7.5 Experimental Verification of 100 MHz Crystal Oscillator using Noise XT (DCNTS)

The feature of cross-correlation techniques in Noise XT satisfies the established criteria; require 2-additional references at exact frequency. Figures 6-26 shows the picture of Noise XT (DCNTS) phase noise measurement equipment, including the measured phase noise plot of 100 MHz crystal oscillator for the purpose of the verification of measurement uncertainty.

The measured phase noise at 100 Hz offset is -140dBc/Hz for LN XO 100 (100 MHz carrier frequency), this shows the capability of close-in measurement. The instrument's specification calls for -190 dBc/Hz floor at offsets greater than 1 MHz. The theoretical expectations of -191dBc/Hz noise floor closely met with this equipment for 14dBm output power. The main concern is the close-in phase noise, which is 7dB inferior as compared to Holzworth for identical correlations. As shown in Figure 6-26, Noise XT Dual Core Noise Test Set (DCNTS) [75] requires two references with similar performance as the DUT (the better the reference performance – the faster the test), the references must have voltage control (ability to change frequency with the change of the voltage on the control terminal), and be calibrated on the frequency of DUT.

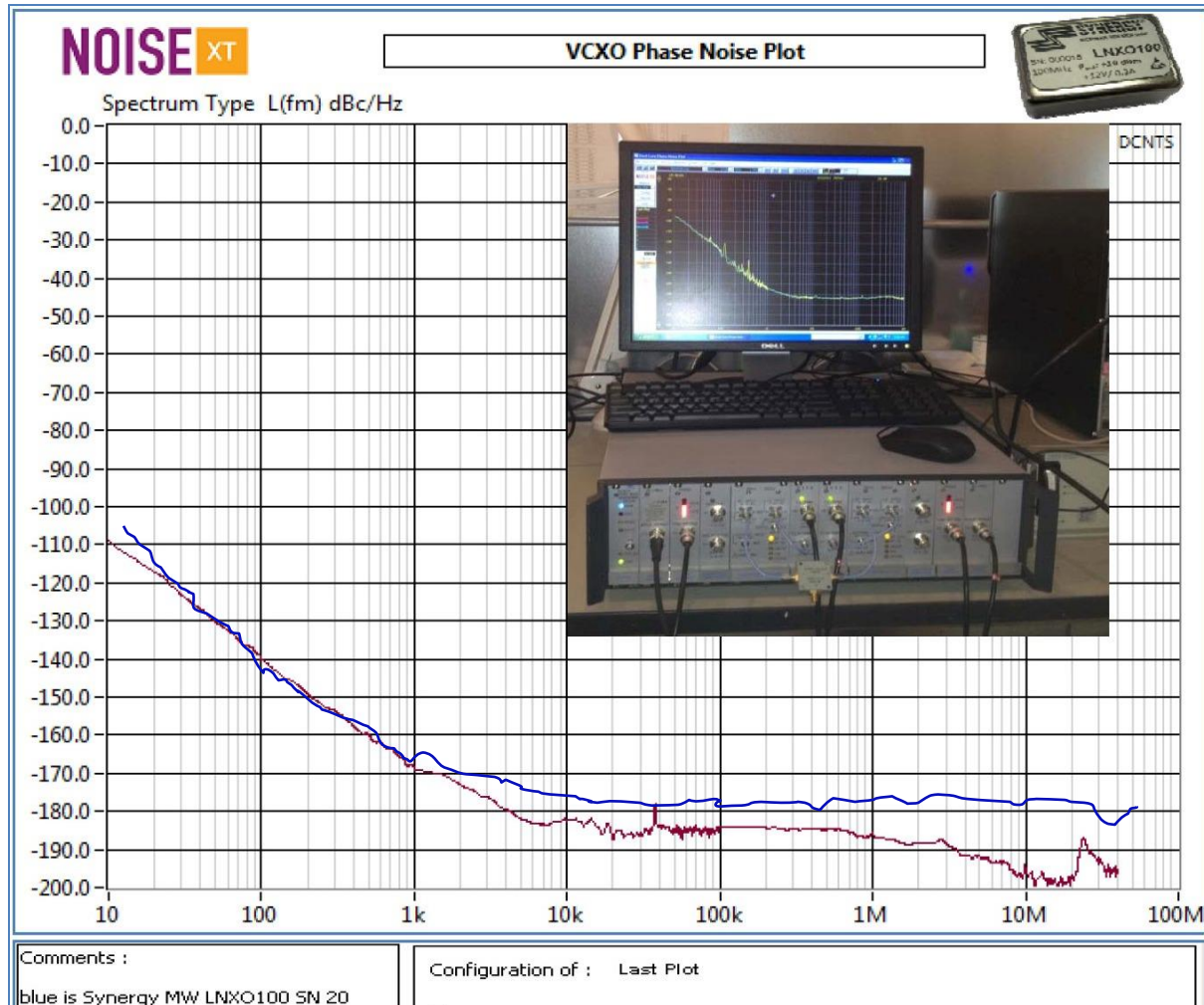


Figure 6-26: Phase noise measurement using cross-correlation techniques using Noise XT DCNTS Engine [3]

6.8 Phase Noise Measurement Evaluation and Uncertainties:

The rigorous measurements are conducted on 100 MHz Crystal oscillator using different Phase Noise Measurement Equipments (Agilent E5052B, R&S FSUP, Holzworth, Noise XT, and Anapico APPH6000-IS) commercially available on the market. Table 6-3 describes the theoretical and measured phase noise on different test equipment for comparative analysis of the measured data under similar phase test condition. The consequence is this set of equations gives the best possible phase noise. If the equipment in use, after many correlations gives out a better number, either it violates the laws of physics and if it gives a worse number, then the correlations settings needs to corrected or the dynamic range of the equipment is insufficient. This measurement is exhaustive, but it was necessary to explain how things fall in place.

At 20dBm output, the output amplifier certainly has a higher noise figure, as it is driven with more power and there is no improvement possible. Phase Inversion may lead to collapse of the cross-spectral function, failure to truly measure noise occurs when a special phase condition exists between the signals being offered to the cross-spectrum function [18][37][38][105]-[109]. This may be favorable condition to see optimistic but wrong phase noise measurement due to the established anti-phase condition of second uncorrelated interfering signal. Therefore, the detection of the desired signal using cross-spectral techniques collapses partially or entirely in the presence of the second uncorrelated interfering signal. Cross-spectral analysis is a mathematical tool for

extracting the power spectral density of a correlated signal from two time series in the presence of uncorrelated interfering signals [37][108]. The cross-spectrum of two signals $x(t)$ and $y(t)$ is defined as the Fourier transform of the cross-covariance function of x and y .

For example, $x(t) = a(t) + c(t) + d(t)$; $y(t) = a(t) + c(t) - d(t)$, where $c(t)$ to be the desired signal, $a(t)$ and $b(t)$ are the uncorrelated interfering signals, $d(t)$ is anti-correlated (phase inverted) in x and y then it leads to an unexpected negative hump (exhibits unexpected very low phase noise) in phase noise plot due to cancellation dynamics. This implies that at any frequency f where the average magnitude of signal $C(f)$ is equal to that of signal $D(f)$, the magnitude of the cross-spectrum collapses to zero [38][109].

Any contribution of the desired signal $c(t)$, or the interferer $d(t)$, to the cross spectral density is eliminated. This occurs even though signals $c(t)$ and $d(t)$ are completely uncorrelated. If $C(f)$ and $D(f)$ have the same shape or slope versus frequency, entire octaves or decades of spectrum can be suppressed and be grossly under-reported. If the PSD (power spectral density) of C and D are not exactly equal, a partial cancellation still occurs. These condition is demonstrated on 100 MHz OCXO measured on different equipments, some of the measurements showing -198dBc/Hz @ 20 MHz offset for 100 MHz OCXO (Figure 6-26, red plot) can be uncertain for exactly these reasons.

The cross correlation technique allows us to look below kT (k is Boltzmann constant and T is temperature in degree Kelvin), however the usefulness of noise contributions below kT is a matter of discussion among scientific community because not understanding when and how this effect occurs can lead to dramatic underreporting of the desired signal [18][38]-[41][109]-[111].

Following is a set of measured results of 100 MHz Crystal Oscillators with different test equipments shown in Table 6-3 for giving good understanding about the discrepancy in phase noise measurement performed on different commercially available equipments in the market.

Table 6-3: Theoretical and measured phase noise on different test equipments available in market [3][36]

100 MHz OCXO O/P=14dBm, NF=7dB	Theoretical Model [24]	Agilent E5052B	R & S FSUP 26	Anapico APPH6000 -IS	Holzworth HA7402-A	Noise XT DCNTS
	dBc/Hz	dBc/Hz	dBc/Hz	dBc/Hz	dBc/Hz	dBc/Hz
PN @ 100 Hz offset	-147	-143	-143	-141	-147	-140
PN @ 1 kHz offset	-175	-167	-163	-170	-170	-170
PN @ 10 kHz offset	-185	-173	-174	-172	-178	-181
PN @ 100 kHz offset	-185	-174	-183	-181	-179	-183
PN @ 1 MHz offset	-185	-174	-184	-182	-179	-186
PN @ 10 MHz offset	-185	-174	-185	-188	-178	-196

6.9 Phase Noise Measurement Issues

There are important measurement issues that, if not well understood, can lead to erroneous results and interpretations [3][29]-[34][99]-[104]. They involve measurement bandwidth masking of, and accurate distinction between, true discrete spurious signals and narrowband noise peaks (typically encountered under vibration). Although the phase noise data displayed by phase noise equipment is usually normalized to 1 Hz measurement bandwidth, most automated phase noise measurement equipments actually measure the phase noise in measurement bandwidths that increase with

increasing carrier offset frequency. This is done for two reasons: (1) it results in shorter, overall measurement time, and (2) at high carrier offset frequency (i.e., > 100 kHz), many measurement systems employ analog spectrum analyzers that are not capable of 1 Hz resolution. Noise measured in a 1 kHz bandwidth, for example, is 30dB higher than that displayed in a 1 Hz bandwidth. That means that low-level discrete spurious signals (and narrowband noise peaks typically encountered under vibration as a result of high Q mechanical resonances) may not be detected. The second problem involves the software employed by the noise measurement system vendor used to discriminate between random noise and discrete spurious signals. Usually, when a reasonably sharp increase in noise level is detected, the system software assumes that the increase marks the presence of a “zero bandwidth” discrete signal.

It therefore (when displaying the phase noise on a 1 Hz bandwidth basis) applies a bandwidth correction factor to the random noise, but does not make a correction to what was interpreted as a discrete signal. This results in an erroneous plot if/when the detected “discrete” is really a narrowband noise peak. Figures 6-27 and Figure 6-28 attempt to depict the various situations that can result from these issues as described above. Figure 6-29 shows the picture of Faraday Cage, demonstrating the phase noise measurement setup using different equipments (Agilent E5052B, R&S FSUP, Holzworth HA7402-A, Noise XT DCNTS, Anapico APPH6000-IS) for the validation purpose. OEwaves-PHENOM™ and Agilent E5500 claim for improved dynamic ranges and capable of measuring noise floor below kT but these equipments were not made available for the validation in our Faraday Cage. The effort is in progress to validate the phase noise measurement using PHENOM™ and E5500 for broader acceptance of the fact and myth linked with variation in measurement phase noise data below the kT .

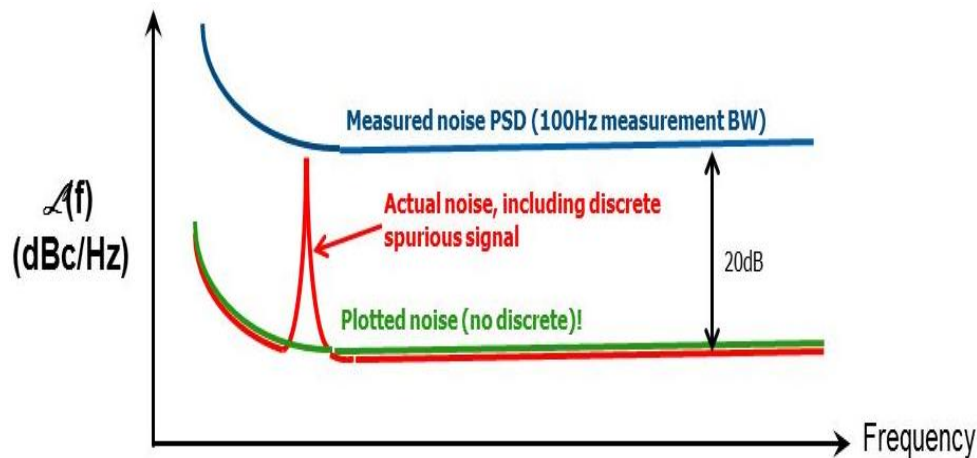


Figure 6-27: Undetected Discrete Spurious Signal [52]

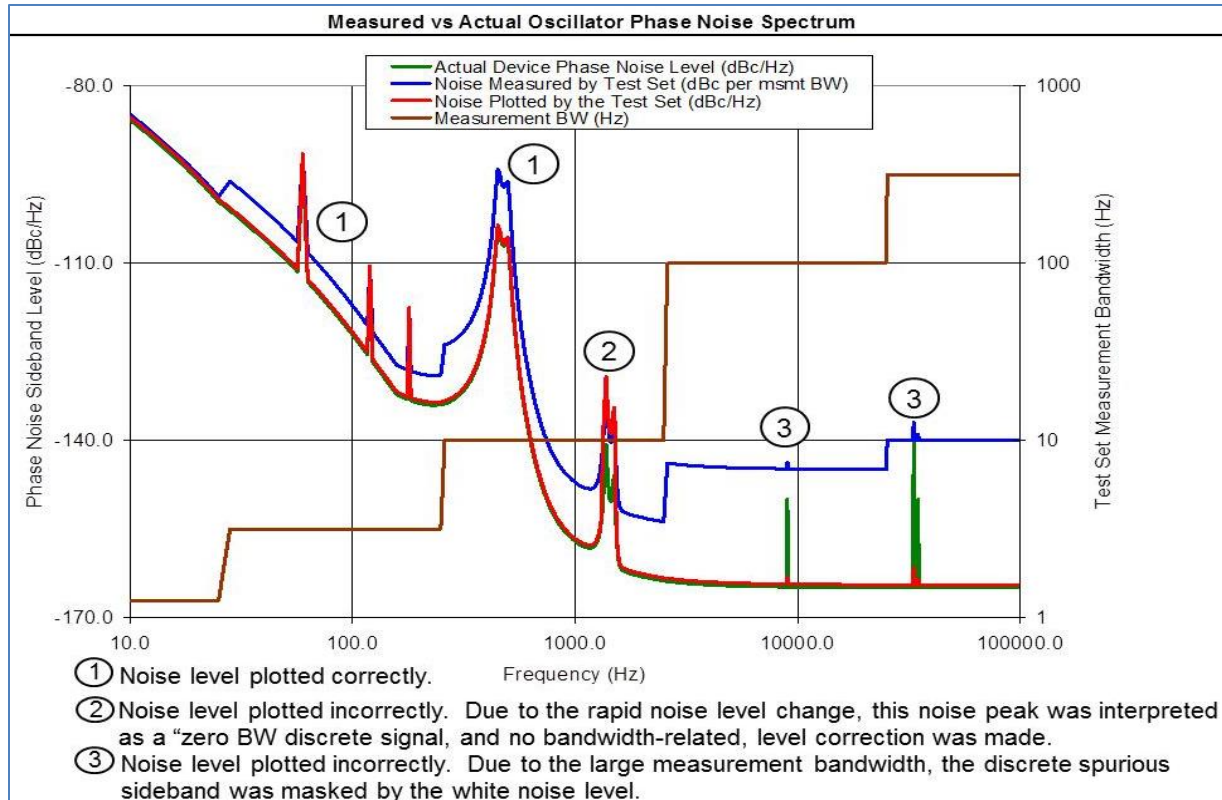
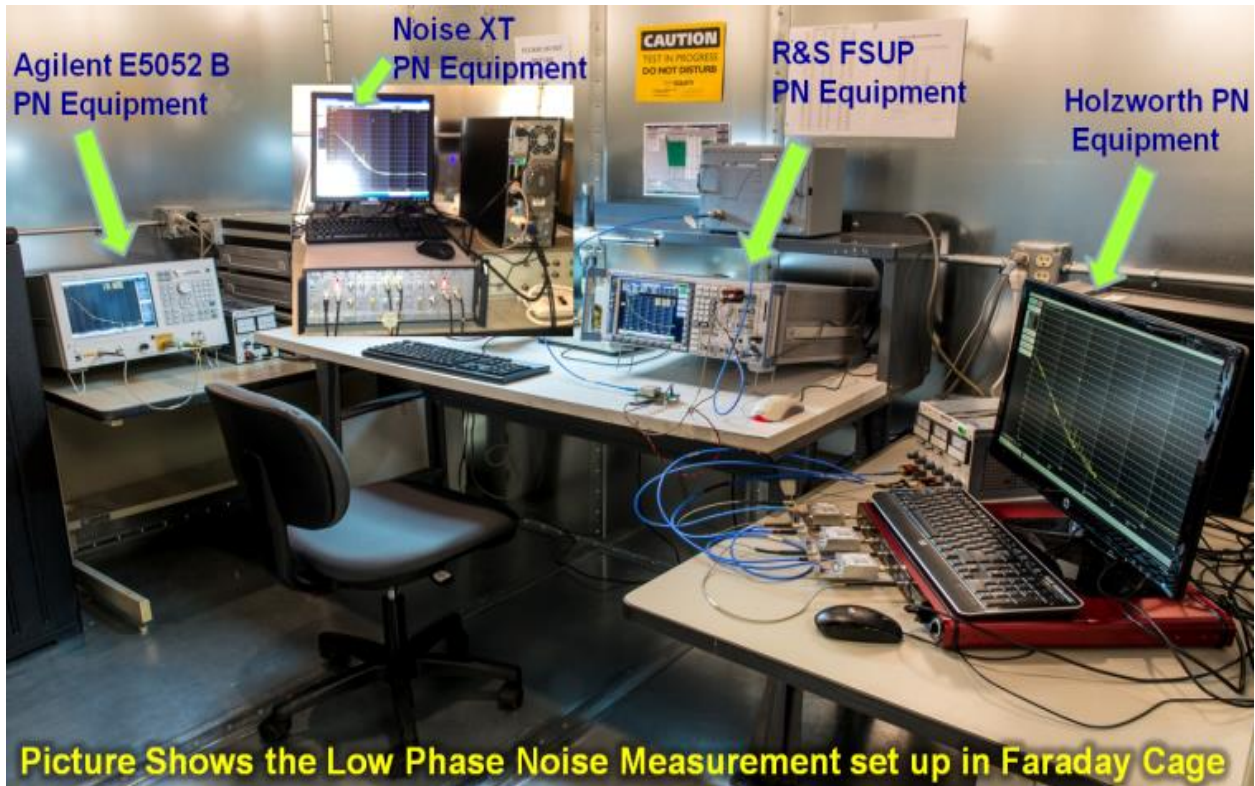


Figure 6-28: Correct and Erroneous Display of Phase Noise Data [3][112]



Picture Shows the Low Phase Noise Measurement set up in Faraday Cage

Figure 6-29 - Picture shows Low Phase Noise Measurement Setup in Faraday Cage [24]

6.10 Applying the Cross-Correlation

The old systems have an FFT analyzer for close-in calculations and are slower in speed. Modern equipments use noise-correlation method. The reason why the cross-correlation method became popular is that most oscillators have an output between zero to 15dBm and what is even more important is that only one signal source is required. The method with a delay line (Fig. 6-30 and Fig. 6-31), in reality required a variable delay line to provide correct phase noise numbers as a function of offset, shown in ref. [9, pp. 148-153, Fig 7.25 and 7.26].

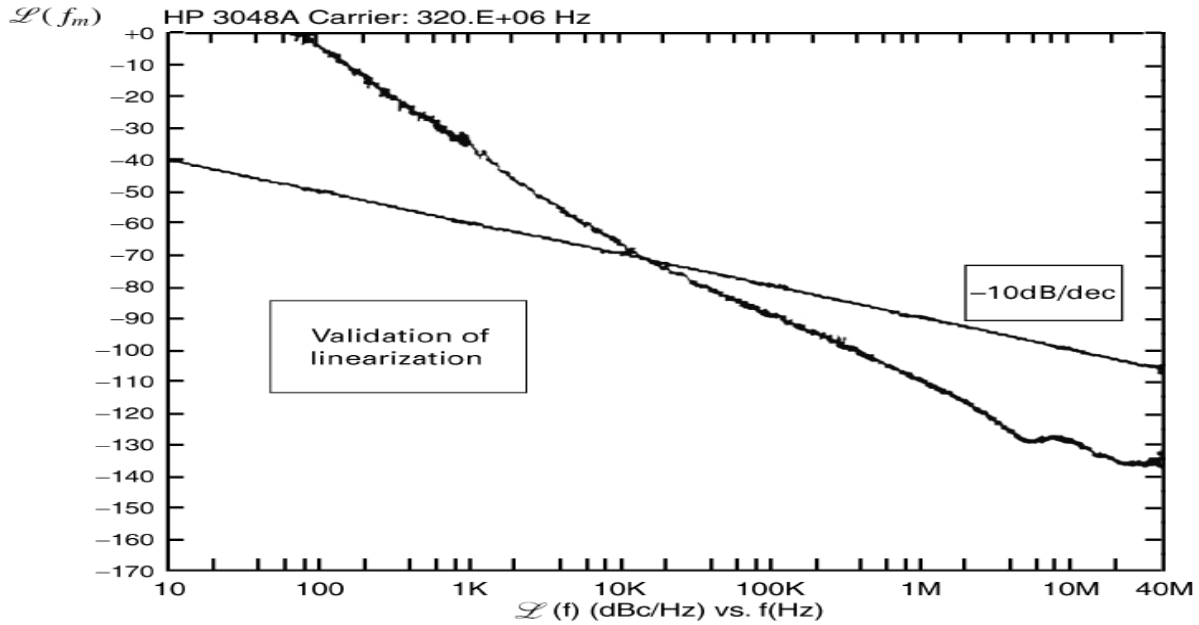


Figure 6-30: Display of a typical phase noise measurement using the delay line principle. This method is applicable only where $x \sin(x)$. The measured values above the solid line violate this relationship and therefore are not valid [9]

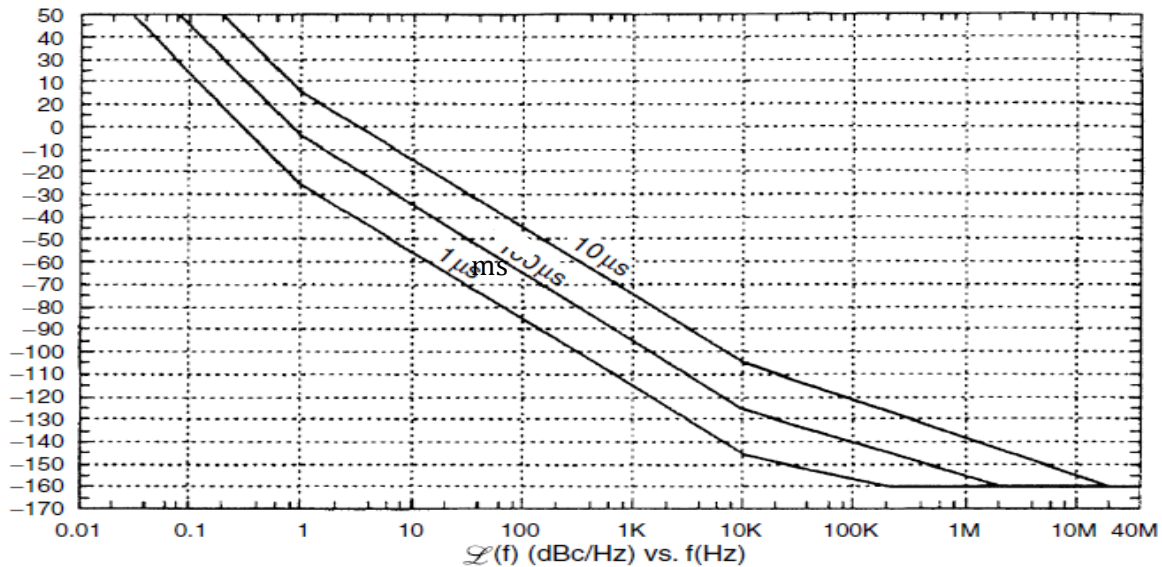


Figure 6-31: Dynamic range as a function of cable delay. A delay line of 1ms is ideal for microwave frequencies [9]

Advantages of the noise correlation technique:

- Increased speed
- Requires less input power
- Single source set-up
- Can be extended from low frequency 1 MHz to 100 GHz - depends on the internal synthesizer

Drawbacks of the noise-correlation technique:

- Different manufacturers have different isolation, so the available dynamic range is difficult to predict
- These systems have a “sweet-spot”, both R&S and Agilent start with an attenuator, not to overload the two channels; 1dB difference in input level can result in quite different measured numbers. These “sweet-spots” are different for each machine.
- The harmonic contents of the oscillator can cause an erroneous measurement, that’s why a switchable-low-pass filter like the R&S Switchable VHF-UHF Low-pass Filter Type PTU-BN49130 or its equivalent should be used.
- Frequencies below 200 MHz, systems such as Anapico or Holzworth using 2 crystal oscillators instead of a synthesizer must be used. There is no synthesizer good enough for this measurement. Example: Synergy LNX0100 Crystal Oscillator measures about -142dBc/Hz, 100 Hz after carrier, limited by the synthesizer of the FSUP and -147dBc/Hz with the Holzworth system. Agilent results are similar to the R&S FSUP, just faster.
- At frequencies like 1 MHz off the carrier, these systems gave different results. The R&S FSUP, taking advantage of the “sweet-spot”, measures -183dBc, Agilent indicates -175dBc/Hz and Holzworth measures -179dBc/Hz.
- We have not researched the “sweet-spots” for Agilent and Holzworth, but we have seen publications for both Agilent and Holzworth showing -190dBc/Hz far-off the carrier. These were selected crystal oscillators from either Wenzel or Pascall [29]-[35][71].
- Another problem is the physical length of the crystal oscillator connection cable to the measurement system. If the length provides something like “quarter-wave-resonance”, incorrect measurements are possible. The list of disadvantages is quite long and there is a certain ambiguity whether or not to trust these measurements or can they be repeated.

6.11 Uncertainties in Phase Noise Measurement [42, Ch-4]

The uncertainties in phase noise measurement due to following:

- Harmonics
- Output Load Mismatch
- Output Phase Mismatch
- Cable Length (Delay)
- Equipment Dynamic Range

RF signals in VCOs, PLLs and synthesizers are characterized by signal power, harmonic content and phase noise; these parameters have to be accurately measured in order to guarantee the system performance. Phase noise measurement methods that use mixers to down-convert the signal to baseband are subject to uncertainty in presence of harmonics.

- Signal Source Analyzer topology
- The conversion characteristic of mixers
- Harmonic Measurement Set-Up

- Effects of fundamental and 3rd harmonic down-conversion on PN measurements
- Harmonic Injection Locking Mechanism
- Harmonic-Injection Locked VCO

6.12 Measurement: This work is to perform analysis of harmonics, phase, and delay and load variations during ultra-low phase noise measurement.

- Commercially available signal source analyzers (SSA) (Figure 6-32) use a phase detector method to measure the phase noise [88] and [89].
- The signal produced by the DUT is mixed with a reference generated by the instrument's internal oscillator and the result is filtered and sampled by an ADC.
- The ADC samples are analyzed and the information is used to extract the phase noise information and to synchronize the internal oscillator.
- Considering practical mixer and oscillator designs used inside the instrument; the harmonics produced by the DUT will also mix with the local oscillator's signal and will produce low frequency components.
- These low frequency components added to the fundamental components are sampled by the ADC resulting in measurement errors.

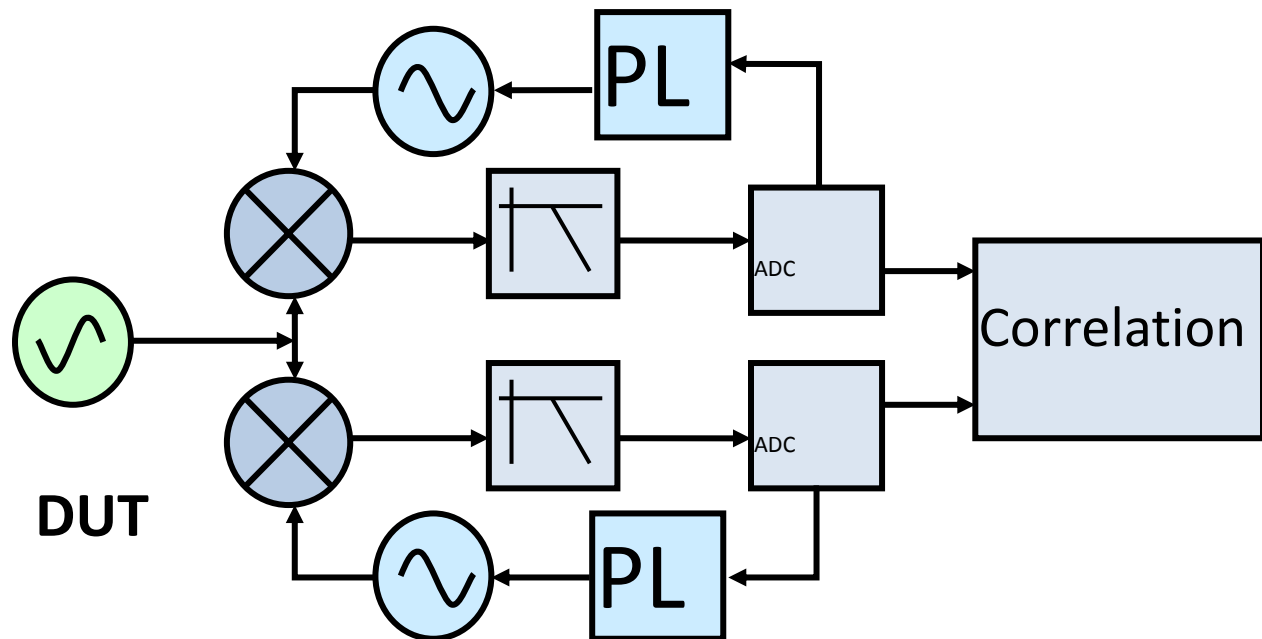


Figure 6-32: A typical Signal source analyzer [[63], ch4]

- The phase detection measurement uses a mixer to down-convert the DUT signal.
- The phase noise is extracted from the ADC's samples
- A PLL locks the internal oscillators to the DUT frequency.
- Correlation between the 2 channels reduces the noise floor of the instrument.
- Because mixers are used, DUT harmonics will influence the measurements.

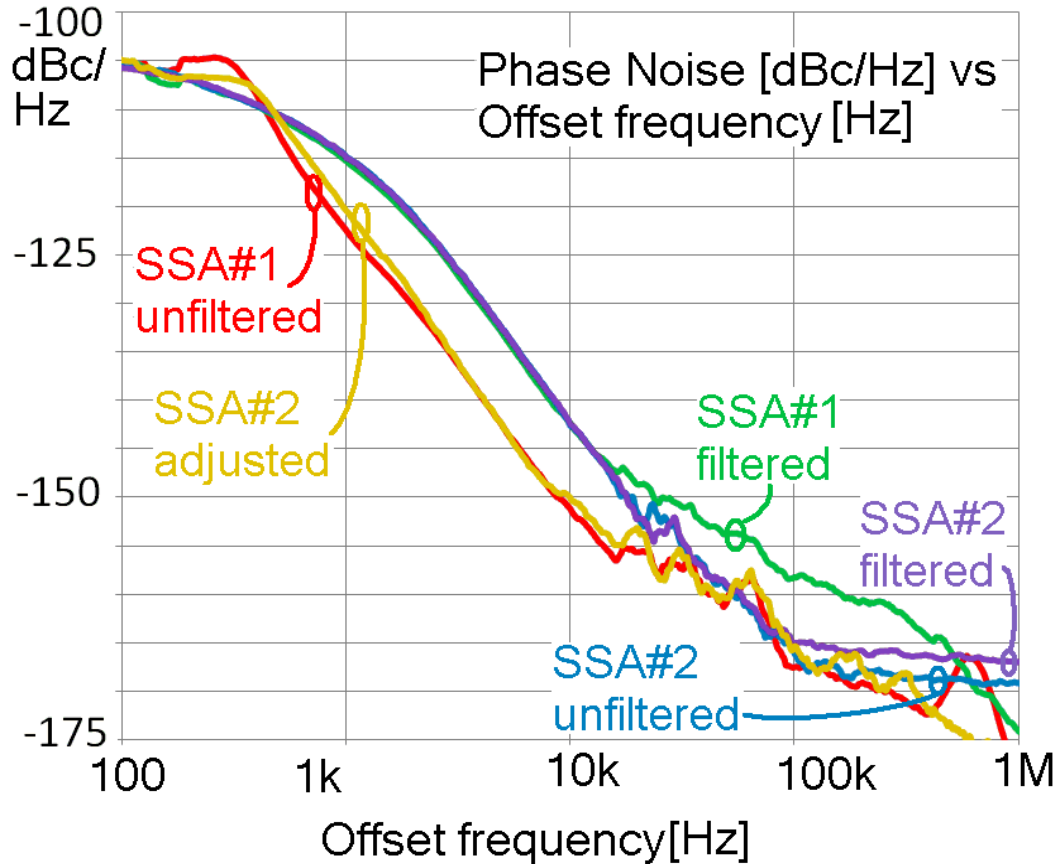


Figure 6-33: Phase noise measurement of 1 GHz SAW Oscillator (SSA#1: -151.9dBc/Hz @ 10 kHz for 1 GHz carrier frequency, SSA#2: -142.3dBc/Hz @ 10 kHz) HFSO 100 [63, ch4]

SSA#2 was adjusted (harmonically tuned injection locked source): -152dBc/Hz @ 10 kHz (HFSO 100). The filtered signal on both instruments reported as -142.34 and -142.41dBc .

The phase noise between 100 Hz and 10 kHz offset show little variation (less than 1dB) when measured on SSA #1 (filtered), SSA #2 (filtered) or SSA#2 (unfiltered) (Figure 6-33).

6.13 Some inferences, findings and suggestions:

- Phase noise measurement methods that use mixers to down-convert the signal to baseband are subject to uncertainty in presence of harmonics.
- If the mixed signals have harmonics, the mechanism that converts the harmonics to baseband will degrade the measurement accuracy.
- We have demonstrated how the harmonics can alter the accuracy of the phase noise measurements based on the mixer characteristics in the test equipment.
- Based on our observations we recommend that phase noise measurements should be performed on clean signals, harmonics level should be kept below -20dBc .
- In the case where harmonic levels are high we recommend that low pass filters be used to suppress the third harmonic to the levels below 20 dBc to get reliable and repeatable phase noise measurements.

- We developed harmonics-injection mechanism to improve the phase noise of SAW, Crystal and Dielectric Resonator Oscillator, including high performance frequency synthesizers.

Testing phase noise of ultra-low noise HPXOs and HFSOs (www.synergymwave.com) requires the cross-correlation technique. Special care must be taken for reduction of RF interference, especially while testing 100 MHz OCXO in the vicinity of strong interference caused due to noisy neighborhood. The choice of conducting the measurement in Faraday cage is welcome approach to minimize the error due to EMI.

6.14 Factors Influence Phase Noise Measurement

It is especially pertinent to production environment, where measurement time and accuracy of each measurement becomes critical. Several test methods and test instruments were investigated.

There's no "one size fits all" solution, but for each frequency range the optimum solutions were propose based on (1) Accuracy, (2) Repeatability, (3) Speed of Test, (4) Operating Range, (5) Cost and (6) Ease of data retrieval. The phase noise of -120dBc/Hz at 1 Hz offset from the carrier and better than -190dBc/Hz at far offset from the carrier (10 MHz offset) is a challenge using existing test equipment and methods and also the measured data should be reliable and repeatable.

As shown in Figure 6-29, phase noise measurement of 100 MHz OCXO using Agilent E5052B, Rohde & Schwarz FSUP 26, Holzworth, Noise XT, Anapico, was conducted, for understanding the capability and limitations of the equipments for a given test condition.

A survey of some of the more common topologies along with some possible trouble spots helps one to review and keep in mind the advantages and limitations of each approach.

Table 6-4 describes the quick summary that addresses phase noise measurement related problems and possible remedy [67].

Table 6-4: Phase noise measurement related problems and possible remedy [63][77]

Sr. No	PN measurement related issue	Possible remedy
1	Reference noise compromise measurement	Obtain lower noise reference or use cross-correlation and two-independent references
2	System noise compromise measurement	Use higher drive levels and /or higher drive level mixer
3	Broadband okay, but 1/f region too high	Look at a better reference or use carrier suppression or replace mixer
4	System overall noise floor is too high	Change over to a cross-correlation topology.
5	Calibration has errors due to mixer/amplifier gain variations with offset frequency	Use an AM/PM calibration standard to measure the system at each offset frequency
6	Residual detection of AM noise from Ref or DUT compromises measurement	See if a mixer with better balance will solve the problem or try to inject AM on the signal and adjust the phase balance (dc offset in the PLL loop) to minimize AM detection or switch to carrier suppression
7	Injection locking is occurring.	Improve the isolation between the sources and the mixer either by using an attenuator or an isolation amplifier. One may also need to look at power supplies or shielding.
8	PLL bandwidth compensating for the phase	Reduce the PLL gain or switch to the delay line discriminator approach or measure the amount of

	noise close to the carrier.	attenuation and compensate. This can be done using an AM/PM calibration standard.
9	PLL doesn't seem to be locking.	Do you have the right tuning voltage for your PLL output matched to the tuning range of your source? Does the source tune far enough to match the frequency of the other source? An external bias to the tune might be necessary to get the source close to the desired operating frequency.
10	PLL still doesn't seem to work	Frequency-divide the sources to a much lower frequency. Since the phase excursion also is divided, much less PLL gain is required and, hence, the PM bias is much less.
11	The final plot has large excursions between the peaks and valleys.	If you don't have a fairly fine line through the noise sections of the plot, the number of averages needs to be increased. See Table 1 for details.
12	Line harmonics are too high or causing excess measurement noise.	Make sure all of the equipment is on the same side of the ac line. Look at using line filters, conditioners, or batteries. Consider using an inside/outside dc block. Move the measurement system away from high ac current sources and transformers.
13	Dynamic range limitation	It is possible to insert a notch filter between the test object and the analyzing receiver (or spectrum analyzer). This way the carrier can be suppressed while the sideband noise is not much affected.

6.15 Conclusion

The task was for conducting rigorous phase noise measurement using most of the equipment that claims to be measuring below the kT noise floor using cross-correlation techniques. It has been noticed that the simultaneous presence of correlated and anti-correlated signals can lead to gross underestimation of the total signal in cross-spectral analysis. Keeping in view of these circumstances, the danger of downfall of cross-correlation techniques used by many equipment companies is high and must be evaluated and used very carefully. The evaluation and analysis described in this thesis was time consuming exercise and for doing so state-of-the art low noise OCXOs and VCXOs (voltage controlled SAW oscillators) were developed that measure typically -147 dBc/Hz @ 100 Hz offset for 100 MHz OCXO and -153 dBc/Hz @ 10 kHz offset for 1 GHz SAW oscillators and exhibit noise floor -178 dBc/Hz at far offset on most of the Phase noise measurement equipment. The challenging exercise was to measure better than kT , -200 dBc/Hz (-177 dBc/Hz- $+20$ dBm) $= -197$ dBc/Hz SSB -3 dB hence -200 dBc/Hz) at 1 MHz offset from the carrier for output power of 20 dBm and the measured data should be reliable and repeatable.

The extensive phase noise measurement was carried out as a part of this research work, reported in IEEE Microwave Magazine, Vol. 14, Sept/Oct 2013 [24].

There are many possibilities in which design engineers can be tricked into false readings or frustrated with the process of trying to achieve a good measurement. Characterizing the phase noise of a system or component is not necessarily very easy. Many different approaches are possible, but the key is to find the best approach for the measurement requirements at hand.

Chapter 7: Experimental Validations-Design Methodology of High Performance Crystal Oscillators

At the heart of today's communication systems lies the autonomous signal sources or oscillators, that are used in test and measurement equipments and communications equipments. The requirements of a system, based on the applications, govern the design criteria of such oscillators. The present day oscillators have evolved over the past century and offer a wide range of options with stringent specifications in terms of power consumption, performance and cost. Optimization for better phase noise and overall performance can be considered as the key design criteria and, a Figure of Merit (FoM) that includes all the important parameters to determine the performance of oscillators. In the case of voltage controlled oscillators, there is noise or hum contribution from the power supply, the tuning diodes, the heater (in case of the crystal), the influence of external magnetic fields and other electrical disturbances [9][29][31][48][49].

This chapter describes the winning entry (*First place*) in the IEEE Microwave Theory and Techniques Society (MTT-S) 2016 International Microwave Symposium (IMS2016) Student Design Competition (SDC) for the category focused on a low-phase-noise 100 MHz crystal oscillator, which was sponsored by Technical Committees IEEE MTT-17 (www.mtt.org/committee/mtt-17-hf-vhf-uhf-technology-committee/) and IEEE MTT-22 (<https://www.mtt.org/committee/mtt-22-signal-generation-and-frequency-conversion-committee/>). All competition participants received identical crystal resonators from the same vendor; hence, the major task was to design a circuit using novel noise-cancellation techniques to realize a low-phase-noise signal source. The methodology opted to win this prestigious design competition was based on considering the various limitations in the design and present a novel approach for achieving high dc-RF conversion efficiency (η) without degrading phase noise and oscillator FOM performance [31].

This chapter discusses the quartz crystal resonator based signal sources and presents a novel approach for achieving high DC-RF conversion efficiency (η) without degrading the PN (phase noise) and oscillator FOM performances [9][10][50].

The design specifications that were given to students at IMS 2016 are used here as a reference.

7.1 Design Specification based on IMS 2016 SDC (Student Design Contest)[31][53]:

- Size of the planar PCB: < 1.5 inch square package
- Steady State DC power consumption: < 2000 mW (I_{dc} Max=150 mA)
- Frequency Tuning range: +/-5ppm (typical)
- Free Running frequency: \cong 100 MHz
- Output Power: > 10 dBm into a 50-ohm load impedance
- The performance of the oscillator circuits based on the FOM (Figure of merit) parameters as measured with a phase noise analyzer, can be given by

$$FOM|_{f_{offset}} = \left[\mathcal{E}(f_{offset}) - 20 \log_{10} \left(\frac{f_o}{f_{offset}} \right) + 10 \log_{10} \left(\frac{P_{DC}}{1mW} \right) \right] \quad \left(\frac{dBc}{Hz} \right) \quad (7-1)$$

where f_o is the oscillation frequency, $E(f_{offset})$ is the phase-noise at the offset frequency f_{offset} , k is the Boltzmann constant, T is temperature in Kelvin, and P_{DC} is the total consumed DC power in milli-watts. The larger values of $|FOM| \left(\frac{dBc}{Hz}\right)$ values relate to superior performance oscillators.

7.2 Example: 100 MHz crystal oscillator

Figures (7-1) and (7-2) show the conventional and modified 5th overtone 100 MHz crystal oscillator, utilizing dynamic phase-injection and mode-coupling to improve the phase noise and stability. As shown in Figure (7-1), which is based on [9, Appendix C], higher order mode is coupled through the output path and fed back to the point where resonator impedance shows steep change of phases, thereby, maximizing the group delay.

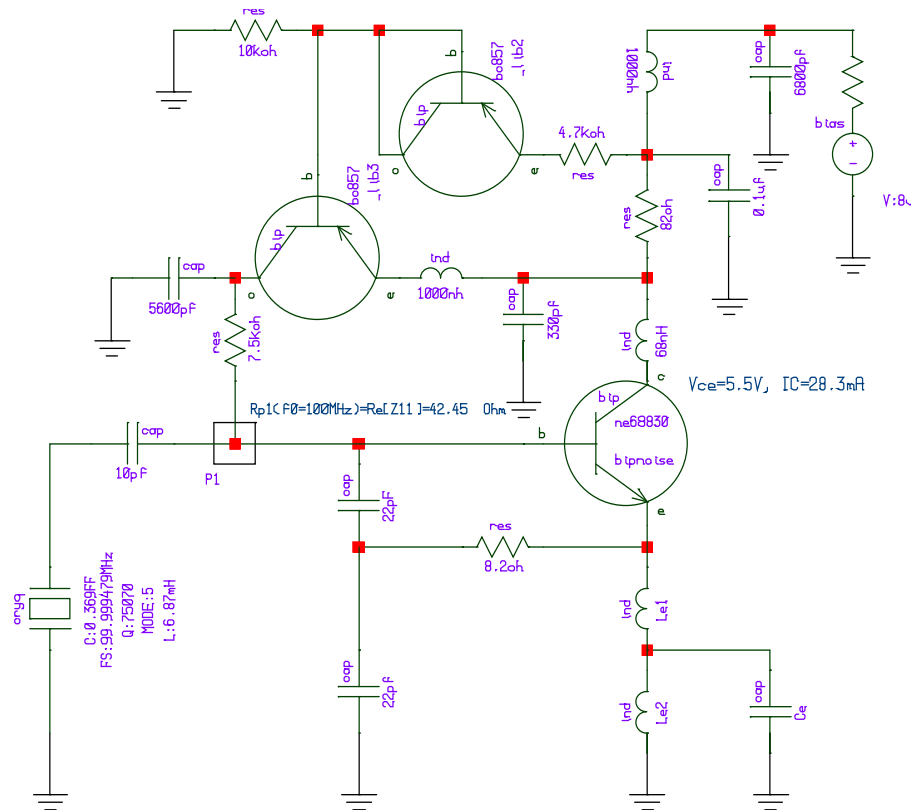


Figure 7-1: A typical 100 MHz conventional crystal oscillator (tuning diodes are not included for simplification) [31]

The CAD simulation circuit schematic as shown in Figure 7-2 was considered for the actual design prototype. As depicted in Figure 7-2, the Mode-Locking and Injection-Phase Locking network improves the overall performances. The Mode-Locking network is comprised of a multiple parallel, series tuned LC circuit for locking the desired overtone modes for operating two crystal resonator connected in parallel for the realization of lower phase noise. It is to note that Injection-Phase Locking network as shown in Figure 7-2 improves the group delay and lowers the close-in carrier phase noise by linearizing and lowering the RF drive level across the crystal resonator. The result of the simulated phase noise is shown in Figure 7-5, which is significantly better than conventional OCXO. This design was then implemented to build a prototype as shown in Figure 7-3. Another revision was made to the prototype to fit the design guidelines for the student design contest at IMS 2016, which can be seen in Figure 7-4. The measured phase noise of this design using the R&S FSWP which had just then become available, is also shown in the Figure 7-4. The measured phase

noise with a significant improvement especially in the noise floor after addition of the crystal filter at the output is shown in Figure 7-7(a) and (b). All these modifications improved the FOM of the circuit under the given criteria for the SDC at IMS 2016.

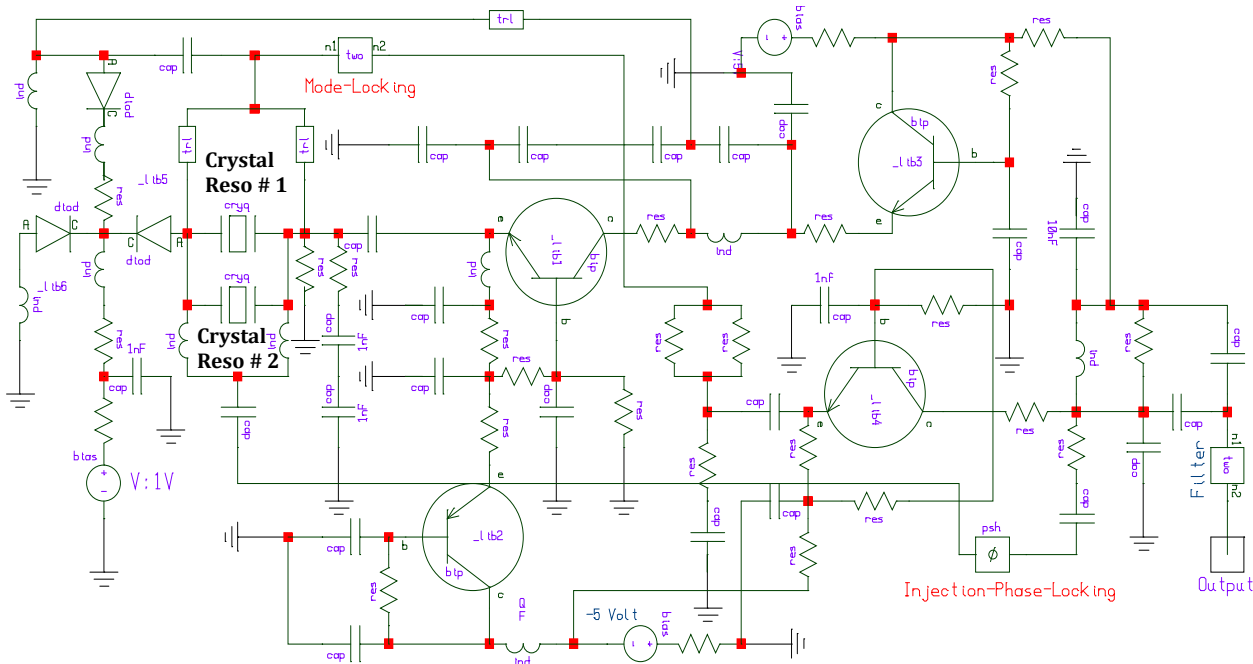


Figure 7-2: 100 MHz 5th overtone crystal oscillator circuit (DC Bias: 5V, 42mA), heater circuit is not included, typical power consumption in steady-state with heater is typically 660mW, startup power consumption with heater 1120 mW) [31]

Figure (7-3) shows the prototype developed for the validation purpose and Figure 7-4 shows the DUT (device under test: 100 MHz OCXO) connected to the phase noise measurement equipment.

Prototype development:

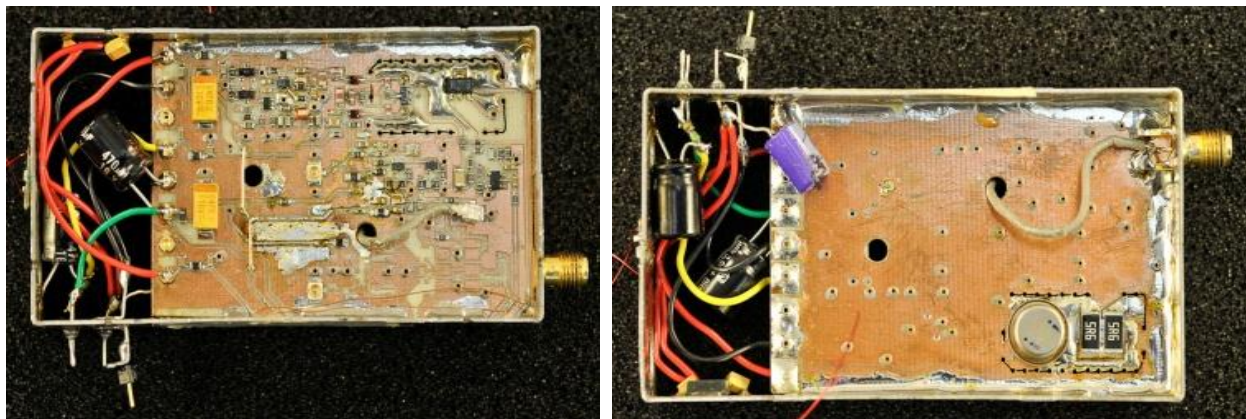


Figure 7-3: Prototype board of the 100 MHz Crystal Oscillator (Top and Bottom sides) [13]

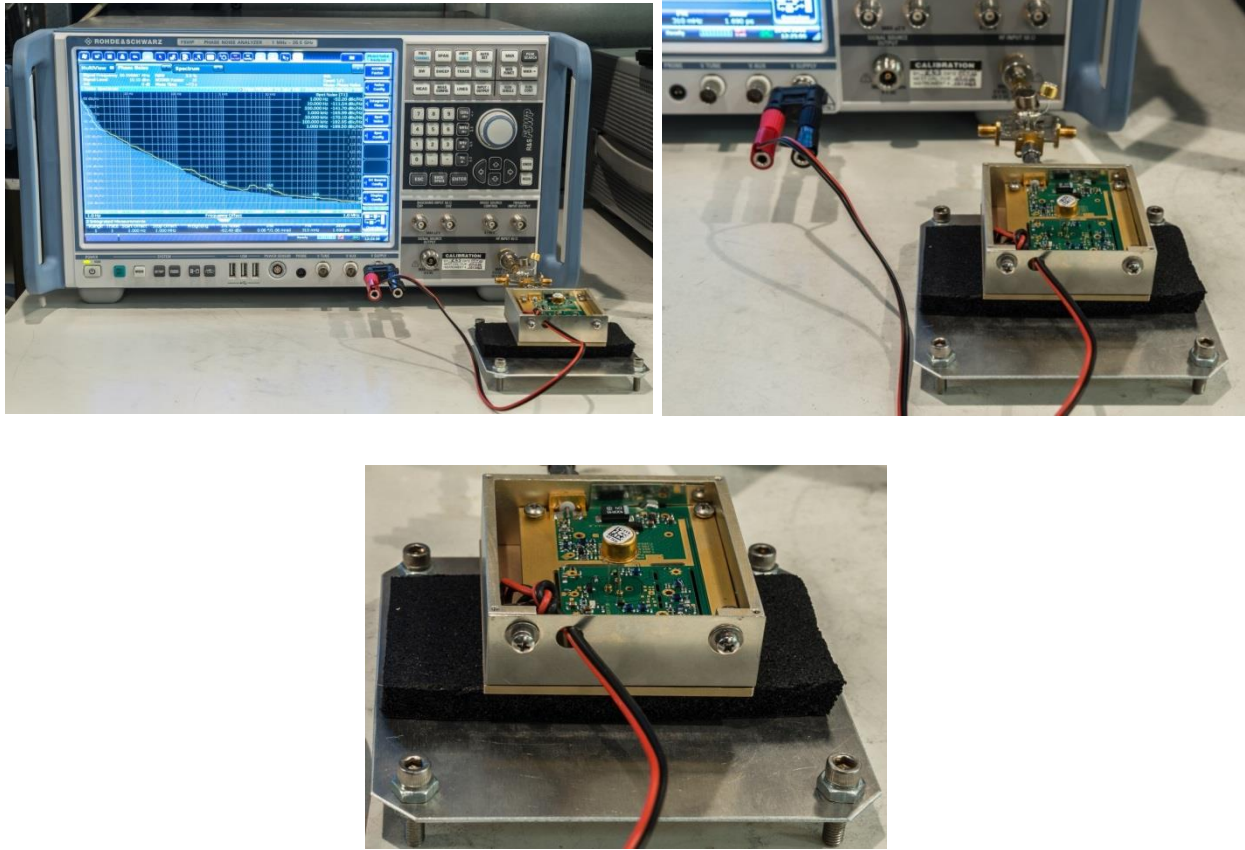
Actual Circuit - IMS 2016 - Student Design Competition

Figure 7-4: Shows the measurement setup with 100 MHz 5th overtone OCXO, the measured Phase Noise is -141dBc/Hz @ 100 Hz offset with -193 dBc/Hz noise floor [31]

Figures (7-5) and (7-6) show the simulated and calculated phase noise for comparative analysis, with crystal resonator unloaded quality factor of 100,000. As illustrated in Figures (7-1) and (7-2), injection-phase-locking and mode-locking are effective methods to minimize the noise and improve the overall performance. Figure 7-7a & Figure 7-7b shows the measured phase noise plots; the measurements closely agree with simulated phase noise depicted in Figure (7-5).

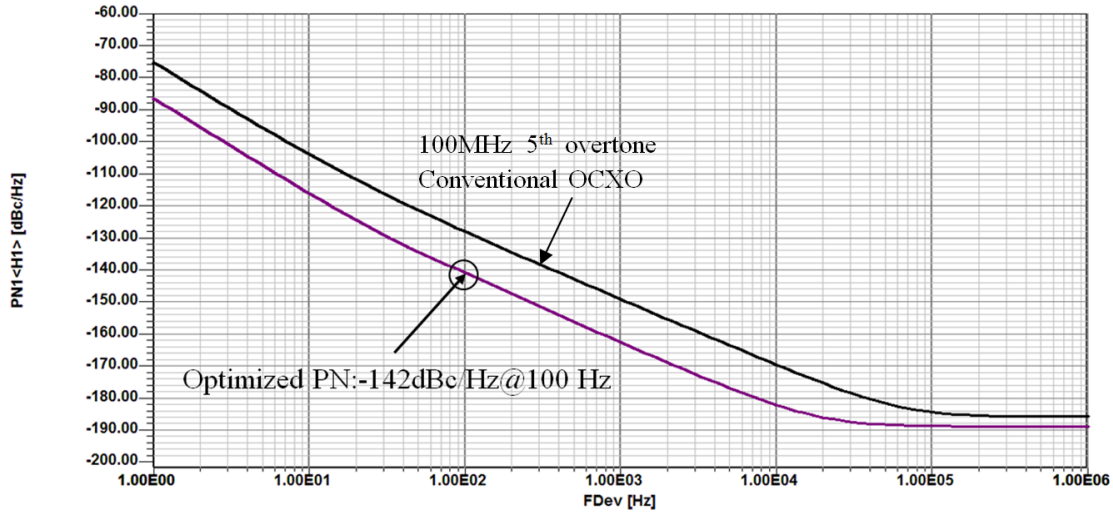


Figure 7-5: CAD simulated PN plots for 100 MHz 5th overtone OCXO (ovenized crystal oscillator): trace T1 and T2 show the conventional 100 MHz OCXO, PI+MC+NF (phase-injection, mode-coupled, and noise filtering), noise floor of trace T2 is -190 dBc/Hz@ 1MHz offset [31]

Calculated Phase Noise Contribution from different noise sources [9]:

$\hat{f} := 100 \cdot 10^6$	$\omega_0 := 2 \cdot \pi \cdot \hat{f}$	$\omega_0 = 6.283 \cdot 10^8$	$I_c := 13 \cdot 10^{-3}$	$I_b := 130 \cdot 10^{-6}$
$R := 7.5 \cdot 10^{11}$	$r := 6.14$	$q := 1.6 \cdot 10^{-19}$	$T := 290$	$L := 15 \cdot 10^{-3}$
$C_0 := 4.7 \cdot 10^{-15}$	$Q := 60000$	$AF := 2$	$C_2 := 4.7 \cdot 10^{-12}$	$n := 2.5$
$\Delta\omega := 1 \cdot 10^2 \cdot (2 \cdot \pi)$		$K := 1.38 \cdot 10^{-23}$	$C_1 := 6.5 \cdot 10^{-12}$	$kf := 1 \cdot 10^{-11}$
$f_m := 100$	$C_{eff}(C_1) := \left[C_0 + \frac{(C_1) \cdot (C_2)}{C_1 + C_2} \right]$		$C_{eff}(C_1) = 2.732 \cdot 10^{-12}$	$\frac{C_1 + C_2}{C_2} = 2.383$
$\left(\frac{C_2}{C_1 + C_2} \right) = 0.42$	$\Delta\omega = 628.319$	$\frac{\omega_0}{\Delta\omega} = 1 \cdot 10^6$	$\frac{C_1}{C_1 + C_2} = 0.58$	$\frac{1}{(2 \cdot Q \cdot C_{eff}(C_1) \cdot \omega_0)} = 4.854 \cdot 10^{-3}$
$PN1_{res} := 10 \cdot \log \left[\frac{(4 \cdot K \cdot T)}{2 \cdot R} \left[\frac{1}{2} \cdot \left(\frac{1}{2 \cdot \omega_0 \cdot C_{eff}(C_1)} \right) \cdot \left(\frac{\omega_0}{\Delta\omega} \right)^2 \right] \right]$				PN1res = -156.453
$PN2_{rb} := 10 \cdot \log \left[(2 \cdot K \cdot T \cdot r) \cdot \left[\frac{1}{2} \cdot \left(\frac{C_1 + C_2}{C_2} \right) \cdot \left(\frac{1}{2 \cdot Q} \right) \cdot \left(\frac{\omega_0}{\Delta\omega} \right)^2 \right] \right]$				PN2rb = -173.147
$PN3_{ibif} := 10 \cdot \log \left[2 \cdot q \cdot I_b + \frac{(2 \cdot \pi \cdot kf \cdot I_b \cdot AF)}{\Delta\omega} \right] \cdot \left[\left(\frac{C_2}{C_1 + C_2} \right) \cdot \left(\frac{1}{4 \cdot Q \cdot C_{eff}(C_1) \cdot \omega_0} \right) \cdot \left(\frac{\omega_0}{\Delta\omega} \right)^2 \right]$				PN3ibif = -147.457
$PN4_{KF} := 10 \cdot \log \left[\frac{kf \cdot (I_b)^{AF}}{f_m} \cdot \left[\frac{1}{2} \cdot \left(\frac{C_2}{C_1 + C_2} \right) \cdot \left(\frac{1}{2 \cdot Q \cdot C_{eff}(C_1) \cdot \omega_0} \right) \cdot \left(\frac{\omega_0}{\Delta\omega} \right)^2 \right] \right]$				PN4KF = -147.562
$PN5_{ic} := 10 \cdot \log \left[2 \cdot q \cdot I_c \cdot \left[\frac{1}{2} \cdot \left(\frac{C_1}{C_1 + C_2} \right) \cdot \left(\frac{1}{2 \cdot Q \cdot C_{eff}(C_1) \cdot \omega_0} \right) \cdot \left(\frac{\omega_0}{\Delta\omega} \right)^2 \right] \right]$				PN5ic = -140.834

Figure 7-6: Calculated Phase Noise from the different noise sources [9]

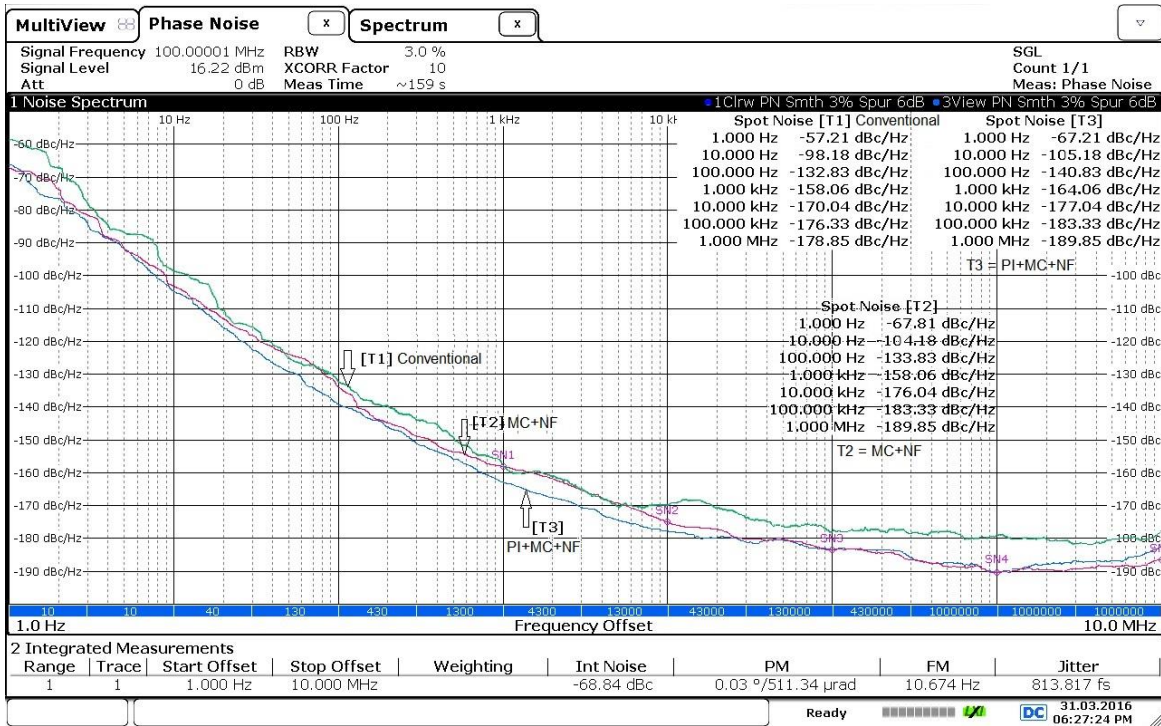


Figure 7-7a: Measured PN plots for 100 MHz 5th overtone OCXO: trace T1, T2, and T3 show the conventional 100 MHz OCXO, MC+NF (mode-coupled and noise filtering), and PI+MC+NF (phase-injection, mode-coupled, noise filtering), noise floor of trace T3 is -189.85dBc/Hz@ 1 MHz offset (with heater) [31]

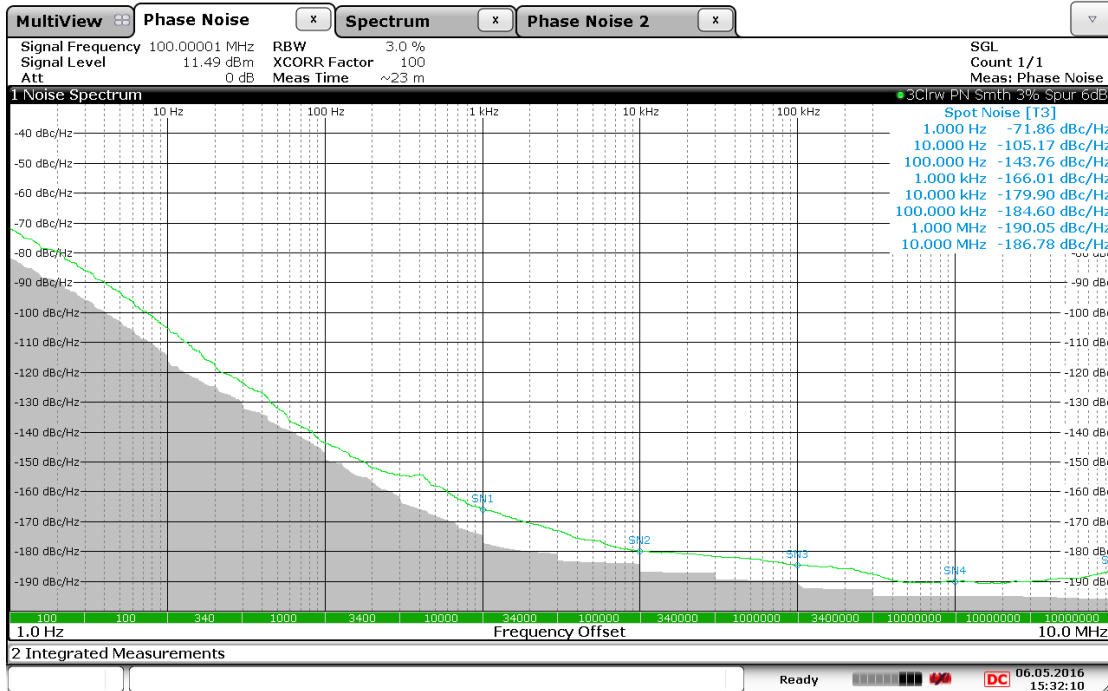
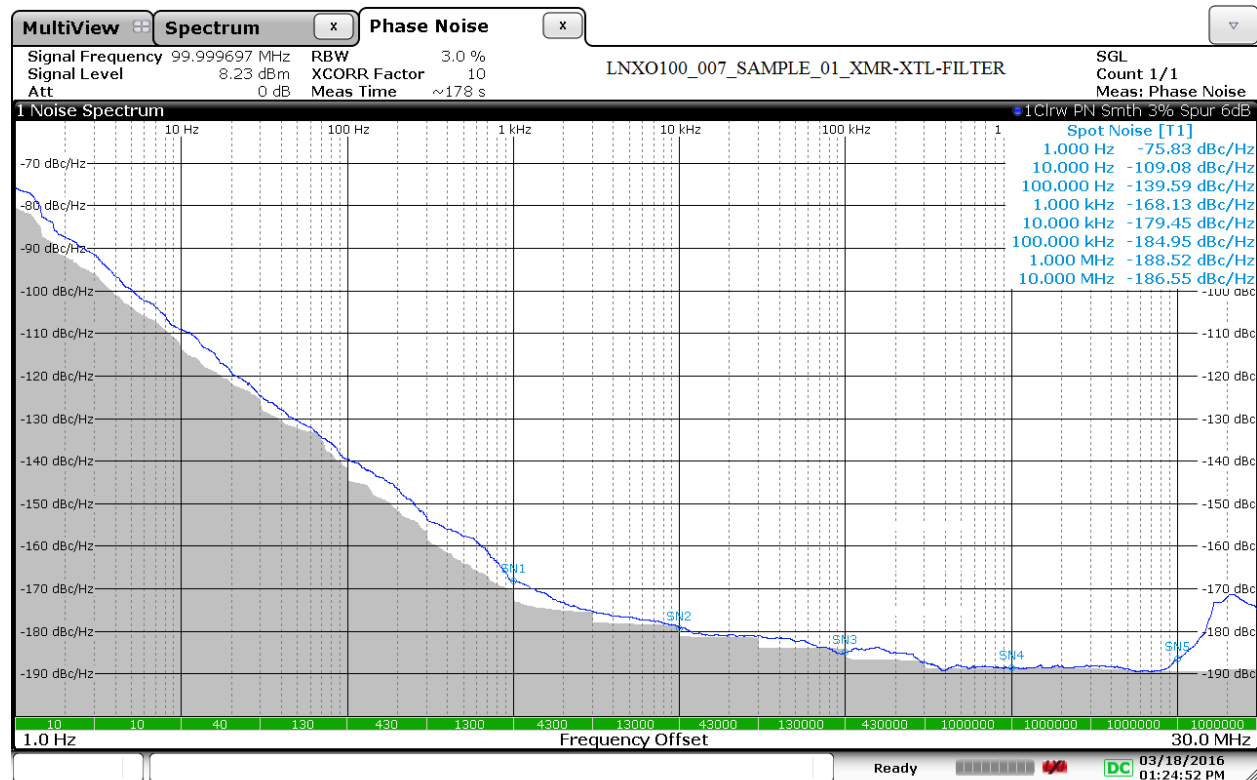


Figure 7-7b: Measured PN plots for 100 MHz 5th overtone OCXO: optimized using PI+MC+NF (phase-injection, mode-coupled, noise filtering) [31]

Figure 7-7a and 7-7b depict measured phase noise plots for the 100 MHz 5th overtone OCXO. As illustrated in Figure 7-7a, trace T1, T2, and T3 show the conventional 100 MHz OCXO, MC+NF (mode-coupled and noise filtering), and PI+MC+NF (phase-injection, mode-coupled, noise filtering) respectively. Noise floor of trace T3 is -189.85dBc/Hz at 1 MHz offset (with heater). Figure 7-7b shows the measured phase noise plot of optimized 100 MHz OCXO as a part of SDC (IMS 2016). The phase noise at 100 Hz offset from the carrier is -143.76dBc/Hz with 16.22 dBm output power as seen in the Figure 7-7a. Attenuation due to the notch filter is approximately 5dBm, as seen in the measured plot of Figure 7-7b. The far offset measured noise floor is -189.85dBm/Hz at 1 MHz offset. The total power consumption in steady state is 660mW (210 mW for crystal resonator oscillator + 350mW for ovenized heater). As illustrated in Figures (7-1) and (7-2), noise filtering at the output of the oscillator circuit (shown as 2-port crystal resonator 100 MHz filter) offers 8-10 dB improvement in noise floor.

The total startup DC power consumption is 1120 mW which includes the heater and oscillator circuit. The measured FOM (figure of merit) is -235.8dBc/Hz at 1 kHz offset for 100 MHz ovenized crystal resonator oscillator.

The noise at close-in, upto 10 Hz, can be improved by using large power, metal film resistors with 1% tolerance. In the circuit designed for the 100 MHz crystal oscillator, the use of such low tolerance resistors was tried out and the following Figure 7-8, shows the improvement in close-in noise when similar low tolerance resistors were used. The phase noise at 1 Hz offset improved by about 6dB. This needs to be optimized and needs to be addressed with a more step by step and thorough research in the future work.



Date: 18.MAR.2016 13:24:52

Figure 7-8a: Improvement in close-in noise is seen after using some low tolerance metal film resistors (this needs to be optimized in future work)

Table 7-1: shows the comparison of simulated and measured results after optimization with phase injection, mode coupling and noise filtering techniques.

Table 7-1: Comparison of Simulated and Measured results after optimization [31]

Offset Frequency	1 Hz	10 Hz	100 Hz	1 kHz	10 kHz	100 kHz	1 MHz
Simulated Phase Noise in dBc/Hz (Optimized)	-86	-116	-142	-163	-182	-189	-189
Measured Phase Noise in dBc/Hz (Optimized)	-72	-105	-144	-166	-179	-184	-190

Wenzel Associates, Inc. Austin, Texas				
Title: 100 MHz-SC Golden Citrine Crystal Oscillator				
P/N: 501-25900	Rev: B	Date: 05-29-13	Drawn:	Ref:
Tolerances: (except as noted) Dimensions are in inches	0.XX Dec: $\pm 0.030''$	0.XXX Dec: $\pm 0.010''$	FSCM: 62821	Page 1 of 1

Phase Noise L(f)	
100 Hz	-138 dBc/Hz
1 kHz	-163 dBc/Hz
10 kHz	-183 dBc/Hz
100 kHz	-188 dBc/Hz

Figure 7-8b: Part of datasheet of a typical crystal oscillator with its phase noise table [Courtesy Wenzel, www.wenzel.com]

The part from the datasheet of one of the leading crystal oscillators on the market is shown above. The measured results of this work are comparable and better at 100 Hz and 1 kHz offsets, and the design in this work is independent of the transistor as the gain is the ratio of two resistors.

Table 7-2 shows the recent published papers on crystal resonator oscillators, compares this work based on DC-RF conversion efficiency, phase noise and FOM at 1 kHz offset from the carrier.

Table 7-2: Recent published Crystal oscillator performance and this work

References	f_o MHz	P_{DC} mW	P_o dBm	DC-RF Conversion Efficiency	$L(f)$ dBc/Hz@ 1 kHz	FOM dBc/Hz @ 1 kHz
[55]	100	300	7.9	2.05%	-157	-232.2
[56] OCXO With heater	100	1000	3.98	3.98%	-163	-233
This Work OCXO With heater (Fig. 7-4)	100	660	16.22	6.31%	-166	-235.8
This Work Without heater (Fig. 7-4)	100	210	15.7	17.69%	-169	-245.7

(Ref. 12 and 13 shown in Table 2 describes crystal oscillator without heater) [31]

The crystal oscillator circuit (Fig. 7-4) exhibits phase noise -169 dBc/Hz and FOM -245 dBc/Hz @ 1 kHz offset with 15.7dBm o/p power and DC-RF conversion efficiency 17.69 % when heating circuit is not connected.

7.3 Example 125 MHz Crystal Oscillator

Using design methodology described in section 7.1, 125 MHz crystal oscillator is built and measured. Figures 7-9 and 7-10 show the prototype of the 125 MHz crystal oscillator and measured phase noise plot. Table 7-1 shows the detailed specification of commercial 125 MHz crystal oscillator built as a part of the research study.



Figure 7-9: shows the prototype 5th overtone 125 MHz crystal (crystal resonator unloaded Q=90,000)[13]

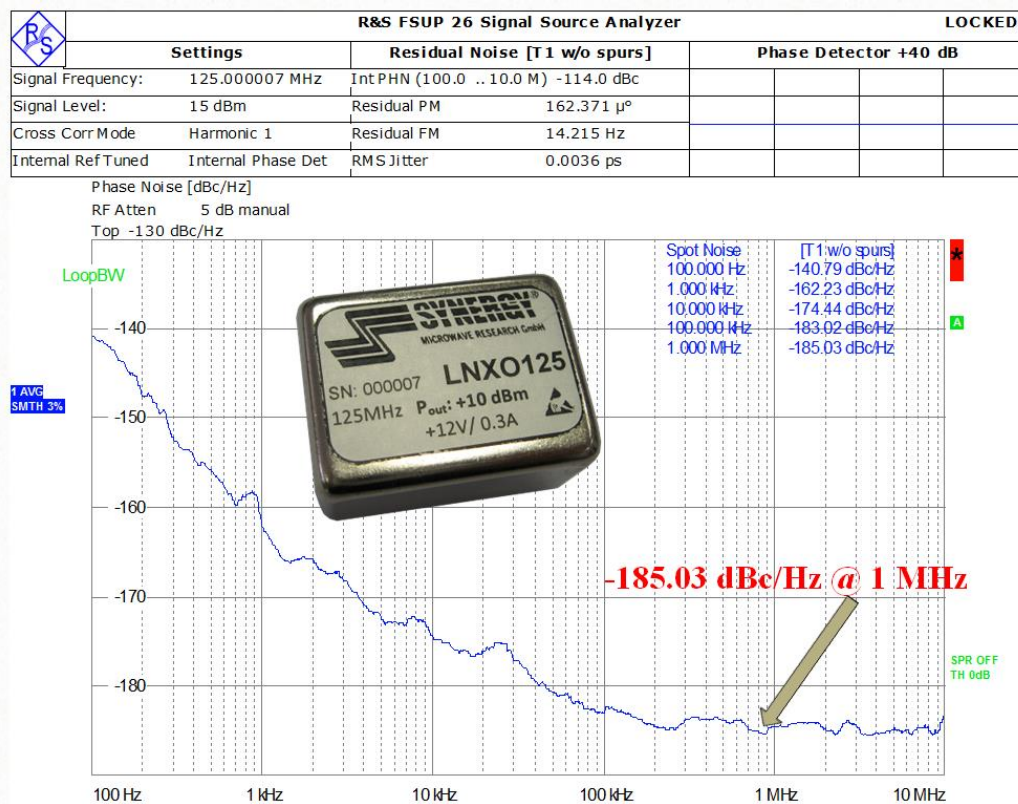


Figure 7-10: Measured Phase Noise of the 125 MHz Crystal Oscillator [13]

Table 7-3: Specification of the 125 MHz Crstal Oscillator circuit [Courtsey: Synergy Microwave Corp.]

Parameter	Unit	Value			Conditions / Notes
		Min.	Typ.	Max.	
<i>All specifications at 25°C ambient Temperature, unless otherwise specified</i>					
Frequency	MHz	125			Other frequency on request
Frequency tuning range	ppm		± 5		Tuning : 1...10V
Frequency stability over temperature	ppm		≤ ±0.2	≤ 0.5	
Aging	ppm/Year		±0.3		after 30 days of continuous operation
Warm up time	sec.	300			
Phase Noise	dBc/Hz				
	100 Hz	≤ - 135	≤ - 140		
	1 KHz	≤ - 160	≤ - 162		
	10 KHz	≤ - 170	≤ - 174		
	1MHz	≤ - 180	≤ - 185		
Jitter	fs		≤ 6	10	
Output power	dBm	+ 10	+ 15		Sine wave at 50Ohm load
Harmonics	dBc		- 35	- 25	
Supply voltage V_s	V	+11.4	+12	+12.6	
Supply current I_s	mA			≤120	
	steady state @+25 °C				
	during warm-up			≤300	
Temperature range (OTR)	operating	°C	-20	+ 60	
	storage		- 35	+ 85	
Mass	kg	max. 0.03			
Dimensions	mm	36 x 27 x 17			

7.4 Example: 155.6 MHz Crystal Oscillator

Another example, a commercial 155.6 MHz VCXO was used and the concept of mode-feedback, and mode-coupling mechanism was applied to the design [10][11]. The promising alternative for high performance VCXO at 155.6 MHz is overtone mode, which is similar in concept to a harmonic, with the exception that crystal oscillation overtones are not exact integer multiples of the fundamental. The new approach includes dynamic noise filtering, mode-feedback, noise-feedback, and mode coupling for optimum group delay to enhance the loaded Q and suppress mode-jumping phenomena (especially when the crystal resonates at higher odd-order overtone modes).

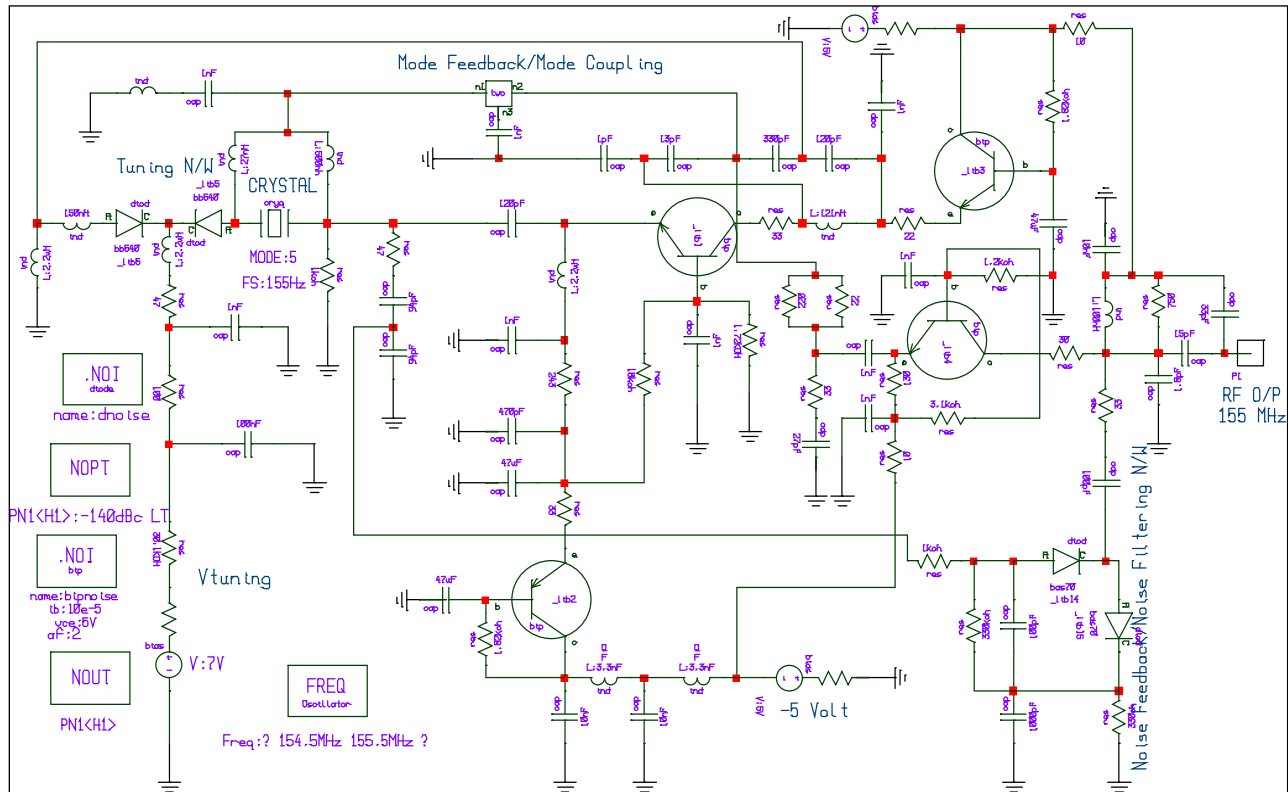


Figure 7-11: 155.6 MHz Mode-Feedback 5th overtone crystal oscillator, resonator Q=100k [122]

Figure 7-11 shows the 5th overtone 155 MHz VCXO circuit in which higher order mode is coupled through output path and feedback to the point where resonator impedance shows steep change of phases, thereby, maximization of group delay. Additional improvement in the phase noise is achieved by dynamically optimizing noise-feedback and mode-coupling mechanism. The dynamic noise-feedback is an effective method to reduce the 1/f noise. By introducing an additional low frequency negative feedback loop, the close-in noise is reduced by approximately 10-15 dB in the flicker region. A mode-feedback and noise filtering offers significant improvement in phase noise performances, 2 shows the measured phase noise plot, -137 dBc/Hz @ 100 Hz offset for 155.6 MHz carrier frequency. At lower offset (1 Hz), improvement in phase noise performance is limited due to the influence 1/f noise, which can be optimized by selecting transistor that has low value of 1/f noise.

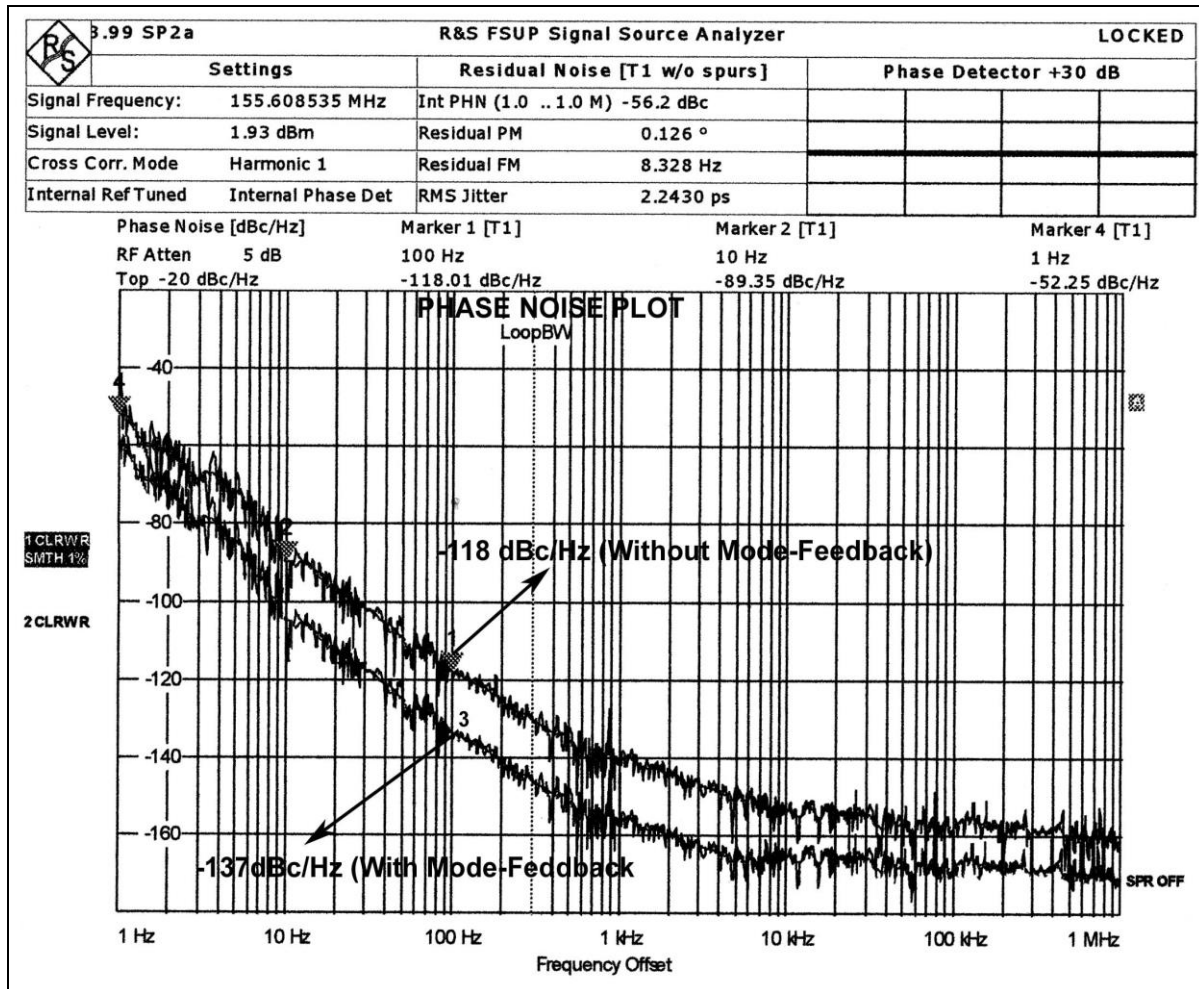


Figure 7-12: Measured phase noise plots for 155.6 MHz 5th overtone crystal oscillator [122]

7.5 Conclusion

This work offers a novel approach for designing power-efficient signal sources for the application in frequency generating and frequency controlled electronic circuits and systems. The novel PI (phase-injection) and ML (mode-locking) techniques can be applied for other variations of oscillator circuits detailed report is published [31]. The measured phase noise performance is the best performance reported too date for this class of the technology.

7.6 Acknowledgement

Author acknowledges the support and help provided by Coven Crystals Wenzel International Inc, Keysight (Agilent), Rohde & Schwarz, and National Instruments (NI).

The experience of meeting with some of the legends and pioneers in the field was extraordinarily overwhelming and I consider myself highly privileged to have my work looked at and appreciated by them.



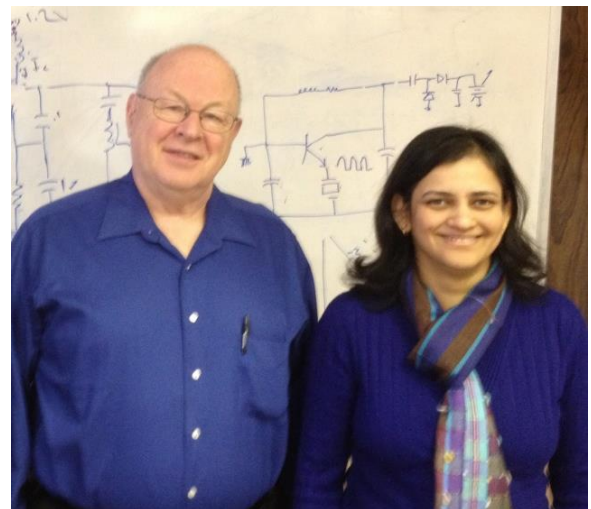
Dr. Paul Khanna (IMS President) verifying the measurements



Anisha Apte with Dr. David Leeson



Prof. Jeremy Everard and Anisha Apte



Michael Driscoll and Anisha Apte



Prof. Ulrich L. Rohde presenting the student award to Anisha Apte

Figure 7-13: Pictures taken at IEEE conferences

Chapter 8: Future Work, Market trends and Conclusions

This closing chapter provides a summary of the key results and proposes additional research. Although further development work will enable even better low noise crystal oscillator circuits; based on what has been demonstrated here, the 100 MHz crystal oscillator reported as a part of this research study is best to date for a given resonator Q-factor and FOM.

8.1 Summary

The crystal technology currently seems to be at a point where it is very stable and reliable and can be said to have reached the limits of physics. In this dissertation, after analyzing the first crystal oscillator by W.G. Cady (1921), other high performance crystal oscillators have been discussed, analyzed and calculated. As most crystal oscillators are phase locked in synthesizer, the phase noise below 10 Hz offset is dependent on the semiconductors and not the crystal. With new techniques of integration and manufacturing of the semiconductor devices, an in-depth study of transistor breakdown voltage and flicker noise etc. and its effect on phase noise and other performances is required, though out of the scope of this dissertation. For the oscillator, the tuning diode sensitivity and flicker noise contribution need to be taken into consideration and should be sufficient but not more than necessary. Noise induced due to infra-red radiation from the heater circuit and power supply needs to be studied.

In this thesis, design methodology is investigated for noise reduction as well as extending the operating frequencies option for future possibility of utilizing high frequency crystals for carrier synthesis in the microwave range. The discussions and observations pointed out are related to circuit schematic simulations, prototype building and experimental validations, which were sufficient for the completion of this thesis. For future study, the effects of vibration and shock, driving sensitivity and amplitude frequency (AF) effect can be addressed.

8.2 Vibration and Shock Sensitivity:

In modern communications a system that includes a clock oscillator, the vibration sensitivity of the crystal oscillator is a requirement that is straightforwardly discounted. Sensitivity to vibration can have a detrimental impact on the overall performance of the communication systems. In this thesis, effect of vibration and shock is not evaluated, though recommended for future study.

Figure 8-1 and 8-2 shows the degradation of the phase noise plots under vibration measured at Rohde & Schwarz facility in Munich, Germany. The DUT (device under test) is 100 MHz crystal oscillator circuit built as a part of the research work for this thesis.

The dependency of quartz crystal resonator frequency on excitation current magnitude is termed as the amplitude frequency (AF) effect. The AF effect sometimes described as a bending of the resonator response characteristics, is an important consideration in oscillator applications, because it limits the maximum resonator current and thereby the signal-to-noise ratio at large offset frequencies. It is also a mechanism for the conversion of amplitude modulation (AM) to phase modulation noise at smaller offset frequencies. The AF effect of a typical crystal resonator is described as

$$\delta = k[I_x]^2 \quad (8-1)$$

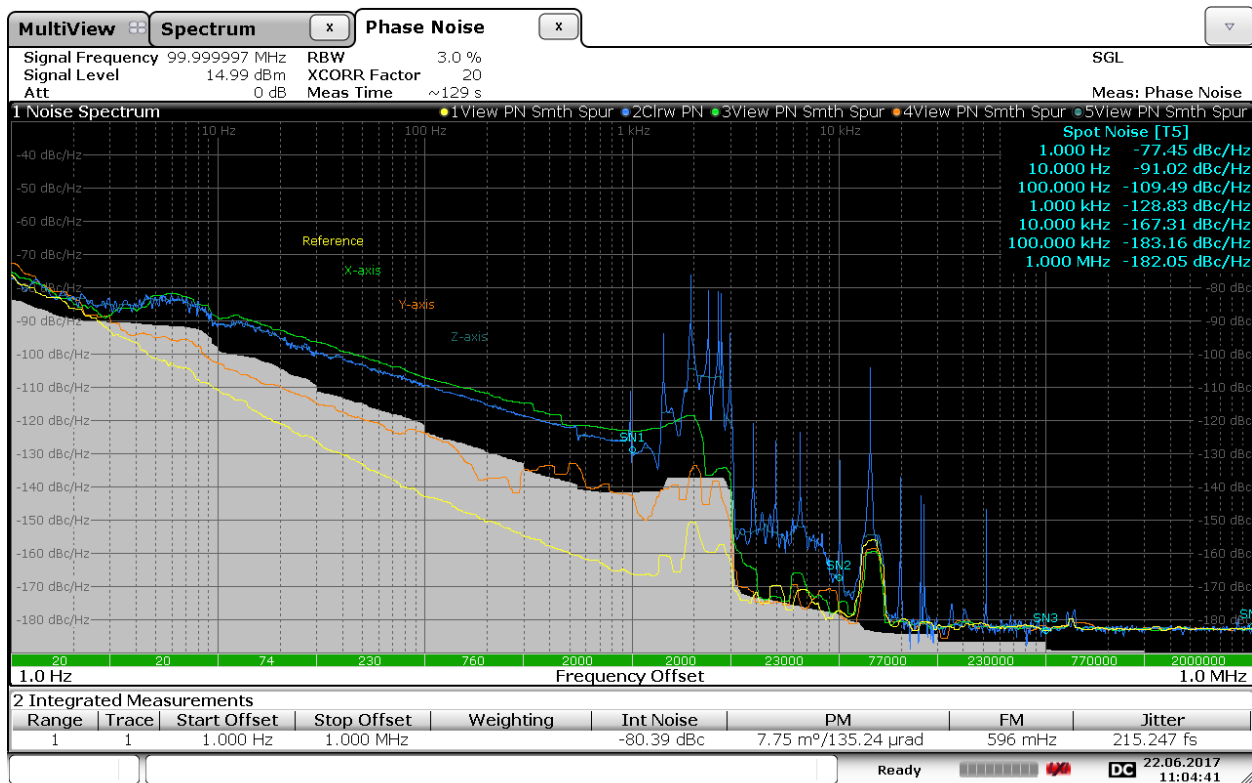
where δ is the fractional frequency change, I_x is the amplitude of the resonator motional arm current, and k is AF coefficient defined as a complex function of material properties and orientation angle (cut), as well as resonator properties such as overtone frequency (f_n), overtone (n), impedance, resonator electrode area (A_e), and mode shape.

From (8-1) k is given by [114]

$$k = \alpha \left[\frac{n}{f_n A_e} \right]^2 \tag{8-2}$$

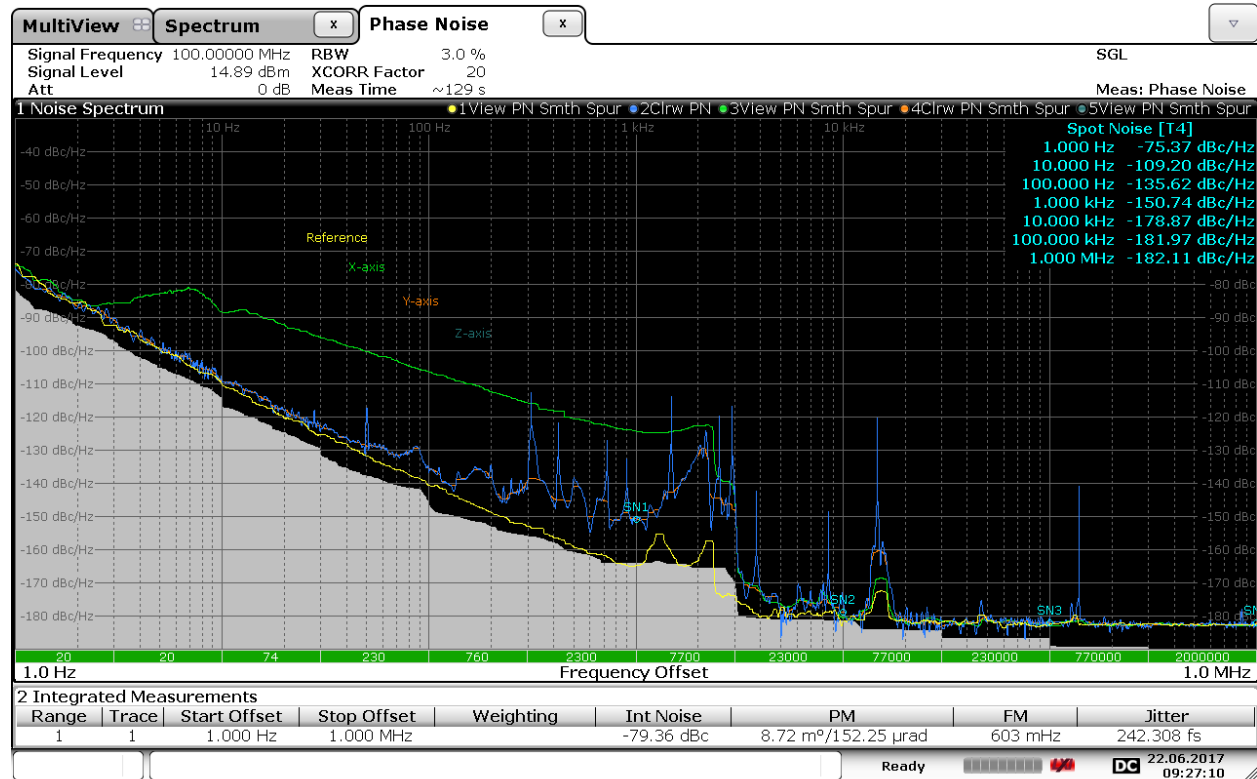
where α is a constant dependent on the resonator cut and material properties.

The challenge associated with accurate AF measurement is the isolation of drive-level-induced frequency shifts caused by nonlinearity from the linear effect of quasi-static temperature changes. A fundamental problem when evaluating AF effects is, how to change the resonator drive level without affecting the accuracy of the measurement system used to determine the associated frequency change. In particular, the phase detector amplitude response determines the accuracy with which small values of the AF effect can be determined using either of the above measurement systems.



Date: 22.JUN.2017 11:04:41

Figure 8.1: shows the phase noise plots of reference and 100 MHz crystal oscillator as DUT (Device under test), yellow plot depicts reference phase noise plot in z-direction and DUT-phase noise plot along x, y, and z-axis directions under vibration



Date: 22.JUN.2017 09:27:10

Figure 8.2: shows the phase noise plots of reference and 100 MHz crystal oscillator as DUT (Device under test), yellow plot depicts reference phase noise plot in XY-direction and DUT-phase noise plot along x, y, and z-axis directions under vibration

8.3 Current and Next Generation Crystal Oscillators:

The crystal oscillators are electromechanical devices that produce an electric signal by using a mechanical resonance of a vibrating quartz crystal of piezoelectric material. Due to low cost and compact size, crystal oscillators are currently employed in a numerous applications that include clocks, radios, computers, cellphones, microcontrollers, space tracking systems, modems, microprocessors, disk drives, sensors, video games, digital systems, measuring instruments, timers, engine controlling, phase locked loop systems, medical devices, global positioning systems (GPS), cable television systems, oscilloscopes and signal generators. The next generation crystal oscillators can play a vital role in improving the performance of automotive electronics for precise timing solutions and frequency.

The alternative low cost and high performance solution is projected by MEMS community claiming that this technology would finally replace quartz crystal oscillator by providing lower costs, shorter design and production cycle times, excellent shock and vibration performance, and superior signal quality [115]. Despite these claims, few studies have been available to help understand the performance characteristics of MEMS oscillators. Due to their material characteristics, silicon-based MEMS oscillators have to use a temperature compensated circuit to tune the resonant frequency back to an acceptable scale. The vibration mechanism of the silicon MEMS resonator is still not very stable in the short term and that makes the MEMS oscillator unable to achieve wide market acceptance at this time [115].

8.4 Conclusion

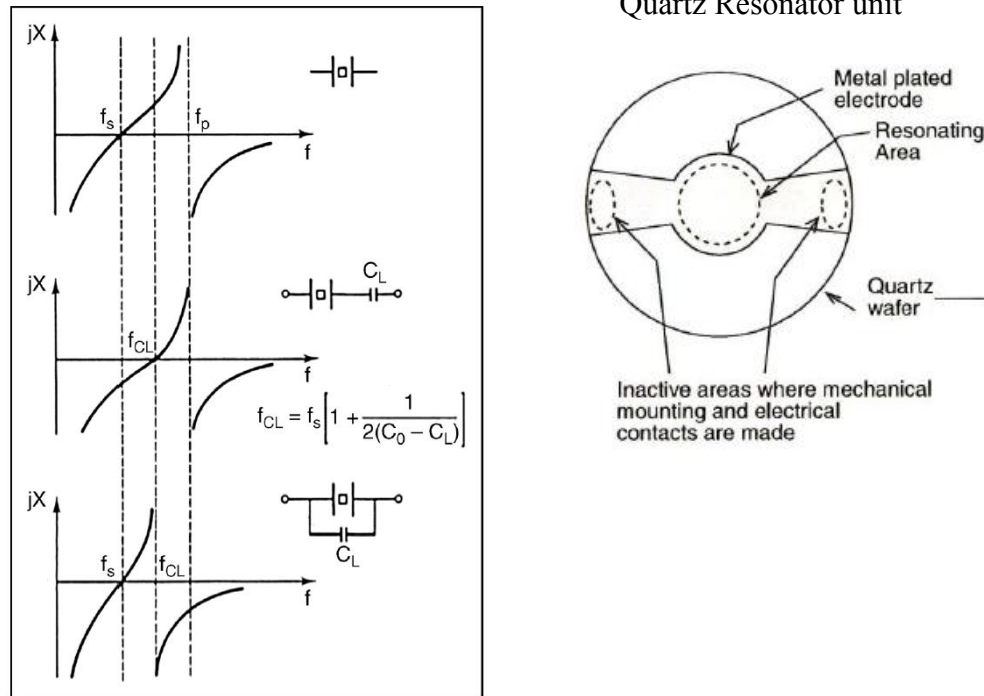
How will market trends for frequency controlled circuits and timing devices shape up? While silicon-based timing devices are still not as capable of sophisticated tasks as crystal oscillators, they are getting better, and will eventually replace crystals in many contexts. That will produce further synergies for the industry as mass production becomes cheaper and easier. These days, designers require higher frequencies and low jitter in oscillators, while buyers demand low cost and quick delivery. Timely oscillator options that can deliver the highest desired performance, while minimally compensating design steps are key to cost-effective solutions [115]-[117].

Fortunately, in the ongoing battle to push the limits of technology and lower component costs, oscillator manufacturers continue to close the gap between high-level performance and cost-effective purchasing, with conventional crystal technology paired with configurable oscillator technology. Like every exciting new technology targeting mass markets driven by start-ups, confusion or exaggeration are present, but all in all, it is believed that MEMS oscillators will follow the successful bulk acoustic wave devices as the second RF MEMS mass product. The current steady, moderate growth in timing solutions revenue is being driven by the expansion of strong consumer electronics and computer applications sectors, as silicon timing solutions are improving. Silicon is increasingly able to handle some of the timing tasks traditionally given to crystals. However, continued under-investment by telecom infrastructure vendors could have a negative effect in the medium term. Overall, it is expected that the market for both non-silicon and silicon resonator oscillators will share 50 percent of the timing solution market down the road.

The knowhow gained in 7 years (2012-19) for the seminal research work carried out for the fulfillment of Dr. Ing study can be extended for future study, especially low phase noise signal sources for modern radio communications that includes 5G and IoT (Internet of Things Applications). The reported publications [3, 4, 24, 31, 71, 128, 129, 130, 131, and 132] provide the knowhow for high frequency generations for X-band Radar applications and also basis for miniaturizations without compromising the quality (Q) factor.

Typical questions in the context of this dissertation:

1. The frequency – impedance diagram



The first graph in the figure shows the relation between the crystal's resonant frequency and the reactive impedance due to the crystal, f_s and f_p are the series and parallel resonant frequencies.

The crystal datasheets specify the holding capacitance (between the two metallized surfaces used as electrodes) C_0 which is 3-15pF for most crystals.

The second graph shows that the capacitor C_L when placed in series with the crystal changes the impedance and shifts the frequency slightly higher than the original series resonance.

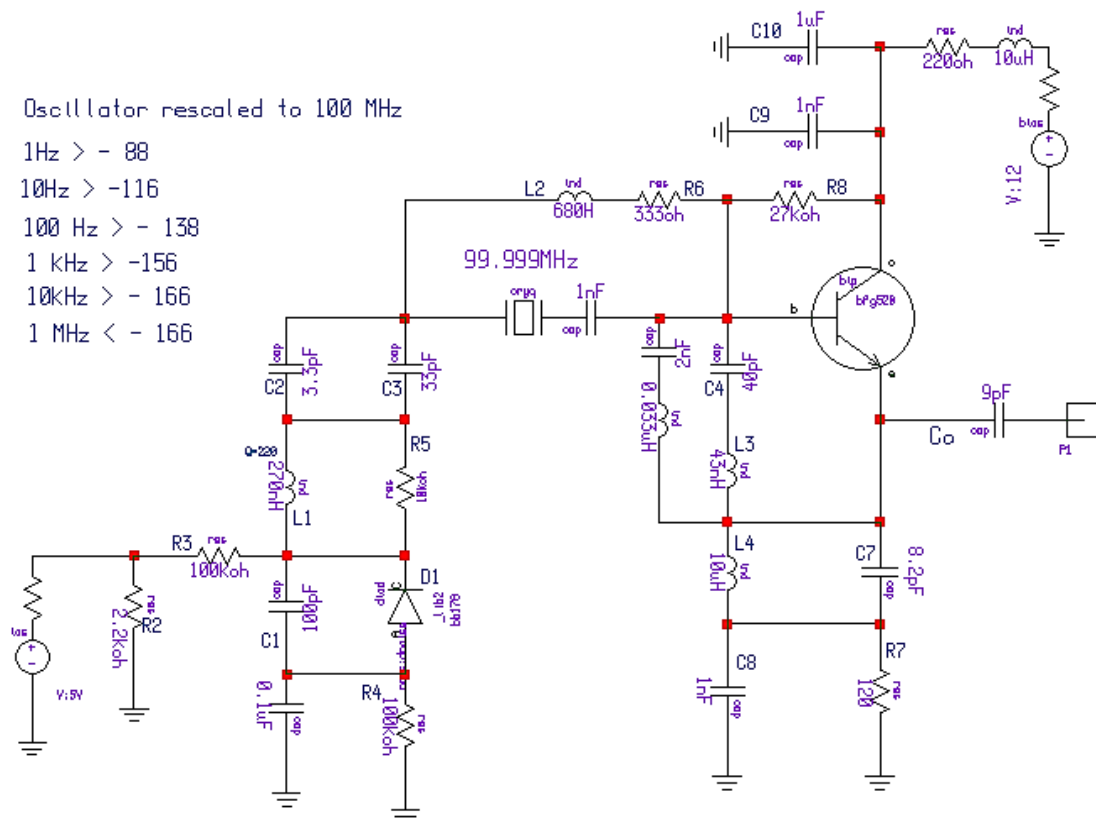
The third graph shows that when the capacitance is placed in parallel to the crystal, the parallel resonant frequency is shifted slightly to a lower value.

Similar approach is used in the design shown below (Fig 5-22a from thesis), by adding an inductance in series to the crystal resonator to pull down the frequency a little and a capacitor in series is used to push it a little higher. This is to compensate for the tolerances of the resonance frequency of the crystal in a production environment.

In the circuit (Fig 5-33a from thesis), the 270nH inductor pulls the frequency further down (by few Hz, as the crystal frequency is a few Hz below the resonant frequency; 99.999MHz).

The 33pF in parallel to 3.3pF capacitor and the tuning diode in parallel with 100pF capacitor, which limits the tuning range, shift the frequency up and tune the circuit to 100MHz. Fig. 4-4 in the thesis explains selection of tuning diode and its effect on phase noise.

The capacitor C4 and inductor L3 parallel to 2nF capacitor and 43nH inductor is the mode suppression circuit; to prevent oscillation at the fundamental frequency.



- The reason why the BFG 540 was selected – As a rule of thumb, the optimum performance can be achieved with the f_T of the transistor at least about 10 times the frequency of operation. The higher the f_T the higher the flicker noise. The BFG 540 has f_T of 9GHz and was found to be best fit for this design. Transistors with lower f_T are now not easily available.

Why not MOSFET or SiGe for this design?

The f_T is higher with different topologies of transistor generally in the order seen here - Ge, Si, SiGe, CMOS or MOSFET, GaAs, GaN – and this will shift the flicker corner frequency higher with higher f_T and hence not good for this frequency of operation (100MHz) or oscillators in general.

- What would be the case if tubes were used?

The table shows phase noise performance of a tube LC oscillator, FET-LC oscillator and a BJT- Crystal oscillator:

Offset from the carrier	Phase Noise in dBc/Hz Tubes circuit	Phase Noise in dBc/Hz FET-LC oscillator	Phase Noise in dBc/Hz Xtal oscillator
1 Hz	-0.70	-16	-72
10 Hz	-37	-50	-105
100 Hz	-74	-77	-145
1 kHz	-105	-97	-165
10 kHz	-140	-135	-175
100 kHz	-165	-148	-180
1 MHz	-181	-150	-185

4. Why does FSUP/FSWP give closer to theoretical measurements? – Since it uses the cross correlation method the uncorrelated noise will be canceled and only DUT noise will be measured. This method gives phase noise measurement with 40dB more dynamic range and now validates the theory.
5. Why measured and simulated phase noise values are not matching below 10Hz – the limitation is due to the lack of a transistor model that includes flicker in the CAD simulation. More research on flicker noise is needed and a physics based model is not yet available and hence the predictions at close-in offsets are not accurate enough.
6. What are Af and Kf – These are curve fitting factors and their values are Af (between 1.7 and 2) and Kf (between 10e-11 to 10e-13) depends upon the transistor used.
7. How did you choose the values for Af and Kf in your simulations – This had to be done with curve fitting techniques where these values are found empirically, based on measured results: used as follows

$$\langle i_{bn}^2 \rangle = 2qI_D \Delta f + KF \frac{I_B^{AF}}{f_{FCF}} \Delta f \quad (\text{Eqn 4-7 in thesis})$$

8. How did the 2 transistor design improve phase noise?
9. Can you explain the mechanism?

8 & 9: Due to the class-C operation the transistor remains off for about 70% of the cycle and thus minimizes the noise contribution from the semiconductor.

The crystal is in the emitter and used as a resonator and filter – improves the phase noise without deteriorating the power output, thus results in a better FoM (figure of merit)

10. What did you do different from HP?

This is a 2-transistor design and the gain is the ratio of two resistors; HP used a single transistor Colpitts configuration and suffers from the unfavorable effect of component tolerances.

The transistors used in the HP oscillator are no longer manufactured.

The mode suppression circuit used in HP design is not required in this design as it is taken care of with the parallel tuned circuit at the collector of both the transistors.

References:

- [1] Terman, "Radio Engineers Handbook", First Edition, Tenth impression, McGraw-Hill Book Company, Inc. 1943
- [2] M. M. Driscoll, "Low Noise Crystal Controlled Oscillator", US Patent No. US4797639A, Jan 10, 1989
- [3] Ajay Poddar, Ulrich Rohde, Anisha Apte, "How Low Can They Go, Oscillator Phase noise model, Theoretical, Experimental Validation, and Phase Noise Measurements", IEEE Microwave Magazine, Vol. 14, No. 6, pp. 50-72, September/October 2013
- [4] U.L. Rohde, Anisha Apte, "Everything You Always Wanted to Know about Colpitts Oscillators," IEEE Microwave Magazine, vol. 17, issue 8, pp. 59-76, Aug. 2016
- [5] U.L. Rohde, "Noise Analysis – Then and today",
https://synergymwave.com/articles/2018/Large-signal-oscillator-noise-analysis-then-and-today_s.pdf (seen in June 2019)
<https://www.microwavejournal.com/articles/29151-noise-analysis-then-and-today?v=preview> (seen in June 2019)
- [6] <http://www.nist.gov/pml/div688/grp50/primary-frequency-standards.cfm> (seen in June 2019)
- [7] Robert J. Matthys, "Crystal Oscillator Circuits", Revised Edition, Krieger Publishing Company, Malabar, Florida, 1992
- [8] <http://http://www.ieee-uffc.org/publications/books/toc.asp?book=10www.ieee-uffc.org/main/history-norton.asp> (seen in June 2019)
- [9] U.L. Rohde, A.K. Poddar, and G. Boeck, "The Design of Modern Microwave Oscillators for Wireless Applications: Theory and Optimization", John Wiley & Sons, New York, NY, May, 2005, ISBN 0-471-72342-8
- [10] U. L. Rohde and A. K. Poddar, "Crystal Oscillators", Wiley Encyclopedia and Electronics Engineering, pp.1-38, October 19, 2012
- [11] U. L. Rohde and A. K. Poddar, "Crystal Oscillator Design", Wiley Encyclopedia of Electrical and Electronics Engineering, pp. 1–47, October 2012
- [12] U. L. Rohde and A. K. Poddar, "Latest Technology, Technological Challenges, and Market Trends for Frequency Generating and Timing Devices", IEEE Microwave Magazine, pp.120-134, October 2012
- [13] U. L. Rohde and A. K. Poddar, "Techniques Minimize the Phase Noise in Crystal Oscillators", 2012 IEEE FCS, pp. 01-07, May 2012
- [14] U. L. Rohde, "Crystal oscillator provides low noise", Electronic Design, 1975
- [15] Stichting Centrum voor Duitse Verbindings- en aanverwante Technologieën (Stg. C.D.V. & T.) Foundation: Centre for German Communication and related Technology, Pater Pirestraat 29 1111 KR Diemen, February 2000
- [16] Cady W.G., "Piezoelectricity", Dover, New York, McGraw Hill Book Company, 1946
- [17] <https://www.keysight.com/en/pd-1000001050%3Aeprsg%3Apro-pn-10811E/10-mhz-crystal-oscillator?cc=US&lc=eng> (seen in May 2019)
- [18] Dieter Scherer, "The "Art" of Phase Noise Measurement", RF & Microwave Measurement Symposium and Exhibition, Hewlett Packard, 1983

- [19] U. L. Rohde, "Microwave and Wireless Synthesizers, Theory and Design", Wiley, New York, ISBN 0-471-52019-5, August 1997
- [20] U. L. Rohde, Matthias Rudolph, "RF/Microwave Circuit Design for Wireless Applications", 2nd Ed. John Wiley & Sons. pp. 745–746, New York, ISBN 1118431405, 2013
- [21] Keysight Technologies phase noise measurement solutions
<https://literature.cdn.keysight.com/litweb/pdf/5990-5729EN.pdf> (Seen on 5/1/2019)
- [22] Dorin Calbaza, Chandra Gupta, Ulrich L. Rohde, and Ajay K. Poddar, "Harmonics Induced Uncertainty in Phase Noise Measurements", 2012 IEEE MTT-S Digest, pp. 1-3, June 2012
- [23] B. Griffiths. (2009). Notes on the Driscoll VHF overtone crystal oscillator. [Online] Available: <http://www.mentby.com/bruce-griffiths/notes-on-the-driscoll-vhf-overtone-crystaloscillator.html> (seen in May 2019)
- [24] Ulrich Rohde, Ajay Poddar, Anisha Apte, "Getting Its Measure", IEEE Microwave Magazine, Vol. 14, No. 6, pp. 73-86, September/October 2013
- [25] George D. Vendelin and Anthony M. Pavio, U. L. Rohde, "Microwave circuit design using linear and nonlinear techniques", Wiley, New York, 2005
- [26] A. L. Lance, W. D. Seal, F. G. Mendozo and N. W. Hudson, "Automating Phase Noise Measurements in the Frequency Domain," Proceedings of the 31st Annual Symposium on Frequency Control, 1977
- [27] U. L. Rohde, Hans Hartnagel, "The Dangers of Simple use of Microwave Software"
- [28] http://www.mes.tu-darmstadt.de/media/mikroelektronische_systeme/pdf_3/ewme2010/proceedings/session_vii/rohde_paper.pdf (seen in May 2019)
- [29] D. Nehring, "Novel high-frequency crystal oscillator cuts jitter and noise", RF Design Journals, pp. 32-42, June 2005
- [30] U. L. Rohde and A. K. Poddar, "Voltage Controlled Crystal Oscillator", IEEE Sarnoff, March 30-April 01, 2009, Princeton, NJ, USA
- [31] Anisha Apte, Ulrich L. Rohde, Ajay Poddar, and Matthias Rudolph, "Low Phase Noise 100MHz Crystal Oscillator – Optimizing Phase-Noise Performance", IEEE Microwave Magazine, June 2017
- [32] K. L. Kotzebue, 'A Technique for the Design of Microwave Transistor Oscillators', *IEEE Trans. Microwave Theory Tech.*, MTT-32, 719–721 (1984)
- [33] I. Bahl and P. Bhartia, Microwave Solid State Circuit Design, 2nd ed., Wiley, New York, April 2003
- [34] John Vig, "Quartz Crystal Resonators and Oscillators: For Frequency Control and Timing Applications - A Tutorial", August 2014
- [35] Benjamin Parzen, "Design of Crystal and Other Harmonic Oscillators", Ch-6, John Wiley & Sons, 1983, ISBN: 0-471-08819-6,
- [36] K. C. Gupta, R. Garg and R. Chadha, *Computer-Aided Design of Microwave Circuits*, Dedham: Artech House (1981)
- [37] R. E. Collin, Foundation for Microwave Engineering, McGraw-Hill, New York, 1966
- [38] D. Pozar, Microwave Engineering, 2nd ed., Wiley, New York 1998

- [39] <http://www.wenzel.com/contact-us/croven-crystals-website/> (seen in July 2019)
- [40] H. K. Gummel and R. C. Poon, "An integral charge control model of bipolar transistor," *Bell Syst. Tech. J.*, vol. 49, pp. 827-852, May-June 1970
- [41] U.L. Rohde, D.P. Newkirk, *RF/Microwave Circuit Design for Wireless Applications*, John Wiley & Sons, April 2000, ISBN 0-471-29818-2, pp782
- [42] K.K. Clarke, D.T. Hess, *Communication Circuits: Analysis and Design*, Chapter 4: Nonlinear Controlled Sources, Addison Wesley, 1971
- [43] <http://www.farnell.com/datasheets/39775.pdf> (seen in May 2019)
- [44] V. Rizzoli, F. Mastri, D. Masotti, "A general-purpose harmonic-balance approach to the computation of near-carrier noise in free-running microwave oscillators", 1993 IEEE MTT-S IMS Digest
- [45] https://www.infineon.com/dgdl/Infineon-BFP193-DS-v01_01-en.pdf?fileId=db3a30431400ef6801142674fdc3061b (seen in May 2019)
- [46] <https://www.keysight.com/en/pd-1000001050%3Aepsg%3Apro-pn-10811E/10-mhz-crystal-oscillator?cc=US&lc=eng> (seen in May 2019)
- [47] <https://www.nist.gov/director/pao/nist-boulder-laboratories-precision-measurements-support-innovation> (seen in May 2019)
- [48] G. Gonzalez, *Foundations of Oscillator Circuit*, Ch-IV, 2007 Artech House, Inc., London
- [49] <http://ieeexplore.ieee.org/stamp/stamp.jsp?arnumber=7348831>
- [50] U. L. Rohde and A. K. Poddar, "A Novel Voltage Controlled Crystal Oscillator (VCXO)", 2009 European Frequency & Time Forum & IEEE Int'l Frequency Control Symposium (EFTF-IFCS 2009), Besancon, France, April 20-24 2009
- [51] T. Yasuda et al., "Nonlinear model of crystal resonator and its application to phase noise simulator of oscillator", IEEE IFCS. pp. 1-3, May 2014
- [52] M. M. Driscoll, "Oscillator AM-to-FM Noise Conversion Due to the Dynamic Frequency- Drive Sensitivity of the Crystal Resonator", 2008 IEEE Frequency Control Symposium FCS, pp. 672-676
- [53] http://ims2016.org/images/files/instructions/IMS2016/SDC_10_2016_SDC_MTT_22_17_crystal_osc_V2.pdf
- [54] X. Huang et al, "Prediction, simulation, and verification of the phase noise in 80-MHz Low-Phase-Noise Crystal Oscillators", IEEE Transaction on UFFC, vol. 62, No. 9, pp. 1599-1604, Sept. 2015
- [55] X. Huang, D. Liu, Y. Wang, P. Chen, and W. Fu", "100-MHz Low-Phase-Noise microprocessor temperature compensated crystal oscillator", IEEE Trans. on Circuits and Systems-II, Express Briefs, vol. 62, No. 7, pp. 636-640, July 2015
- [56] R. Boroditsky, J. Gomez, "Micro miniature, SMD, Ultra low phase noise, high frequency OCXO", EFTF, pp. 360-362, 2014
- [57] Ji Wang, "Consideration of Stiffness and Mass Effects of Relatively Thicker Electrodes with Mindlin Plate Theory", IEEE Transactions on UFFC, Vol. 53, No. 6, June 2006
- [58] <http://www.wenzel.com/documents/circuits1.htm>

- [59] Xuezhen Wang, Russell Radke, Jay E. Ackerman, Michael Baker , “Multimode Crystal Oscillator for Power Management Unit with Digitally Controlled AGC Loop in 0.18 μ m CMOS Technology”, 2015 ISCAS, pp.874-877
- [60] Y Tsuzuki, T. Adachi, and J. W. Zhang, “ Fast Start-up Crystal Oscillator Circuits”, 1995 IEEE International Frequency Control Symposium Digest, pp. 565-568
- [61] Y Tsuzuki, T. Adachi, and J. W. Zhang, “Formulation of Nonlinear Negative Resistance For Calculation of Start-up Characteristics of Crystal Oscillator Circuits”, 1996 IEEE IFCS Digest, pp. 710-713
- [62] Y Tsuzuki, T. Adachi, and H. Yokohara, “Low Drive Level Crystal Oscillator Circuit”, 1997 IEEE International Frequency Control Symposium Digest, pp. 966-969
- [63] A. K. Poddar, “Slow Wave Resonator Based Tunable Multi-Band Multi-Mode Injection-Locked Oscillators”, Dr.-Ing.-habil Thesis, Chapter 5, pp. 163-177, BTU Cottbus, Germany, 2014
- [64] ANSI/IEEE Std. 176-1987, IEEE Standard on Piezoelectricity, 1987
- [65] U. L. Rohde, “Mathematical Analysis and Design of an Ultra Stable Low Noise 100MHz Crystal Oscillator with Differential Limiter and its Possibilities in Frequency Standards”, Proceedings of the 32nd Annual Symposium on Frequency Control, p418, 1978”
- [66] U. L. Rohde, “A New Efficient Method of Designing Low Noise Microwave Oscillators,” Dr.-Ing. Dissertation, Faculty IV, EEC (Electrical Engineering and Computer Sciences), TU-Berlin, Germany, Feb. 2004
- [67] U. L. Rohde, “A Novel Approach for Generating Active Inductors for Microwave Oscillators,” Dr.-Ing. Habil, Dissertation, Technical University of Berlin, 2011
- [68] U. L. Rohde, A. K. Poddar, “Phase Noise Measurement Techniques, Associated Uncertainty and Limitations”, IEEE joint UFFC Symposia with European Frequency and Time Forum (EFTF) and Piezo response Force Microscopy, July 21-25, 2013
- [69] Ulrich L. Rohde, Ajay K. Poddar, “Emerging Technology and Technological Challenges in Low Phase Noise Oscillator Circuit Designs”, workshop, IMS 2012, June 18, 2012
- [70] U. L. Rohde and A. K. Poddar, “Impact of Radiated EMI in High Frequency Crystal Oscillator”,, IEEE IMS 2010, May 23-28, 2010, Anaheim, California, USA
- [71] U. L. Rohde, A. K. Poddar, Anisha Apte, “Phase noise measurement and its limitations”, Microwave journal, April 2013
- [72] R. L. Filler, “The acceleration sensitivity of quartz crystal oscillators: A review”, IEEE Trans. on UFFC Vol. 35, Mo. 3, May 1985, pp.297-305
- [73] <https://synergymwave.com/articles/2010/05/>
- [74] <https://www.alliedmarketresearch.com/press-release/crystal-oscillator-market.html>
- [75] https://industryarc.com/PressRelease/608/Next-Generation-Crystal-Oscillators-Market-Research.html?gclid=EAIaIQobChMIu6uXz_yv4QIVDisMCh22vw_1EAMYASAAEgIfd_BwE
- [76] Agilent Phase Noise Measurement Solution (www.home.agilent.com/agilent/application), 2012 (seen in 2012)
- [77] W. F. Walls, “Practical problems involving phase noise measurements, 33th annual precise time interval (PTTI) meeting, pp 407-416, Nov 2001.

- [78] "Sideband Noise in Oscillators", <http://www.sm5bsz.com/osc/osc-design.htm>, 2009
- [79] Jeff Cartwright, "Choosing an AT or SC cut for OCXOs", http://www.conwin.com/pdfs/at_or_sc_for_ocxo.pdf, 2008
- [80] M. M. Driscoll, "Low Frequency Noise Quartz Crystal Oscillators", *Instrumentation and Measurement*, IEEE Trans. Vol 24, pp 21-26, Nov 2007,
- [81] M. M. Driscoll, "Reduction of quartz crystal oscillator flicker-of-frequency and white phase noise (floor) levels and acceleration sensitivity via use of multiple resonators", *IEEE Trans. UFFCC*, Vol. 40, pp 427-430, Aug 2002.
- [82] U. L. Rohde, A. K. Poddar, "Technique to minimize phase noise in crystal oscillator", *Microwave Journal*, pp132-150, May 2013
- [83] O. Rajala, "Oscillator Phase Noise Measurements using the Phase Lock Method", MS thesis, Department of Electronics, Tampere University of Technology, June 2010.
- [84] W. F. Walls, "Cross-Correlation Phase Noise Measurements", *IEEE FCS*, pp. 257-261, 1992
- [85] J. Breitbarth, "Cross Correlation in phase noise analysis", *Microwave Journal*, pp 78-85, Feb 2011.
- [86] F. L. Walls et al. Extending the Range and Accuracy of Phase Noise Measurements, *Proceedings of the 42nd Annual Symposium on Frequency Control*, 1988.
- [87] Noise XT, DCNTS manual, http://www.noisext.com/pdf/noisext_DCNTS.pdf, 2013, (seen in 2013)
- [88] Agilent E5052A Signal Source Analyzer 10 MHz to 7, 26.5, or 110 GHz – Datasheet", Agilent document 5989-0903EN, p. 12, May 2007
- [89] Frequency Extension for Phase Noise Measurements with FSUP26/50 and Option B60 (Cross-Correlation)", Rhode & Schwarz Application Note 1EF56, p. 3 Jan 2007.
- [90] M. Jankovic, "Phase noise in microwave oscillators and amplifiers", PhD thesis, Faculty of graduate School of the University of Colorado, Department of Electrical, Computer and Energy Engineering, 2010
- [91] Hewlett Packard, *RF and Microwave Phase Noise Measurement Seminar*, Available at: http://www.hparchive.com/seminar_notes/HP_PN_seminar.pdf, June 1985.
- [92] Stephan R. Kurz, *WJ Tech note – Mixers as Phase Detectors*, Available at: http://www.triquint.com/prodserv/tech_info/docs/WJ_classics/Mixers_phase_detectors.pdf, [Cited 2010-05-11]
- [93] Agilent Technologies, *Phase Noise Characterization of Microwave Oscillators – Phase Detector Method – Product Note 11729B-1*
Available at: <http://tycho.usno.navy.mil/ptti/ptti2001/paper42.pdf>, May 2010
- [94] Aeroflex, Application Note #2 – PN9000 automated Phase Noise Measurement System Available at: <http://www.datasheetarchive.com/datasheet-pdf/010/DSA00173368.html>, April 2010
- [95] Hewlett Packard. *HP 3048A Phase Noise Measurement System Reference Manual* [online]. Available: <http://cp.literature.agilent.com/litweb/pdf/03048-90002.pdf>, 1989, Sept 01
- [96] E. Rubiola and F. Vernotte, "The cross-spectrum experimental method", [online]. Available: <http://arxiv.org/>, document arXiv:1003.0113v1 [physics.ins-det], 2010, Feb 27
- [97] Hewlett Packard *HP 3048A Phase Noise Measurement System Operating Manual* [online]. Available: <http://cp.literature.agilent.com/litweb/pdf/03048-61004.pdf>, (1990, Jun 01)
- [98] *HP 11848A Phase Noise Interface Service Manual*, 1st ed., Hewlett-Packard Company Spokane, Washington 1987.

- [99] M. Sampietro, L. Fasoli, and G. Ferrari, "Spectrum analyzer with noise reduction by cross-correlation technique on two channels," *Rev. Sci. Instrum.*, vol. 70, no. 5, May 1999.
- [100] Samuel J. Bale, David Adamson, Brett Wakley, Jeremy Everard, "Cross Correlation Residual Phase Noise Measurements using Two HP3048A Systems and a PC Based Dual Channel FFT Spectrum Analyzer", 24th European Frequency and Time Forum, pp 1-8, (April 13-16, 2010)
- [101] Jeremy Everard, Min Xu, Simon Bale, "Simplified Phase Noise Model for Negative-Resistance Oscillators and a Comparison With Feedback Oscillator Models", *IEEE Transactions on Ultrasonics, Ferroelectrics, and Frequency Control*, Vol. 59, No. 3, March 2012
- [102] Jeremy Everard, Min Xu, "Simplified Phase Noise Model for Negative-Resistance Oscillators", *IEEE Frequency Control Symposium, 2009 Joint with the 22nd European Frequency and Time forum*, pp. 338-343, April 2009
- [103] Time Domain Oscillator Stability Measurement Allan variance, application note, Rohde & Schwarz, pp. 1-16, <http://www.crya.unam.mx/radiolab/recursos/Allan/RS.pdf>, 2009.
- [104] M. M. Driscoll, "Modeling Phase Noise in Multifunction Subassemblies", *IEEE Transactions on Ultrasonics, Ferroelectrics, and Frequency Control*, vol. 59, no. 3, pp. 373-381, March 2012
- [105] E. Rubiola, *Phase Noise and Frequency Stability in Oscillators*. Cambridge University Press, 2009, ISBN: 978-0-521-12328-7
- [106] G. Cibiel, M. Regis, E. Tournier, and O. Llopis, "AM noise impact on low level phase noise measurements", *IEEE Transactions on Ultrasonics, Ferroelectrics and Frequency Control*, vol. 49, no. 6, pp. 784-788, 2002
- [107] E. Rubiola and R. Boudot, "The effect of AM noise on correlation phase-noise measurements", *IEEE Transactions on Ultrasonics, Ferroelectrics and Frequency Control*, vol. 54, no. 5, pp. 926-932, May 2007.
- [108] E. Rubiola, "Primary calibration of AM and PM noise measurements," arXiv e-print 0901.1073, Jan. 2009
- [109] C. W. Nelson, A. Hati, and D. A. Howe, "Collapse of the Cross-spectral Function", *IEEE Frequency Control Symposium, FCS proceedings 2014*, pp.590-591, Taipei May 2014
- [110] C.W. Nelson, A. Hati, and D.A. Howe, "A Collapse of the Cross spectral Function in Phase Noise Metrology," *Electronics Letters.*, vol. 49, no. 25, pp. 1640-1641, Dec. 2013
- [111] C. W. Nelson, A. Hati, and D. A. Howe, "A collapse of the cross spectral function in phase noise metrology," *Rev. Sci. Instrum.*, vol. 85, pp. 024705-7, Feb. 2014
- [112] M.M. Driscoll, "Low Noise Signal Generation and Verification Techniques", *IEEE Ultrasonics, Ferroelectrics, and Frequency Control Society, Distinguished Lecture 2012-2013*
- [113] D. B. Leeson, "A Simple Model of Feedback Oscillator Noise Spectrum", *IEEE, Proc.* pp. 329-332, 1966
- [114] R. L. Filler, "The acceleration sensitivity of quartz crystal oscillators: A review", *IEEE Trans. on UFFC* Vol. 35, Mo. 3, May 1985, pp.297-305.
- [115] <https://synergymwave.com/articles/2010/05/>
- [116] <https://www.alliedmarketresearch.com/press-release/crystal-oscillator-market.html>
- [117] https://industryarc.com/PressRelease/608/Next-Generation-Crystal-Oscillators-Market-Research.html?gclid=EAIaIQobChMIu6uXz_yv4QIVDisMCh22vw_1EAMYASAAEgIf1fD_BwE
- [118] M. E. Frerking, "Crystal Oscillator Design and Temperature Compensation, Van Nostrand Reinhold Co., ISBN:0-442-22459-1, 1978
- [119] W. P. Robins, "Phase Noise in Signal Sources", Peter Peregrinus 1984, ISBN: 0-86341-026-X

- [120] Frank W. Harris, "Crystal Sets to Sideband", REV 12, Chapter 14, pp. 1-25, 2010 (www.qrparci.org/wa0itp/chap14.pdf)
- [121] Ulrich L. Rohde, "Introduction to modern signal generation; from analog to digital: Advantages and disadvantages and "solutions",
https://www.unibw.de/inf/aktuelles/6_4_18_uni_bw_june18-safe.pdf
- [122] Ulrich L. Rohde, Ajay K. Poddar, "Dynamic Noise-Feedback and Mode-Coupling Mechanism Silences The VCXOs Phase Noise", IEEE IFCS 2008
- [123] https://www.infineon.com/dgdl/Infineon-BB535SERIES_BB555SERIES-DS-v01_01-en.pdf?fileId=db3a304313d846880113d99d5153013c (seen on Aug 7 2019)
- [124] <https://www.axtal.com/cms/docs/doc86667.pdf> (seen on Aug 7 2019)
- [125] <https://www.infineon.com/cms/en/product/rf-wireless-control/rf-transistor/high-linearity-si-and-sigec-transistors-for-use-up-to-6-ghz/bfp196w/> (seen on Aug 7 2019)
- [126] https://www.infineon.com/dgdl/Infineon-BFP196W-DS-v01_01-en.pdf?fileId=db3a30431400ef680114267ecec60628 (seen on Aug 7 2019)
- [127] https://www.infineon.com/dgdl/Infineon-RFTransistor-SPICE.lib-SM-v02_10-EN.lib?fileId=5546d46256fb43b30157577dff04549 (seen on Aug 7 2019)
- [128] Anisha Apte, Ajay Poddar, Ulrich Rohde, Enrico Rubiola, "Colpitts Oscillator: A new Criterion of Energy Saving for high performance signal sources", IEEE International Frequency Control Symposium (IFCS), pp. 1-7, 2016
- [129] Ajay Poddar, Ulrich Rohde, Vivek Madhavan, Anisha Apte, Shibam Koul. "Ka-Band Metamaterial Möbius Oscillator (MMO) Circuit", IEEE International Microwave Symposium, MTT-S Digest, pp. 1-4, 2016
- [130] Anisha Apte, Ajay Poddar, Matthias Rudolph, and Ulrich Rohde, "A Novel Low Phase Noise X-Band Oscillator", IEEE Microwave Magazine, Vol. 16, Issue 1, pp. 127-135, 2015.
- [131] Anisha Apte, Vivek Madhavan, Ajay Poddar, Ulrich Rohde, and Matthias Rudolph, "A Novel Low Phase Noise X-band Oscillator", 2014 IEEE Benjamin Franklin Symposium on Microwave and Antenna Sub-systems for RADAR, Telecommunications, and Biomedical Applications (BenMAS), pp. 1-3, 2014
- [132] Ajay Poddar, Ulrich Rohde, Anisha Apte, Vivek Madhavan, Tatsuo Itoh, "Phase Noise Measurement: Uncertainty & Limitations", 2014 IEEE Benjamin Franklin Symposium on Microwave and Antenna Sub-systems for RADAR, Telecommunications, and Biomedical Applications (BenMAS), pp. 1-3, 2014

Chapter 9

Abbreviations and Symbols

<u>Symbol</u>	<u>Description</u>
$\Delta A(t)$	Amplitude fluctuation
$\Delta \varphi(t)$	Phase fluctuation
Δf	Noise bandwidth
B	Bandwidth
$\Delta \theta$	Steady state phase difference
DUT	Device under test
LTV	Linear time variant
LTIV	Linear time invariant
NLTV	Nonlinear time variant
$I_c(t)$	Collector current
I_{cob}	Collector reverse current
Y_n	Normalized noise admittance
Y_e	Even mode admittance
Y_o	Odd mode admittance
λ_e	Even mode Eigen value
λ_o	Odd mode Eigen value
G_n	In-phase component of noise source
B_n	Quadrature component of noise source
R_p	Parallel loss resistance
m	Ratio of loaded and unloaded Q
m_{opt}	Optimum value of m for minimum phase noise
Q_L	Loaded quality factor
Q_o	Unloaded quality factor
β_{ij}	Coupling parameter
α_i	Free-running amplitude of the i^{th} oscillator
$A_i(t)$	Instantaneous amplitude of the i^{th} oscillator
$\varphi_i(t)$	Instantaneous phase of the i^{th} oscillator
ω_i	Free-running frequency of the i^{th} oscillator
g_m	Small signal transconductance
$g_m(t)$	Large signal transconductance
f_0	Center frequency
f_c	Flicker corner frequency
f_m	Frequency offset
P_0	Average power at oscillator output
K_0	Oscillator voltage gain
R_p	Parallel loss resistance associated with the resonator
NF	Noise Figure

MEMS	Micro-electro-mechanical-system
SMD	Surface mounted device
SRF	Self resonance frequency
MSL	Microstripline
$\mathcal{L}(f_m)$	Ratio of sideband power in a 1 Hz bandwidth at f_m
$e_n(t)$	Noise signal voltage
$e_{inj}(t)$	Injected signal voltage
$\Delta\omega_{lock}$	Locking bandwidth
ω_{inj}	Injected signal frequency
λ_{ij}	Magnitude of the coupling coefficient
φ_{ij}	Phase of the coupling coefficient
r	Capacitance ratio of the tuning diode
C_{V0}	Capacitance of tuning diode at zero bias voltage
C_{VB}	Capacitance of tuning diode at breakdown bias voltage
P_n	Average power dissipated by the network
μ	Empirical nonlinear parameter
$R_n(t)$	Time variant negative resistance
K	Boltzmann's constant (1.38E-23 J/K)
$\Gamma(x)$	Impulse sensitivity function
C_n	Fourier series coefficient
$[C]$	Matrix representation of arbitrary coupling topology
C	Coefficient of correlation
θ_n	Phase of the n^{th} harmonic
W_e	Average stored electrical energy
W_m	Average stored magnetic energy
ω_{diff}	Modulation frequency
VNA	Vector network analyzer
VDP	Van der Pol
kT	4.1×10^{-21} at 300K (room temperature)
$\overline{i_{bn}^2} = 2qI_b\Delta f$	Mean square value of noise due to base current
$\overline{i_{cn}^2} = 2qI_c\Delta f$	Mean square value of noise due to collector current
$\overline{i_{con}^2} = 2qI_{cob}\Delta f$	Mean square of noise due to reverse collector current
$\overline{v_{bn}^2} = 4kTR_b\Delta f$	Mean square of noise voltage due to base resistance
$\overline{v_{sn}^2} = 4kTR_s\Delta f$	Mean square of noise voltage due to base resistance
$S(i_{cn}) = 2KTg_m$	Noise power spectral densities due to collector current
$S(i_{bn}) = \frac{2KTg_m}{\beta}$	Noise power spectral densities due to base current
$S(v_{bn}) = 4KTR_b$	Noise power spectral densities due to base resistance
$S(v_{sn}) = 4KTR_s$	Noise power spectral densities due to source resistance